SIMULATION AND ANALYSIS OF HUMAN PHANTOMS EXPOSED TO HEAVY CHARGED PARTICLE IRRADIATIONS USING THE PARTICLE AND HEAVY ION TRANSPORT SYSTEM (PHITS)

A Thesis

by

DONGYOUL LEE

Submitted to the Office of Graduate Studies of
Texas A&M University
in partial fulfillment of the requirements for the degree of

MASTER OF SCIENCE

December 2011

Major Subject: Nuclear Engineering

Simulation and Analysis of Human Phantoms Exposed to Heavy Charged Particle Irradiations Using the Particle and Heavy Ion Transport System (PHITS)

SIMULATION AND ANALYSIS OF HUMAN PHANTOMS EXPOSED TO HEAVY CHARGED PARTICLE IRRADIATIONS USING THE PARTICLE AND HEAVY ION TRANSPORT SYSTEM (PHITS)

A Thesis

by

DONGYOUL LEE

Submitted to the Office of Graduate Studies of
Texas A&M University
in partial fulfillment of the requirements for the degree of

MASTER OF SCIENCE

Approved by:

Co-Chairs of Committee,	Stephen Guetersloh
	Leslie Braby
Committee Member,	John Lawler
Head of Department,	Raymond Juzaitis

December 2011

Major Subject: Nuclear Engineering

ABSTRACT

Simulation and Analysis of Human Phantoms Exposed to Heavy Charged Particle Irradiations Using the Particle and Heavy Ion Transport System (PHITS).

(December 2011)

Dongyoul Lee, B. S., Korea Military Academy

Co-Chairs of Advisory Committee: Dr. Stephen Guetersloh
Dr. Leslie Braby

Anthropomorphic phantoms are commonly used for testing radiation fields without the need to expose human subjects. One of the most widely known is RANDO phantom. This phantom is used primarily for medical X-ray applications, but a similar design known as "MATROSHKA" is now being used for space research and exposed to heavy ion irradiations from the Galactic environment. Since the radiation field in the phantom should respond in a similar manner to how it would act in human tissues and organs under an irradiation, the tissue substitute chosen for soft tissue and the level of complexity of the entire phantom are crucial issues. The phantoms, and the materials used to create them, were developed mainly for photon irradiations and have not been heavily tested under the conditions of heavy ion exposures found in the space environment or external radiotherapy.

The Particle and Heavy-Ion Transport code System (PHITS) was used to test the phantoms and their materials for their potential as human surrogates for heavy ion irradiation. Stopping powers and depth-dose distributions of heavy charged particles

(HCPs) important to space research and medical applications were first used in the simulations to test the suitability of current soft tissue substitutes. A detailed computational anthropomorphic phantom was then developed where tissue substitutes and ICRU-44 tissue could be interchanged to verify the validation of the soft tissue substitutes and and determine the required level of complexity of the entire phantom needed to achieve a specified precision as a replacement of the human body.

The materials tested were common soft tissue substitutes in use and the materials which had a potential for the soft tissue substitute. Ceric sulfate dosimeter solution was closest to ICRU-44 tissue; however, it was not appropriate as the phantom material because it was a solution. A150 plastic, ED4C (fhw), Nylon (Du Pont Elvamide 8062), RM/SR4, Temex, and RW-2 were within 1% of the mean normalized difference of mass stopping powers (or stopping powers for RW-2) when compared to the ICRU-44 tissue, and their depth-dose distributions were close; therefore, they were the most suitable among the remaining solid materials.

Overall, the soft tissue substitutes which were within 1% of ICRU-44 tissue in terms of stopping power produced reasonable results with respect to organ dose in the developed phantom. RM/SR4 is the best anthropomorphic phantom soft tissue substitute because it has similar interaction properties and identical density with ICRU-44 tissue and it is a rigid solid polymer giving practical advantages in manufacture of real phantoms.

ACKNOWLEDGEMENTS

I would like to extend a tremendous amount of gratitude to my committee co-chairs, Dr. Stephen Guetersloh and Dr. Braby, and my committee member, Dr. Lawler, for their guidance and support throughout my graduate career.

I also want to extend my gratitude to the Korean Army, which provided full support over the years.

To my lovely family, thanks for making the past two years an unforgettable happy memory of my life. Especially to my wife, thanks for your continued support and encouragement throughout my entire life. I couldn't have finished my degree without your patience and love.

Finally, I would like to thank all my great friends I have met here; Shin Kyu Kang, Hyocheol Lee, Donghoon Kim, Sangjun An, Junsoo Ryu, and Saya Lee.

TABLE OF CONTENTS

CHAPTER Page

LIST OF FIGURES

FIGURE Page

FIGURE Page

FIGURE Page

LIST OF TABLES

TABLE Page

CHAPTER I

INTRODUCTION

Anthropomorphic phantoms have been used in various fields such as medical fields and space studies for testing radiation fields as a safe replacement to exposing human subjects when testing, calibration, and research are required. A physical phantom can be defined as a volume of tissue substitute materials used to simulate radiation interactions, where each individual tissue substitute is designed to simulate a particular body tissue with respect to a set of physical characteristics [1].

While the conventional phantoms used in medical field, representing body parts with a simple geometric shapes such as cylinders, were designed to be scanned or imaged to evaluate, analyze, and tune the performance of various imaging devices such as X-ray, CT (X-ray computed tomography), or MRI (magnetic resonance imaging), the anthropomorphic phantoms, in which more boundaries and materials exist, were mainly used to study non-uniform dose distribution within the phantom or to observe modality of absorbed dose on specific organ.

One of the most widely known anthropomorphic phantoms is RANDO phantom introduced by Alderson Research Laboratories in 1960's. RANDO phantom is a three compartment model having a soft tissue substitute for most of the body and a low density lung tissue substitute, as well as a real human skeleton [2]. The phantom has

---

This thesis follows the style of *IEEE Transactions on Nuclear Science*.

been used mainly for medical needs, but a similar design based on RANDO is now used for space research applications and is known as “MATROSHKA” [3].

However, the question of what makes a phantom ‘good enough’ in simulating a real human body has been posed. Since the phantom should respond in a similar manner to how human tissues and organs would act under an irradiation, the tissue substitute chosen for soft tissue and the level of complexity of the entire phantom are crucial issues. The materials of the RANDO phantom were developed for X-ray irradiations and have not been tested under heavy charged particle exposures.

Heavy charged particles (HCPs) are becoming a focus topic in the medical field because of the growing use in external radiotherapy where protons are common and accelerated carbon is emerging, offering better localization of dose than conventional radiotherapy [4]. HCPs are also important in space research since the long term chronic Galactic Cosmic Ray (GCR) exposures are from particles spanning the periodic table [5].

However, there is limited information available about the suitability of the current phantoms in studies of HCP exposures because the Heavy Charged Particle Therapy (HCPT) is relatively new technology, and the Galactic exposures were not coupled with detailed benchmarking. The suitability of typical tissue substitutes currently used for phantoms is in question when applied to HCP exposures.

It is beneficial to be able to simulate the phantom computationally to observe how well the phantom behaves as a true replacement of the human body, especially regarding the tissue substitute materials, before the expense of manufacture and testing. Early computational phantoms such as Medical Internal Radiation Dose (MIRD)

approach [6], and others derived from MIRD, were based on A General Monte Carlo N-Particle Transport Code (MCNP) and are, therefore, limited only to neutron, photon, and electron exposures [7].

A new detailed anthropomorphic computational phantom was developed using the Particle and Heavy-Ion Transport code System (PHITS) in which the transport of heavy ions and other charged particles is available [8]. ICRU-44 definition of average soft tissue was used in simulation, as well as commonly found tissue substitutes. Simulations were performed to see if the tissue substitutes remain valid surrogates when used both in isolation and with a detailed geometry containing multiple boundaries and materials. The goal of this study is therefore not only to find the most suitable tissue substitutes among commonly available materials, but also to determine the level of complexity required in the overall anthropomorphic phantom design using PHITS.

CHAPTER II

BACKGROUND

Heavy charged particle (HCP)

Heavy charged particles are defined as charged particles having masses greater than or equal to a proton's mass [9]. They interact with matter primarily through coulomb forces between their positive charge and the negative charge of the orbital electrons within the medium that the particle passes through. Since the interactions with nuclei are rare, the heavy charged particles lose their energy primarily by excitation or ionization, depending on the proximity of the coulomb interaction. By the frequent interactions, the HCP gradually loses its energy depositing a dose along its path until the particle is stopped. Near the end of the range of the HCP, a pronounced peak in the energy loss distribution, known as Bragg-peak, appears immediately before the particle comes to rest. The Bragg-peak is a characteristic feature of HCP dose delivery. The peak occurs because the interaction cross section increases as the charged particle's energy decreases [10, 11].

As shown in Fig. 1, provided by the Japanese National Institute of Radiological Sciences (NIRS), the energy loss modality of HCPs is different than that of photons because of the characteristic Bragg-peak. While the depth-dose distribution of uncharged radiations has a maximum near the surface of the body, maximum doses of HCPs occur

at significant depths. This trend of depth-dose distribution of HCP and its high biological effect allows precise dose localization in radiotherapy.

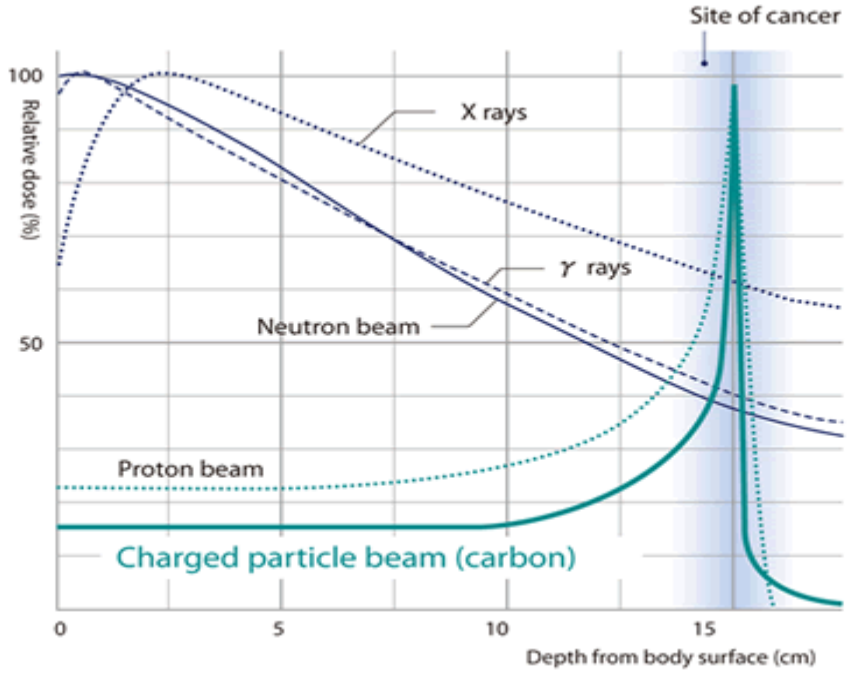

Fig. 1. Relative depth-dose distributions of charged and uncharged radiations within the human body. Charged radiations impart a relatively low dose on healthy tissues but a higher dose on the cancerous tissues. Uncharged radiations impart a relatively high dose near surface of the body and exponentially decrease as they pass through [12].

External beam radiotherapy that uses charged particles is referred to as charged particle therapy (CPT) and is dived into two subsections: proton therapy (PT) and heavy charged particle therapy (HCPT). The therapeutic use of protons was first suggested by Robert R. Wilson in 1946 and the first treatment by PT was performed at the Berkeley Radiation Laboratory in 1954. After modifying and connecting the low energy heavy ion accelerator (HILAC) to the high energy proton accelerator (BEVATRON), the combination now referred to as the BEVALAC, HCPT also began at Berkeley in 1974.

The NIRS in Chiba, Japan began using HCP for cancer treatment in June 1994 with carbon ions that were generated by the heavy ion medical accelerator (HIMAC) [13-15].

Fig. 2 shows the differences in the dose distributions between the X-rays and the protons when used for radiotherapy. As shown in this figure, the conventional radiotherapy using the X-rays tends to affect more of the surrounding healthy tissues due to the broad dose delivery. For the CPT, however, the dose can be localized in the cancerous area minimizing negative effects to the healthy tissues.

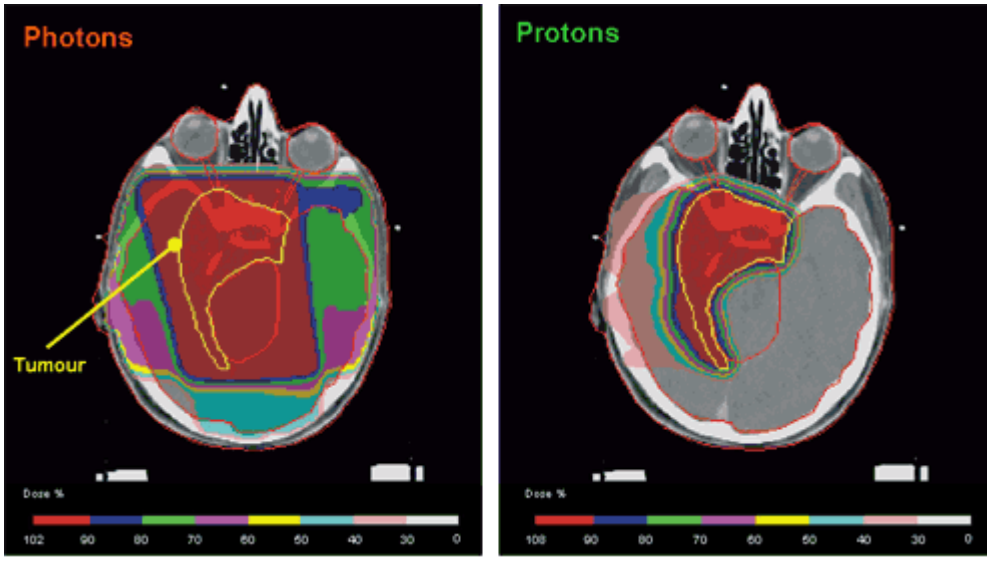

Fig. 2. Dose distribution contrast between the photon therapy (left) and the proton therapy (right) [16]. Inner section of the yellow line indicates a meningioma. The photon therapy gives a high dose throughout a wide area (red section), but the proton therapy localizes the dose near the tumor section.

HCPs are advantageous for tumor control; however, they are disadvantageous if the Bragg-peaks are misplaced on normal tissues due to problems in range determination from using tissue substitutes developed for photon interaction. Therefore, careful positioning on the cancerous cells is necessary [17].

RANDO phantom

RANDO, shown in Fig. 3, is one of the most widely known commercial phantoms and has provided a detailed mapping of dose distribution that is essential for evaluating radiotherapy treatment plans. The phantom body is sliced as 2.5 cm intervals and inserted several dosimeters into the sliced sections as shown in Fig. 3-(b).

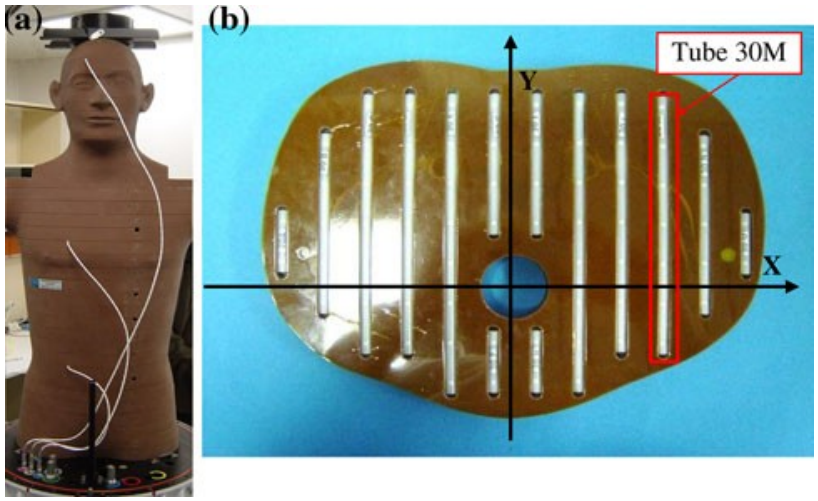

Fig. 3. RANDO phantom used in space study [(a) is the front view and (b) is the top view of a slice equipped with thermo-luminescent detectors (TLDs) mounted in polyethylene tubes.] [3].

RANDO phantom is constructed using a three compartment model: skeleton, lung, and a bulk soft tissue compartment. It has a natural human skeleton and lung tissue substitute that represents the lungs in a median respiratory state and is molded to fit the contours of the natural rib cage. The soft tissue substitute simulates the muscle tissue assuming randomly distributed fat [18]. The elemental compositions of the tissue substitutes used in RANDO phantom are presented in Table 1. Two different compositions are listed for the soft tissue because the product has been modified since its introduction. The tissue substitutes used for soft tissue and lungs in RANDO phantom are called Alderson muscle and Alderson lung, respectively. For Alderson muscle, the first manufactured product is called Alderson muscle (A) and the modified product is called Alderson muscle (B) [1].

TABLE 1
Elemental compositions of the tissue substitutes used in RANDO phantom (percentage by weight) [1].

Element	Alderson muscle (A)	Alderson muscle (B)	Lungs
Carbon	66.8	64.4	74.0
Oxygen	21.1	20.4	18.1
Hydrogen	8.9	8.8	5.7
Nitrogen	3.1	4.1	2.0
Chlorine	-	2.2	-
Antimony	0.1	0.1	0.2
Density (g/cm^3)	1.00	1.00	0.32

MATROSHKA facility [3]

RANDO phantom had been used routinely in X-ray radiotherapy for the treatment of patients, but its application was expanded to heavy ion studies at the end of the 1980s to evaluate the organ dose and the dose distribution inside the human body in the space environment. Until the end of the 1980s, the dose characterization of astronauts and cosmonauts exposures was performed only with personal dosimeters and monitoring instruments at fixed locations inside the spacecraft; therefore, only skin dose with no information about dose distribution inside the body could be achieved. Furthermore, it was emphasized that dose 'Hot Spots' could arise in the human body owing to stopping heavy ions. Because it was difficult to determine overall radiation risk precisely by using only skin dose, the accurate and detailed determination of the radiation exposure on human body was necessitated. Phantom experiments were therefore started to gain information on energy deposition and dose distribution from the Galactic environment. The MATROSHKA experiment, led by the German Aerospace Center (DLR) and supported by European Space Agency (ESA), was therefore launched on 29 January 2004. As shown in Fig. 4, MATROSHKA is a RANDO phantom design mimicking the astronaut in space work environment, which consists of the phantom, a base structure, and a container that simulates spacesuit. It contains more than 6,000 passive thermo-luminescent detectors (TLDs), and they are used to measure the absorbed doses from space radiation both inside and outside the International Space Station (ISS).

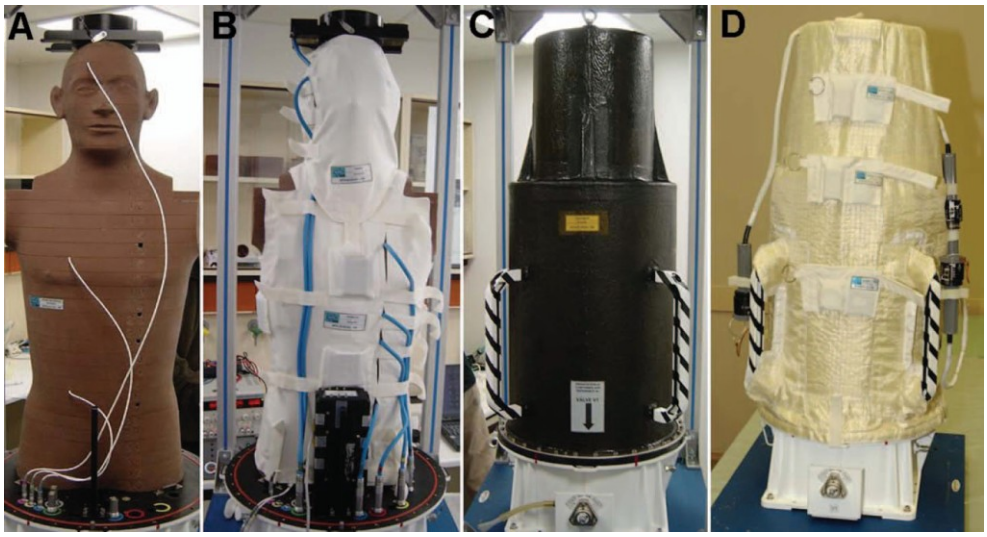

Fig. 4. MATROSHKA facility mounted with various equipment to represent the space work environment. The RANDO phantom was equipped with a poncho and hood which had passive detector systems for skin dose measurements, and then carbon fiber container was also equipped to simulate the astronaut's spacesuit. The facility close to launch was equipped with multilayer insulation for thermal protection (Picture courtesy of DLR) [19].

Fig. 5 shows the depth distribution of dose rates including the skin measurement. From this depth-dose distribution, an average organ dose rate was determined for each critical organ. The experimental results showed that the absorbed dose generally decreased with depth and no hot spot inside the human body existed.

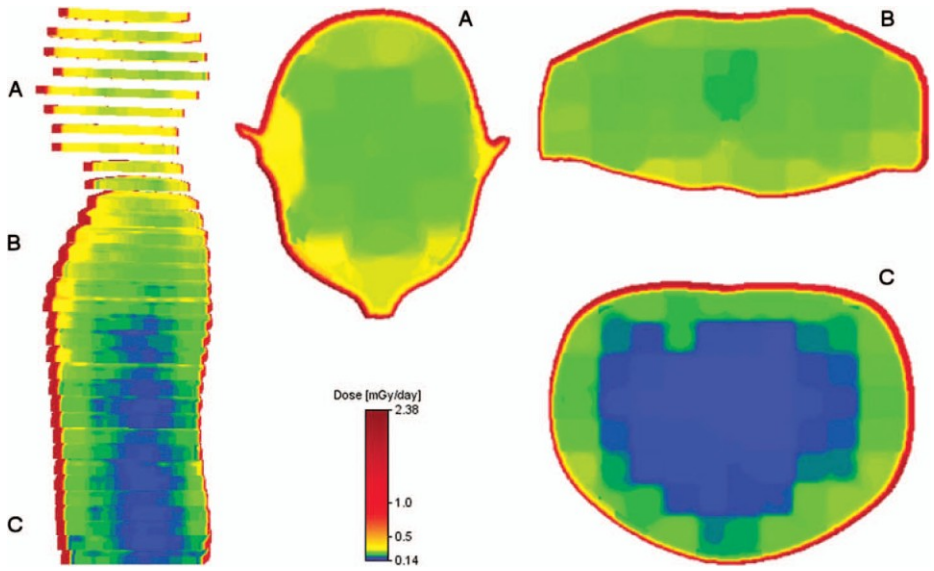

Fig. 5. Dose distributions as the result of the MASTOSHKA experiment. Panel A, B, and C represents the dose distribution for the slices in the head, the shoulder region, and the lower torso, respectively. The skin had the maximum dose and there was no hot spot inside of the phantom in this experiment [19].

Soft tissue and tissue substitute

The reference values for human body tissues are available in the International Commission on Radiation Units and measurements (ICRU) report 46. In this report, the data of elemental compositions and densities for organs, several types of tissues such as muscle, adipose tissue, and cortical bone are available. Data also exist for average values of a group of similar body tissues such as soft tissues. Soft tissues are defined as the body tissues in a human subject other than osseous tissue, teeth, hair, and nails, and include all the body fluid, muscle-like tissues, and fatty tissues [20].

The data for adipose tissue, skeletal muscle, and averaged soft tissues of male adults are given in Table 2. Since the cross sections of related interactions are dependent on the chemical composition and densities of the tissues, the different weight ratios of elemental compositions between adipose tissue and skeletal muscle would result in a large deviation depending on the amount of the adipose tissue composing the soft tissue.

TABLE 2
Elemental compositions and densities of adipose tissue, skeletal muscle, and average soft tissues. (percentage by mass) ICRU-33 tissue and ICRU-44 tissue are based on adult male data [20].

Tissue	H	C	N	O	Others	Density (g/cm^3)
Adipose tissue	11.4	59.8	0.7	27.8	0.1Na, 0.1S, 0.1Cl	0.95
Muscle(skeletal)	10.2	14.3	3.4	71.0	0.1Na, 0.2P, 0.3S,0.1Cl, 0.4K	1.05
ICRU-33 tissue	10.1	11.1	2.6	76.2	-	1.00
ICRU-44 tissue	10.5	25.6	2.7	60.2	0.1Na, 0.2P, 0.3S, 0.2Cl, 0.2K	1.03

The average body tissue composition was required because a single elemental composition is necessary to ease the manufacture of a human phantom. An average muscle-like tissue composition was introduced in ICRU report 33 which is called "ICRU-33 tissue" and has only four components to simplify computational process. An additional average soft tissue composition was suggested in ICRU report 44 which is called "ICRU-44 tissue" [1, 20]. The average data of ICRU-44 tissue was based on the

reassessment of published body tissue compositions given by Woodard and White (1986) and White et al. (1987) [21, 22], and the tissue proportions suggested by the International Commission on Radiological Protection (1975) for reference adults [23].

To be a suitable substitute, the material chosen should have ideally the same interaction properties under a given irradiation as the body tissue. As a soft tissue substitute, water has been conventionally used because of its high content (almost 70%) in the human body. Several materials including Acrylic (PMMA, Polymethyl-methacrylate), Polystyrene, and Nylon-6 have also been used as the tissue substitute for muscle due to their similar elemental compositions. A150 tissue equivalent plastic, a mixture of polyethylene and nylon with carbon and calcium fluoride additives, is a well known tissue substitute. Several investigators also have tried to find more suitable tissue substitute for the muscle by mixing or manipulating several materials. The elemental compositions and description of the materials were well summarized in ICRU report 44 [1].

As mentioned earlier, the HCP can produce adverse dose distributions if the Bragg-peaks were to be misplaced on healthy tissues, and thus a precise substitute for soft tissue in the phantom is essential. Furthermore, for the space study, the trend of the depth-dose distribution would change depending on tissue substitutes used in the phantom, and a hot spot might exist because of the change of characteristic depth-dose trend if a different tissue substitute was used. Therefore, precise tissue substitute study for the charged particle transport is important.

Stopping power and range

The slowing down process of charged particle in matter is expressed by the rate of energy loss in a given material, known as stopping power, S. The stopping power is defined as the differential energy loss for that particle within the material divided by the corresponding differential path length as

$$S = -\frac{dE}{dx} \tag{1}$$

Dividing the stopping power by density of medium to make it independent with the density leads a quantity known as mass stopping power. The mass stopping power is very well described by the Bethe formula and it is written as [24]

$$-\frac{dE}{\rho dx} = \frac{4\pi r_0^2 N_A Z}{A}\frac{m_0 c^2 z^2}{\beta^2}\left[\ln\frac{2m_0 c^2\beta^2}{I(1-\beta^2)} - \beta^2\right] \tag{2}$$

where $m_0c^2 =$ rest mass of an electron,
$r_0 =$ classical electron radius,
$N_A =$ Avogadro constant,
$Z =$ atomic number of medium,
$A =$ mass number of medium,
$z =$ atomic number of charged particle,
$\beta = V/c =$ speed of the particle relative to speed of light (c), and
$I =$ mean excitation energy of the medium.

Eq. (2) can be simplified with several known constants as [24]

$$-\frac{dE}{\rho dx} = 0.3071 \frac{Z}{A\beta^2} z^2 \left[13.8373 + \ln\left(\frac{\beta^2}{1-\beta^2} \right) - \beta^2 - \ln I \right] \tag{3}$$

As shown in the Eq. (3), the inverse β^2 term outside of the bracket strongly illustrates how the stopping power rapidly increases as particle velocity is decreased. And the factor z^2 shows that the stopping power increases with square of particle's charge. For the compound or mixture materials as the medium, the Bragg additive rule can be used to estimate the Z/A in the Eq. (3) as [25]

$$\frac{Z}{A} = \sum w_j \frac{Z_j}{A_j} \tag{4}$$

where w_j is the fraction by weight and index j refers to the jth constituent. For example, for the water, the calculation for Z/A can be done as

$$\begin{aligned} \left(\frac{Z}{A} \right)_{water} &= w_H \frac{Z_H}{A_H} + w_O \frac{Z_O}{A_O} \\ &= 0.112 + 0.888 \cdot \frac{1}{2} \\ &= 0.556 \end{aligned}$$

The range of a charged particle is defined as the distance it travels before coming to rest. The integral of inverse mass stopping power from kinetic energy T of the particle to zero gives this quantity as [24]

$$R(T) = \int_0^T \left(-\frac{dE}{\rho dx} \right)^{-1} dE \tag{5}$$

In the slowing down process of HCPs in the medium, the tracks tend to be quite straight because the particle is not greatly deflected by any single electron interaction and the interactions take place in all directions simultaneously with the same possibility when the medium is uniform. Charged particles are therefore characterized by a definite range in a given material [10]. In this context, when the property of a charged particle is fixed in the transport and the material is varied, the range can be used as a quantity for comparison when the range straggling is negligible.

Stopping power tables and codes

The study of the stopping power of charged particles has been done by several investigators and institutes. The ICRU published a table for the stopping of protons and alpha particles in report 49 and that of ions heavier than helium in report 73 [25, 26]. Based on the table in ICRU report 49, PSTAR and ASTAR, which are computer codes capable of computing the stopping power of protons and helium ions with energies

between 1 keV and 10 GeV in 74 materials, were developed because of the increasing demand for computer-readable databases that can quickly generate reference values [27].

Likewise, SRIM (The Stopping and Range of Ions in Matter) and MSTAR are also available for estimating the stopping power and range. SRIM is a software package capable of calculating the stopping and range of ions up to 2 GeV in materials using a quantum mechanical treatment of ion-atom collisions [28]. MSTAR is a program that calculates electronic stopping powers for heavy ions $(3 \le Z \le 18)$ and it is based on a fit of ratios between massive experimental stopping data base and the alpha stopping table of ICRU report 49 [25, 29]. The accuracy for the tables of ICRU reports, SRIM, and MSTAR has been investigated using actual experimental data in the several papers [28, 30, 31].

History of computational phantom

The computational phantom, designed to represent human anatomy, started with a simple geometry of cylinders and spheres of homogeneous composition. The first heterogeneous model was introduced by Fisher and Snyder of Oak Ridge National Laboratory (ORNL) for Medical Internal Radiation Dose (MIRD) in the 1970s using the anatomical data of the "Reference Man" publication of the International Commission on Radiological Protection (ICRP). Reference Man is defined as a Western European or North American adult male of 170cm in height, weighing 70 kg, and 20 to 30 years of age. The organs and body of the MIRD model were modeled using simple geometry

such as planes, elliptical cylinders, and ellipsoid and well defined by corresponding mathematical equations [6, 23].

The computational phantom has gone through continuous revisions since its initial development. Based on the early MIRD model which was an adult hermaphrodite model with gender-specific organs, ORNL had developed not only a series of age-specific models but also pregnant female models at different stages of pregnancy [32]. And GSF (National Research Center for Environment and Health, Germany) developed gender-specific adult models, known as ADAM and EVA, based on the original MIRD model [33].

The University of Florida (UF), under the direction of Wesley Bolch and in conjunction with Keith Eckerman, recently updated the ORNL phantom model to include detailed representation of the tissues of the head and more organs of interest [34]. The early model had only three material compositions: lung, bone, and soft tissue, but recently revised phantom by UF (ORNL-UF phantom) has 23 different tissue compositions using the updated data of ICRP Publication 89 (Basic Anatomical and Physiological Data for Use in Radiological Protection: Reference Values) [35].

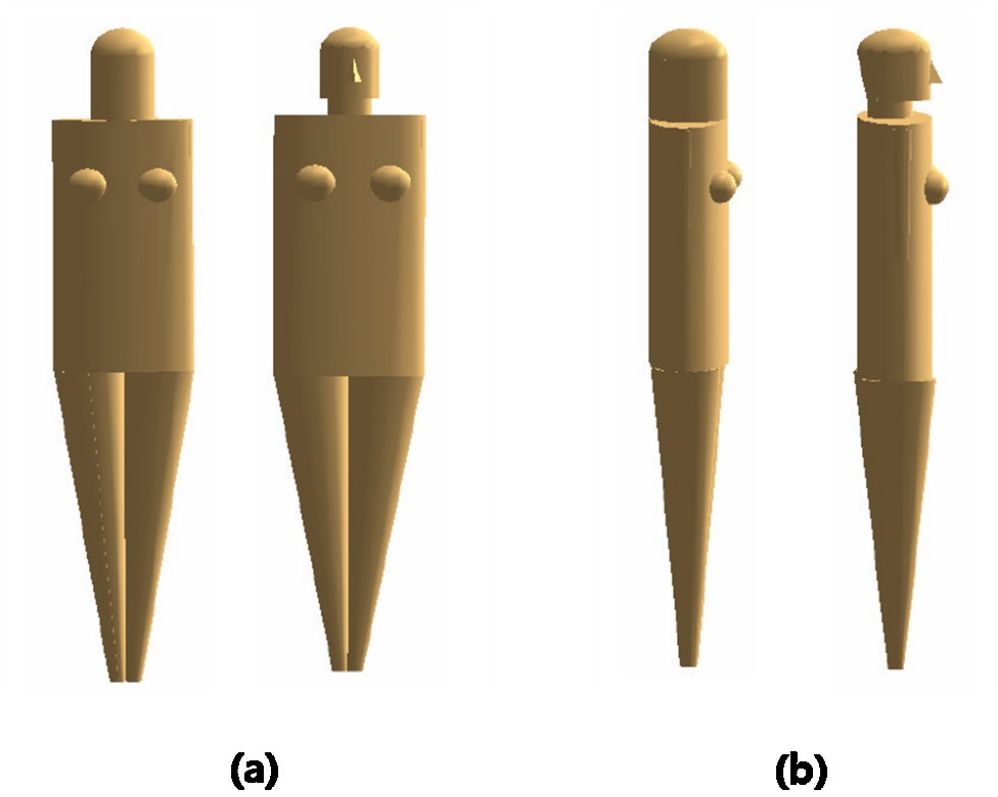

Fig. 6. The exterior shapes of the MIRD-5 (left) and ORNL-UF (right) phantom models [(a) is the front view and (b) is the side view.] [36].

As the MIRD model has been a standard for computational dose assessment for internal and external exposures to radiation, many organizations including the Nuclear Regulatory Commission (NRC) have used it. The phantom model currently used by the NRC is the MIRD-5 phantom, published in 1974, and this model was developed in Monte Carlo N-Particle (MCNP) code [36].

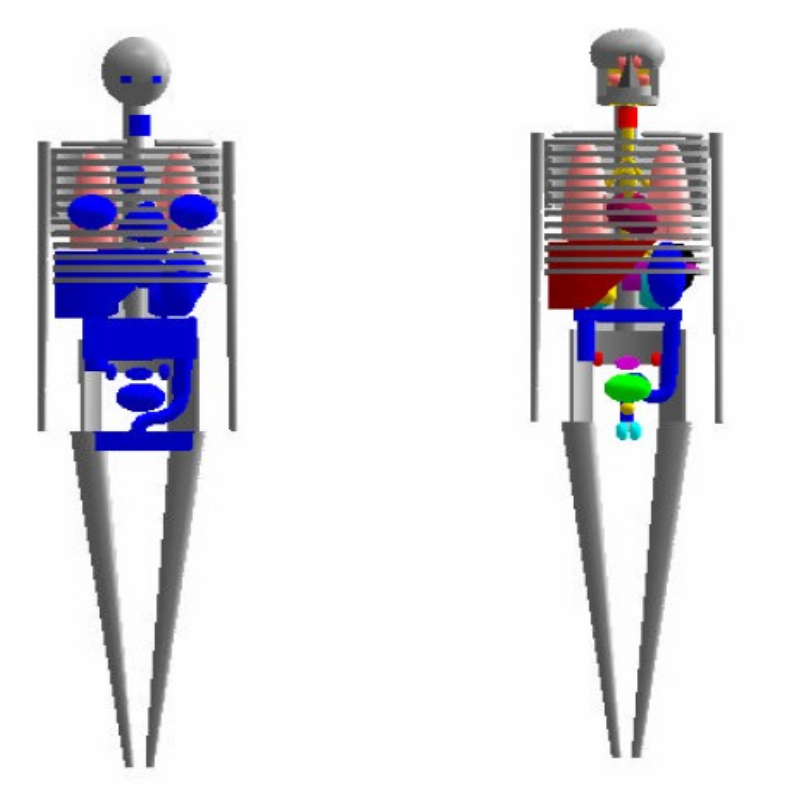

Fig. 7. The interior shapes of the MIRD-5 (left) and the ORNL-UF phantom models (right) [36].

Absorbed dose (D) and dose equivalent (H) [10, 37]

The energy absorbed from any type of radiation per unit mass of the absorber is defined as the absorbed dose and the SI unit is called the *gray* (Gy)

$$1Gy = 1J/kg \tag{6}$$

The absorbed dose should be a reasonable measure of the radiological effects created by a given radiation exposure in an absorbing material. Even though an equal amount of dose may be delivered from different types of radiation, the biological effect may be different depending on the specific radiation used in the exposure. The different biological effects for different types of radiations giving the same absorbed dose are characterized by the *quality factor,* Q. For heavy charged particles, Q is a function of the local energy deposition rate along the particle track, known as the linear energy transfer (*LET*), and as shown in Table 3. The *LET* is a similar quantity with the stopping power, but while the stopping power focuses on the energy loss of particle, *LET* focuses on energy loss at the microscopic scale, having units of energy per micrometer (keV/μm).

TABLE 3
Quality factors with respect to *LET* of the different radiations in water.

LET in water ($keV/\mu m$)	Q
<10	1
$10-100$	$0.32L-2.2$
>100	$300/\sqrt{L}$

Therefore, the dose equivalent (H) can be defined to quantify the biological effect of the given radiation as the product of the absorbed dose (D) and the quality factor (Q), and SI unit of dose equivalent is the *Sievert* (*Sv*).

$$H = D \cdot Q \tag{7}$$

CHAPTER III

METHODS AND BENCHMARKING

Particle and heavy-ion transport code system (PHITS)

PHITS is a general-purpose three-dimensional Monte Carlo code specially designed for the transport of heavy ions and all varieties of charged particles with energies up to around 100 GeV/nucleon. It was developed and maintained by Research organization for Information Science and Technology (RIST), Japan Atomic Energy Agency (JAEA) and High Energy Accelerator Research Organization (KEK) in Japan together with Sihver et al. at Chalmers University of Technology in Sweden [38].

Benchmarking

ICRU has suggested the primary interaction quantities with respect to several radiation sources, and for the proton mass stopping power is recommended as shown in Table 4 [1, 20]. Thus, this study began by benchmarking PHITS treatment of mass stopping powers against the Bethe formula and the other codes mentioned above.

TABLE 4
Primary interaction quantities suggested by ICRU for the radiation sources. For the proton, the mass stopping power is the primary interaction quantity [1, 20].

Source	Primary interaction quantities
Photons	$\tau/\rho,\ \sigma_{coh}/\rho,\ \sigma_c/\rho,\ \kappa/\rho,\ \mu/\rho,\ \mu_{en}/\rho$
Electrons	$(S/\rho)_{col},\ (S/\rho)_{rad},\ S/\rho,\ \mathrm{T}/\rho$
Protons	S/ρ
Neutrons	$[E(\mu_{tr}/\rho)]$ (kerma factors)

Fig. 8 gives a representation of the geometry used in the PHITS simulations to obtain stopping power. Water was used as the target and proton, ${}^{12}_{6}C$, and ${}^{56}_{26}Fe$ pencil beams with 0.25 cm radii were used as the beam. Proton and carbon beams were used because of their importance in therapy, and iron was used because iron ions deliver about 8% of the total dose from the GCR and 27% of the dose equivalent at times near solar maximum, even though they contribute less than 1% of the total GCR flux [39].

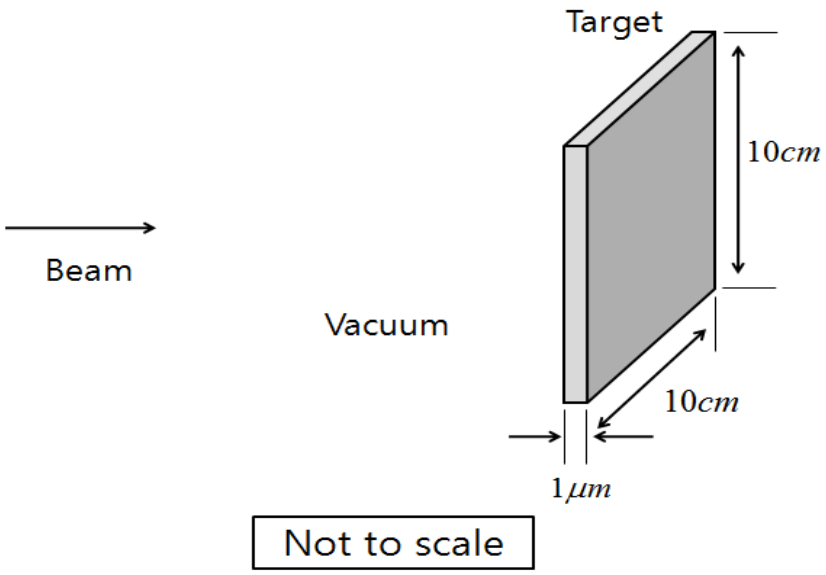

Fig. 8. Geometry used in PHITS simulations to obtain stopping powers. The beam is a pencil beam which is directed at the center of the target.

The stopping power can be thought of as the energy lost by incident particles within the thin target divided by the thickness of target. The simulations were repeated in PHITS varying the energy of beam from 1keV to 10GeV, and total 100,000 particles were used to simulate each case. For the low energies, the target thickness was changed because the range is below the original thickness and the stopping power could be underestimated. Therefore, the thickness when it is in the low energy was $0.2\mu m$ and the results were multiplied by 5 after simulation. By simply diving the acquired stopping powers by the density of target, the mass stopping powers were found. The results were then compared to Bethe formula calculations and the results of several codes to verify the use of PHITS. Figures 9-11 indicate comparisons of the mass stopping powers of the Bethe formula calculations, codes, and PHITS simulations in the water target varying the

beam as proton (Fig. 9), carbon (Fig. 10), and iron (Fig. 11). For the proton, experimental results for a small range of energy between 1.1 MeV and 15.243 MeV were added in the comparison [40]. The limited amount of experimental data is available for liquid water for a small range of energies. In all cases, the mass stopping power calculated using PHITS for beam energies below about 1 MeV is higher than using other methods. For the low energies below about 40-50 keV, the stopping power could not be computed using the Bethe formula calculations because the value inside of the bracket of Eq. (3) became negative.

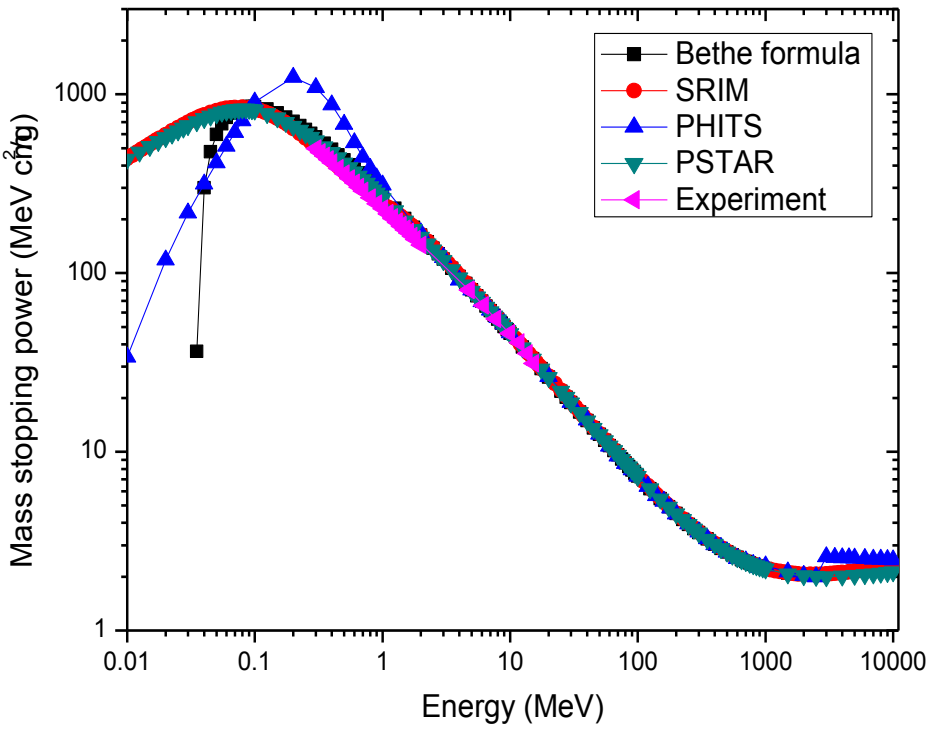

Fig. 9. The comparison of the mass stopping powers of proton beam in the water obtained by Bethe formula calculations, SRIM, PHITS simulations, PSTAR, and experimental results.

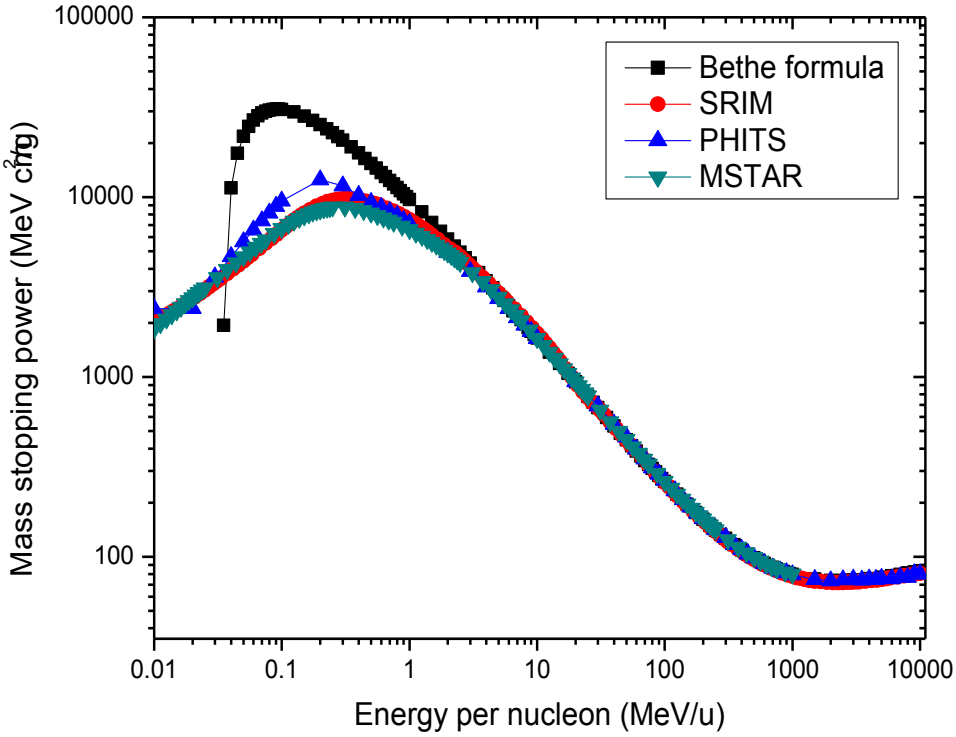

Fig. 10. The comparison of the mass stopping powers of carbon beam in the water obtained by Bethe formula calculations, SRIM, PHITS simulations, and MSTAR.

Since MSTAR program gives the stopping powers only for limited heavy ions which have the atomic number between 3 and 18, only stopping powers of Bethe formula calculations were compared with that of PHITS for the iron beam. Furthermore, MSTAR gives only electronic stopping power, not total stopping power, thus the given stopping power was underestimated by the amount of the nuclear stopping power. Fig. 12 and Fig. 13 show the electronic, nuclear, and total stopping powers of proton and helium in liquid water, respectively. These were given by PSTAR and ASTAR code available in NIST web page [41]. As shown these figures, since the nuclear stopping

power is not significant except when it is in very low energy, it is acceptable to use only electronic stopping power for the comparison.

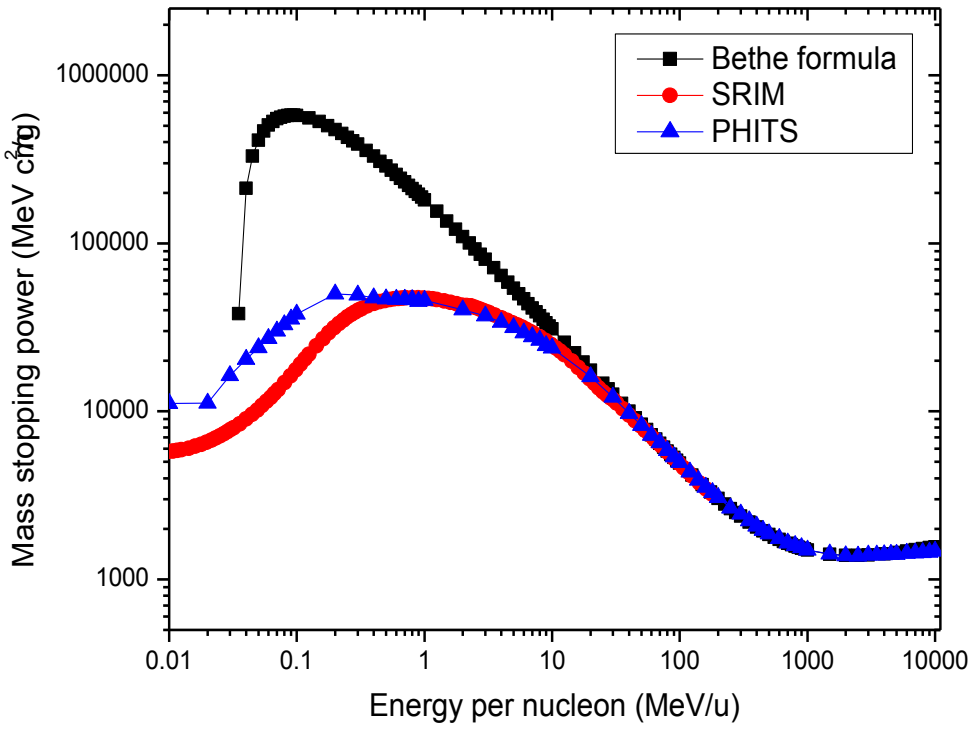

Fig. 11. The comparison of the mass stopping powers of iron beam in the water obtained by Bethe formula calculations, SRIM, and PHITS simulations.

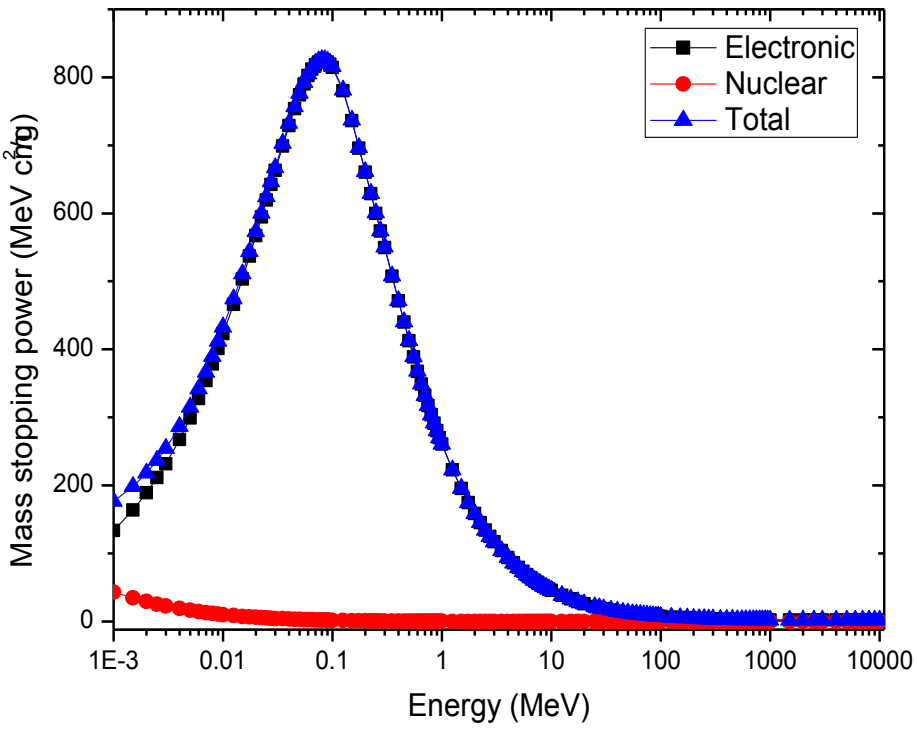

Fig. 12. Electronic, nuclear, and total stopping powers of the proton beam in the medium of liquid water which was given by the PSTAR code [41].

Overall, the stopping powers of PHITS simulations, Bethe formula calculations, and codes are close for each case except when the energy of the particle is below 1 MeV. Therefore, since the general trend of stopping powers for each beam given by PHITS simulations is appropriate, especially in the energy ranges above 1MeV, PHITS can be thought as a good tool to estimate the stopping power. By an assumption that this trend would be same with not only water but also the other materials, PHITS was then used to study compounds and study whether current tissue substitutes remain valid for use under heavy ion irradiations.

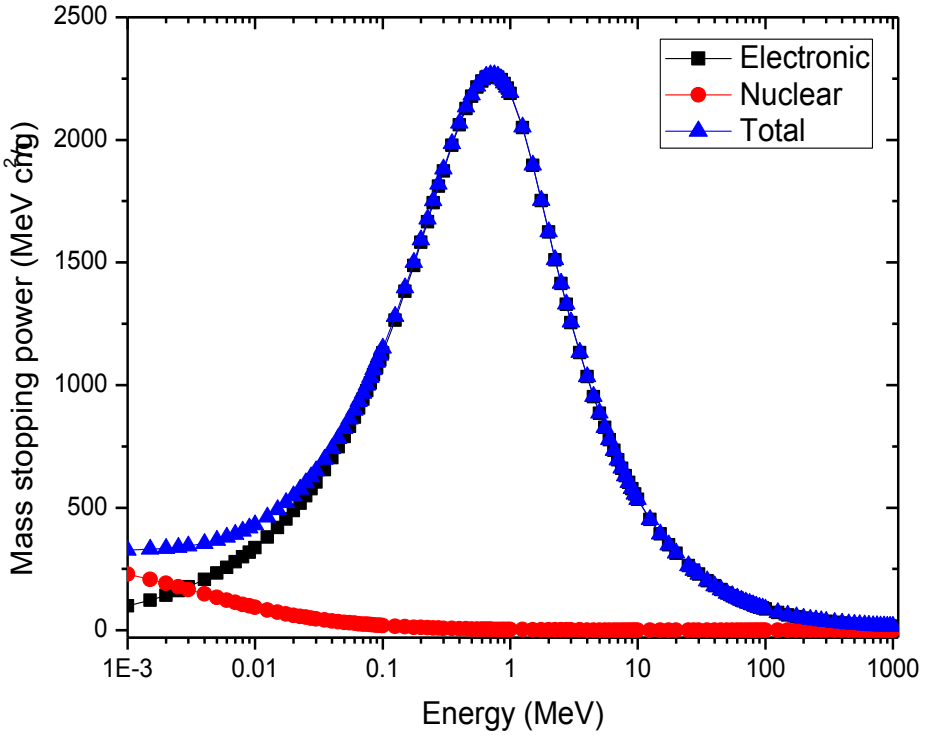

Fig. 13. Electronic, nuclear, and total stopping powers of the helium beam in the medium of liquid water which was given by the ASTAR code [41].

Reference data for soft tissue

As shown in Table 2, the muscle tissue and adipose tissue exhibit the difference in their material composition ratios. Because of the difference, the simulation results could be affected by the extent of how much muscle or adipose tissue is in the phantom. ICRU-44 tissue was used as the reference value for the soft tissue because normally a

single material had been used in manufacturing a phantom and thus the averaged data would be appropriate to use.

Soft tissue substitutes

The soft tissue substitutes and their elemental compositions considered in this study are listed in Table 5. ED1S and ED4C are crosslinked copolymers which consist of a combination of MMA (methyl methacrylate) and VP (vinylpyrolidone) with different ratios presented in Table 6. These were developed by S. Bauk *et al*. for breast phantom materials because they had the potential to be made to have similar elemental composition to that of soft tissue by hydration. Since the ratio of constituents would be changed when it was fully hydrated in water, the exact elemental composition was calculated using the data of equilibrium water content (EWC) [42]. Therefore, ED1S and ED4C, that was fully hydrated in water, will be represented as ED1S (fhw) and ED4C (fhw) to distinguish from the copolymers prior to the hydration. The other information about soft tissue substitutes in Table 5 were referred from ICRU report 44 and NIST website [1, 43].

TABLE 5
Elemental compositions and densities of the materials of concern [1, 42, 43].

Material	Elemental composition (percent by mass)					Density (g/cm^3)
	H	C	N	O	Others	
A150	10.1	77.7	3.5	5.2	1.7F, 1.8Ca	1.12
Acrylic (PMMA)	8.0	60.0	-	32.0	-	1.17
Alderson muscle (A)	8.9	66.8	3.1	21.1	0.1Sb	1.00
Alderson muscle (B)	8.8	64.4	4.1	20.4	2.2Cl, 0.1Sb	1.00
Amber	10.59	78.9	-	10.51	-	1.10
Ceric Sulfate Dosimeter Solution	10.76	-	0.08	87.5	1.46S, 0.20Ce	1.03
ED1S (fhw)	9.82	28.67	4.36	57.14	-	1.01
ED4C (fhw)	10.31	18.54	2.98	68.16	-	1.01
Ethyl Cellulose	9.00	58.52	-	32.48	-	1.13
Ferrous Sulfate Dosimeter Solution	10.83	-	0.002 7	87.86	0.0022Na, 1.30S, 0.0034Cl, 0.0054Fe	1.02
Frigerio gel	10.0	12.0	4.0	73.3	0.4Na, 0.2S, 0.1Cl	1.12
Frigerio liquid	10.2	12.3	3.5	72.9	0.1Na, 0.02Mg, 0.2P, 0.3S, 0.1Cl, 0.4K, 0.01Ca	1.08
Goodman liquid	10.2	12.0	3.6	74.2	-	1.07
Griffith muscle	9.0	60.2	2.8	26.6	1.4Ca, 0.01Sn	1.12
Lincolnshire bolus	5.9	37.9	-	52.7	3.5Mg	1.05
Mylar/Melinex	4.2	62.5	-	33.3	-	1.40
Nylon-6	9.8	63.7	12.4	14.1	-	1.13
Nylon, Du Pont Elvamide 8062	10.35	64.84	9.95	14.85	-	1.08
Polyethylene	14.4	85.6	-	-	-	0.92
PEG-200	9.34	49.47	-	41.19	-	1.12
Polystyrene	7.7	92.3	-	-	-	1.05
Polyvinyl Butyral	9.28	68.06	-	22.66	-	1.12
Rice powder	6.2	44.4	-	49.4	-	0.84
RM-1	12.2	73.4	-	6.4	6.0Mg, 2.0Ca	1.03
RM/G1	10.2	9.4	2.4	77.4	0.1Na, 0.03P, 0.1S, 0.2Cl, 0.2K	1.07
RM/L3	10.2	12.8	2.2	74.1	0.1Na, 0.03P, 0.2S, 0.2Cl, 0.2K	1.04
RM/SR4	10.1	73.6	2.2	13.7	0.01Na, 0.003Mg, 0.03P, 0.1S, 0.1Cl, 0.2K	1.03

TABLE 5
(*continued*)

Material	Elemental composition (percent by mass)					Density (g/cm^3)
	H	C	N	O	Others	
Rossi gel	9.8	15.7	3.6	70.9	-	1.10
Rossi liquid	9.8	15.6	3.6	71.0	-	1.11
RW-2	7.0	83.0	-	4.0	6.0Ti	1.11
Temex	9.6	87.5	0.1	0.5	1.5S, 0.3Ti, 0.5Zn	1.01
TH/L2	10.0	13.6	2.2	73.5	0.2Na, 0.1P, 0.1Cl, 0.2K, 0.06I	1.08
Water	11.2	-	-	88.8	-	1.00

TABLE 6
The material compositions of ED1S and ED4C [42].

	MMA	VP
ED1S	1	3
ED4C	1	4

Stopping power and depth-dose comparisons

The mass stopping powers of each tissue substitute were obtained at specific beam energies in PHITS simulations and compared to ICRU tissue to find the most suitable soft tissue substitutes. The simulation geometry was same as that of Fig. 8 using a total of 48 beam energies between 1MeV and 10GeV. For the comparison, the normalized difference was calculated to compare the similarity of mass stopping powers with ICRU-44 tissue as

$$\delta = \frac{\left|(S/\rho)_{Tissue\ substitute} - (S/\rho)_{ICRU-44}\right|}{(S/\rho)_{ICRU-44}} \times 100 \quad (8)$$

After calculating the normalized difference at every beam energy, the mean normalized difference $\Delta = \langle \delta \rangle$ and standard deviation $\sigma = \sqrt{\langle \delta^2 \rangle - \langle \delta \rangle^2}$ was determined. In this case, a small Δ means good agreement between ICRU-44 tissue and the tissue substitute and σ is related to the mean difference accuracy. The relative ratios of mass stopping powers between ICRU-44 tissue and the soft tissue substitutes were then compared to observe the trend of mass stopping powers of a soft tissue substitute at each energy point.

Fig. 14 represents the geometry used for simulations of dose as a function of depth in the ICRU-44 tissue and soft tissue substitutes. The simulations were done with 100 MeV proton, 200 MeV/u carbon, and 400MeV/u iron pencil beams also having a radius of 0.25 cm. The energies of the beams were chosen to be appropriate for therapy use, having the projected ranges by SRIM calculations of 7.603 cm for the proton beam, 8. 756 cm for the carbon beam, and 6.938 cm for the iron beam.

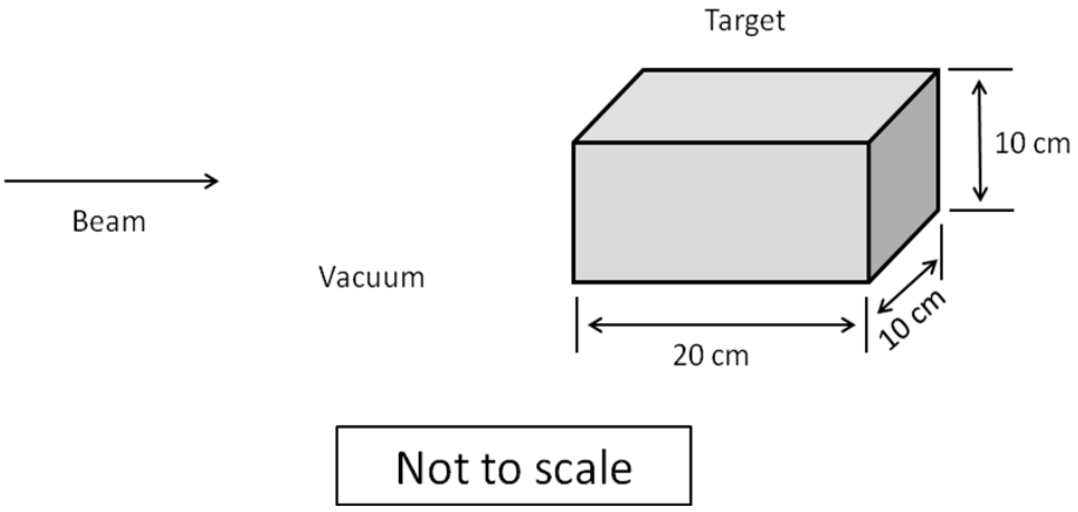

Fig. 14. Geometry used for simulations of range for body tissues and tissue substitutes.

The depth-dose distributions acquired by PHITS simulations were modified to make them independent of the densities. These modifications could be done by multiplying each energy point of simulation data by material density. This manipulation was done because the goal of the simulation was to see the interaction properties only rather than the density effect.

However, in the manufacture point of view of a real human phantom, ignoring the material density can be an issue. The dimension of the phantom should be corrected by the simple equation shown in Eq. (9) to get the same mass and thus the same interaction probability.

$$\rho_A dx_A = \rho_B dx_B \tag{9}$$

where ρ_A is the density of material A; dx_A is x dimension of material A; ρ_B is the density of material B; and dx_B is x dimension of material B.

The correction is easy for simple geometries such as a rectangular solid (box) or a cylinder; however, it is not easy for the anthropomorphic human phantom, because the phantom has several boundaries, complicate shapes, and irregular dimensions as shown in RANDO phantom. Because of that, it is common to use a fixed dimension of the phantom without the correction; therefore, this can be a considerable error source.

If a material has similar interaction properties and density as the human soft tissue, the material is the best tissue substitute. On the other hand, even though the material has fairly different interaction properties (e.g. mass stopping power) and the density, but if the material has similar result (e.g. stopping power) by compensating the differences each other when the both are taken into account, the material can be also treated as a suitable tissue substitute. Therefore, this study is including the both cases: the interaction property only that is independent of the density and the interaction property combined with density.

Application to the developed anthropomorphic phantom

After the suitable soft tissue substitutes were achieved, they were put into the developed phantom and observed if they would still valid in the condition of multiple regions and boundaries. Two types of beam describing the radiotherapy and the Galactic environments were irradiated into the phantom, pencil beam with 0.25cm radius and broad (rectangle) beam, and the same energies as the depth-dose simulations for the beams were used.

CHAPTER IV

PHANTOM DEVELOPMENT

In this work, a heterogeneous phantom was developed based on the information of ICRP publication 89 [35]. Except for a voxel (volume pixel) phantom in which each organ or tissue is represented by small volume elements (voxels) identified from the CT images, since most of computational phantoms were developed based on the early MIRD model, basic geometrical concepts of organs and body structure have not changed. New simple geometrical concepts and better characterization of features of the human anatomy were therefore considered here.

An adult male 176 cm in height was constructed in PHITS as discussed below. Three organs, brain, lung, and heart, have been included to observe the dose differences on each organ when the surrounding soft tissue substitute is changed.

Heart

The heart model developed by Coffey has been employed for the most of computational phantoms including MIRD model. The outer surface of the heart is represented by four quarter-ellipsoids. Within this space, the heart is divided into regions representing the muscular walls and the four chambers [44]. However, in this work, a simplified geometry of a sphere was developed for the heart of new computational model

Since the heart is located inside of lung, another sphere with larger radius than the heart radius was considered to give some space between the heart and the lung. For the heart, therefore total three regions, one for outside space between the heart and lungs one for heart tissue itself, and the other representing the blood inside of heart, were considered as shown in Fig. 15 and the three regions were represented by spheres with different radii.

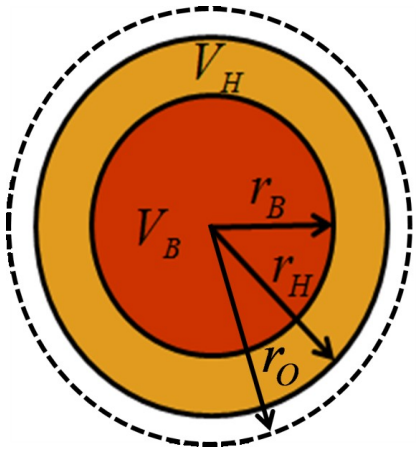

Fig. 15. Development of the heart geometry. (V_B is the volume of blood, V_H is the volume of heart tissue, r_B is the radius of the sphere for blood, r_H is the radius of the sphere for the heart, and r_O is the radius of the outside sphere.)

The radii of three spheres was found by calculation using the information about density in ICRU Report 46 and mass in ICRP Publication 89 [20, 35]. The reference value for the heart including blood is 840g and heart tissue only is 330g. Therefore, the blood mass occupied inside of the heart is 510g by simply subtracting heart tissue only

mass from the heart including blood mass. Table 7 summarizes the information for heart tissue only and the blood occupied inside the heart.

TABLE 7
Information for calculating the radii of spheres that consist of the heart [20, 35].

	Mass (g)	Density (g/cm^3)
Heart including blood	840	-
Heart tissue only	330	1.05
Blood inside of the heart	510	1.06

Since the blood inside the heart has 510g of mass and specific gravity of 1.06, the volume and the corresponding radius can be calculated as

$$V_B = 510 \text{ g} \times \frac{1 \text{ ml}}{1.06 \text{ g}} = 481.132 \text{ ml}$$

$$\frac{4}{3}\pi r_B^{\,3} = 481.132 \text{ cm}^3$$

$$\therefore \; r_B = \sqrt[3]{\frac{3}{4\pi}(481.132 \text{ cm}^3)}$$

$$= 4.861 \text{ cm}$$

And the further calculation can be made for the heart with the information of 330g of heart tissue mass and specific gravity of 1.05 as

$$V_H = 330 \text{ g} \times \frac{1 \text{ ml}}{1.05 \text{ g}} = 314.286 \text{ ml}$$

$$\frac{4}{3}\pi {r_H}^3 - \frac{4}{3}\pi {r_B}^3 = 314.286 \text{ cm}^3$$

$$\frac{4}{3}\pi {r_H}^3 = 481.132 \text{ cm}^3 + 314.286 \text{ cm}^3 = 795.418 \text{ cm}^3$$

$$\therefore \ r_H = \sqrt[3]{\frac{3}{4\pi}(795.418 \text{ cm}^3)}$$

$$= 5.748 \text{ cm}$$

The radius of outer space of heart is assumed as 5.8cm, and thus corresponding statements that must be satisfied are

$$(x-x_0)^2 + (y-y_0)^2 + (z-z_0)^2 \le {r_B}^2 \quad \text{for the blood,} \tag{10}$$

$${r_B}^2 \le (x-x_0)^2 + (y-y_0)^2 + (z-z_0)^2 \le {r_H}^2 \quad \text{for the heart tissue, and} \tag{11}$$

$${r_H}^2 \le (x-x_0)^2 + (y-y_0)^2 + (z-z_0)^2 \le {r_O}^2 \quad \text{for the outer space of the heart.} \tag{12}$$

where x_0, y_0, and z_0 are -2, 1.5, and 28.5, respectively for all the spheres, and radii of each spheres are summarized in Table 8.

TABLE 8
Radii of the spheres that represent the blood, the heart, and the space between the heart and lungs.

Region	Radius (cm)
Blood inside of heart (r_B)	4.861
Heart (r_H)	5.748
Space for outside of heart (r_O)	5.8

Lungs

For the right lung geometry, an ellipsoid was used and was cut by a horizontal plane and a vertical plane as shown in Fig. 16. By changing only the cutting direction of the vertical plane, the left lung also could be achieved.

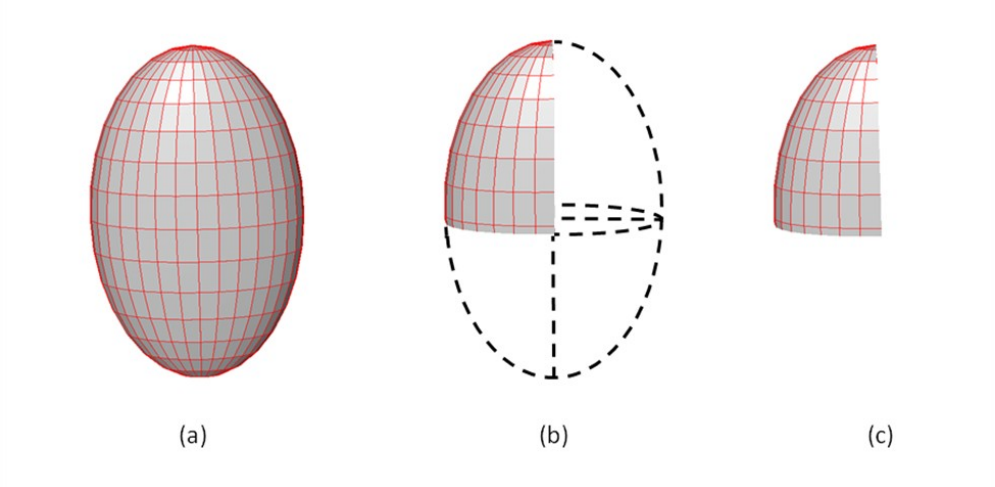

Fig. 16. Development of the lung geometry [(a) An ellipsoid was prepared, (b) The ellipsoid was cut by horizontal and vertical planes, (c) The right lung geometry was prepared.].

Since the heart is located inside of lungs (biased to the left), some volume was excluded from the original lung geometry as shown in Fig 17. The dotted sphere represents the outer void that will accommodate the heart. The real heart will be located inside of the void with small dimension compared to the space.

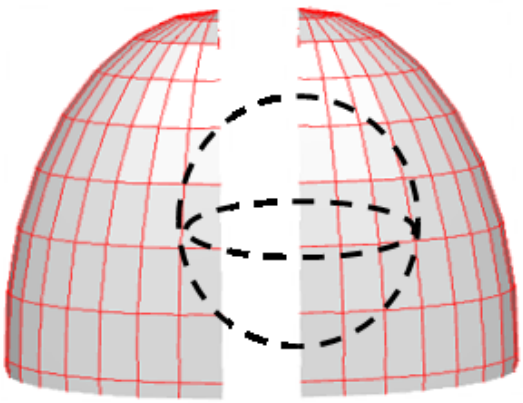

Fig. 17. The geometrical concept to exclude a space for the heart.

For the lung mass, there is considerable variability in reported values depending on investigators because of the difference in the amount of blood drained from the lungs at autopsy and accumulated fluid in the lungs after death that may cause an overestimate in lung mass in some studies [35]. French investigators recently published autopsy data on Caucasoid adults who died from external causes and showed no pathological changes [45]. All autopsies were conducted within 48 h of death, the masses were obtained before the lungs were opened and the techniques used in these studies are such that the lung masses are presumed to include blood as well as lung tissue. This data of lung mass for 355 males was chosen to represent lung geometry and the specific data of lung mass is shown in Table 9.

TABLE 9
The masses of the lungs used to represent the lungs geometry.

Lung	Mass (g)
Left lung	583 ± 216 g.
Right lung	663 ± 239 g
Total lung	1246 ± 322 g

In this work, the mean masses of lungs were used, and since density of adult lungs containing air is 0.26 g/cm^3 as listed in ICRU report 46, the corresponding volumes were shown in Table 10.

TABLE 10
Mean masses and corresponding volumes of each lung.

Parameter	Left lung	Right lung
Mass (g)	583	663
Volume (cm^3)	2242.3	2550

However, as mentioned before, the additional volume which would be subtracted for the space of the heart was considered in preparing the lung geometry. The final lung geometry excludes the space for the heart from the geometry and the volumes were

calculated by integrating the overlapping portion between the lungs and the space for heart as shown in Fig 18.

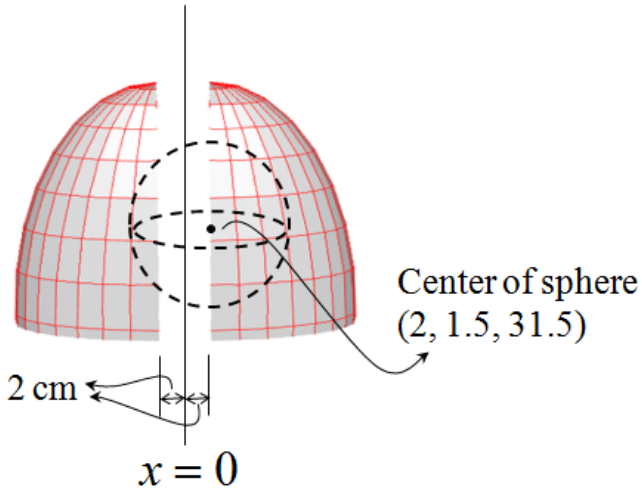

Fig. 18. Dimensions for calculating the subtracting volumes.

For the left lung, the subtracting volume is the half of the sphere such as

$$V_{l,s} = \frac{1}{2} V_s = \frac{2}{3} \pi \cdot R^3 \tag{13}$$

where $V_{l,s}$ is the subtracting volume in the left lung, V_s is volume of the sphere, and R is the radius of the sphere (5.8cm).

For the right lung, the subtracting volume can be achieved by integrating of the overlapped volume such as

$$V_{r,s} = \frac{1}{2}V_s - \pi\int_0^4 (R^2 - r^2)dr \tag{14}$$

where $V_{r,s}$ is the subtracting volume in the right lung, and r is a variable as shown in Fig. 19.

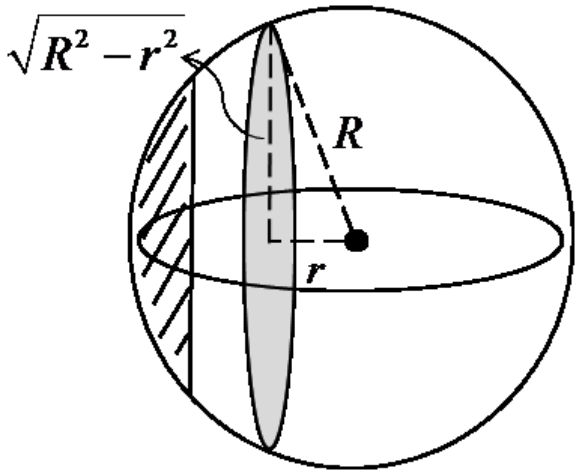

Fig. 19. Integration to calculate the subtracting volume of right lung.

Therefore, the subtracting volume and the total volume (original volume + subtracting volume) are shown in the Table 11. Lung geometry was first made using the total volume for determining the basic shapes of lungs. After subtracting the space of heart from the geometry, the desired geometry of lungs was completed acquiring the original volume.

TABLE 11
Original volume, subtracting volume, and total volume for each lung.

Lung	Original volume	Subtracting volume	Total volume
Left lung	2242.3	408.64	2650.94
Right lung	2550	52.93	2602.93

Since the volume of the lung geometry is one fourth of an ellipsoid's volume as shown in Fig. 16-(c), the total volumes of lungs in Table 11 can be written as

$$V = \frac{1}{4} V_e = \frac{1}{3} \pi abc \tag{15}$$

where V is the total volume of left or right lung, V_e is the volume of the ellipsoid, a is the minor axis with x-direction of the ellipsoid, b is the minor axis with y-direction of the ellipsoid, and c is the major axis with z-direction of the ellipsoid. When the values of a and b are fixed to 15cm and 7cm respectively, the major axis (c) can be calculated using Eq. (15). Thus, the statements that must be satisfied, with corresponding values in Table 11, are below.

For the left lung,

$$\begin{aligned} &\frac{(x-x_0)^2}{15^2}+\frac{(y-1)^2}{7^2}+\frac{(z-z_0)^2}{c^2}\le 1, \\ &x\le -2, \\ &z\ge z_0, \\ &\textit{and}\ \ (x+2)^2+(y-1.5)^2+(z-28.5)^2\ge {r_O}^2. \end{aligned} \tag{16}$$

For the right lung,

$$\begin{aligned} &\frac{(x-x_0)^2}{15^2}+\frac{(y-1)^2}{7^2}+\frac{(z-z_0)^2}{c^2}\le 1, \\ &x\ge 2, \\ &z\ge z_0, \\ &\textit{and}\ \ (x+2)^2+(y-1.5)^2+(z-28.5)^2\ge {r_O}^2. \end{aligned} \tag{17}$$

where r_O is the radius of sphere for the outer region of heart, and variables used in Eq. (16) and (17) are summarized in Table 12.

TABLE 12
Values used to define each lung in Eq. (16) and Eq. (17).

Lung	x_0	z_0	c
Left lung	2	21.79085	24.10915
Right lung	-2	22.22748	23.67252

Fig. 20 shows a cross sectional view for the geometry of heart and lungs prepared in PHITS code.

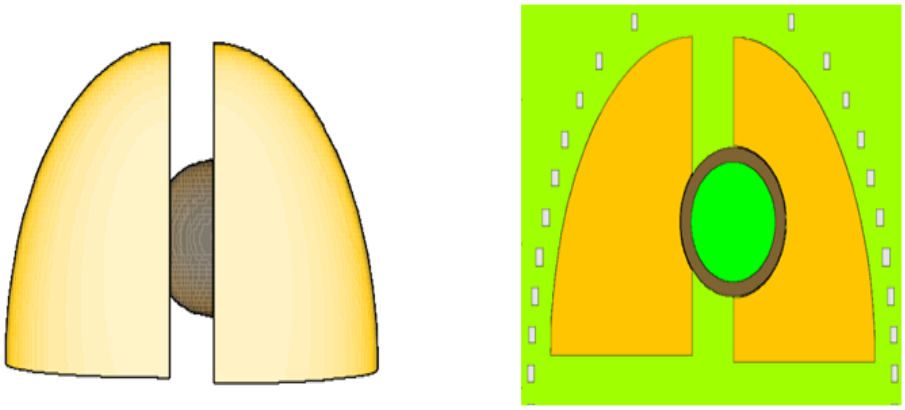

Fig. 20. 3D view and cross sectional view of the heart and the lungs prepared in PHITS.

Spine

The spine is divided into 3 portions: vertebrae lumbales, thoracic vertebrae and cervical vertebrae. They were represented simply by a cylinder and several horizontal dividing planes. For any single vertebra, two horizontal planes were used to cut the upper boundary and lower boundary of the common cylinder used for all. In this work, the same dimension was used for the thoracic vertebrae and lumbal vertebrae, but the cervical vertebrae had smaller heights than the others as shown in Fig. 21.

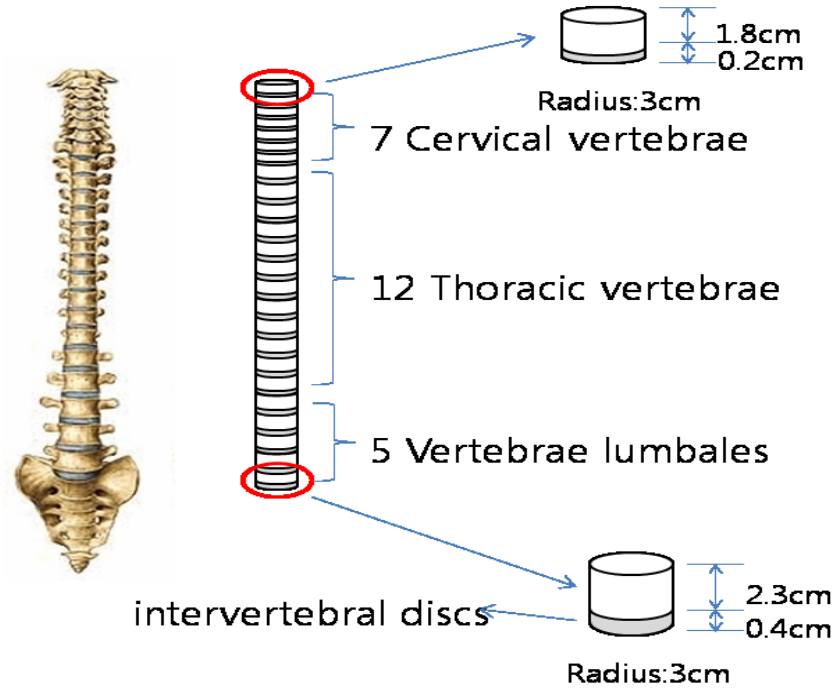

Fig. 21. Geometrical concept and specific dimensions of the spine. Each vertebra will be represented with a cylinder and two horizontal planes with different dimensions depending on the kind of the vertebra.

Fig. 22 shows the cross sectional view of the body prepared by the PHITS. Since beam was set to pass through from +y to –y and the center of the trunk is located at the origin, the spine should be located at -7.8 cm away from the origin.

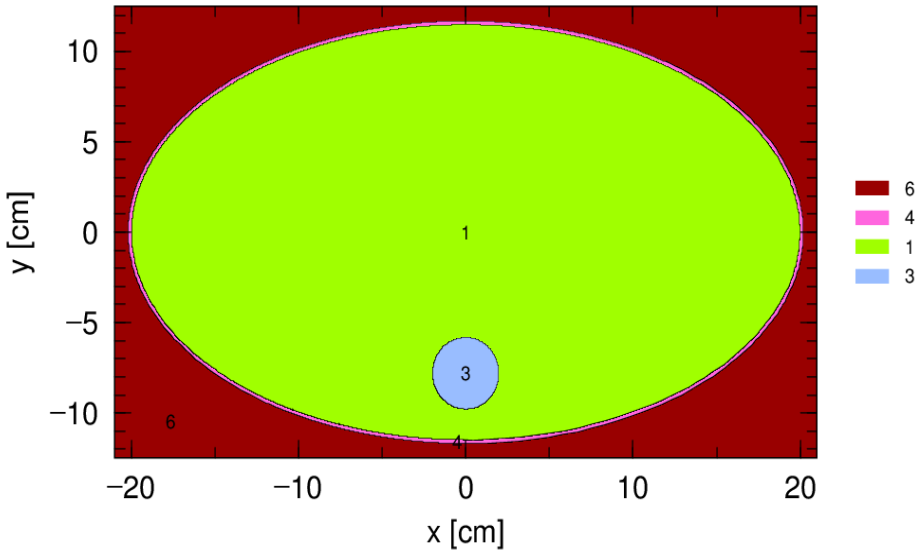

Fig. 22. Cross sectional view of the phantom prepared in PHITS. (material 1 : Soft tissue of trunk, material 3 : spine, material 4 : skin, material 6 : Air)

The final statements for the spine and the corresponding values are given by

$$x^2 + (y + 7.8)^2 \le 2^2 \tag{18}$$

and $z_1 \le z \le z_2$.

TABLE 13
Values used to define the height of the vertebrae and the intervertebral discs consisting of the spine.

Region	z_1	z_2
Cervical vertebra 1	58.1	59.9
Intervertebral disc 1	57.9	58.1
Cervical vertebra 2	56.1	57.9
Intervertebral disc 2	55.9	56.1
Cervical vertebra 3	54.1	55.9
Intervertebral disc 3	53.9	54.1
Cervical vertebra 4	52.1	53.9
Intervertebral disc 4	51.9	52.1
Cervical vertebra 5	50.1	51.9
Intervertebral disc 5	49.9	50.1
Cervical vertebra 6	48.1	49.9
Intervertebral disc 6	47.9	48.1
Cervical vertebra 7	46.1	47.9
Intervertebral disc 7	45.9	46.1
Thoracic vertebra 1	43.6	45.9
Intervertebral disc 8	43.2	43.6
Thoracic vertebra 2	40.9	43.2
Intervertebral disc 9	40.5	40.9
Thoracic vertebra 3	38.2	40.5
Intervertebral disc 1	37.8	38.2
Thoracic vertebra 4	35.5	37.8
Intervertebral disc 10	35.1	35.5
Thoracic vertebra 5	32.8	35.1
Intervertebral disc 11	32.4	32.8
Thoracic vertebra 6	30.1	32.4

TABLE 13
(*continued*)

Region	z_1	z_2
Intervertebral disc 12	29.7	30.1
Thoracic vertebra 7	27.4	29.7
Intervertebral disc 13	27.0	27.4
Thoracic vertebra 8	24.7	27.0
Intervertebral disc 14	24.3	24.7
Thoracic vertebra 9	22.0	24.3
Intervertebral disc 15	21.6	22.0
Thoracic vertebra 10	19.3	21.6
Intervertebral disc 16	18.9	19.3
Thoracic vertebra 11	16.6	18.9
Intervertebral disc 17	16.2	16.6
Thoracic vertebra 12	13.9	16.2
Intervertebral disc 18	13.5	13.9
Lumbal vertebra 1	11.2	13.5
Intervertebral disc 19	10.8	11.2
Lumbal vertebra 2	8.5	10.8
Intervertebral disc 20	8.1	8.5
Lumbal vertebra 3	5.8	8.1
Intervertebral disc 21	5.4	5.8
Lumbal vertebra 4	3.1	5.4
Intervertebral disc 22	2.7	3.1
Lumbal vertebra 5	0.4	2.7
Intervertebral disc 23	0	0.4

In the MIRD computational phantom, the spine is divided into only 3 portions: upper, middle, and lower sections to estimate dose or absorbed fractions separately for each rough portion [32]. In this work, since the spine was divided into each region of vertebrae, comparison of important information such as dose can be done between each vertebra. Moreover, since the intervertebral discs were introduced here, which also have different material properties than the vertebrae, more applications can be made.

Rib cage

The rib cage surrounds the lungs and the heart which are the most important organs for this study related to absorbed dose. Therefore, the geometry of the rib cage can be thought of the most important part since it may give rise to differences in absorbed dose depending on the geometry, boundary conditions, and material properties such as the density and the elemental composition. Each rib was made using two concentric, right-vertical, elliptical cylinders and two horizontal planes. Because of the limited availability of information found for the rib anatomy, the rib cage in the MIRD model used arbitrary values and identical geometry for all of the ribs. In this work, actual data of human rib anatomy was used to develop more appropriate rib geometry.

As shown in Fig. 23, a cross section of a human rib is too complicated to be represented exactly. The bounding box shown in the right figure was considered to adequately represent the human rib and therefore the averaged height (h) and width (w)

of the box was used. Table 14 shows the geometric parameters of rib cross-sections along human cadaveric ribs three through nine [46].

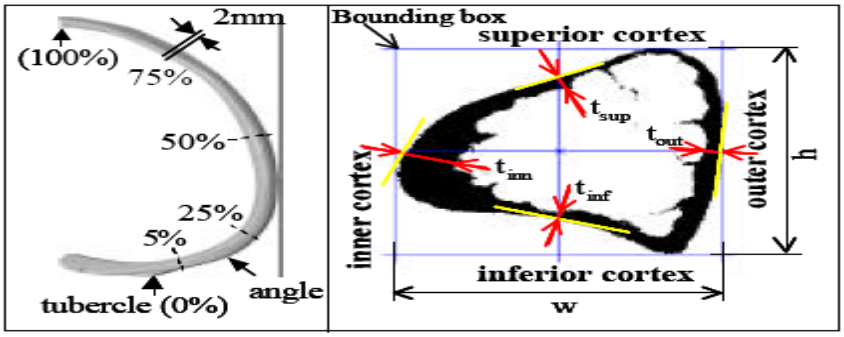

Fig. 23. Locations cut for the cross-section study of human ribs and the geometric parameters of the cross-section of a rib. For this study, the rectangular bounding box will be considered to represent the human rib geometry [46].

TABLE 14
Dimensions of the bounding boxes surrounding the ribs. 'h' is the height and 'w' is the width of the bounding box. All dimensions are in mm [46].

	Rib 3	Rib 4	Rib 5	Rib 6	Rib 7	Rib 8	Rib 9
h	11.3±2.5	11.6±2.6	11.4±2.6	11.8±2.6	12.8±2.8	13.1±3.6	12.0±3.8
w	6.0±2.0	6.8±2.0	7.2±1.9	7.6±1.8	7.4±1.7	6.5±2.1	6.4±1.9

Fig. 24 shows the development of the human rib configuration using the information of the height (h) and width (w) of the bounding box in the right panel of Fig. 18. The median values of each dimension of the bounding boxes were used. As an

example, the height for rib 3 was 11.3 mm and the width was 6.0 mm. Furthermore, since there is no data about rib 1, 2, 10, 11, and 12, an assumption was made that rib 1 and 2 are the same as rib3 and rib 10, 11, and 12 are the same as rib 9.

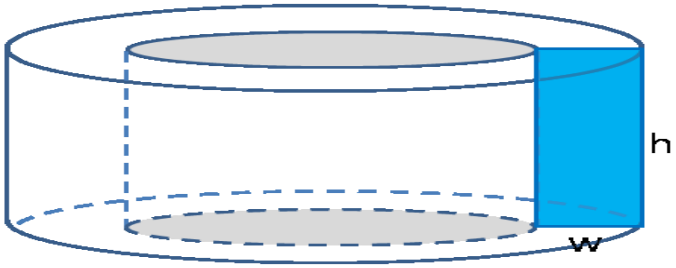

Fig. 24. Geometrical concept how to develop the human rib configuration.

Fig. 25 represents the development of the rib geometries using the data given in Table 14. The respective ribs were made with two cylinders with different radii to define the different rib widths, and two planes to define the different heights.

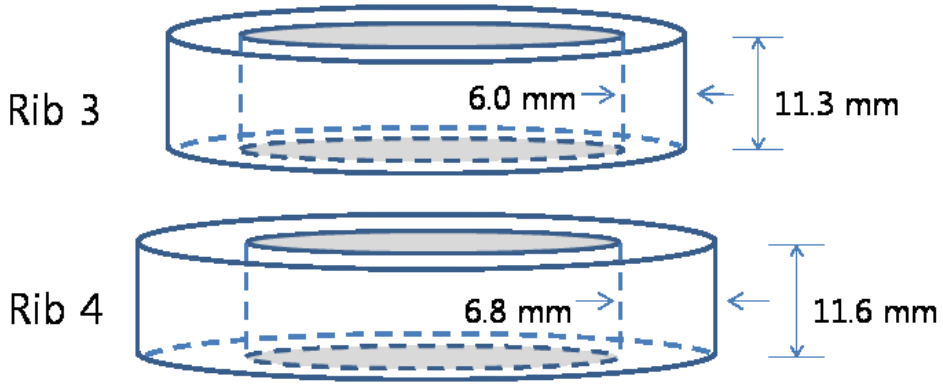

Fig. 25. An example of how to apply the dimensions of the bounding boxes to developing rib cage geometry.

The radii of the inner elliptical cylinder of the ribs were determined along the contour of the lungs and the radii of the outer elliptical cylinder were determined by adding the dimensions of inner radii and the widths (w). The corresponding statement for the rib cage therefore becomes

$$\begin{aligned} &\frac{x^2}{a^2}+\frac{(y-y_0)^2}{b^2}\geq 1, \\ &\frac{x^2}{a'^2}+\frac{(y-y_0)^2}{b'^2}\leq 1, \\ &and\ z_3\leq z\leq z_4 \end{aligned} \tag{19}$$

For the rib 11 and 12, however, since they do not have a perfect shape in real human ribs, the ribs that defined from Eq. (19) are cut by planes of $y=0.55$ and $y=-2$, respectively. Table 15 represents the values used to define the ribs in Eq. (19).

TABLE 15
Values used to define the ribs in Eq. (19).

Rib	a	b	a'	b'	y_0	z_3	z_4
Rib 1	7.447	7.1	8.047	7.7	-2.1	44.77	45.9
Rib 2	10.936	8.05	11.536	8.65	-1.15	42.07	43.2
Rib 3	12.882	8.55	13.482	9.15	-0.65	39.37	40.5
Rib 4	14.393	8.885	15.073	9.565	-0.235	36.64	37.8
Rib 5	15.411	9.13	16.131	9.85	0.05	33.96	35.1
Rib 6	16.374	9.295	17.134	10.055	0.255	31.22	32.4
Rib 7	17.052	9.465	17.792	10.205	0.405	28.42	29.7
Rib 8	17.585	9.625	18.235	10.275	0.475	25.69	27
Rib 9	17.897	9.73	18.537	10.37	0.57	23.1	24.3
Rib 10	18.000	9.75	18.640	10.39	0.59	20.4	21.6
Rib 11	18.000	9.75	18.640	10.39	0.59	17.7	18.9
Rib 12	18.000	9.75	18.640	10.39	0.59	15	16.2

Sternum

The sternum is a long flat bony plate shaped like a capital "T" located anterior to the heart in the center of the thorax. It connects the rib bones via cartilage, forming the anterior section of the rib cage, and thus helps to protect the lungs, heart and major blood vessels from physical trauma [47]. Therefore, because its location is anterior to the heart, it will affect the absorbed dose to the heart when the beam is incident on the front of the body and, unlike the MIRD model, is included here.

Since sternum connects the ribs in the human and the ribs exist along the contour of lungs, its shape should be a bending plate along the contour of the lungs. To maintain the contour of the lung for the shape of the sternum, two identical ellipsoids as represented in the lung but with different y coordinates were used. As shown in Fig. 26, each ellipsoid was used for the outer and inner shape respectively and two horizontal planes cut the upper and lower boundaries. The designated region represents the sternum.

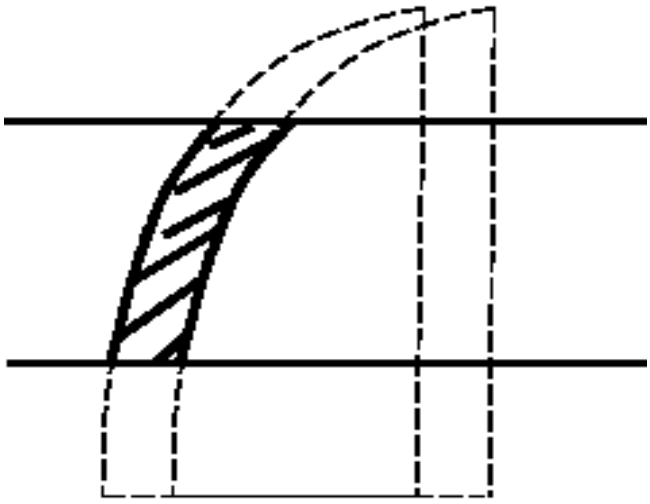

Fig. 26. Geometrical concept for development of the sternum. Two identical ellipsoids as represented in the lung but with different y coordinates were used to maintain the contour of the lung for the shape of the sternum.

Fig. 27 is the front and the side views of the final geometry of the rib cage prepared in PHITS. The rib cage surrounds the lungs and the sternum is located anterior to the heart in the center of the thorax connecting the rib bones.

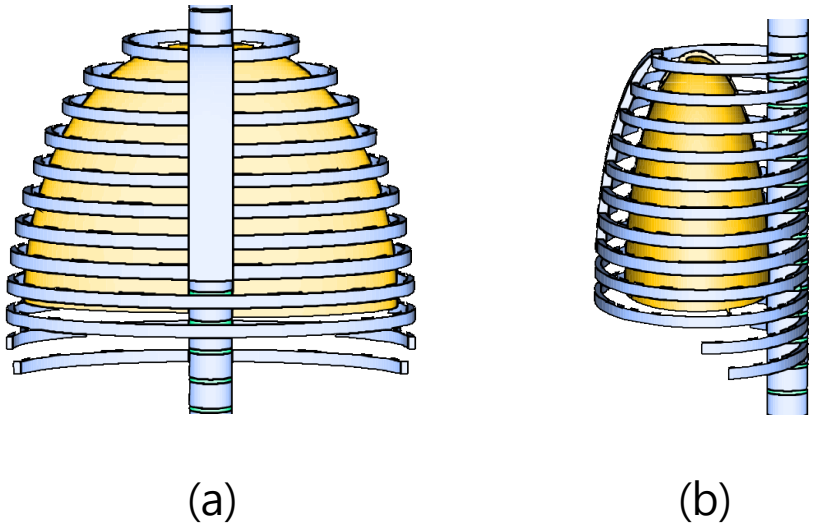

Fig. 27. Front (a) and side (b) views of the rib cage geometry prepared in PHITS.

Head

The head section consists of neck, skull, face, and brain. The neck was simply represented by using a right cylinder with 8cm height and 5cm radius as

$$x^2 + (y + 6.5)^2 = 5^2 \quad \text{and} \quad 48 \le z \le 56 \tag{20}$$

The brain, one of the important organs of concern for radiation dose, is enclosed within the skull. It can therefore be represented by the inner ellipsoid which used as the inner boundary of the skull. Since the mass and density of brain is 1450 g and 1.04 g/cm^3, the specific dimension for brain can be determined by simple calculation as [35]

$$V_{Br} = 1450\ \text{g} \times \frac{1\ \text{cm}^3}{1.04\ \text{g}} = 1394.23\ \text{cm}^3$$

$$\therefore\ \frac{4}{3}\pi \cdot a_{Br} \cdot b_{Br} \cdot c_{Br} = 1394.23\ \text{cm}^3$$

where a_{Br} is a minor axis of x-direction, b_{Br} is major axis of y-direction, and c_{Br} is another minor axis of z-direction. The values of a_{Br} and b_{Br} were assumes as 7cm, 8.5cm respectively, and thus, c_{Br} was found to be 5.594cm by calculation. Thus the statement that must be satisfied is

$$\frac{x^2}{7^2} + \frac{(y+2)^2}{8.5^2} + \frac{(z-66.266)^2}{5.594^2} \le 1 \tag{21}$$

After determining the brain dimension, the skull was completed by using an outer ellipsoid with 1cm larger dimension than that of the brain as

$$\frac{x^2}{7^2} + \frac{(y+2)^2}{8.5^2} + \frac{(z-66.266)^2}{5.594^2} \ge 1 \quad \textit{and} \quad \frac{x^2}{8^2} + \frac{(y+2)^2}{9.5^2} + \frac{(z-66.266)^2}{6.594^2} \le 1 \tag{22}$$

For the facial representation, an elliptical cylinder for the outer boundary was used and facial bone was included in this section by using another concentric cylinder with 1cm smaller dimension than that of the outer elliptical cylinder. A vertical plane

was also used to cut the boundary between facial bone and soft tissue. The facial bone excluding the chin could be expressed as

$$\begin{aligned}
&\frac{x^2}{7^2}+\frac{(y+2)^2}{8.5^2}\geq 1,\\
&\frac{x^2}{8^2}+\frac{(y+2)^2}{9.5^2}\leq 1,\\
&57\leq z\leq 66.266,\\
&y\geq -0.605,\\
&\textit{and}\ \ \frac{x^2}{8^2}+\frac{(y+2)^2}{9.5^2}+\frac{(z-66.266)^2}{6.594^2}\geq 1
\end{aligned} \tag{23}$$

The soft tissue was filled inside of the head excluding the cervical vertebrae, skull, facial bone, and brain. Fig. 28 is the cross sectional view of the head section with soft tissue represented in green.

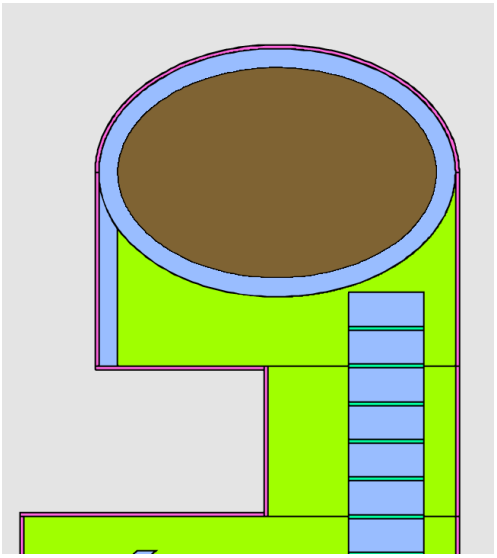

Fig. 28. Cross sectional view of the head section prepared in PHITS.

Trunk

The trunk was represented by an elliptical cylinder specified by

$$\frac{x^2}{20^2}+\frac{y^2}{11.5^2}\le 1 \quad and \quad -3.07\le z\le 48 \tag{24}$$

Arms

The arms which contain bones were represented by several cylinders. They are separated by two sections, forearms and upper arms, and they are represented by cylinders with different radii. For the tissue of each arm, the statement that must be satisfied is

$$r_{B,A}{}^2\le\left(x-x_1\right)^2+y^2\le r_A{}^2 \quad and \ z_5\le z\le z_6. \tag{25}$$

And for the bone of each arm, the statement is the below.

$$\left(x-x_1\right)^2+y^2\le r_{B,A}{}^2 \quad and \ z_5\le z\le z_6. \tag{26}$$

where $r_{B,A}$ is the radius of cylinder for bone of arm and it is 3cm for all bones, r_A is the radius of cylinder for outer boundary of arm. Table 16 represents the values used to define each section of arms in Eq. (25) and Eq. (26).

TABLE 16
Values used to define each section of arms in Eq. (25) and Eq. (26).

Arms	x_1	r_A	z_5	z_6
Left upper arm	- 5.290	5	18	48
Left forearm	- 5.3290	4	-12	18
Right upper arm	25.3290	5	18	48
Right forearm	25.3290	4	-12	18

Legs

The legs can be represented in the similar way as the arms, and they are also separated into two sections, lower legs and thighs. For the tissue of each leg, the statement that must be satisfied is

$$r_{B,L}{}^2 \le (x - x_2)^2 + y^2 \le r_L{}^2 \quad \textit{and} \quad z_7 \le z \le z_8. \tag{27}$$

And for the bone of each arm, the statement is the below.

$$\left(x-x_2\right)^2+y^2\le {r_{B,L}}^2 \quad and\ z_7\le z\le z_8. \tag{28}$$

where $r_{B,L}$ is the radius of cylinder for bone of leg and it is 5cm for all of the bones, r_L is the radius of cylinder for outer boundary of leg. Table 17 represents the values used to define each section of legs in Eq. (27) and Eq. (28).

TABLE 17
Values used to define each section of legs in Eq. (27) and Eq. (28).

Legs	x_2	r_L	z_7	z_8
Left thigh	-11	9	-53.105	-3.07
Left lower leg	-11	8	-103.14	-53.105
Right thigh	11	9	-53.105	-3.07
Right lower leg	11	8	-103.14	-53.105

Skin

Estimates of epidermal, dermal, or total skin thickness have been done by several investigators and a re-assessment was performed based on the reported information and typical values for skin thickness including epidermal and dermal thickness and are presented in Table 18 [34]. Skin is represented as a layer of thickness extending over the exterior of the phantom based on the information of Table 18.

TABLE 18
Typical values for epidermal and dermal thickness (Total skin thickness is the sum of epidermis and dermis thickness) [34].

Body site	Epidermis (μm)	Dermis (μm)	Total skin (μm)
Head and trunk	45	2000	2045
Upper arms and thighs	45	1200	1245
Forearms and lower legs	90	1200	1290

Elemental compositions and densities of the organs and the body tissues

The elemental compositions of the organs and the body tissues are summarized in Table 19. For soft tissue, ICRU-44 tissue was used because commercially manufactured phantoms generally use only one soft tissue compartment. The elemental information of skeleton-femur, skeleton-humerus, and skeleton-mandible was used as representatives for leg bones, arm bones, and facial bone respectively. Furthermore, the fragmentary information of ribs (2^{nd}, 6^{th}), ribs (10^{th}), vertebral column (C4), and vertebral column (D6, L3) was used to represent ribs (1^{st} - 9^{th}) and sternum, ribs (10^{th} - 12^{th}), whole cervical vertebrae, and whole thoracic and lumbal vertebrae respectively. Since the information used above for the skeletal system is for whole bone, the osseous tissue, bone (red, yellow) marrow are included, but excluded any cartilage in the information. Because of the lack of information of elemental composition of intervertebral disks, the information of skeleton-cartilage was substituted.

TABLE 19
Elemental compositions and densities of the organs and the body tissues [20].

Tissue	Elemental composition (percentage by mass)					Density (g/cm^3)	Data used
	H	C	N	O	Others		
Soft tissue	10.5	25.6	2.7	60.2	0.1Na, 0.2P, 0.3S, 0.2Cl, 0.2K	1.03	ICRU-44
Heart tissue	10.4	13.9	2.9	71.8	0.1Na, 0.2P, 0.2S, 0.2Cl, 0.3K	1.05	Heart (healthy)
Blood	10.2	11.0	3.3	74.5	0.1Na, 0.1P, 0.2S, 0.3Cl, 0.2K, 0.1Fe	1.06	Blood (whole)
Lung	10.3	10.5	3.1	74.9	0.2Na, 0.2P, 0.3S, 0.3Cl, 0.2K	0.26	Lung (hearthy, inflated)
Brain	10.7	14.5	2.2	71.2	0.2Na, 0.4P, 0.2S, 0.3Cl, 0.3K	1.04	Brain (whole)
Skin	10.0	20.4	4.2	64.5	0.2Na, 0.1P, 0.2S, 0.3Cl, 0.1K	1.09	-
Skull	5.0	21.2	4.0	43.5	0.1Na, 0.2Mg, 8.1P, 0.3S, 17.6Ca	1.61	Cranium (whole)
Leg bone	7.0	34.5	2.8	36.8	0.1Na, 0.1Mg, 5.5P, 0.2S, 0.1Cl, 12.9Ca	1.33	Femur (whole)
Arm bone	6.0	31.4	3.1	36.9	0.1Na, 0.1Mg, 7.0P, 0.2S, 15.2Ca	1.46	Humerus (whole)
Facial bone	4.6	19.9	4.1	43.5	0.1Na, 0.2Mg, 8.6P, 0.3S, 18.7Ca	1.68	Mandible (whole)
Ribs (1^{st} - 9^{th}) / sternum	6.4	26.3	3.9	43.6	0.1Na, 0.1Mg, 6.0P, 0.3S, 0.1Cl, 0.1K,13.1Ca	1.41	Ribs (2^{nd}, 6^{th}) (whole)
Ribs (10^{th} - 12^{th})	5.6	23.5	4.0	43.4	0.1Na, 0.1Mg, 7.2P, 0.3S, 0.1Cl, 0.1K,15.6Ca	1.52	Ribs (10^{th}) (whole)
Cervical vertebrae	6.3	26.1	3.9	43.6	0.1Na, 0.1Mg, 6.1P, 0.3S, 0.1Cl, 0.1K, 13.3Ca	1.42	Vertebral column (C4) (whole)
Thoracic / Lumbal vertebrae	7.0	28.7	3.8	43.7	0.1Mg, 5.1P, 0.2S, 0.1Cl, 0.1K, 11.1Ca, 0.1Fe	1.33	Vertebral column (D6,L3) (whole)
Intervertebral disks	9.6	9.9	2.2	74.4	0.5Na, 2.2P, 0.9S, 0.3Cl	1.10	Cartilage

Fig. 29 shows the total body skeletal system with differing material properties represented by arbitrary color based on the information available in ICRU report 46 [20]. Fig. 30 shows the total body from two directions.

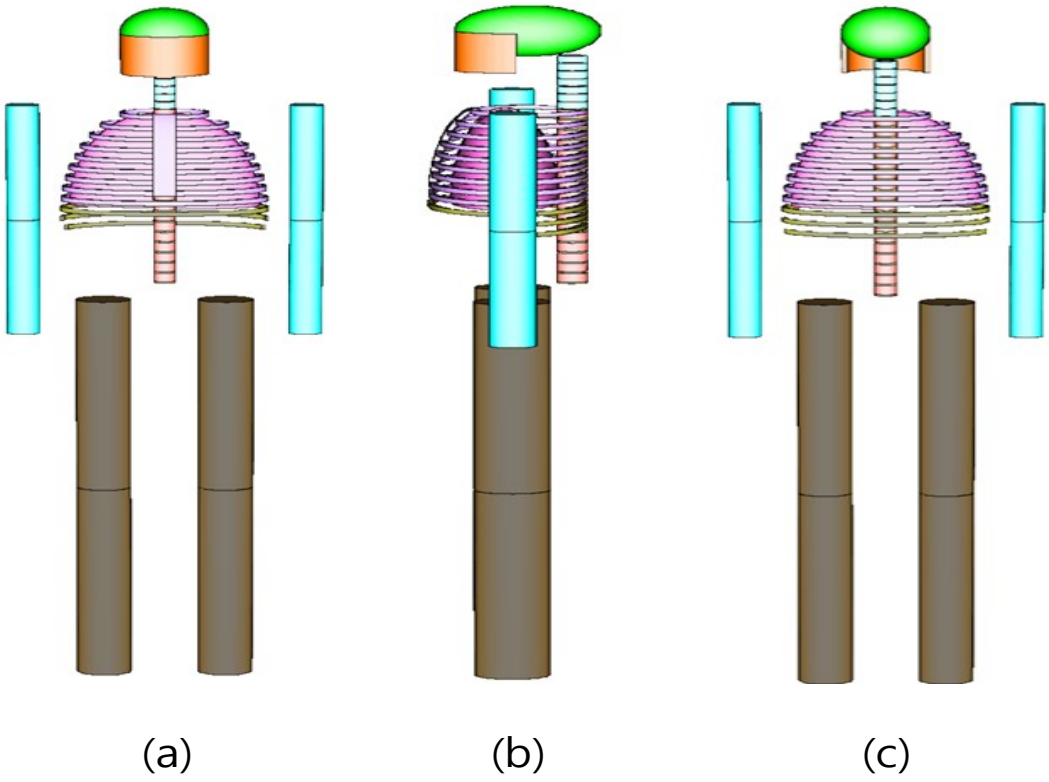

Fig. 29. 3D view of the skeleton system including organs prepared in PHITS. [(a) is the front view, (b) is the side view, and (c) is the rear view.]

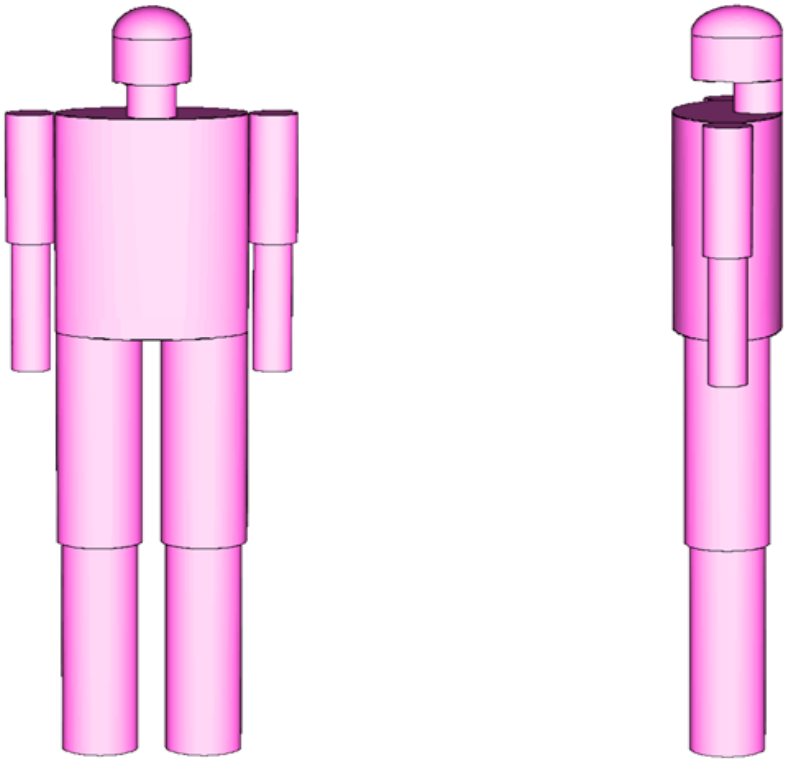

Fig. 30. 3D view of the total body prepared in PHITS. [(a) is the front view and (b) is the side view.)

CHAPTER V

RESULT AND DISCUSSION

Stopping power and depth-dose distribution comparisons

Tables 20-22 are the final results of the mass stopping power comparisons between the ICRU-44 tissue and the soft tissue substitutes by the irradiations of the proton, the carbon, and the iron beams. They are represented by maximum normalized differences and the mean normalized differences and corresponding standard deviations.

As shown in Tables 20-22, the three HCPs have similar trends in the mean normalized differences. In this result, if a material is suitable for the soft tissue substitute of the proton beam, it is also suitable for the carbon or iron beam.

For the mass stopping power comparison, Alderson muscle (A) has mean normalized differences of $2.69 \pm 1.28\%$ for the proton beam, $2.26 \pm 0.47\%$ for the carbon beam, and $2.21 \pm 0.49\%$ for the iron beam. However, Alderson muscle (B) has $3.04 \pm 1.30\%$ for the proton beam, $2.65 \pm 0.47\%$ for the carbon beam, and $2.60 \pm 0.50\%$ for the iron beam; Alderson muscle (A) is therefore more appropriate as the soft tissue substitute even though Alderson muscle (A) has been modified since its introduction and replaced with Alderson muscle (B).

TABLE 20
Maximum and mean normalized differences of mass stopping powers and stopping powers of the proton beam between ICRU-44 tissue and the soft tissue substitutes.

Tissue substitute	Density (g/cm^3)	Mass stopping power		Stopping power	
		Maximum differ. (%)	Mean differ. ($\Delta \pm \sigma$, %)	Maximum differ. (%)	Mean differ. ($\Delta \pm \sigma$, %)
A150	1.12	7.43	0.79 ± 1.22	9.95	8.19 ± 1.48
Acrylic (PMMA)	1.17	10.07	4.43 ± 1.16	9.84	8.55 ± 1.31
Alderson muscle A	1.00	8.92	2.69 ± 1.28	11.57	5.51 ± 1.28
Alderson muscle B	1.00	9.11	3.04 ± 1.30	11.75	5.86 ± 1.27
Amber	1.10	6.74	1.29 ± 0.99	9.11	7.45 ± 1.53
Ceric Sulfate Dosimeter Solution	1.03	0.96	0.21 ± 0.19	0.96	0.21 ± 0.19
ED1S (fhw)	1.01	4.41	1.97 ± 0.45	6.48	4.09 ± 0.44
ED4C (fhw)	1.01	0.62	0.41 ± 0.39	5.22	2.75 ± 0.39
Ethyl Cellulose	1.13	8.75	2.56 ± 1.15	8.19	6.90 ± 1.26
Ferrous Sulfate Dosimeter Solution	1.02	1.11	0.24 ± 0.22	0.98	0.41 ± 0.21
Frigerio gel	1.12	2.69	1.14 ± 0.41	8.20	7.50 ± 0.44
Frigerio liquid	1.08	1.55	0.76 ± 0.26	4.52	4.06 ± 0.27
Goodman liquid	1.07	1.53	0.69 ± 0.24	3.49	3.16 ± 0.25
Griffith muscle	1.12	8.76	2.61 ± 1.12	7.10	5.94 ± 1.05
Lincolnshire bolus	1.05	12.91	9.04 ± 1.60	11.22	7.28 ± 1.64
Mylar/Melinex	1.40	16.75	11.94 ± 1.88	23.18	19.70 ± 2.55
Nylon-6	1.13	7.74	1.07 ± 1.26	9.99	8.56 ± 1.41
Nylon, Du Pont Elvamide 8062	1.08	7.03	0.85 ± 1.07	7.26	5.08 ± 0.98
Polyethylene	0.92	9.79	7.53 ± 1.86	11.36	3.98 ± 1.77
PEG-200	1.12	3.19	1.73 ± 0.47	8.08	7.23 ± 0.51
Polystyrene	1.05	10.49	4.53 ± 1.26	8.75	2.68 ± 1.28
Polyvinyl Butyral	1.12	8.40	1.96 ± 1.25	8.07	6.62 ± 1.28
Rice powder	0.84	12.51	8.37 ± 1.63	28.65	25.27 ± 1.33
RM-1	1.03	5.93	3.47 ± 1.01	5.93	3.47 ± 1.01
RM/G1	1.07	1.62	0.78 ± 0.26	3.48	3.07 ± 0.27
RM/L3	1.04	1.03	0.73 ± 0.18	0.57	0.24 ± 0.18
RM/SR4	1.03	7.38	0.77 ± 1.18	7.38	0.77 ± 1.18
Rossi gel	1.10	3.03	1.37 ± 0.38	5.81	5.33 ± 0.41
Rossi liquid	1.11	2.99	1.42 ± 0.41	6.80	6.24 ± 0.45
RW-2	1.11	12.34	7.52 ± 1.01	5.53	0.74 ± 0.87
Temex	1.01	8.10	1.37 ± 1.32	9.88	3.28 ± 1.30
TH/L2	1.08	1.86	1.08 ± 0.28	4.15	3.72 ± 0.29
Water	1.00	16.06	9.22 ± 2.09	18.51	11.87 ± 2.03

TABLE 21
Maximum and mean normalized differences of mass stopping powers and stopping powers of the carbon beam between ICRU-44 tissue and the soft tissue substitutes.

Tissue substitute	Density (g/cm^3)	Mass stopping power		Stopping power	
		Maximum differ. (%)	Mean differ. ($\Delta \pm \sigma$, %)	Maximum differ. (%)	Mean differ. ($\Delta \pm \sigma$, %)
A150	1.12	5.14	0.54 ± 0.92	9.46	8.45 ± 1.13
Acrylic (PMMA)	1.17	7.85	4.24 ± 0.91	9.76	8.78 ± 1.03
Alderson muscle A	1.00	3.49	2.26 ± 0.47	6.30	5.11 ± 0.45
Alderson muscle B	1.00	3.87	2.65 ± 0.47	6.67	5.49 ± 0.45
Amber	1.10	4.44	1.28 ± 0.71	8.94	7.71 ± 1.26
Ceric Sulfate Dosimeter Solution	1.03	0.38	0.18 ± 0.12	0.38	0.18 ± 0.12
ED1S (fhw)	1.01	2.43	1.90 ± 0.23	4.54	4.03 ± 0.22
ED4C (fhw)	1.01	0.62	0.41 ± 0.14	2.90	2.68 ± 0.15
Ethyl Cellulose	1.13	6.51	2.40 ± 0.86	7.85	7.08 ± 0.94
Ferrous Sulfate Dosimeter Solution	1.02	0.49	0.21 ± 0.17	0.74	0.39 ± 0.19
Frigerio gel	1.12	5.17	1.31 ± 0.74	8.02	7.31 ± 0.81
Frigerio liquid	1.08	4.91	0.96 ± 0.75	4.44	3.86 ± 0.73
Goodman liquid	1.07	4.89	0.90 ± 0.76	3.50	3.00 ± 0.57
Griffith muscle	1.12	6.52	2.46 ± 0.84	6.78	6.06 ± 0.91
Lincolnshire bolus	1.05	12.16	8.70 ± 1.57	10.46	6.93 ± 1.60
Mylar/Melinex	1.40	15.91	11.78 ± 1.90	23.59	19.91 ± 2.59
Nylon-6	1.13	5.46	0.84 ± 0.95	9.65	8.79 ± 1.04
Nylon, Du Pont Elvamide 8062	1.08	4.75	0.70 ± 0.77	6.06	5.07 ± 1.05
Polyethylene	0.92	9.73	7.70 ± 1.47	6.37	3.80 ± 1.31
PEG-200	1.12	6.05	1.91 ± 0.84	7.76	7.03 ± 0.91
Polystyrene	1.05	6.07	4.11 ± 0.73	4.24	2.24 ± 0.75
Polyvinyl Butyral	1.12	6.15	1.74 ± 0.92	7.71	6.85 ± 1.00
Rice powder	0.84	11.84	7.75 ± 1.87	28.10	24.77 ± 1.53
RM-1	1.03	4.42	3.43 ± 0.85	4.42	3.43 ± 0.85
RM/G1	1.07	4.90	0.98 ± 0.75	3.48	2.91 ± 0.56
RM/L3	1.04	1.01	0.74 ± 0.19	0.58	0.23 ± 0.18
RM/SR4	1.03	0.75	0.34 ± 0.18	0.75	0.34 ± 0.18
Rossi gel	1.10	5.42	1.58 ± 0.75	5.81	5.11 ± 0.80
Rossi liquid	1.11	5.41	1.59 ± 0.74	6.77	6.05 ± 0.80
RW-2	1.11	8.85	7.18 ± 0.85	1.77	0.66 ± 0.64
Temex	1.01	1.54	0.84 ± 0.41	3.46	2.77 ± 0.40
TH/L2	1.08	5.17	1.28 ± 0.75	4.16	3.54 ± 0.67
Water	1.00	12.91	9.21 ± 1.79	15.45	11.86 ± 1.74

TABLE 22
Maximum and mean normalized differences of mass stopping powers and stopping powers of the iron beam between ICRU-44 tissue and the soft tissue substitutes.

Tissue substitute	Density (g/cm^3)	Mass stopping power		Stopping power	
		Maximum differ. (%)	Mean differ. ($\Delta \pm \sigma$, %)	Maximum differ. (%)	Mean differ. ($\Delta \pm \sigma$, %)
A150	1.12	1.27	0.38 ± 0.35	9.47	8.59 ± 0.55
Acrylic (PMMA)	1.17	5.60	4.14 ± 0.62	9.60	8.89 ± 0.71
Alderson muscle A	1.00	3.41	2.21 ± 0.49	6.22	5.06 ± 0.47
Alderson muscle B	1.00	3.80	2.60 ± 0.50	6.61	5.44 ± 0.49
Amber	1.10	2.04	1.03 ± 0.54	8.97	7.83 ± 0.70
Ceric Sulfate Dosimeter Solution	1.03	0.43	0.17 ± 0.13	0.43	0.17 ± 0.13
ED1S (fhw)	1.01	2.41	1.83 ± 0.32	4.52	3.96 ± 0.32
ED4C (fhw)	1.01	3.00	0.47 ± 0.17	2.90	2.64 ± 0.24
Ethyl Cellulose	1.13	3.21	2.26 ± 0.40	7.73	7.22 ± 0.44
Ferrous Sulfate Dosimeter Solution	1.02	5.04	2.51 ± 2.27	4.43	2.34 ± 1.82
Frigerio gel	1.12	2.32	1.19 ± 0.27	7.98	7.45 ± 0.29
Frigerio liquid	1.08	2.16	0.83 ± 0.25	4.43	3.99 ± 0.27
Goodman liquid	1.07	2.13	0.75 ± 0.25	3.50	3.10 ± 0.26
Griffith muscle	1.12	3.33	2.31 ± 0.38	6.66	6.22 ± 0.41
Lincolnshire bolus	1.05	11.96	8.65 ± 1.65	10.26	6.87 ± 1.69
Mylar/Melinex	1.40	16.18	11.65 ± 1.88	23.30	20.08 ± 2.56
Nylon-6	1.13	1.65	0.72 ± 0.42	9.60	8.92 ± 0.46
Nylon, Du Pont Elvamide 8062	1.08	1.07	0.53 ± 0.20	5.98	5.19 ± 0.49
Polyethylene	0.92	9.68	7.74 ± 1.41	6.16	3.76 ± 1.26
PEG-200	1.12	2.77	1.78 ± 0.34	7.64	7.18 ± 0.37
Polystyrene	1.05	5.93	4.05 ± 0.77	4.10	2.19 ± 0.79
Polyvinyl Butyral	1.12	2.55	1.59 ± 0.42	7.66	7.01 ± 0.45
Rice powder	0.84	11.34	7.72 ± 1.78	27.69	24.74 ± 1.46
RM-1	1.03	4.47	3.44 ± 0.78	4.47	3.44 ± 0.78
RM/G1	1.07	2.23	0.84 ± 0.27	3.48	3.01 ± 0.28
RM/L3	1.04	1.01	0.75 ± 0.18	0.63	0.22 ± 0.17
RM/SR4	1.03	0.80	0.33 ± 0.19	0.80	0.33 ± 0.19
Rossi gel	1.10	2.66	1.45 ± 0.29	5.77	5.25 ± 0.30
Rossi liquid	1.11	2.61	1.45 ± 0.29	6.73	6.21 ± 0.31
RW-2	1.11	8.86	7.18 ± 0.85	1.78	0.66 ± 0.63
Temex	1.01	1.45	0.80 ± 0.36	3.36	2.70 ± 0.41
TH/L2	1.08	2.47	1.14 ± 0.27	4.16	3.66 ± 0.29
Water	1.00	12.74	9.10 ± 1.91	15.28	11.75 ± 1.86

Water, commonly used as a tissue equivalent material, has a mean difference of $9.22 \pm 2.09\%$ for the proton beam, $9.21 \pm 1.79\%$ for the carbon beam, and $9.10 \pm 1.91\%$ for the iron beam. It is therefore less appropriate for use as a soft tissue substitute. A150 tissue equivalent plastic, however, has better interaction characteristics than the Alderson muscle by having the mean normalized differences of $0.79 \pm 1.22\%$ for the proton beam, $0.54 \pm 0.92\%$ for the carbon beam, and $0.38 \pm 0.35\%$ for the iron beam.

The relative ratios of the mass stopping powers between the ICRU-44 tissue and the tissue substitutes were compared to observe the trends of the mass stopping powers of the soft tissue substitutes at all energies of the beams. If a soft tissue substitute had the similar interaction properties with the ICRU-44 tissue, then the relative ratios should be close to unity. The errors tended to be larger when the energy or the charge of a beam became larger. A total of 1,000,000 particles were used for the proton beam, and 100,000 particles were used for both of the carbon and the iron beams. Fig. 31 represents the relative ratios of the mass stopping powers between A150 tissue equivalent plastic and ICRU-44 tissue. For A150 plastic, the relative ratios are close to unity at all energies of beams, and this means it has similar interaction properties with ICRU-44 tissue for the HCPs and thus it can be treated as a suitable soft tissue substitute in the entire energy range considered.

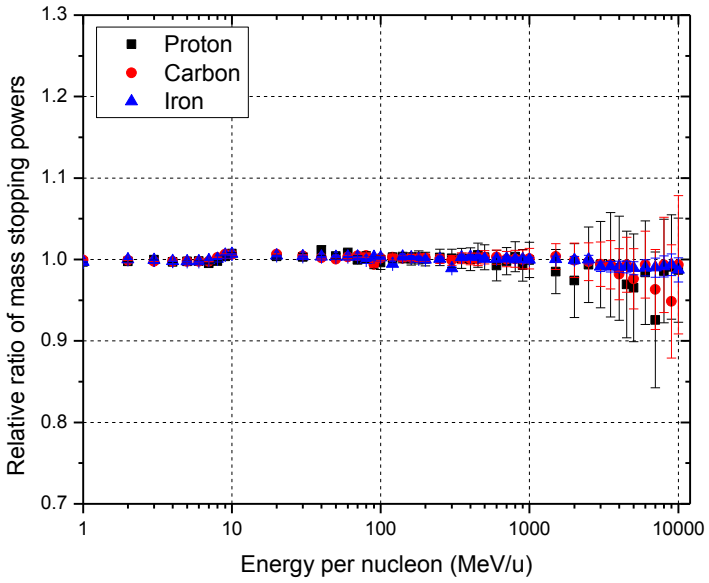

Fig. 31. Relative ratios of the mass stopping powers between A150 tissue equivalent plastic and ICRU-44 tissue. ($(S/\rho)_{A150}/(S/\rho)_{ICRU-44}$)

The relative ratios of the mass stopping powers between ICRU-44 tissue and Alderson muscle (A) are shown in Fig. 32. For Alderson muscle (B), they are shown in Fig. 33. The general trends of two cases are similar because the densities of Alderson muscle (A) and Alderson muscle (B) are identical and the elemental compositions of them are close. The results show that the relative ratios between the Alderson muscles (both of 'A' and 'B') and the ICRU-44 tissue are below unity at all energies of beams points (about 3-4% lower). This means the Alderson muscles have smaller mass stopping power than the ICRU-44 tissue at all energies of beams; therefore, this will lead HCPs to have larger ranges and the Bragg-peaks will occur on the depths slightly far from that of the ICRU-44 tissue.

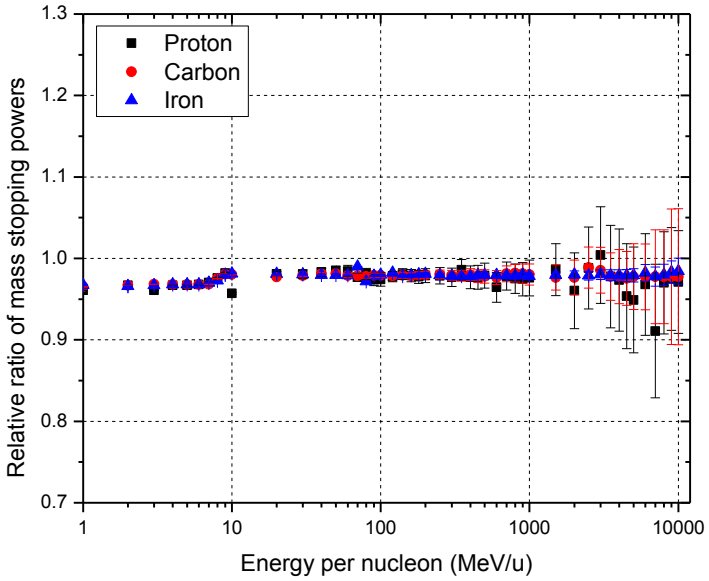

Fig. 32. Relative ratios of the mass stopping powers between Alderson muscle (A) and ICRU-44 tissue. ($(S/\rho)_{Alderson\ (A)}/(S/\rho)_{ICRU-44}$)

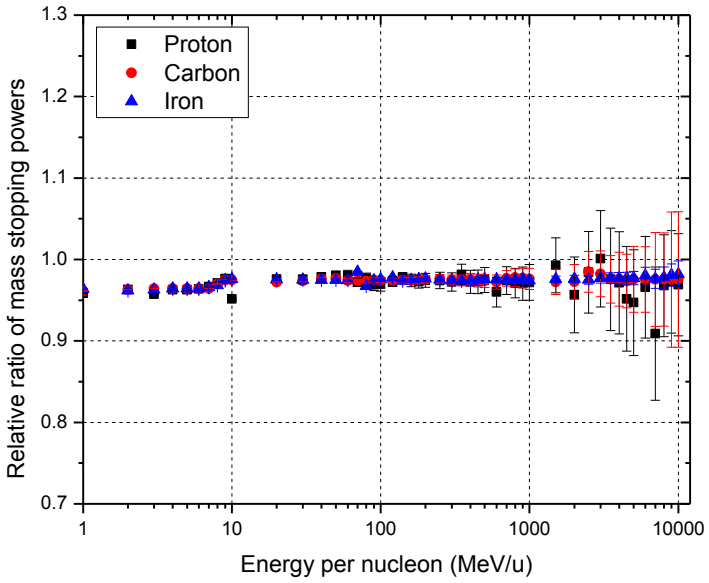

Fig. 33. Relative ratios of the mass stopping powers between Alderson muscle (B) and ICRU-44 tissue. ($(S/\rho)_{Alderson\ (B)}/(S/\rho)_{ICRU-44}$)

Fig. 34 shows the relative ratios of the mass stopping powers between the water and ICRU-44 tissue at all energies of beams. The relative ratios of the water are relatively much lower than unity at all energies of beams (by about 10%). From this result, the ranges of the HCPs within the water medium are expected to be longer than in either ICRU-44 tissue or Alderson muscles substitute. The Bragg-peak should occur at depths far from them of ICRU-44 tissue and Alderson muscles.

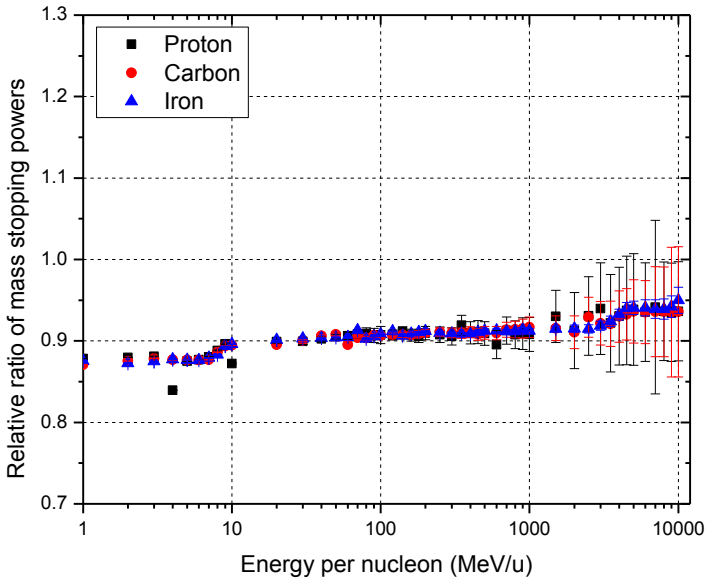

Fig. 34. Relative ratios of the mass stopping powers between the water and ICRU-44 tissue. ($(S/\rho)_{water}/(S/\rho)_{ICRU-44}$)

Fig. 35 is the depth-dose distributions of the proton, the carbon, and the iron beams incident on ICRU-44 tissue, A150 plastic, water, and Alderson muscles. As shown in this figure, the depth-dose distributions have similar trends regardless of whichever HCPs is used for the irradiation. These results correspond to the expectations based on relative ratios of the mass stopping powers. A150 plastic has similar depth-dose distributions as exhibited in ICRU-44 tissue. All HCPs transported showed larger ranges using Alderson muscles, and the Bragg-peaks occurred at deeper depths when compared to ICRU-44 tissue. These trends were much more pronounced with using water in the comparison.

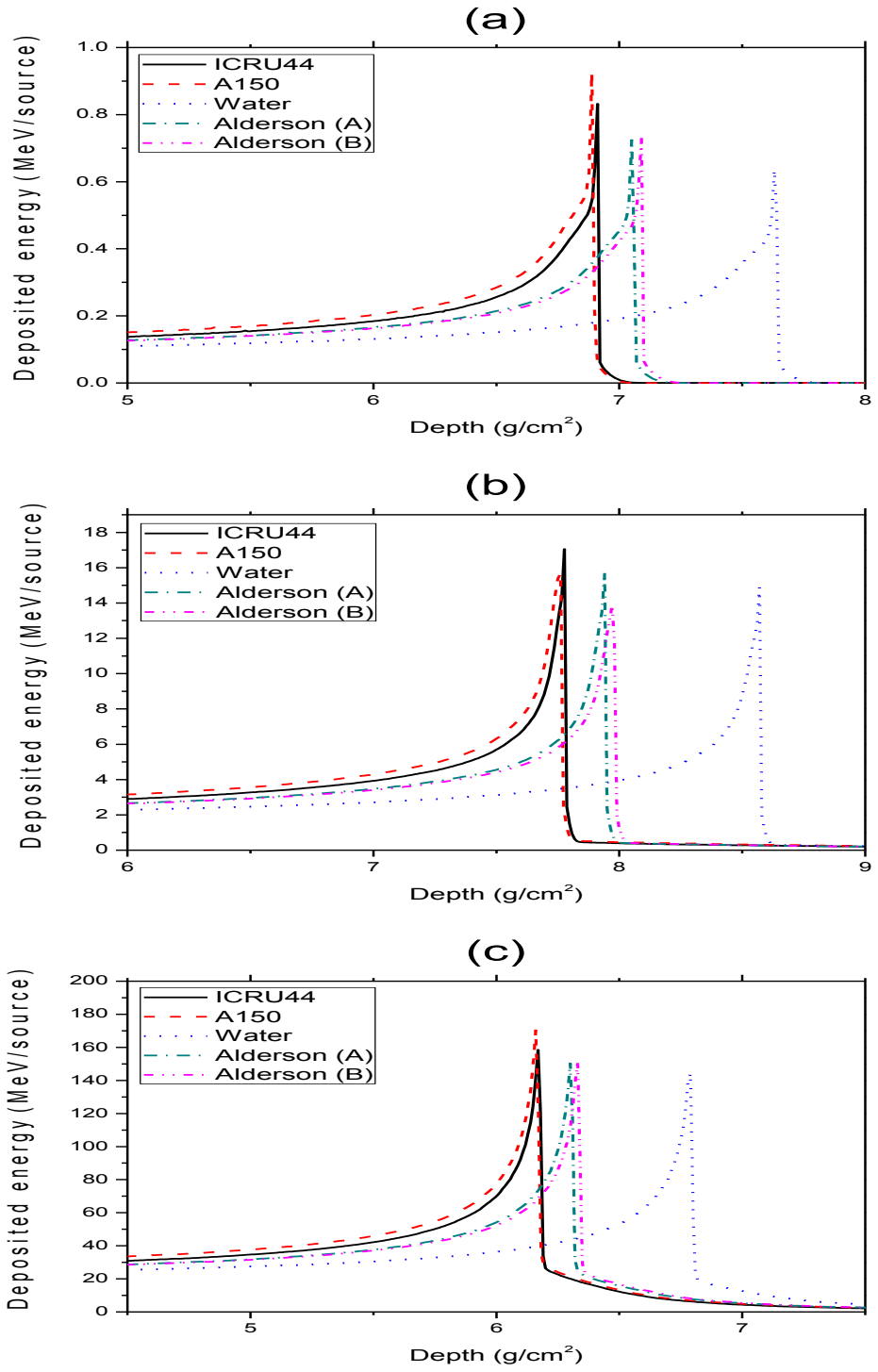

Fig. 35. Depth-dose distributions of the proton(a), the carbon(b), and the iron(c) beams within the media of ICRU-44 tissue, A150, the water, and Alderson muscles.

Even though the Alderson muscles showed small differences in mass stopping powers at all beam energies, which are below 5%, and the depth-dose distributions of the HCPs are acceptable, other soft tissue substitutes listed in Tables 20-22 such as A150 tissue equivalent plastic apparently can give more accuracy for simulating the human soft tissue. Based on these simulation results, the "MATROSHKA" experiments or any experiments related to RANDO phantom therefore may have better experimental results if the Alderson muscle was substituted with a better soft tissue substitute such as A150.

As shown in Tables 20-22, the mean normalized differences of the mass stopping powers of all soft tissue substitutes except for Lincolnshire bolus, Mylar/Melinex, Polyethylene, Rice powder, RW-2, and water are below 5% for all HCPs. Notably, a total of 10 soft tissue substitutes had the mean normalized differences below 1% for all HCPs; A150, Ceric Sulfate Dosimeter Solution, ED4C (fhw), Ferrous Sulfate Dosimeter Solution, Frigerio liquid, Goodman liquid, Nylon (Du Pont Elvamide 8062), RM/G1, RM/L3, RM/SR4. Furthermore, Nylon-6 and Temex had the mean normalized difference of 1.07 ± 1.26 and 1.37 ± 1.32 for proton beam, but for carbon and iron beams, they also showed differences below 1%.

The most suitable soft tissue substitute among the materials of concern was Ceric sulfate dosimeter solution having the mean normalized difference of $0.21 \pm 0.19\%$ for proton beam, $0.18 \pm 0.12\%$ for carbon beam, and $0.17 \pm 0.13\%$ for iron beam, and the depth-dose distributions in this solution are almost identical as ICRU-44 tissue as shown in Fig. 36.

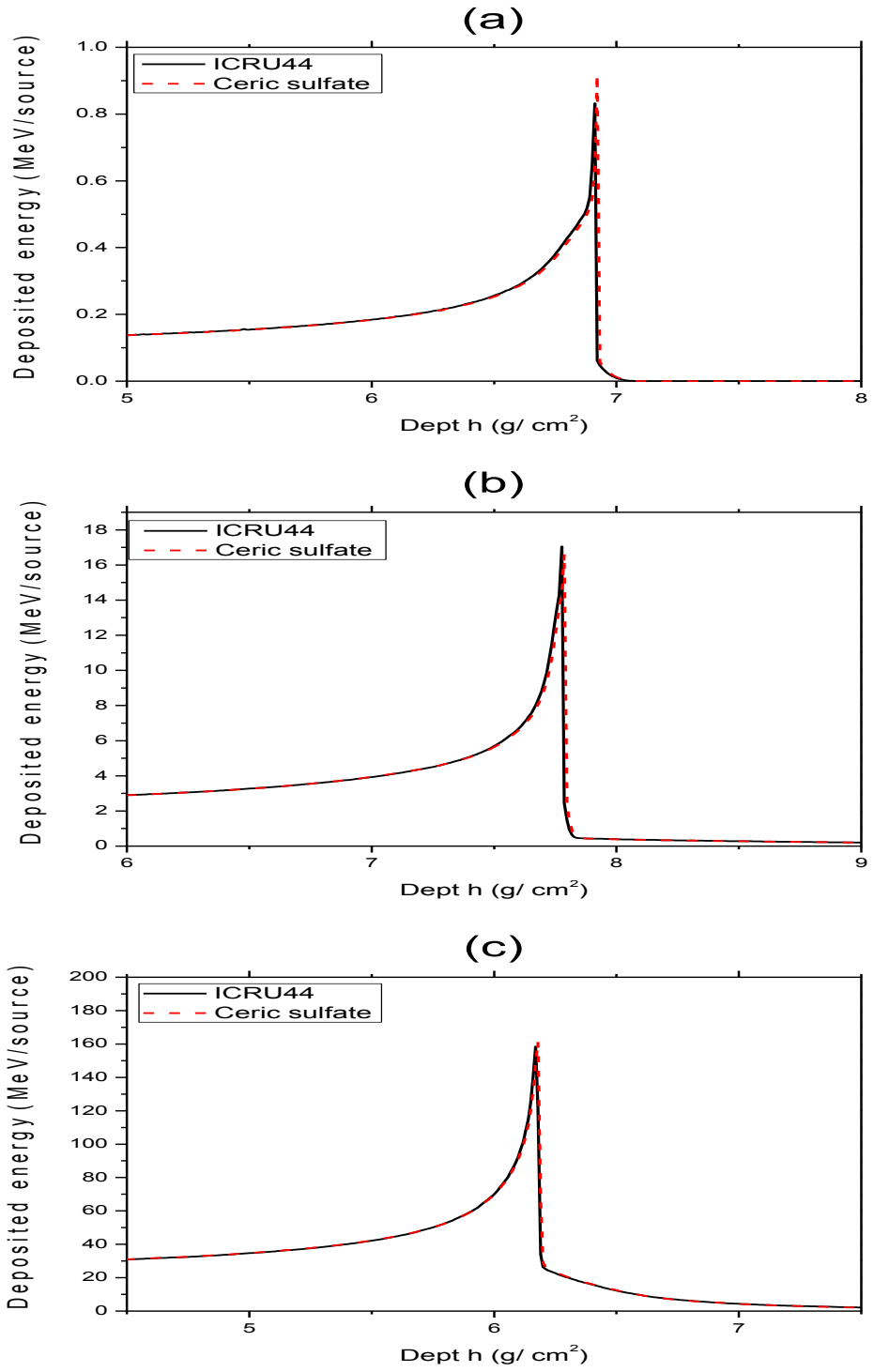

Fig. 36. Depth-dose distributions of the proton(a), the carbon(b), and the iron(c) beams within the media of ICRU-44 tissue and Ceric sulfate dosimeter solution.

Thus far, the selection for the suitable soft tissue substitute was analyzed by using the mass stopping power comparison. When a density is considered as a characteristic of the soft tissue substitute, the situation is somewhat different. That is, when it comes to the comparisons of the stopping powers which are dependent of the densities of the soft tissue substitutes, some soft tissue substitutes such as A150 plastic and Nylon (Du Pont Elvamide 8062) are no longer suitable showing around 8% and 5% mean normalized differences, respectively. Furthermore, Alderson muscles also have a negative effect by having larger mean differences above 5%. Therefore, in order to use these soft tissue substitutes for phantom creation, the dimensions of the phantom should be corrected in relation to their different densities.

Ceric Sulfate Dosimeter Solution, RM/L3, and RM/SR4 remain suitable soft tissue substitutes because they have identical or similar densities with ICRU-44 tissue. (ICRU-44 tissue - 1.03 g/cm^3, Ceric Sulfate Dosimeter Solution - 1.03 g/cm^3, RM/L3 - 1.04 g/cm^3, and RM/SR4 - 1.03 g/cm^3) RM/L3 has even better results by taking account of the density effect.

One interesting result was found in use of RW-2 having better result. RW-2 had relatively large mean normalized differences of around 7% when only mass stopping powers were compared, but it is a suitable soft tissue substitutes by taking

into account its density. The mean normalized differences became $0.74 \pm 0.87\%$ for the proton beam, $0.66 \pm 0.64\%$ for the carbon beam, and $0.66 \pm 0.63\%$ for the iron beam after taking account of the density.

In a view of manufacturing a real phantom and its practical use in the real world, solution or gel type soft tissue substitutes may have several defects. Since the Ceric sulfate dosimeter solution is a liquid, it may lead unexpected problems. For example, the phantom would require an outer solid frame also made of one of the suitable tissue substitutes surrounding the liquid or gel, and then considerations such as corrosion and leakage may be required. Furthermore, the use of liquid or gel type tissue substitute makes it more difficult to mount the detectors and to cast the real human skeletons inside of the phantom. Inevitably, more structures to mount or cast the skeletons will be needed and these structures may affect the results. Thus, the physical property of a soft tissue substitute is a critical factor. Table 23 summarizes the general descriptions of several suitable soft tissue substitutes and their physical properties.

Finally, A150, ED4C (fhw), Nylon-6, Nylon (Du Pont Elvamide 8062), RM/SR4, Temex, and RW-2 are the most suitable soft tissue substitutes for the phantoms due to their added benefits of handling the materials and manufacturing into phantoms.

TABLE 23
Description of the suitable soft tissue substitutes and their physical properties [1, 42].

Tissue substitute	Description	Physical property
A150	Mixture of polyethylene and nylon, with fillers carbon and calcium fluoride	Solid
Ceric Sulfate Dosimeter Solution	Dosimeter solution for radiation absorbed dose measurements using spectrophotometry by the radiation-induced changes in ion concentrations by the reduction of ceric (Ce4+) to cerous ions (Ce3+)	Liquid
ED4C (fhw)	Crosslinked and fully hydrated in water copolymer from a combination of methyl metahcrylate (MMA) and vinylpyrolidone (VP)	Solid
Ferrous Sulfate Dosimeter Solution	Dosimeter solution for radiation absorbed dose measurements using spectrophotometry by the radiation-induced changes in ion concentrations by the oxidation of ferrous (Fe2+) to ferricions (Fe3+)	Liquid
Frigerio liquid	Aqueous solution containing urea, ethylene glycol, and glycerol	Liquid
Goodman liquid	Aqueous solution containing urea and glycerol	Liquid
Nylon-6	Nylon multipolymer resin	Rigid solid
Nylon, Du Pont Elvamide 8062	Nylon multipolymer resin	Flexible solid
RM/G1	Water based gel comprising gelatin and glucose; manufactured for red marrow	Soft gel
RM/L3	Aqueous solution containing urea and glycerol; manufactured for red marrow	Liquid
RM/SR4	Epoxy CB4 with fillers ammonium nitrate, polyethylene and phenolic microspheres; manufactured for red marrow	Rigid solid
RW-2	Polystyrene with filler titanium dioxide	Rigid solid
Temex	Natural rubber with fillers including oil, carbon, sulfur, stearic acid, and titanium dioxide	Flexible solid

Nylon-6 and Nylon (Du Pont Elvamide 8062) are both nylon multipolymer resins and have similar elemental compositions; therefore, only Nylon (Du Pont Elvamide 8062), which had better result than Nylon-6, was dealt with and analyzed throughout simulations. Table 24 is a summary of the maximum and the mean normalized differences between ICRU-44 tissue and the soft tissue substitutes. The only RW-2 data is from the stopping power comparison, and the others are from the mass stopping power comparisons.

TABLE 24
Summary for the maximum and the mean normalized differences from the mass stopping power or stopping power comparisons between the ICRU-44 tissue and the suitable soft tissue substitutes. For only RW-2, the stopping powers were used to compare.

Tissue substitute	Charged particle	Maximum difference (%)	Mean difference ($\Delta \pm \sigma$, %)
A150	Proton	7.43	0.79 ± 1.22
	Carbon	5.14	0.54 ± 0.92
	Iron	1.27	0.38 ± 0.35
ED4C (fhw)	Proton	0.62	0.41 ± 0.39
	Carbon	0.62	0.41 ± 0.14
	Iron	3.00	0.47 ± 0.17
Nylon (Du Pont Elvamide 8062)	Proton	7.03	0.85 ± 1.07
	Carbon	4.75	0.70 ± 0.77
	Iron	1.07	0.53 ± 0.20
RM/SR4	Proton	7.38	0.77 ± 1.18
	Carbon	0.75	0.34 ± 0.18
	Iron	0.80	0.33 ± 0.19
Temex	Proton	8.10	1.37 ± 1.32
	Carbon	1.54	0.84 ± 0.41
	Iron	1.45	0.80 ± 0.36
RW-2 (stopping power)	Proton	5.53	0.74 ± 0.87
	Carbon	1.77	0.66 ± 0.64
	Iron	1.78	0.66 ± 0.63

As shown in Figs. 37-41, the all solid soft tissue substitutes show that the relative ratios of the mass stopping powers or stopping powers with ICRU-44 tissue are close to unity at all beam energies. Especially, the relative ratios of ED4C (fhw) have a stable and ideal distribution at all energies of the beams except for just one energy of the proton beam (10 MeV), and this trend therefore leads smaller standard deviations of the normalized difference of the mass stopping powers.

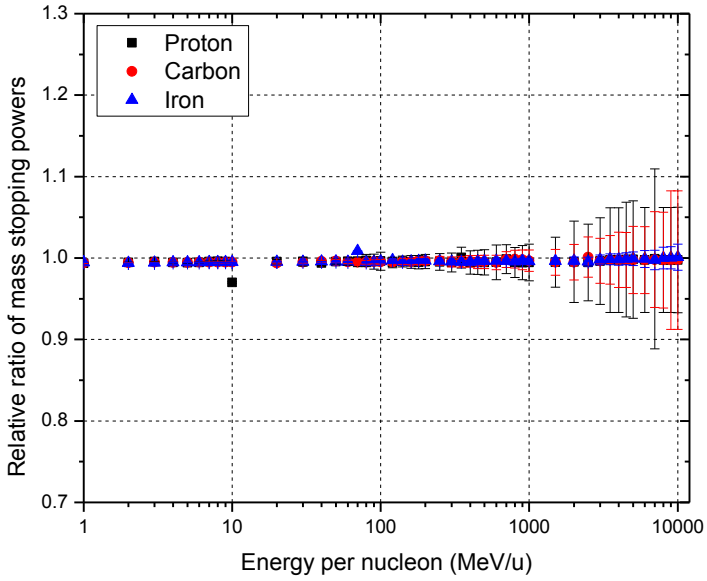

Fig. 37. Relative ratios of the mass stopping powers between ED4C (fhw) and ICRU-44 tissue. ($(S/\rho)_{ED4C(fhw)}/(S/\rho)_{ICRU-44}$)

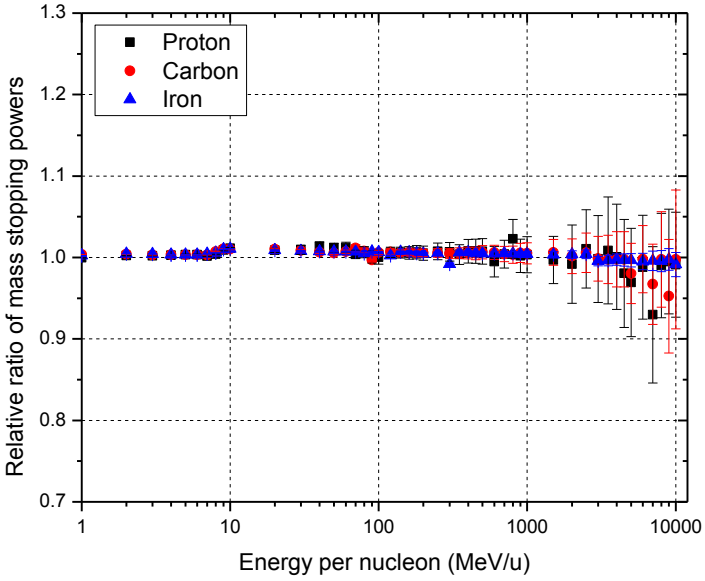

Fig. 38. Relative ratios of the mass stopping powers between Nylon (Du Pont, Elvamide 8062) and ICRU-44 tissue. ($(S/\rho)_{Nylon,Elvamide\ 8062}/(S/\rho)_{ICRU-44}$)

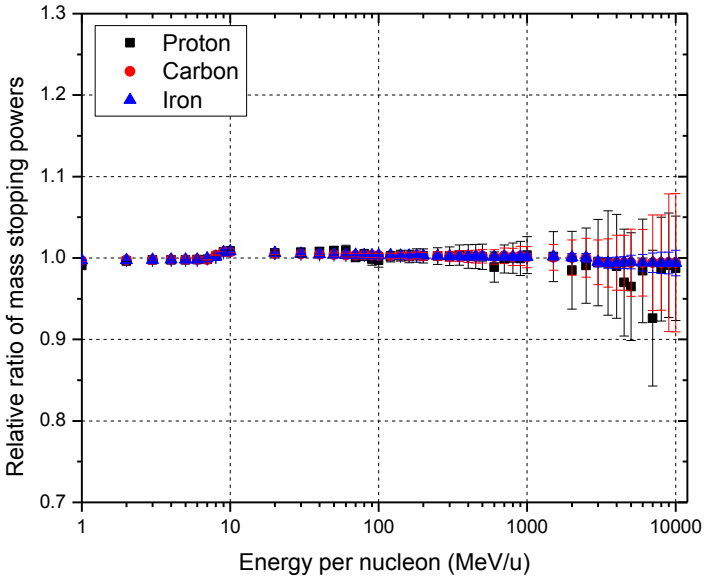

Fig. 39. Relative ratios of the mass stopping powers between RM/SR4 and ICRU-44 tissue. ($(S/\rho)_{RM/SR4}/(S/\rho)_{ICRU-44}$)

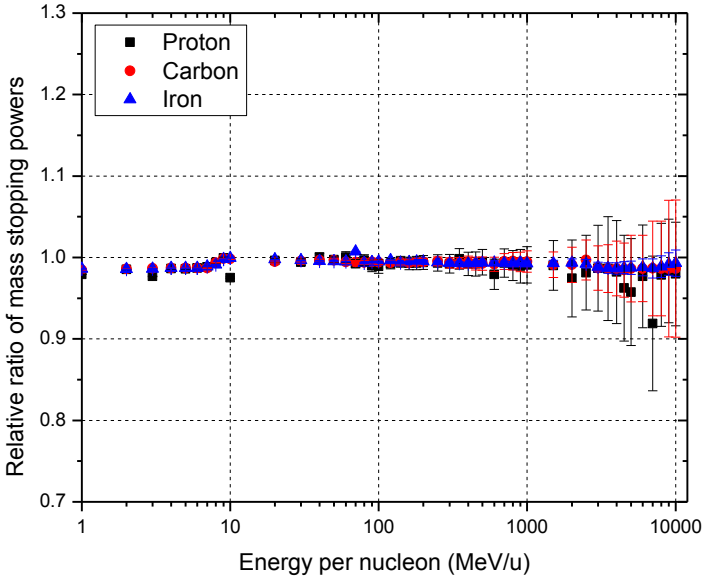

Fig. 40. Relative ratios of the mass stopping powers between Temex and ICRU-44 tissue. $((S/\rho)_{Temex}/(S/\rho)_{ICRU-44})$

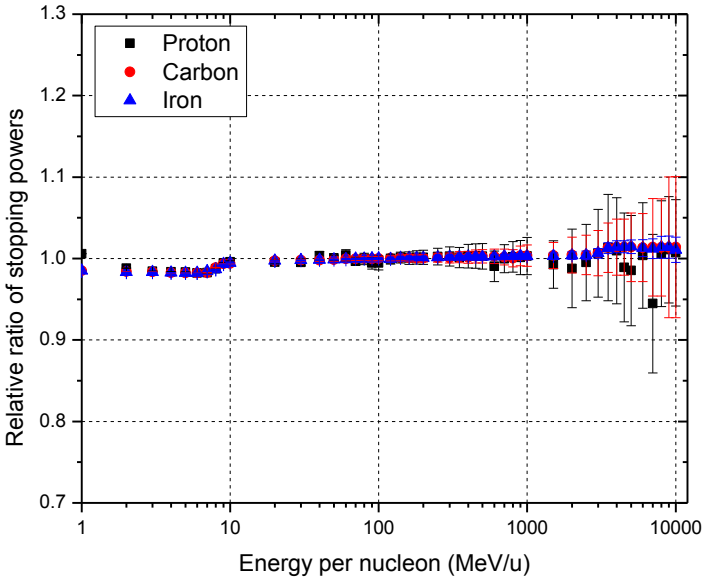

Fig. 41. Relative ratios of the stopping powers between RW-2 and ICRU-44 tissue. $(S_{RW-2}/S_{ICRU-44})$

Fig. 42 is the depth-dose distributions within the media of the ICRU-44 tissue and the suitable solid soft tissue substitutes for each beam and the horizontal scale is extended to observe the differences of the distributions. All soft tissue substitutes described in this figure have similar distributions and all Bragg-peaks occur within just 0.1cm difference. In a view of the depth-dose distribution, A150 tissue equivalent plastic is the best soft tissue substitute among the solid tissue substitutes even though the differences are small.

Fig. 43 is the depth-dose distributions within the media of the ICRU-44 tissue and the RW-2 for each beam. RW-2 also has similar distribution with ICRU-44 tissue. The unit of the abscissa is ‘cm’ and this means the depth-dose distributions is taking into account the density effect.

The interaction data of the mass stopping powers and the stopping powers including the standard deviations for the ICRU-44 tissue and the soft tissue substitutes of concern in this study are listed in Appendix B, and the depth-dose distributions about the soft tissue substitutes which were not represented are shown in Appendix C.

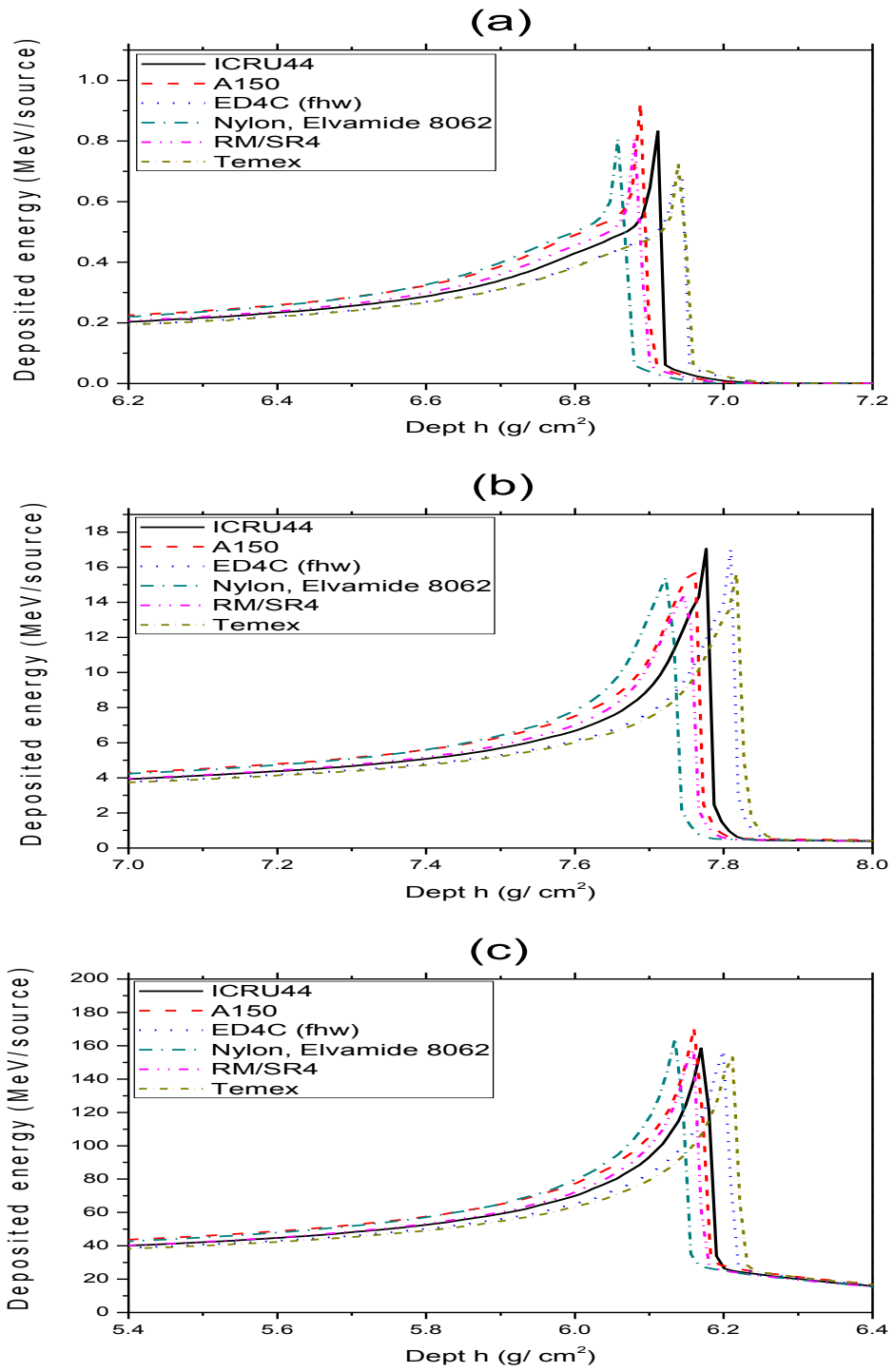

Fig. 42. Depth-dose distributions of the proton(a), the carbon(b), and the iron(c) beams within the media of ICRU-44 tissue and the suitable solid tissue substitutes.

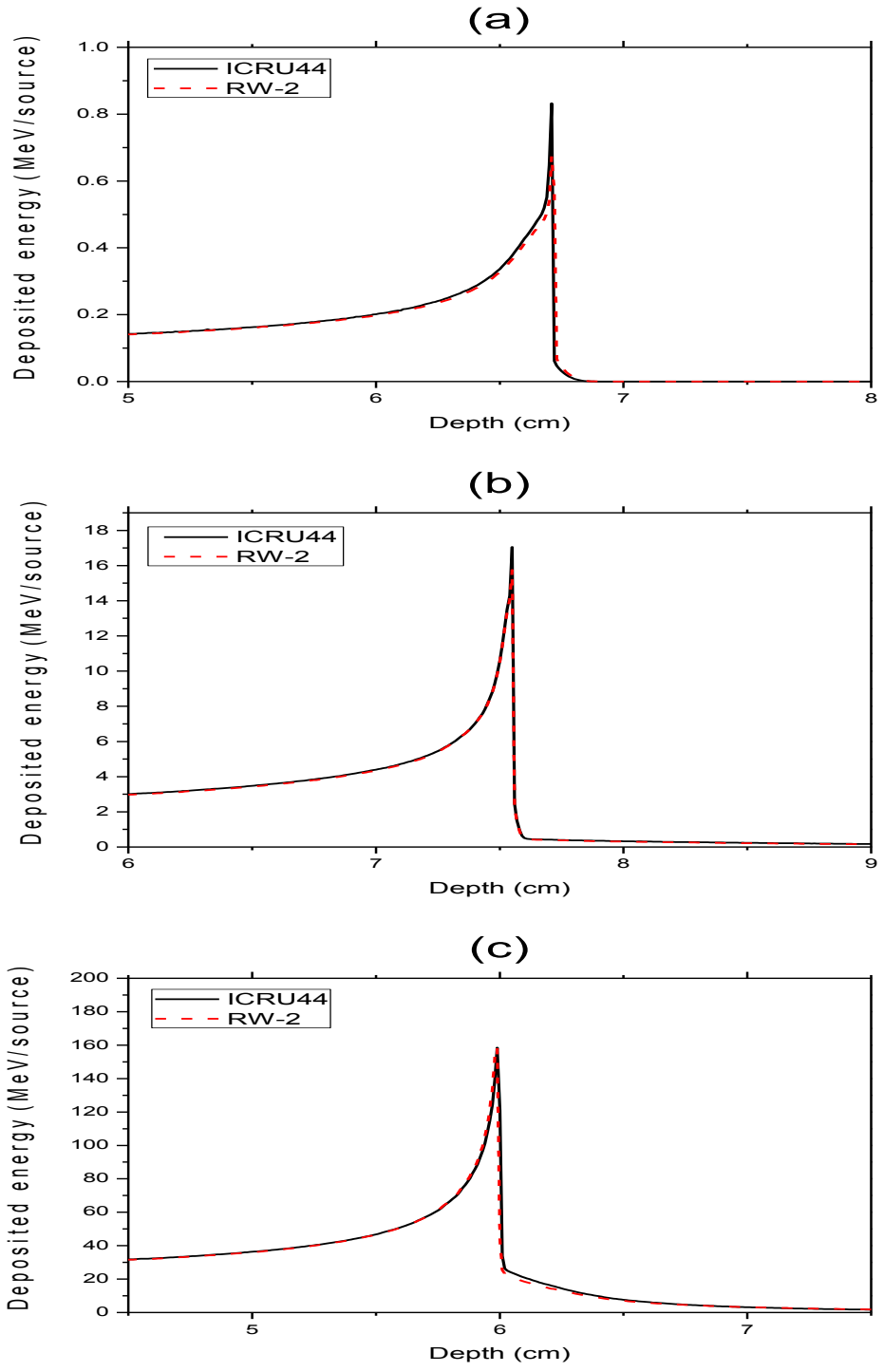

Fig. 43. Depth-dose distributions of the proton(a), the carbon(b), and the iron(c) beams within the media of ICRU-44 tissue and RW-2.

PHITS simulations in the developed phantom

As the next step, the most suitable soft tissue substitutes listed in Table 24 were used in the anthropomorphic computational phantom developed to observe whether they would still valid under conditions containing multiple regions, materials, and boundaries. Fig. 44 is the beam geometries irradiated into the phantom. The pencil beams of 0.25cm radius were irradiated into the center of the heart and the rectangle beams (broad beam) were also irradiated into an entire of the trunk. The energies used for irradiations were 100MeV for the proton beam, 200MeV/u for the carbon beam, 400MeV/u for the iron beam. From each irradiation, organ doses for the heart (heart tissue and the blood) and the left and right lungs were acquired.

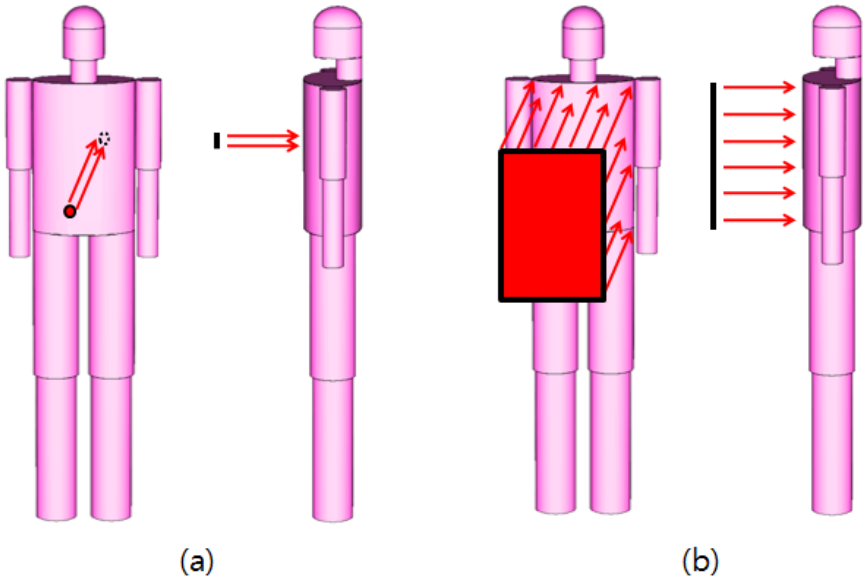

Fig. 44. Source geometries used to estimate the organ doses in the developed anthropomorphic computational phantom. Pencil beam of 0.25cm radius irradiating into the center of the heart (a) and rectangle beam covering an entire of the trunk (b) were used.

As shown in Fig. 45, when the pencil beams were irradiated into the phantom, since the beams are proximal to the heart and biased to the left side, the uncertainty or error in the right lung was higher than that of the left lung. This is because that there is no direct irradiation of the primary beam on the right lung and thus the dose came from the interactions with only secondary particles such as the fragments. Since the PHITS does not transport the secondary delta-ray electrons in this study, this is not included in the secondary particle spectrum. The corresponding uncertainty of the dose for the right lung was relatively higher than the others as shown in Table 25. As the charge of beam became larger, the transport modalities of the secondary particles were more remarkable.

Fig. 46 is the deposited energy distributions inside of the phantom in which ICRU-44 tissue was used as the soft tissue by the irradiations of 100MeV proton, 200MeV/u carbon, 400MeV/u iron rectangle beams. For the pencil beams, a total of 1,000,000 particles for the proton beam, 100,000 particles for the carbon beam, and 40,000 particles for the iron beams were used. For the broad beams, a total of 2,000,000 particles for the proton beam, 200,000 particles for the carbon beam, and 80,000 particles for the iron beams were used.

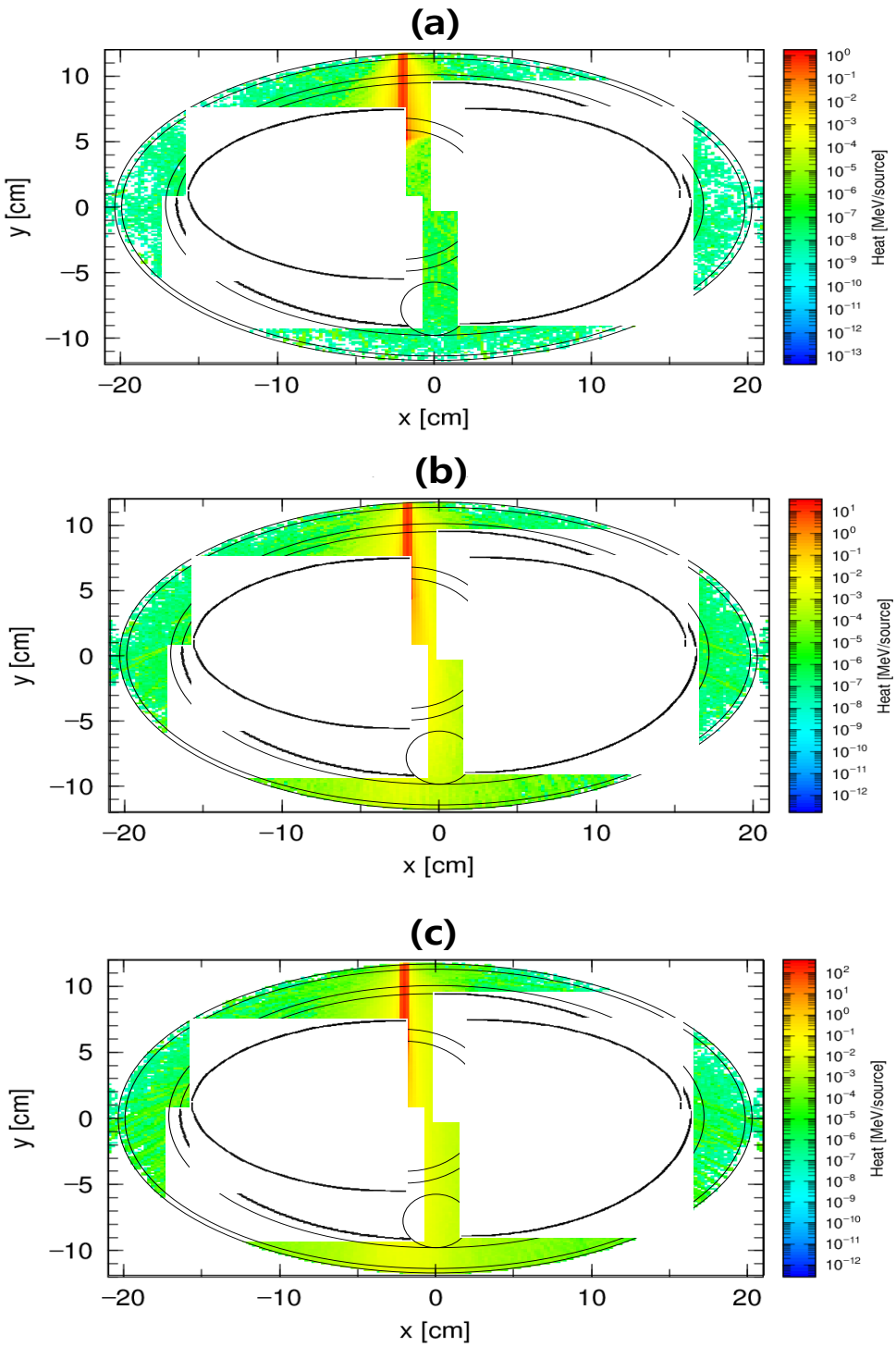

Fig. 45. Energy depositions by the pencil beams inside the phantom that ICRU-44 tissue was used for the soft tissue. The100 MeV proton (a), the 200 MeV/u carbon (b), the 400 MeV/u (c) pencil beams were used. The deposited energy distribution was represented by averaging 1cm height between z=31 and z=32.

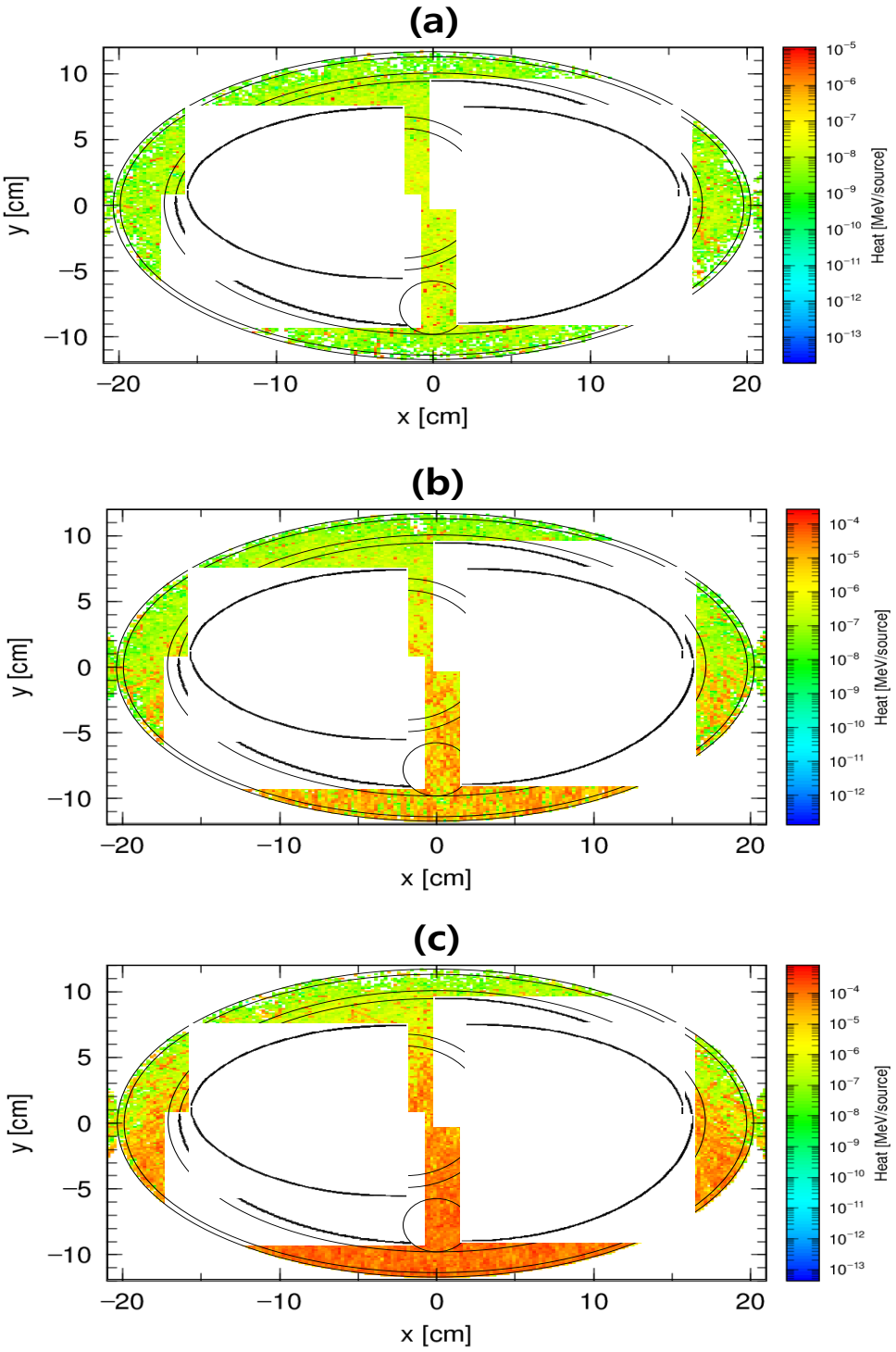

Fig. 46. Energy depositions by the broad beams inside the phantom that ICRU-44 tissue was used for the soft tissue. The100 MeV proton (a), the 200 MeV/u carbon (b), the 400 MeV/u (c) broad beams were used. The deposited energy distribution was represented by averaging 1cm height between z=31 and z=32.

Table 25 is the simulation result for the absorbed doses of each organ using ICRU-44 tissue with irradiations of each beam. In this table, the blood means the blood occupied inside of the heart. The dose of the heart (all) is simply the sum of the doses of the heart tissue and the blood, and similarly, the dose of the lungs (all) is the sum of the doses of the left lung and the right lung. The reason why the standard deviations do not exist for the carbon pencil beam in the heart is that the particles used for the carbon beam were so many that the errors were below the minimum limit that PHITS could display.

TABLE 25
Absorbed doses and the corresponding standard deviations of the organs by the irradiations of each beam when ICRU-44 tissue was used as the soft tissue of the phantom. Units are Gy.

Type of beam		Heart tissue	Blood	Heart (all)	Left lung	Right lung	Lungs (all)
Pencil beam	Proton	7.25E-12± 2.18E-15	9.14E-12± 2.74E-15	1.64E-11± 3.50E-15	2.80E-13± 3.63E-16	1.97E-15± 7.33E-17	2.82E-13± 3.71E-16
	Carbon	1.22E-10	3.01E-10	4.24E-10	5.66E-12± 1.59E-14	1.89E-13± 3.49E-15	5.85E-12± 1.62E-14
	Iron	2.12E-09± 3.82E-12	1.01E-09± 2.84E-12	3.13E-09± 4.75E-12	7.02E-11± 3.51E-13	1.34E-12± 1.24E-14	7.16E-11± 3.51E-13
Broad beam	Proton	2.66E-15± 1.19E-16	1.03E-15± 4.42E-17	3.69E-15± 1.27E-16	3.50E-12± 4.19E-15	2.82E-12± 3.39E-15	6.32E-12± 5.39E-15
	Carbon	1.34E-13± 3.24E-15	7.98E-14± 2.37E-15	2.14E-13± 4.01E-15	5.79E-11± 2.14E-13	5.04E-11± 1.86E-13	1.08E-10± 2.84E-13
	Iron	6.84E-13± 1.04E-14	5.14E-13± 9.87E-15	1.20E-12± 1.43E-14	7.62E-10± 4.27E-12	6.66E-10± 3.73E-12	1.43E-09± 5.67E-12

For the pencil beams, since the beams are proximal to the heart, the heart has relatively higher doses than the lungs (about 60 times). As mentioned before, the right lung has lower dose than the others because there was no direct irradiation of the beam; therefore, it depends on the transports of the secondary particles and the errors were relatively high. On the other hand, for the broad beams (rectangle beams), the lungs have more dose than the heart (about 1000 times) because the interaction areas of the lungs were larger than that of the heart and more particles therefore interacted with lungs than the heart. Since the heart doses are 3 orders of magnitude less than them of lungs, the doses from the secondary particles are significant leading to the high relative errors in the heart. Therefore, the heart should be the main organ of concern for the pencil beams and the lungs should be the main organs of concern for the broad beams to observe the validation of early selection by the stopping power comparisons and the depth-dose distributions.

By using the result of ICRU-44 tissue in Table 25 and more simulation results for the suitable soft tissue substitutes, the normalized differences and mean normalized differences of the organ doses between ICRU-44 tissue and all suitable soft tissue substitutes of concern were acquired and are shown in Tables 26-27. Table 26 is for the pencil beam irradiations, and Table 27 is for the broad beam irradiations. For the reference, the Alderson muscle (B) which is of concern in this study and Ceric sulfate dosimeter solution which had close interaction properties and the same density as ICRU-44 tissue were also simulated. The results came from uncorrected physical dimensions of the phantom, and thus unexpected errors occurred for some soft tissue substitutes.

TABLE 26

Simulation results for the pencil beam irradiations into the developed phantom. The results are represented with the normalized difference of each organ dose, the mean normalized differences of all organ doses, and the mean normalized differences of the only heart doses between ICRU-44 tissue and the suitable soft tissue substitutes.

Tissue substitute	HCP	Heart tissue	Blood	Heart (all)	Left lung	Right lung	Lung (all)	Mean differ. (all) ($\Delta \pm \sigma$)	Mean differ. (heart only) ($\Delta \pm \sigma$)
A150	P	14.12	23.88	7.07	6.00	0.63	5.95	9.61±7.50	15.02±6.89
	C	5.43	10.04	5.58	0.90	4.18	0.73	4.48±3.16	6.97±2.12
	Fe	2.59	33.55	12.60	5.86	1.99	5.72	10.38±10.92	16.24±12.90
ED4C (fhw)	P	3.15	6.40	2.17	1.35	6.03	1.38	3.41±2.07	3.91±1.81
	C	1.50	2.64	1.45	1.65	0.15	1.59	1.49±0.73	1.86±0.55
	Fe	6.26	18.52	1.75	2.08	1.51	2.02	5.36±6.11	8.84±7.08
Nylon, Elvamide	P	7.76	14.04	4.40	3.86	0.24	3.83	5.69±4.32	8.73±4.00
	C	3.08	6.08	3.44	0.60	1.55	0.53	2.55±1.93	4.20±1.34
	Fe	1.53	19.82	7.44	2.97	0.77	2.90	5.90±6.57	9.60±7.62
RM/SR4	P	0.44	0.92	0.32	0.85	0.34	0.84	0.62±0.26	0.56±0.26
	C	0.05	0.52	0.38	1.16	1.71	1.06	0.81±0.55	0.32±0.20
	Fe	0.51	0.64	0.55	0.43	0.00	0.42	0.42±0.20	0.57±0.06
Temex	P	2.75	5.46	1.83	0.59	2.16	0.57	2.23±1.65	3.35±1.54
	C	1.68	2.38	1.20	1.90	0.43	1.83	1.57±0.62	1.75±0.48
	Fe	6.24	17.44	1.42	2.70	0.89	2.67	5.23±5.72	8.37±6.71
RW-2	P	0.30	0.62	0.48	0.10	18.36	0.03	3.31±6.73	0.46±0.13
	C	0.65	0.60	0.61	1.29	4.87	1.09	1.52±1.52	0.62±0.03
	Fe	0.61	1.48	0.89	1.32	1.85	1.26	1.24±0.40	1.00±0.36
Ceric Sulfate	P	0.23	0.48	0.17	0.25	6.44	0.29	1.31±2.30	0.29±0.14
	C	0.03	0.03	0.03	1.70	2.29	1.72	0.97±0.96	0.03±0.00
	Fe	0.43	0.35	0.18	0.36	0.06	0.35	0.29±0.13	0.32±0.11
Alderson muscle(B)	P	5.45	12.26	4.42	1.28	4.35	1.24	4.83±3.68	7.38±3.48
	C	3.18	5.14	2.74	2.70	2.33	2.54	3.11±0.94	3.69±1.04
	Fe	13.95	37.87	2.81	4.24	0.62	4.15	10.61±12.89	18.21±14.63
A150 (corrected)	P	0.32	0.69	0.24	0.72	0.37	0.71	0.51±0.20	0.42±0.19
	C	0.16	0.44	0.36	1.10	0.37	1.05	0.58±0.36	0.32±0.12
	Fe	0.46	0.30	0.41	0.83	0.23	0.81	0.51±0.23	0.39±0.06

TABLE 27

Simulation results for the broad beam irradiations into the developed phantom. The results are represented with the normalized difference of each organ dose, the mean normalized differences of all organ doses, and the mean normalized differences of the only lung doses between ICRU-44 tissue and the suitable soft tissue substitutes.

Tissue substitute	HCP	Heart tissue	Blood	Heart (all)	Left lung	Right lung	Lung (all)	Mean differ. (all) ($\Delta \pm \sigma$)	Mean differ. (lungs only) ($\Delta \pm \sigma$)
A150	P	1.20	3.06	0.01	2.48	2.81	2.63	2.03±1.08	2.64±0.13
	C	1.28	5.26	1.16	5.56	5.44	5.51	4.03±1.99	5.50±0.05
	Fe	2.58	3.02	2.77	2.20	2.15	2.18	2.48±0.33	2.18±0.02
ED4C (fhw)	P	6.40	2.92	3.80	1.33	1.28	1.31	2.84±1.86	1.31±0.02
	C	0.46	1.31	0.20	1.52	1.39	1.46	1.06±0.52	1.45±0.05
	Fe	0.64	4.80	2.42	0.17	0.01	0.09	1.35±1.75	0.09±0.06
Nylon, Elvamide	P	0.04	5.19	1.48	1.81	2.19	1.98	2.11±1.54	1.99±0.16
	C	0.26	1.65	0.45	3.04	2.81	2.93	1.86±1.15	2.92±0.09
	Fe	1.97	1.19	1.63	1.29	1.55	1.41	1.51±0.26	1.42±0.11
RM/SR4	P	13.51	3.60	10.74	0.06	0.53	0.27	4.78±5.38	0.28±0.19
	C	0.07	2.33	0.91	0.21	0.32	0.26	0.68±0.78	0.26±0.05
	Fe	1.33	0.17	0.83	0.53	1.00	0.75	0.77±0.36	0.76±0.19
Temex	P	20.66	5.99	16.57	1.32	0.82	1.10	7.74±7.97	1.08±0.20
	C	1.93	4.93	3.04	1.83	1.74	1.79	2.54±1.16	1.79±0.04
	Fe	0.79	1.28	0.10	0.53	0.87	0.69	0.71±0.36	0.69±0.14
RW-2	P	30.83	21.76	28.29	0.64	1.84	1.17	14.09±13.16	1.22±0.49
	C	5.29	5.39	5.33	0.79	0.76	0.78	3.05±2.28	0.78±0.01
	Fe	3.49	1.11	2.47	0.83	1.16	0.99	1.67±0.97	0.99±0.14
Ceric Sulfate	P	2.81	6.50	3.84	0.01	0.30	0.14	2.27±2.39	0.15±0.12
	C	3.00	2.69	0.88	0.26	0.20	0.23	1.21±1.18	0.23±0.02
	Fe	0.35	1.40	0.80	0.14	0.29	0.21	0.53±0.44	0.21±0.06
Alderson muscle(B)	P	24.61	5.10	19.16	3.06	2.70	2.90	9.59±8.87	2.88±0.15
	C	4.70	10.27	0.88	3.20	2.96	3.09	4.18±2.94	3.08±0.10
	Fe	0.82	0.84	0.10	0.25	0.55	0.39	0.49±0.27	0.40±0.12
A150 (corrected)	P	12.50	2.57	9.72	0.01	0.43	0.19	4.24±5.00	0.21±0.17
	C	1.09	6.76	1.84	0.30	0.38	0.34	1.78±2.29	0.34±0.03
	Fe	0.00	2.52	1.08	0.56	0.97	0.75	0.98±0.77	0.76±0.17

As shown in Fig. 45, the range of the iron beam is shortest and closer to the boundary between the heart tissue and the blood region, while the carbon beam had the longest range such that most of the particles were stopped inside the blood region. Therefore, the doses of the heart tissue and the blood region by the iron irradiation should be more sensitive by the range straggling and the density differences of materials than them by the carbon beam irradiation. This results in the higher differences of the doses on the heart sections when the iron beam was irradiated, especially on the blood region. This corresponds with the relatively low differences of the doses when the carbon beam was irradiated.

Tables 26-27 show that Ceric sulfate dosimeter solution remains valid as a suitable soft tissue substitute, but the Alderson muscle (B) still showed relatively high differences. This trend corresponds with the results of the mass stopping power comparisons and the depth-dose distributions.

As shown in Table 26, A150 and Nylon (Du Pont Elvamide 8062) exhibited relatively large differences than expected. This is mainly because the dimensions of the phantom were not changed to compensate for the differences in material densities, and thus give the same interaction probabilities. However, the dimensions of the developed phantom could not be corrected here by the amount of thickness that should be corrected using Eq. (9) because the phantom uses the fixed dimensions for the ribs and some outer rib dimensions are larger than the soft tissue dimension that would be under corrected conditions. Even though the density of a soft tissue substitute is close to that of the ICRU-44 tissue and the correction therefore can be done, it is difficult to apply the

correction into the developed phantom in which the shapes and dimensions are complex and irregular. This situation may be same with some anthropomorphic phantom including RANDO phantom which use the real human skeletons and has human-like shapes and dimensions. Namely, the correction can be done only with the phantoms which have the simple geometry and few regions and boundaries. This illustrates the point that choosing a given phantom and replacing the tissue substitutes is an inadequate approach. However, the relatively low differences in Table 27 show that the density differences of the materials are insignificant when the broad beam is used.

For the pencil beams, RM/SR4 and RW-2 have acceptable normalized differences for all concerned regions expect for the right lungs under the proton irradiations. The right lungs of the RM/SR4 and the RW-2 have the normalized differences of 7.19% and 17.78%, respectively, which are much larger than expected. Thus, though RM/SR4 and RW-2 have similar interactions as ICRU-44 tissue from primary interaction, they have slightly different secondary particle characterizations. For the heart, even though the secondary particles may deposit their energies, the effect should be very small compared to that of the primary beams, and it should be insignificant. However, for the right lungs, since the doses do not depend on the direct irradiation of the primary beams, slightly different generation and transport characteristics of the secondary particles within the media of RM/SR4 and RW-2 are significant and are shown in the results. This is similar with the broad beams having dose differences below 2% for the lungs, but relatively large for the heart because only a small portion of the primary beam energy is deposited to the heart and the dose by the

secondary particles became significant. Even so, both are adequately suitable exhibiting values below around 1% for all beams if the mean normalized differences for the main organs only are considered.

In an effort to match the transport interaction probability with ICRU-44 tissue, A150 was simulated again after changing the density itself to 1.03 g/cm^3 instead of changing the phantom's dimensions, referred to as 'A150_corrected'. The simulation result for the pencil beams, shown in Table 26, shows that the A150 is a still suitable soft tissue substitute when it is used after the compensation is made, showing relative differences below 1% for all concerned organs. For the broad beams, as shown in Table 27, since the mean normalized differences for all organ doses were obtained by averaging the differences of all organ doses equally without any weighting into the organ that has higher dose, this indicator produced unexpected results, by not showing notably better results when the correction was made. However, the mean normalized difference for only the main organ (the lungs only in this case) is appropriate as an indicator of performance in the agreement of results.

The suitable soft tissue substitutes obtained by the stopping power comparisons and depth-dose comparisons are still valid for the simulations in the computational phantom with most of them having mean normalized differences below 5% except for a few, such as the A150 and the Nylon (Elvamide), in which their densities need to be corrected and the RW-2 which has slightly different secondary particle transport. A150, Nylon (Elvamide), and even the other soft tissue substitutes will show improved results when the dimensions of phantom are corrected to compensate for density. RW-2 is also

suitable because of its similar interaction properties in comparison to ICRU-44 tissue for the primary beams, but the slightly different generation and transport of secondary particles should be taken account for some studies in which the secondary particles' transports are important.

Overall, RM/SR4 is the best material tested as an anthropomorphic phantom soft tissue substitute because it not only showed very similar interaction properties with ICRU-44 tissue, and phantom dimensions do not need to be corrected because of its density, but it also has the advantage of easy construction and application because of its solid state.

CHAPTER VI

CONCLUSIONS

The study show that PHITS simulations for estimating the stopping power of soft tissue substitutes with HCPs are in agreement with other codes and experimental results. In the results, water which has conventionally been used as a tissue equivalent material had mean normalized differences of $9.22 \pm 2.09\%$ for proton, $9.21 \pm 1.79\%$ for carbon, and $9.10 \pm 1.91\%$ for iron, and thus it is not appropriate as soft tissue substitute. Alderson muscle (A) had the mean normalized differences of $2.69 \pm 1.28\%$ for proton, $2.26 \pm 0.47\%$ for carbon, and $2.21 \pm 0.49\%$ for iron. And Alderson muscle (B) had the $3.04 \pm 1.30\%$ for proton, $2.65 \pm 0.47\%$ for carbon, and $2.60 \pm 0.50\%$ for iron. These differences are acceptable for use of Alderson muscles as the soft tissue substitute by having small differences of mass stopping powers at all energy points compared to ICRU-44 tissue which are below 5% and show similar depth-dose distributions.

However, the simulation results for the other tissue substitutes such as A150 plastic show the opportunity to change the tissue substitute currently used in the RANDO phantom to materials more suited to HCP irradiations to obtain better accuracy in simulating human soft tissue. And thus the MATROSHKA experiments or any experiments related to RANDO phantom will have better experimental results if the Alderson muscle is replaced with a better tissue substitute under the conditions of the specific exposure.

The most suitable tissue substitute among these tissue substitutes is Ceric Sulfate Dosimeter Solution having the normalized % difference of 0.21 ± 0.19 for proton, 0.18 ± 0.12 for carbon, and 0.17 ± 0.13 for iron, and the depth-dose distributions in the solution are almost identical with those of ICRU-44 tissue. In the view of manufacturing a real phantom and its practical use in real world, solution or gel type tissue substitutes may have several additional considerations such as leakage. Therefore, in this context, A150, ED4C (fhw), Nylon (Du Pont Elvamide 8062), RM/SR4, and Temex can be treated as better tissue substitutes by their having the added benefits of molding, machining, and handling during manufacture.

These solid state tissue substitutes have been shown to be good soft tissue substitutes by having normalized differences below 1%. A150 had the differences of 0.79 ± 1.22 for proton, 0.54 ± 0.92 for carbon, and 0.38 ± 0.35 for iron; ED4C (fhw) had the differences of 0.41 ± 0.39 for proton, 0.41 ± 0.14 for carbon, and 0.47 ± 0.17 for iron; Nylon (Du Pont Elvamide 8062) had the differences of 0.85 ± 1.07 for proton, 0.70 ± 0.77 for carbon, and 0.53 ± 0.20 for iron; RM/SR4 had the differences of 0.77 ± 1.18 for proton, 0.34 ± 0.18 for carbon, and 0.33 ± 0.19 for iron; and Temex had the differences of 1.37 ± 1.32 for proton, 0.84 ± 0.41 for carbon, and 0.80 ± 0.36 for iron. Furthermore, all of these solid tissue substitutes had very similar depth-dose distributions and the bragg-peaks occurred within 0.1 cm difference with that of ICRU-44 tissue.

When the suitable soft tissue substitutes were put into the developed phantom and simulated within the computational phantom, they remained valid as surrogates by having the mean normalized differences below 5% except for a few, such as the A150

and the Nylon (Elvamide) for which correction for their densities need to be made, and RW-2 which showed slightly different secondary particle characteristics.

Overall, RM/SR4 is the most suited as an anthropomorphic phantom soft tissue substitute because not only did it show very similar interaction properties when compared to ICRU-44 tissue, but also phantom dimensions do not need to be corrected for density differences and it is a rigid solid polymer giving practical advantages in manufacture of real phantoms.

REFERENCES

[1] International Commission on Radiation Units and measurements (ICRU), "Tissue Substitutes in Radiation Dosimetry and Measurement," ICRU Report 44, 1989.

[2] J. H. Kleck, J. B. Smathers, F. E. Holly, and L. T. Myers, "Anthropomorphic radiation therapy phantoms: a quantitative assessment of tissue substitutes," *Med Phys,* vol. 17, pp. 800-6, Sep-Oct 1990.

[3] G. Reitz and T. Berger, "The MATROSHKA facility--dose determination during an EVA," *Radiat Prot Dosimetry,* vol. 120, pp. 442-5, 2006.

[4] G. T. Chen, J. R. Castro, and J. M. Quivey, "Heavy charged particle radiotherapy," *Annu Rev Biophys Bioeng,* vol. 10, pp. 499-529, 1981.

[5] J. S. Rigden, *Macmillan Encyclopedia of Physics*. New York: Simon & Schuster Macmillan, 1996.

[6] W. S. Snyder, H. L. Fisher, Jr., M. R. Ford, and G. G. Warner, "Estimates of absorbed fractions for monoenergetic photon sources uniformly distributed in various organs of a heterogeneous phantom," *J Nucl Med,* Suppl 3: pp. 7-52, Aug 1969.

[7] Los Alamos National Laboratory, "Criticality Calculations with MCNP5: A Primer," LA-UR-04-0294, Available: http://mcnp-green.lanl.gov/pdf/Criticality PrimerII-release1.pdf

[8] Japan Atomic Energy Agency (JAEA). (13 September 2011). *Overview of PHITS*. Available: http://phits.jaea.go.jp/Overview.html

[9] J. K. Shultis and R. E. Faw, *Radiation Shielding*. La Grange Park, IL: American Nuclear Society, 2000.

[10] G. F. Knoll, *Radiation Detection and Measurement*, 4th ed. Hoboken, N.J.: John Wiley, 2010.

[11] J. E. Turner, *Atoms, Radiation, and Radiation Protection*, 3rd completely rev. and enl. ed. Weinheim: Wiley-VCH, 2007.

[12] Japanese National Institute of Radiological Sciences (NIRS). (2 August 2011). *Human-friendly Cancer Therapy*. Available: http://www.nirs.go.jp/ENG/research /charged_particle/index.shtml

[13] R. R. Wilson, "Radiological use of fast protons," *Radiology,* vol. 47, pp. 487-491, 1946.

[14] M. R. Raju, "Particle radiotherapy: historical developments and current status," *Radiat Res,* vol. 145, pp. 391-407, Apr 1996.

[15] T. Okada, T. Kamada, H. Tsuji, J. Mizoe, M. Baba, *et al.*, "Carbon ion radiotherapy: clinical experiences at National Institute of Radiological Science (NIRS)," *J Radiat Res (Tokyo),* vol. 51, pp. 355-64, 2010.

[16] A. J. Lomax, T. Bortfeld, G. Goitein, J. Debus, C. Dykstra, *et al.*, "A treatment planning inter-comparison of proton and intensity modulated photon radiotherapy," *Radiotherapy and Oncology,* vol. 51, pp. 257-271, Jun 1999.

[17] B. Jones, R. G. Dale, and A. Carabe-Fernandez, "Charged particle therapy for cancer: the inheritance of the Cavendish scientists?," *Appl. Radiat. Isotopes* vol. 67, pp. 371-7, Mar 2009.

[18] The Phantom Laboratory. (10 August 2011). *The RANDO® Phantom, RAN100 and RAN110*. Available: http://www.phantomlab.com/library/pdf/rando_datasheet.pdf

[19] G. Reitz, T. Berger, P. Bilski, R. Facius, M. Hajek, *et al.*, "Astronaut's organ doses inferred from measurements in a human phantom outside the International Space Station," *Radiat Res,* vol. 171, pp. 225-35, Feb 2009.

[20] International Commission on Radiation Units and Measurements (ICRU), "Photon, Electron, Proton and Neutron Interaction Data for Body Tissues," ICRU Report 46, 1992.

[21] H. Q. Woodard and D. R. White, "The composition of body tissues," *Br J Radiol,* vol. 59, pp. 1209-18, Dec 1986.

[22] D. R. White, H. Q. Woodard, and S. M. Hammond, "Average soft-tissue and bone models for use in radiation dosimetry," *Br J Radiol,* vol. 60, pp. 907-13, Sep 1987.

[23] International Commission on Radiological Protection (ICRP), "Report of the Task Group on Reference Man," ICRP Publication 23, 1975.

[24] F. H. Attix, *Introduction to Radiological Physics and Radiation Dosimetry*. New York: Wiley & Sons, 1986.

[25] International Commission on Radiation Units and measurements (ICRU), "Stopping Power and Ranges for Protons and Alpha Particles," ICRU Report 49, 1993.

[26] International Commission on Radiation Units and measurements (ICRU), "Stopping of Ions Heavier Than Helium " ICRU Report 73, 2005.

[27] National Institute of Standards and Technology (NIST). (9 August 2011). *Introduction*. Available: http://physics.nist.gov/PhysRefData/Star/Text/intro.html

[28] J. F. Ziegler, M. D. Ziegler, and J. P. Biersack, "SRIM - The stopping and range of ions in matter (2010)," *Nuclear Instruments and Methods in Physics Research Section B,* vol. 268, pp. 1818-1823, 2010.

[29] H. Paul and A. Schinner, "An empirical approach to the stopping power of solids and gases for ions from $_{3}$Li to $_{18}$Ar," *Nuclear Instruments and Methods in Physics Research B,* vol. 179, pp. 299-315, 2001.

[30] H. Paul, "A comparison of recent stopping power tables for light and medium-heavy ions with experimental data, and applications to radiotherapy dosimetry," *Nuclear Instruments & Methods in Physics Research Section B-Beam Interactions with Materials and Atoms,* vol. 247, pp. 166-172, Jun 2006.

[31] H. Paul and A. Schinner, "Statistical analysis of stopping data for protons and alphas in compounds," *Nuclear Instruments & Methods in Physics Research Section B-Beam Interactions with Materials and Atoms,* vol. 249, pp. 1-5, Aug 2006.

[32] M. Cristy and K. F. Eckerman, "Specific absorbed fractions of energy at various ages from internal photon sources. I. Methods," Oak Ridge National Laboratory ORNL/TM-8381/V1, 1987.

[33] G. Williams, M. Zankl, W. Abmayr, R. Veit, and G. Drexler, "The calculation of dose from external photon exposures using reference and realistic human phantoms and Monte-Carlo methods," *Physics in Medicine and Biology,* vol. 31, pp. 449-452, Apr 1986.

[34] E. Han, "Revised Series of Stylized Anthropometric Phantoms for Internal and External Radiation Dose Assessment," Ph.D. Dissertation, University of Florida, 2005.

[35] International Commission on Radiological Protection (ICRP), "Basic anatomical and physiological data for use in radiological protection reference values," ICRP Publication 89, 2002.

[36] H. Akkurt and K. F. Eckerman, "Development of PIMAL: athematical Phantom with Moving Arms and Legs," Oak Ridge National Laboratory ORNL/TM-2007/14, 2007.

[37] J. R. Lamarsh and A. J. Baratta, *Introduction to Nuclear Engineering*, 3rd ed. Upper Saddle River, N.J.: Prentice Hall, 2001.

[38] L. Sihver*, et al.*, "An update about recent developments of the PHITS code," *Advances in Space Research,* vol. 45, pp. 892-899, Apr 1 2010.

[39] G. D. Badhwar and P. M. O' Neill, "An improved model of GCR for space exploration missions," *Nuclear Tracks and Radiation Measurements,* vol. 20, pp. 403-410, 1992.

[40] H. Paul. (9 September 2011). *Stopping Power for Light Ions*. Available: http://www.exphys.uni-linz.ac.at/Stopping/

[41] M. J. Berger, J. S. Coursey, M. A. Zucker, and J. Chang. (August 17). *Stopping-Power and Range Tables for Electrons, Protons, and Helium Ions*. Available: http://www.nist.gov/pml/data/star/index.cfm

[42] S. Bauk, M. J. Farquharson, D. J. Highgate, and N. M. Spyrou, "Hydrophilic crosslinked copolymers as tissue-equivalent materials for breast cancer detection," *Biol Trace Elem Res,* vol. 71-72, pp. 603-9, Winter 1999.

[43] National Institute of Standards and Technology (NIST). (11 September 2011). *Compositions of materials used in STAR databases,* Available: http://physics.nist.gov/cgi-bin/Star/compos.pl

[44] J. L. Coffey, "A Revised Mathematical Model of the Heart for Use in Radiation Absorbed Dose Calculations," M.S. Thesis, University of Tennessee, Knoxville, 1978.

[45] G. L. de la Grandmaison, I. Clairand, and M. Durigon, "Organ weight in 684 adult autopsies: new tables for a Caucasoid population," *Forensic Sci Int,* vol. 119, pp. 149-54, Jun 15 2001.

[46] M. Mohr, E. Abrams, C. Engel, W. B. Long, and M. Bottlang, "Geometry of human ribs pertinent to orthopedic chest-wall reconstruction," *J Biomech,* vol. 40, pp. 1310-7, 2007.

[47] K. S. Saladin, *Anatomy and Physiology: The Unity of Form and Function*, 5th ed. New York: McGraw-Hill, 2010.

APPENDIX A

PHITS input representing the developed anthropomorphic human phantom. The input deck excludes the parameter, source, and tally sections.

```
[ T i t l e ]
A new anthropomorphic phantom geometry

[ M a t e r i a l ]
m1  1000  -10.5          $ TISSUE, SOFT (ICRU-44)
    6000  -25.6          $ Density(g/cm3) = 1.03
    7000  -2.7
    8000  -60.2
    11000  -0.1
    15000  -0.2
    16000  -0.3
    17000  -0.2
    19000  -0.2

m2  1000  -10.4          $ Heart tissue(healthy)
    6000  -13.9          $ Density(g/cm3) = 1.05
    7000  -2.9
    8000  -71.8
    11000  -0.1
    15000  -0.2
    16000  -0.2
    17000  -0.2
    19000  -0.3

m3  1000  -10.2          $ Blood(whole)
    6000  -11.0          $ Density(g/cm3) = 1.06
    7000  -3.3
    8000  -74.5
    11000  -0.1
    15000  -0.1
    16000  -0.2
    17000  -0.3
    19000  -0.2
    26000  -0.1

m4  1000  -10.3          $ Lung(healthy, inflated)
    6000  -10.5          $ Density(g/cm3) = 0.26
    7000  -3.1
    8000  -74.9
    11000  -0.2
    15000  -0.2
    16000  -0.3
    17000  -0.3
    19000  -0.2

m5  1000  -10.7          $ Brain(whole)
    6000  -14.5          $ Density(g/cm3) = 1.04
    7000  -2.2
    8000  -71.2
    11000  -0.2
    15000  -0.4
    16000  -0.2
    17000  -0.3
```

```
     19000  -0.3

m6   1000  -10.0        $ Skin
     6000  -20.4        $ Density(g/cm3) = 1.09
     7000  -4.2
     8000  -64.5
     11000  -0.2
     15000  -0.1
     16000  -0.2
     17000  -0.3
     19000  -0.1

m7   1000  -5.0         $ Skull(ICRU)
     6000  -21.2        $ Density(g/cm3) = 1.61
     7000  -4.0
     8000  -43.5
     11000  -0.1
     12000  -0.2
     15000  -8.1
     16000  -0.3
     20000  -17.6

m8   1000  -7.0         $ Leg bone
     6000  -34.5        $ Density(g/cm3) = 1.33
     7000  -2.8
     8000  -36.8
     11000  -0.1
     12000  -0.1
     15000  -5.5
     16000  -0.2
     17000  -0.1
     20000  -12.9

m9   1000  -6.0         $ Arm bone
     6000  -31.4        $ Density(g/cm3) = 1.46
     7000  -3.1
     8000  -36.9
     11000  -0.1
     12000  -0.1
     15000  -7.0
     16000  -0.2
     20000  -15.2

m10  1000  -4.6         $ Facial bone
      6000  -19.9       $ Density(g/cm3) = 1.68
      7000  -4.1
      8000  -43.5
      11000  -0.1
      12000  -0.2
      15000  -8.6
      16000  -0.3
      20000  -18.7
```

```
m11  1000  -6.4          $ Ribs (1st - 9th)
     6000  -26.3         $ Density(g/cm3) = 1.41
     7000  -3.9
     8000  -43.6
     11000  -0.1
     12000  -0.1
     15000  -6.0
     16000  -0.3
     17000  -0.1
     19000  -0.1
     20000  -13.1

m12  1000  -5.6          $ Ribs (10th - 12th)
     6000  -23.5         $ Density(g/cm3) = 1.52
     7000  -4.0
     8000  -43.4
     11000  -0.1
     12000  -0.1
     15000  -7.2
     16000  -0.3
     17000  -0.1
     19000  -0.1
     20000  -15.6

m13  1000  -6.3          $ Cervical vertebrae
     6000  -26.1         $ Density(g/cm3) = 1.42
     7000  -3.9
     8000  -43.6
     11000  -0.1
     12000  -0.1
     15000  -6.1
     16000  -0.3
     17000  -0.1
     19000  -0.1
     20000  -13.3

m14  1000  -7.0          $ Thoracic / Lumbal vertebrae
     6000  -28.7         $ Density(g/cm3) = 1.33
     7000  -3.8
     8000  -43.7
     12000  -0.1
     15000  -5.1
     16000  -0.2
     17000  -0.1
     19000  -0.1
     20000  -11.1

m15   1000  -9.6          $ Intervertebral disks
      6000  -9.9         $ Density(g/cm3) = 1.10
      7000  -2.2
      8000  -74.4
      11000  -0.5
      15000  -2.2
```

```
      16000  -0.9
      17000  -0.3

m16   6000  -0.000124          $ AIR, DRY (NEAR SEA LEVEL)
      7000  -0.755267          $ Density(g/cm3) = 1.20479E-03
      8000  -0.231781
      18000  -0.012827


[ S u r f a c e ]
$ LUNG(Left)
100    sq 0.00444444 0.02040816 0.001720426 0 0 0 -1 -2 1 21.79084544
101    px -2
102    pz 21.79084544

$ LUNG(Right)
110    sq 0.00444444 0.02040816 0.001784477 0 0 0 -1 2 1 22.22747566
111    px 2
112    pz 22.22747566

$ Sphere for outside of the heart in the lung(r=5.8cm)
200    s -2 1 31.5 5.8

$ HEART(r=5.762cm)
210    s -2 1 31.5 5.748
211    s -2 1 31.5 4.861  $ Blood inside of the heart

$ SPINE
300    c/z 0 -7.8 2
301    pz 0
302    pz 0.4
303    pz 2.7 $1
304    pz 3.1
305    pz 5.4 $2
306    pz 5.8
307    pz 8.1 $3
308    pz 8.5
309    pz 10.8 $4
310    pz 11.2
311    pz 13.5 $5
312    pz 13.9
313    pz 16.2 $6
314    pz 16.6
315    pz 18.9 $7
316    pz 19.3
317    pz 21.6 $8
318    pz 22.0
319    pz 24.3 $9
320    pz 24.7
321    pz 27.0 $10
322    pz 27.4
323    pz 29.7 $11
324    pz 30.1
```

```
325     pz 32.4 $12
326     pz 32.8
327     pz 35.1 $13
328     pz 35.5
329     pz 37.8 $14
330     pz 38.2
331     pz 40.5 $15
332     pz 40.9
333     pz 43.2 $16
334     pz 43.6
335     pz 45.9 $17
336     pz 46.1
337     pz 47.9 $18
338     pz 48.1
339     pz 49.9 $19
340     pz 50.1
341     pz 51.9 $20
342     pz 52.1
343     pz 53.9 $21
344     pz 54.1
345     pz 55.9 $22
346     pz 56.1
347     pz 57.9 $23
348     pz 58.1
349     pz 59.9 $24

$ RIBS
$ RIB12
400     sq 0.00308642 0.010519395 0 0 0 0 -1 0 0.59 0       $inner
401     sq 0.002878115 0.009263368 0 0 0 0 -1 0 0.59 0      $outer
402     pz 15 $313
480     py -2                                   $for cutting the rib
$ RIB11
403     sq 0.00308642 0.010519395 0 0 0 0 -1 0 0.59 0
404     sq 0.002878115 0.009263368 0 0 0 0 -1 0 0.59 0
405     pz 17.7 $315
490     py 0.55                                 $for cutting the rib
$ RIB10
406     sq 0.00308642 0.010519395 0 0 0 0 -1 0 0.59 0
407     sq 0.002878115 0.009263368 0 0 0 0 -1 0 0.59 0
408     pz 20.4 $317
$ RIB9
409     sq 0.003121945 0.010562685 0 0 0 0 -1 0 0.57 0
410     sq 0.002910096 0.009299134 0 0 0 0 -1 0 0.57 0
411     pz 23.1 $319
$ RIB8
412     sq 0.003233681 0.0107944 0 0 0 0 -1 0 0.475 0
413     sq 0.00300726 0.009471883 0 0 0 0 -1 0 0.475 0
414     pz 25.69 $321
$ RIB7
415     sq 0.003439128 0.01116243 0 0 0 0 -1 0 0.405 0
416     sq 0.003158999 0.009602272 0 0 0 0 -1 0 0.405 0
417     pz 28.42 $323
```

```
$ RIB6
418     sq 0.003729807 0.011574473 0 0 0 0 -1 0 0.255 0
419     sq 0.003406266 0.009890901 0 0 0 0 -1 0 0.255 0
420     pz 31.22 $325
$ RIB5
421     sq 0.00421031 0.011996607 0 0 0 0 -1 0 0.05 0
422     sq 0.003842857 0.010306888 0 0 0 0 -1 0 0.05 0
423     pz 33.96 $327
$ RIB4
424     sq 0.004827003 0.012667331 0 0 0 0 -1 0 -0.235 0
425     sq 0.004401307 0.010930249 0 0 0 0 -1 0 -0.235 0
426     pz 36.64 $329
$ RIB3
427     sq 0.006026361 0.013679423 0 0 0 0 -1 0 -0.65 0
428     sq 0.005501892 0.01194422 0 0 0 0 -1 0 -0.65 0
429     pz 39.37 $331
$ RIB2
430     sq 0.008361921 0.015431503 0 0 0 0 -1 0 -1.15 0
431     sq 0.007514695 0.013364964 0 0 0 0 -1 0 -1.15 0
432     pz 42.07 $333
$ RIB1
433     sq 0.018032466 0.019837334 0 0 0 0 -1 0 -2.1 0
434     sq 0.015443598 0.016866251 0 0 0 0 -1 0 -2.1 0
435     pz 44.77 $335

$ STERNUM
450     sq 0.00444444 0.02040816 0.001609643 0 0 0 -1 0 4 21.8
451     sq 0.00444444 0.02040816 0.001609643 0 0 0 -1 0 3 21.8
452     px -2
453     px 2
454     pz 25.6
455     pz 46.2
456     py 0

$ NECK
500     RCC 0 -6.5 48 0 0 8 5
$SKIN of the Neck
501     RCC 0 -6.5 48 0 0 8 5.2045

$ HEAD, FACE
600     sq 0.020408163 0.01384083 0.031956196 0 0 0 -1 0 -2 66.266   $ inner
601     sq 0.015625 0.011080332 0.022998638 0 0 0 -1 0 -2 66.266     $ outer
602     sq 0.020408163 0.01384083 0 0 0 0 -1 0 -2 0                  $inner cylinder
603     sq 0.015625 0.011080332 0 0 0 0 -1 0 -2 0                    $outer cylinder
604     pz 56
605     pz 66.266
606     py -0.605

$ SKIN of the Head
608     sq 0.01485579 0.010618268 0.021635842 0 0 0 -1 0 -2 66.266     $outer
609     sq 0.01485579 0.010618268 0 0 0 0 -1 0 -2 0                    $outer cylinder
610     pz 55.7955
```

```
$ ARM(Left)
700     RCC -25.3290 0 -12 0 0 30 4     $Fore
701     RCC -25.3290 0 18 0 0 30 5      $Upper
$ ARM Bone(Left)
702     RCC -25.3290 0 -12 0 0 30 3     $Fore
703     RCC -25.3290 0 18 0 0 30 3      $Upper
$ ARM(Right)
704     RCC 25.3290 0 -12 0 0 30 4      $Fore
705     RCC 25.3290 0 18 0 0 30 5       $Upper
$ ARM Bone(Right)
706     RCC 25.3290 0 -12 0 0 30 3      $Fore
707     RCC 25.3290 0 18 0 0 30 3       $Upper

$ SKIN of Arms
$Fore
708     RCC -25.3290 0 -12.1290 0 0 30.1290 4.1290    $Left
709     RCC 25.3290 0 -12.1290 0 0 30.1290 4.1290     $Right

$Upper
710     RCC -25.3290 0 18 0 0 30.1245 5.1245        $Left
711     RCC 25.3290 0 18 0 0 30.1245 5.1245         $Right

$ LEG(Left)
800     RCC -11 0 -103.14 0 0 50.035 8   $Lower
801     RCC -11 0 -53.105 0 0 50.035 9   $Thigh
$ LEG Bone(Left)
802     RCC -11 0 -103.14 0 0 50.035 5   $Lower
803     RCC -11 0 -53.105 0 0 50.035 5   $Thigh
$ LEG(Right)
804     RCC 11 0 -103.14 0 0 50.035 8   $Lower
805     RCC 11 0 -53.105 0 0 50.035 9   $Thigh
$ LEG Bone(Right)
806     RCC 11 0 -103.14 0 0 50.035 5   $Lower
807     RCC 11 0 -53.105 0 0 50.035 5   $Thigh

$ SKIN of legs
$ Lower
808     RCC -11 0 -103.269 0 0 50.164 8.1290    $Left
809     RCC 11 0 -103.269 0 0 50.164 8.1290     $Right

$ Thigh
810     RCC -11 0 -53.105 0 0 50.035 9.1245     $Left
811     RCC 11 0 -53.105 0 0 50.035 9.1245      $Right

$ TRUNK
900     sq 0.0025 0.00756144 0 0 0 0 -1 0 0 0
901     pz -3.07
902     pz 48

$ SKIN of Trunk
903     sq 0.002449649 0.007299523 0 0 0 0 -1 0 0 0
904     pz -3.2745
905     pz 48.2045
```

```
$ Outer boundary
990     so 2000


[ C e l l ]
$ Lung(Left)
100    4 -0.26 -100 -101 102 200
$ Lung(Right)
101    4 -0.26 -110 111 112 200

$ Heart
200    2 -1.05 -210 211   $heart tissue
201    3 -1.06 -211       $blood

$ Spine
300     15 -1.10 -300 301 -302   $Disc 24
301     14 -1.33 -300 302 -303   $Vertebrae lumbale 5
302     15 -1.10 -300 303 -304   $Disc 23
303     14 -1.33 -300 304 -305   $Vertebrae lumbale 4
304     15 -1.10 -300 305 -306   $Disc 22
305     14 -1.33 -300 306 -307   $Vertebrae lumbale 3
306     15 -1.10 -300 307 -308   $Disc 21
307     14 -1.33 -300 308 -309   $Vertebrae lumbale 2
308     15 -1.10 -300 309 -310   $Disc 20
309     14 -1.33 -300 310 -311   $Vertebrae lumbale 1
310     15 -1.10 -300 311 -312   $Disc 19
311     14 -1.33 -300 312 -313   $Thoracic vertebrae 2
312     15 -1.10 -300 313 -314   $Disc 18
313     14 -1.33 -300 314 -315   $Thoracic vertebrae 11
314     15 -1.10 -300 315 -316   $Disc 17
315     14 -1.33 -300 316 -317   $Thoracic vertebrae 10
316     15 -1.10 -300 317 -318   $Disc 16
317     14 -1.33 -300 318 -319   $Thoracic vertebrae 9
318     15 -1.10 -300 319 -320   $Disc 15
319     14 -1.33 -300 320 -321   $Thoracic vertebrae 8
320     15 -1.10 -300 321 -322   $Disc 14
321     14 -1.33 -300 322 -323   $Thoracic vertebrae 7
322     15 -1.10 -300 323 -324   $Disc 13
323     14 -1.33 -300 324 -325   $Thoracic vertebrae 6
324     15 -1.10 -300 325 -326   $Disc 12
325     14 -1.33 -300 326 -327   $Thoracic vertebrae 5
326     15 -1.10 -300 327 -328   $Disc 11
327     14 -1.33 -300 328 -329   $Thoracic vertebrae 4
328     15 -1.10 -300 329 -330   $Disc 10
329     14 -1.33 -300 330 -331   $Thoracic vertebrae 3
330     15 -1.10 -300 331 -332   $Disc 9
331     14 -1.33 -300 332 -333   $Thoracic vertebrae 2
332     15 -1.10 -300 333 -334   $Disc 8
333     14 -1.33 -300 334 -335   $Thoracic vertebrae 1
334     15 -1.10 -300 335 -336   $Disc 7
335     13 -1.42 -300 336 -337   $Cervical vertebrae 7
336     15 -1.10 -300 337 -338   $Disc 6
```

```
337    13 -1.42 -300 338 -339   $Cervical vertebrae 6
338    15 -1.10 -300 339 -340   $Disc 5
339    13 -1.42 -300 340 -341   $Cervical vertebrae 5
340    15 -1.10 -300 341 -342   $Disc 4
341    13 -1.42 -300 342 -343   $Cervical vertebrae 4
342    15 -1.10 -300 343 -344   $Disc 3
343    13 -1.42 -300 344 -345   $Cervical vertebrae 3
344    15 -1.10 -300 345 -346   $Disc 2
345    13 -1.42 -300 346 -347   $Cervical vertebrae 2
346    15 -1.10 -300 347 -348   $Disc 1
347    13 -1.42 -300 348 -349   $Cervical vertebrae 1

$ RIB CAGE
400    12 -1.52 300 400 -401 402 -313 -480  $Rib12
401    12 -1.52 300 403 -404 405 -315 -490  $Rib11
402    12 -1.52 300 406 -407 408 -317       $Rib10
403    11 -1.41 300 409 -410 411 -319       $Rib9
404    11 -1.41 300 412 -413 414 -321       $Rib8
405    11 -1.41 300 415 -416 417 -323       $Rib7
406    11 -1.41 300 418 -419 420 -325       $Rib6
407    11 -1.41 300 421 -422 423 -327       $Rib5
408    11 -1.41 300 424 -425 426 -329       $Rib4
409    11 -1.41 300 427 -428 429 -331       $Rib3
410    11 -1.41 300 430 -431 432 -333       $Rib2
411    11 -1.41 300 433 -434 435 -335       $Rib1

$ STERNUM
450    11 -1.41 -450 451 452 -453 454 -455 456

$ NECK
500    1 -1.03 -500 #335 #336 #337 #338 #339 #340
           #341 #342 #343 #344 #345 #346 #347
501    6 -1.09 500 -501                $Neck skin

$ HEAD&FACE
600    7 -1.61 600 -601                                                    $SKULL
601    5 -1.04 -600                                                       $ Brain
602   10 -1.68 602 -603 -605 604 606 #600                                 $ Facial bone
603    1 -1.03 -603 -605 604 #600 #601 #602 #344 #345 #346 #347           $Soft tissue
604    6 -1.09 -608 601 605                                               $ Head skin
605    6 -1.09 -609 603 604 -605                                          $ Face skin
606    6 -1.09 -609 -604 610 #344 #345 #346 #347 #500 #501          $Lower face skin

$ ARMS,LEGS
$ ARMS
700    1 -1.03 -700 702      $ Lower Left arm soft tissue
701    1 -1.03 -701 703      $ Upper Left arm soft tissue
702    9 -1.46 -702          $ Lowr Left arm bone
703    9 -1.46 -703          $ Upper Left arm bone
704    1 -1.03 -704 706      $ Lower Right arm soft tissue
705    1 -1.03 -705 707      $ Upper Right arm soft tissue
706    9 -1.46 -706          $ Lower Right arm bone
707    9 -1.46 -707          $ Upper Right arm bone
```

```
$ Skin of arms
708     6 -1.09 700 -708     $Lower, left
709     6 -1.09 704 -709     $Lower, right
710     6 -1.09 701 -710     $Upper, left
711     6 -1.09 705 -711     $Upper, right

$ LEGS
800     1 -1.03 -800 802    $ Lower Left leg soft tissue
801     1 -1.03 -801 803    $ Upper Left leg soft tissue
802     8 -1.33 -802        $ Lowr Left leg bone
803     8 -1.33 -803        $ Upper Left leg bone
804     1 -1.03 -804 806    $ Lower Right leg soft tissue
805     1 -1.03 -805 807    $ Upper Right leg soft tissue
806     8 -1.33 -806        $ Lower Right leg bone
807     8 -1.33 -807        $ Upper Right leg bone

$ Skin of legs
808     6 -1.09 800 -808    $Lower, left
809     6 -1.09 804 -809    $Lower, right
810     6 -1.09 801 -810    $Upper, left
811     6 -1.09 805 -811    $Upper, right

$ TRUNK
900     1 -1.03 -900 901 -902 #100 #101 #200 #201 #300 #301 #302 #303 #304 #305
                              #306 #307 #308 #309 #310 #311 #312 #313 #314 #315
                              #316 #317 #318 #319 #320 #321 #322 #323 #324 #325
                              #326 #327 #328 #329 #330 #331 #332 #333 #334 #335
                              #336 #337 #338 #339 #340 #341 #342 #343 #344 #345
                              #346 #347 #400 #401 #402 #403 #404 #405 #406 #407
                              #408 #409 #410 #411 #450

$ Skin of trunk
901     6 -1.09 900 -903 901 -902
902     6 -1.09 -903 904 -901 #801 #803 #805 #807 #810 #811
903     6 -1.09 -903 902 -905 #344 #345 #346 #347 #500 #501

$ Vaccuum (Or the Air)
990     0 -990 #100 #101 #200 #201 #300 #301 #302 #303 #304 #305 #306 #307 #308
               #309 #310 #311 #312 #313 #314 #315 #316 #317 #318 #319 #320 #321
               #322 #323 #324 #325 #326 #327 #328 #329 #330 #331 #332 #333 #334
               #335 #336 #337 #338 #339 #340 #341 #342 #343 #344 #345 #346 #347
               #400 #401 #402 #403 #404 #405 #406 #407 #408 #409 #410 #411 #450
               #500 #501 #600 #601 #602 #603 #604 #605 #606 #700 #701 #702 #703
               #704 #705 #706 #707 #708 #709 #710 #711 #800 #801 #802 #803 #804
               #805 #806 #807 #808 #809 #810 #811 #900 #901 #902 #903

$ Outer universe
999     -1 #990

[END]
```

APPENDIX B

The interaction data (mass stopping power) for ICRU-44 tissue and the soft tissue substitutes of interest.

TABLE B. 1
Mass stopping powers of ICRU-44 tissue for the proton, the carbon, and the iron beams. (MeV-cm^2/g)

Energy (MeV/u)	Proton	Carbon	Iron
1	3.54E+02 ± 3.54E-02	8.21E+03 ± 8.21E-01	5.23E+04 ± 5.23E+00
2	1.91E+02 ± 3.83E-02	5.63E+03 ± 5.63E-01	4.61E+04 ± 4.61E+00
3	1.39E+02 ± 2.77E-02	4.41E+03 ± 4.41E-01	4.22E+04 ± 4.22E+00
4	1.09E+02 ± 3.27E-02	3.62E+03 ± 7.23E-01	3.87E+04 ± 3.87E+00
5	9.19E+01 ± 2.76E-02	3.12E+03 ± 6.24E-01	3.61E+04 ± 3.61E+00
6	7.90E+01 ± 3.16E-02	2.74E+03 ± 5.48E-01	3.36E+04 ± 3.36E+00
7	7.04E+01 ± 2.81E-02	2.44E+03 ± 4.89E-01	3.17E+04 ± 3.17E+00
8	6.36E+01 ± 3.18E-02	2.20E+03 ± 6.59E-01	3.00E+04 ± 3.00E+00
9	5.78E+01 ± 3.47E-02	2.00E+03 ± 6.01E-01	2.76E+04 ± 2.76E+00
10	5.31E+01 ± 3.72E-02	1.83E+03 ± 5.49E-01	2.66E+04 ± 2.66E+00
20	2.95E+01 ± 5.60E-02	1.05E+03 ± 6.32E-01	1.79E+04 ± 1.79E+00
30	2.12E+01 ± 8.05E-02	7.65E+02 ± 6.12E-01	1.35E+04 ± 2.70E+00
40	1.68E+01 ± 3.85E-02	6.03E+02 ± 6.03E-01	1.08E+04 ± 2.16E+00
50	1.40E+01 ± 3.07E-02	5.10E+02 ± 6.64E-01	9.14E+03 ± 2.74E+00
60	1.21E+01 ± 3.87E-02	4.44E+02 ± 6.65E-01	7.95E+03 ± 2.38E+00
70	1.07E+01 ± 4.51E-02	3.87E+02 ± 5.80E-01	7.11E+03 ± 2.13E+00
80	9.70E+00 ± 5.04E-02	3.47E+02 ± 5.55E-01	6.48E+03 ± 2.59E+00
90	8.91E+00 ± 5.70E-02	3.18E+02 ± 5.73E-01	5.93E+03 ± 2.37E+00
100	8.22E+00 ± 6.33E-02	2.94E+02 ± 5.87E-01	5.46E+03 ± 2.73E+00
120	7.15E+00 ± 3.29E-02	2.57E+02 ± 5.65E-01	4.78E+03 ± 2.39E+00
140	6.36E+00 ± 2.99E-02	2.29E+02 ± 5.73E-01	4.30E+03 ± 2.58E+00
160	5.84E+00 ± 3.21E-02	2.09E+02 ± 5.64E-01	3.89E+03 ± 2.73E+00
180	5.39E+00 ± 3.12E-02	1.93E+02 ± 5.78E-01	3.62E+03 ± 2.53E+00
200	4.99E+00 ± 3.05E-02	1.79E+02 ± 5.73E-01	3.37E+03 ± 2.70E+00
250	4.34E+00 ± 3.13E-02	1.56E+02 ± 5.92E-01	2.92E+03 ± 3.21E+00
300	3.93E+00 ± 3.22E-02	1.41E+02 ± 6.21E-01	2.69E+03 ± 2.96E+00
350	3.58E+00 ± 3.15E-02	1.29E+02 ± 6.19E-01	2.46E+03 ± 2.95E+00
400	3.38E+00 ± 3.45E-02	1.20E+02 ± 6.26E-01	2.29E+03 ± 2.74E+00
450	3.19E+00 ± 3.35E-02	1.14E+02 ± 6.39E-01	2.15E+03 ± 2.80E+00
500	3.02E+00 ± 3.32E-02	1.08E+02 ± 6.27E-01	2.05E+03 ± 2.86E+00
600	2.84E+00 ± 4.26E-02	1.01E+02 ± 6.25E-01	1.92E+03 ± 2.88E+00
700	2.63E+00 ± 3.21E-02	9.46E+01 ± 6.44E-01	1.81E+03 ± 3.07E+00
800	2.53E+00 ± 3.32E-02	9.13E+01 ± 6.85E-01	1.74E+03 ± 3.13E+00
900	2.47E+00 ± 3.65E-02	8.90E+01 ± 7.47E-01	1.69E+03 ± 3.38E+00
1000	2.39E+00 ± 3.82E-02	8.64E+01 ± 7.95E-01	1.64E+03 ± 3.44E+00
1500	2.27E+00 ± 4.94E-02	8.18E+01 ± 9.17E-01	1.55E+03 ± 4.03E+00
2000	2.33E+00 ± 8.26E-02	8.07E+01 ± 1.24E+00	1.51E+03 ± 4.99E+00
2500	2.27E+00 ± 7.59E-02	8.01E+01 ± 1.36E+00	1.51E+03 ± 5.72E+00
3000	2.30E+00 ± 8.66E-02	8.15E+01 ± 1.59E+00	1.52E+03 ± 6.39E+00
3500	2.32E+00 ± 1.06E-01	8.07E+01 ± 1.70E+00	1.51E+03 ± 7.08E+00
4000	2.31E+00 ± 1.05E-01	8.09E+01 ± 1.94E+00	1.50E+03 ± 7.51E+00
4500	2.34E+00 ± 1.17E-01	8.04E+01 ± 1.93E+00	1.50E+03 ± 7.79E+00
5000	2.33E+00 ± 1.19E-01	8.09E+01 ± 2.37E+00	1.50E+03 ± 8.83E+00
6000	2.28E+00 ± 1.04E-01	8.07E+01 ± 2.36E+00	1.52E+03 ± 1.11E+01
7000	2.40E+00 ± 1.86E-01	8.25E+01 ± 3.44E+00	1.53E+03 ± 1.30E+01
8000	2.25E+00 ± 1.03E-01	8.24E+01 ± 3.43E+00	1.54E+03 ± 1.43E+01
9000	2.24E+00 ± 1.02E-01	8.61E+01 ± 5.19E+00	1.54E+03 ± 1.46E+01
10000	2.24E+00 ± 1.03E-01	8.58E+01 ± 5.18E+00	1.55E+03 ± 1.72E+01

TABLE B. 2
Mass stopping powers of A150 tissue equivalent plastic for the proton, the carbon, and the iron beams. (MeV-cm^2/g)

Energy (MeV/u)	Proton	Carbon	Iron
1	3.53E+02 ± 3.53E-02	8.20E+03 ± 8.20E-01	5.21E+04 ± 5.21E+00
2	1.91E+02 ± 3.82E-02	5.63E+03 ± 5.63E-01	4.61E+04 ± 4.61E+00
3	1.38E+02 ± 2.77E-02	4.40E+03 ± 4.40E-01	4.22E+04 ± 4.22E+00
4	1.09E+02 ± 3.26E-02	3.61E+03 ± 7.22E-01	3.87E+04 ± 3.87E+00
5	9.16E+01 ± 2.75E-02	3.11E+03 ± 6.22E-01	3.60E+04 ± 3.60E+00
6	7.88E+01 ± 3.15E-02	2.73E+03 ± 5.47E-01	3.35E+04 ± 3.35E+00
7	7.00E+01 ± 3.50E-02	2.44E+03 ± 4.88E-01	3.17E+04 ± 3.17E+00
8	6.35E+01 ± 3.81E-02	2.20E+03 ± 4.40E-01	3.00E+04 ± 3.00E+00
9	5.80E+01 ± 4.06E-02	2.02E+03 ± 6.05E-01	2.78E+04 ± 2.78E+00
10	5.35E+01 ± 4.28E-02	1.84E+03 ± 5.53E-01	2.68E+04 ± 2.68E+00
20	2.96E+01 ± 3.25E-02	1.06E+03 ± 5.30E-01	1.80E+04 ± 1.80E+00
30	2.13E+01 ± 4.89E-02	7.68E+02 ± 5.38E-01	1.35E+04 ± 2.71E+00
40	1.69E+01 ± 9.32E-02	6.04E+02 ± 5.43E-01	1.08E+04 ± 2.16E+00
50	1.40E+01 ± 3.09E-02	5.11E+02 ± 6.13E-01	9.17E+03 ± 2.75E+00
60	1.22E+01 ± 6.71E-02	4.45E+02 ± 6.23E-01	7.98E+03 ± 2.39E+00
70	1.07E+01 ± 2.90E-02	3.89E+02 ± 5.44E-01	7.14E+03 ± 2.14E+00
80	9.72E+00 ± 4.08E-02	3.48E+02 ± 5.23E-01	6.48E+03 ± 2.59E+00
90	8.87E+00 ± 3.02E-02	3.16E+02 ± 5.06E-01	5.94E+03 ± 2.38E+00
100	8.19E+00 ± 3.03E-02	2.94E+02 ± 5.59E-01	5.48E+03 ± 2.74E+00
120	7.16E+00 ± 2.94E-02	2.57E+02 ± 5.40E-01	4.76E+03 ± 2.38E+00
140	6.38E+00 ± 2.87E-02	2.30E+02 ± 5.51E-01	4.32E+03 ± 2.59E+00
160	5.85E+00 ± 2.98E-02	2.09E+02 ± 5.44E-01	3.90E+03 ± 2.34E+00
180	5.40E+00 ± 2.97E-02	1.93E+02 ± 5.41E-01	3.62E+03 ± 2.53E+00
200	5.00E+00 ± 2.90E-02	1.79E+02 ± 5.56E-01	3.37E+03 ± 2.70E+00
250	4.35E+00 ± 3.00E-02	1.56E+02 ± 5.61E-01	2.92E+03 ± 2.92E+00
300	3.93E+00 ± 3.07E-02	1.41E+02 ± 5.78E-01	2.67E+03 ± 2.93E+00
350	3.59E+00 ± 3.01E-02	1.29E+02 ± 5.94E-01	2.46E+03 ± 2.96E+00
400	3.38E+00 ± 3.28E-02	1.21E+02 ± 5.91E-01	2.29E+03 ± 2.75E+00
450	3.20E+00 ± 3.33E-02	1.14E+02 ± 6.05E-01	2.16E+03 ± 2.59E+00
500	3.03E+00 ± 3.21E-02	1.08E+02 ± 6.07E-01	2.05E+03 ± 2.66E+00
600	2.82E+00 ± 3.21E-02	1.01E+02 ± 6.17E-01	1.92E+03 ± 2.88E+00
700	2.63E+00 ± 2.99E-02	9.47E+01 ± 6.06E-01	1.81E+03 ± 2.89E+00
800	2.54E+00 ± 3.30E-02	9.14E+01 ± 6.58E-01	1.74E+03 ± 2.96E+00
900	2.45E+00 ± 3.16E-02	8.90E+01 ± 7.03E-01	1.69E+03 ± 3.21E+00
1000	2.38E+00 ± 3.53E-02	8.65E+01 ± 7.61E-01	1.64E+03 ± 3.28E+00
1500	2.23E+00 ± 3.75E-02	8.21E+01 ± 9.12E-01	1.55E+03 ± 3.87E+00
2000	2.27E+00 ± 6.89E-02	8.06E+01 ± 1.18E+00	1.51E+03 ± 4.68E+00
2500	2.26E+00 ± 7.34E-02	7.99E+01 ± 1.27E+00	1.51E+03 ± 5.57E+00
3000	2.28E+00 ± 8.61E-02	8.10E+01 ± 1.58E+00	1.51E+03 ± 6.18E+00
3500	2.30E+00 ± 1.05E-01	8.02E+01 ± 1.69E+00	1.49E+03 ± 6.87E+00
4000	2.28E+00 ± 1.04E-01	7.94E+01 ± 1.68E+00	1.49E+03 ± 7.29E+00
4500	2.27E+00 ± 1.03E-01	7.99E+01 ± 1.92E+00	1.48E+03 ± 7.57E+00
5000	2.25E+00 ± 1.03E-01	7.90E+01 ± 1.89E+00	1.48E+03 ± 8.29E+00
6000	2.24E+00 ± 1.02E-01	8.02E+01 ± 2.34E+00	1.50E+03 ± 1.04E+01
7000	2.22E+00 ± 1.02E-01	7.95E+01 ± 2.33E+00	1.51E+03 ± 1.24E+01
8000	2.22E+00 ± 1.01E-01	8.18E+01 ± 3.40E+00	1.52E+03 ± 1.39E+01
9000	2.22E+00 ± 1.01E-01	8.17E+01 ± 3.40E+00	1.53E+03 ± 1.45E+01
10000	2.21E+00 ± 1.01E-01	8.52E+01 ± 5.15E+00	1.53E+03 ± 1.56E+01

TABLE B. 3
Mass stopping powers of Acrylic (PMMA) for the proton, the carbon, and the iron beams. (MeV-cm^2/g)

Energy (MeV/u)	Proton	Carbon	Iron
1	3.36E+02 ± 3.36E-02	7.76E+03 ± 7.76E-01	4.93E+04 ± 4.93E+00
2	1.81E+02 ± 3.62E-02	5.33E+03 ± 5.33E-01	4.37E+04 ± 4.37E+00
3	1.31E+02 ± 2.63E-02	4.16E+03 ± 4.16E-01	4.00E+04 ± 4.00E+00
4	1.03E+02 ± 3.08E-02	3.42E+03 ± 6.83E-01	3.66E+04 ± 3.66E+00
5	8.67E+01 ± 2.60E-02	2.94E+03 ± 5.89E-01	3.40E+04 ± 3.40E+00
6	7.46E+01 ± 2.98E-02	2.59E+03 ± 5.17E-01	3.17E+04 ± 3.17E+00
7	6.63E+01 ± 3.31E-02	2.31E+03 ± 4.62E-01	3.00E+04 ± 3.00E+00
8	6.02E+01 ± 3.61E-02	2.09E+03 ± 6.28E-01	2.85E+04 ± 2.85E+00
9	5.53E+01 ± 3.87E-02	1.92E+03 ± 5.77E-01	2.65E+04 ± 2.65E+00
10	5.11E+01 ± 4.09E-02	1.76E+03 ± 5.27E-01	2.56E+04 ± 2.56E+00
20	2.83E+01 ± 5.10E-02	1.01E+03 ± 5.07E-01	1.72E+04 ± 1.72E+00
30	2.04E+01 ± 7.95E-02	7.35E+02 ± 5.88E-01	1.30E+04 ± 2.59E+00
40	1.62E+01 ± 7.61E-02	5.78E+02 ± 5.20E-01	1.04E+04 ± 2.07E+00
50	1.35E+01 ± 6.34E-02	4.89E+02 ± 5.87E-01	8.78E+03 ± 2.63E+00
60	1.17E+01 ± 6.43E-02	4.27E+02 ± 5.97E-01	7.64E+03 ± 2.29E+00
70	1.03E+01 ± 2.78E-02	3.73E+02 ± 5.59E-01	6.84E+03 ± 2.05E+00
80	9.33E+00 ± 4.01E-02	3.34E+02 ± 5.01E-01	6.21E+03 ± 2.48E+00
90	8.51E+00 ± 2.89E-02	3.03E+02 ± 4.85E-01	5.70E+03 ± 2.28E+00
100	7.89E+00 ± 5.68E-02	2.82E+02 ± 5.36E-01	5.25E+03 ± 2.63E+00
120	6.88E+00 ± 3.24E-02	2.47E+02 ± 5.18E-01	4.56E+03 ± 2.28E+00
140	6.12E+00 ± 2.82E-02	2.20E+02 ± 5.29E-01	4.15E+03 ± 2.49E+00
160	5.62E+00 ± 2.92E-02	2.01E+02 ± 5.22E-01	3.75E+03 ± 2.25E+00
180	5.19E+00 ± 2.90E-02	1.85E+02 ± 5.19E-01	3.47E+03 ± 2.43E+00
200	4.80E+00 ± 2.79E-02	1.72E+02 ± 5.34E-01	3.23E+03 ± 2.59E+00
250	4.18E+00 ± 2.93E-02	1.50E+02 ± 5.39E-01	2.81E+03 ± 2.81E+00
300	3.78E+00 ± 2.99E-02	1.35E+02 ± 5.55E-01	2.56E+03 ± 2.82E+00
350	3.44E+00 ± 2.85E-02	1.24E+02 ± 5.71E-01	2.37E+03 ± 2.84E+00
400	3.25E+00 ± 3.19E-02	1.16E+02 ± 5.79E-01	2.20E+03 ± 2.64E+00
450	3.08E+00 ± 3.23E-02	1.10E+02 ± 5.93E-01	2.08E+03 ± 2.70E+00
500	2.91E+00 ± 3.11E-02	1.04E+02 ± 5.94E-01	1.97E+03 ± 2.56E+00
600	2.71E+00 ± 3.12E-02	9.73E+01 ± 5.93E-01	1.84E+03 ± 2.77E+00
700	2.53E+00 ± 2.91E-02	9.11E+01 ± 5.83E-01	1.74E+03 ± 2.78E+00
800	2.44E+00 ± 3.20E-02	8.79E+01 ± 6.33E-01	1.67E+03 ± 2.85E+00
900	2.36E+00 ± 3.06E-02	8.56E+01 ± 6.85E-01	1.62E+03 ± 3.09E+00
1000	2.29E+00 ± 3.39E-02	8.31E+01 ± 7.31E-01	1.58E+03 ± 3.15E+00
1500	2.15E+00 ± 3.60E-02	7.91E+01 ± 8.86E-01	1.49E+03 ± 3.73E+00
2000	2.19E+00 ± 6.67E-02	7.76E+01 ± 1.16E+00	1.45E+03 ± 4.50E+00
2500	2.18E+00 ± 7.14E-02	7.70E+01 ± 1.24E+00	1.45E+03 ± 5.36E+00
3000	2.22E+00 ± 8.36E-02	7.87E+01 ± 1.53E+00	1.46E+03 ± 5.85E+00
3500	2.24E+00 ± 1.02E-01	7.79E+01 ± 1.64E+00	1.45E+03 ± 6.53E+00
4000	2.22E+00 ± 1.01E-01	7.72E+01 ± 1.63E+00	1.45E+03 ± 7.08E+00
4500	2.20E+00 ± 1.01E-01	7.76E+01 ± 1.86E+00	1.44E+03 ± 7.35E+00
5000	2.19E+00 ± 1.00E-01	7.68E+01 ± 1.84E+00	1.44E+03 ± 7.91E+00
6000	2.18E+00 ± 9.93E-02	7.79E+01 ± 2.28E+00	1.46E+03 ± 9.92E+00
7000	2.16E+00 ± 9.89E-02	7.72E+01 ± 2.26E+00	1.47E+03 ± 1.20E+01
8000	2.16E+00 ± 9.86E-02	7.95E+01 ± 3.31E+00	1.48E+03 ± 1.33E+01
9000	2.15E+00 ± 9.84E-02	7.94E+01 ± 3.30E+00	1.48E+03 ± 1.41E+01
10000	2.14E+00 ± 9.82E-02	8.28E+01 ± 5.00E+00	1.49E+03 ± 1.52E+01

TABLE B. 4
Mass stopping powers of Alderson muscle (A) for the proton, the carbon, and the iron beams. (MeV-cm^2/g)

Energy (MeV/u)	Proton	Carbon	Iron
1	3.40E+02 ± 3.40E-02	7.92E+03 ± 7.92E-01	5.05E+04 ± 5.05E+00
2	1.85E+02 ± 3.70E-02	5.45E+03 ± 5.45E-01	4.46E+04 ± 4.46E+00
3	1.33E+02 ± 2.66E-02	4.27E+03 ± 4.27E-01	4.08E+04 ± 4.08E+00
4	1.05E+02 ± 3.16E-02	3.50E+03 ± 7.00E-01	3.75E+04 ± 3.75E+00
5	8.88E+01 ± 3.55E-02	3.02E+03 ± 6.04E-01	3.49E+04 ± 3.49E+00
6	7.65E+01 ± 3.06E-02	2.65E+03 ± 5.31E-01	3.25E+04 ± 3.25E+00
7	6.83E+01 ± 3.41E-02	2.37E+03 ± 4.73E-01	3.08E+04 ± 3.08E+00
8	6.20E+01 ± 3.72E-02	2.14E+03 ± 6.42E-01	2.91E+04 ± 2.91E+00
9	5.67E+01 ± 4.54E-02	1.96E+03 ± 5.89E-01	2.71E+04 ± 2.71E+00
10	5.09E+01 ± 4.58E-02	1.80E+03 ± 5.39E-01	2.61E+04 ± 2.61E+00
20	2.89E+01 ± 5.78E-02	1.03E+03 ± 6.18E-01	1.75E+04 ± 1.75E+00
30	2.08E+01 ± 8.31E-02	7.49E+02 ± 5.99E-01	1.32E+04 ± 2.64E+00
40	1.65E+01 ± 7.25E-02	5.91E+02 ± 5.91E-01	1.06E+04 ± 2.11E+00
50	1.38E+01 ± 7.29E-02	5.01E+02 ± 6.51E-01	8.95E+03 ± 2.69E+00
60	1.19E+01 ± 7.39E-02	4.34E+02 ± 6.51E-01	7.78E+03 ± 2.34E+00
70	1.05E+01 ± 3.04E-02	3.79E+02 ± 5.68E-01	7.04E+03 ± 2.82E+00
80	9.51E+00 ± 4.28E-02	3.39E+02 ± 5.42E-01	6.30E+03 ± 2.52E+00
90	8.67E+00 ± 3.12E-02	3.12E+02 ± 5.61E-01	5.80E+03 ± 2.32E+00
100	8.00E+00 ± 3.12E-02	2.88E+02 ± 5.75E-01	5.35E+03 ± 2.68E+00
120	6.99E+00 ± 3.07E-02	2.51E+02 ± 5.78E-01	4.70E+03 ± 2.82E+00
140	6.24E+00 ± 3.06E-02	2.24E+02 ± 5.84E-01	4.21E+03 ± 2.53E+00
160	5.72E+00 ± 3.15E-02	2.04E+02 ± 5.72E-01	3.81E+03 ± 2.67E+00
180	5.26E+00 ± 3.05E-02	1.89E+02 ± 5.66E-01	3.54E+03 ± 2.84E+00
200	4.89E+00 ± 3.03E-02	1.75E+02 ± 5.79E-01	3.31E+03 ± 2.98E+00
250	4.25E+00 ± 3.10E-02	1.53E+02 ± 5.96E-01	2.86E+03 ± 3.15E+00
300	3.83E+00 ± 3.14E-02	1.38E+02 ± 6.22E-01	2.64E+03 ± 2.90E+00
350	3.53E+00 ± 3.35E-02	1.26E+02 ± 6.19E-01	2.40E+03 ± 2.88E+00
400	3.30E+00 ± 3.37E-02	1.18E+02 ± 6.26E-01	2.23E+03 ± 2.90E+00
450	3.11E+00 ± 3.27E-02	1.12E+02 ± 6.37E-01	2.11E+03 ± 2.74E+00
500	2.95E+00 ± 3.31E-02	1.06E+02 ± 6.24E-01	2.00E+03 ± 2.81E+00
600	2.74E+00 ± 3.15E-02	9.85E+01 ± 6.11E-01	1.88E+03 ± 3.01E+00
700	2.57E+00 ± 3.27E-02	9.29E+01 ± 6.59E-01	1.77E+03 ± 3.01E+00
800	2.47E+00 ± 3.24E-02	8.97E+01 ± 7.17E-01	1.70E+03 ± 3.24E+00
900	2.41E+00 ± 3.56E-02	8.73E+01 ± 7.68E-01	1.66E+03 ± 3.31E+00
1000	2.33E+00 ± 3.73E-02	8.47E+01 ± 8.05E-01	1.60E+03 ± 3.37E+00
1500	2.24E+00 ± 5.37E-02	7.99E+01 ± 8.95E-01	1.52E+03 ± 4.10E+00
2000	2.24E+00 ± 7.44E-02	7.88E+01 ± 1.21E+00	1.48E+03 ± 5.04E+00
2500	2.25E+00 ± 8.63E-02	7.92E+01 ± 1.50E+00	1.47E+03 ± 5.75E+00
3000	2.31E+00 ± 1.05E-01	8.03E+01 ± 1.69E+00	1.49E+03 ± 6.41E+00
3500	2.27E+00 ± 1.03E-01	7.89E+01 ± 1.66E+00	1.48E+03 ± 6.93E+00
4000	2.25E+00 ± 1.02E-01	7.91E+01 ± 1.90E+00	1.47E+03 ± 7.50E+00
4500	2.23E+00 ± 1.02E-01	7.84E+01 ± 1.87E+00	1.47E+03 ± 7.77E+00
5000	2.21E+00 ± 1.01E-01	7.91E+01 ± 2.32E+00	1.47E+03 ± 8.80E+00
6000	2.21E+00 ± 1.01E-01	7.89E+01 ± 2.30E+00	1.49E+03 ± 1.13E+01
7000	2.19E+00 ± 1.00E-01	8.07E+01 ± 3.36E+00	1.49E+03 ± 1.27E+01
8000	2.18E+00 ± 9.98E-02	8.05E+01 ± 3.35E+00	1.51E+03 ± 1.43E+01
9000	2.18E+00 ± 9.97E-02	8.42E+01 ± 5.07E+00	1.51E+03 ± 1.54E+01
10000	2.17E+00 ± 9.94E-02	8.38E+01 ± 5.06E+00	1.52E+03 ± 1.83E+01

TABLE B. 5
Mass stopping powers of Alderson muscle (B) for the proton, the carbon, and the iron beams. (MeV-cm^2/g)

Energy (MeV/u)	Proton	Carbon	Iron
1	3.39E+02 ± 3.39E-02	7.89E+03 ± 7.89E-01	5.04E+04 ± 5.04E+00
2	1.84E+02 ± 3.69E-02	5.43E+03 ± 5.43E-01	4.44E+04 ± 4.44E+00
3	1.33E+02 ± 2.65E-02	4.25E+03 ± 4.25E-01	4.07E+04 ± 4.07E+00
4	1.05E+02 ± 3.14E-02	3.49E+03 ± 6.97E-01	3.74E+04 ± 3.74E+00
5	8.84E+01 ± 3.54E-02	3.01E+03 ± 6.01E-01	3.48E+04 ± 3.48E+00
6	7.61E+01 ± 3.05E-02	2.64E+03 ± 5.28E-01	3.23E+04 ± 3.23E+00
7	6.80E+01 ± 3.40E-02	2.36E+03 ± 4.71E-01	3.06E+04 ± 3.06E+00
8	6.18E+01 ± 3.71E-02	2.13E+03 ± 6.39E-01	2.90E+04 ± 2.90E+00
9	5.64E+01 ± 4.51E-02	1.95E+03 ± 5.86E-01	2.69E+04 ± 2.69E+00
10	5.05E+01 ± 4.55E-02	1.79E+03 ± 5.36E-01	2.60E+04 ± 2.60E+00
20	2.87E+01 ± 5.75E-02	1.02E+03 ± 6.15E-01	1.74E+04 ± 1.74E+00
30	2.07E+01 ± 8.27E-02	7.45E+02 ± 5.96E-01	1.32E+04 ± 2.63E+00
40	1.64E+01 ± 7.21E-02	5.88E+02 ± 5.88E-01	1.05E+04 ± 2.10E+00
50	1.37E+01 ± 7.26E-02	4.99E+02 ± 6.48E-01	8.91E+03 ± 2.67E+00
60	1.19E+01 ± 7.47E-02	4.32E+02 ± 6.48E-01	7.75E+03 ± 2.32E+00
70	1.04E+01 ± 3.02E-02	3.77E+02 ± 5.65E-01	7.00E+03 ± 2.80E+00
80	9.47E+00 ± 4.26E-02	3.37E+02 ± 5.40E-01	6.27E+03 ± 2.51E+00
90	8.63E+00 ± 3.11E-02	3.10E+02 ± 5.58E-01	5.77E+03 ± 2.89E+00
100	7.97E+00 ± 3.11E-02	2.86E+02 ± 5.72E-01	5.33E+03 ± 2.66E+00
120	6.96E+00 ± 3.06E-02	2.50E+02 ± 5.75E-01	4.68E+03 ± 2.81E+00
140	6.22E+00 ± 3.11E-02	2.23E+02 ± 5.81E-01	4.19E+03 ± 2.52E+00
160	5.69E+00 ± 3.13E-02	2.03E+02 ± 5.70E-01	3.80E+03 ± 2.66E+00
180	5.24E+00 ± 3.04E-02	1.88E+02 ± 5.64E-01	3.53E+03 ± 2.82E+00
200	4.87E+00 ± 3.02E-02	1.75E+02 ± 5.77E-01	3.29E+03 ± 2.96E+00
250	4.23E+00 ± 3.13E-02	1.52E+02 ± 5.93E-01	2.85E+03 ± 3.13E+00
300	3.82E+00 ± 3.13E-02	1.38E+02 ± 6.19E-01	2.63E+03 ± 2.89E+00
350	3.52E+00 ± 3.37E-02	1.26E+02 ± 6.16E-01	2.39E+03 ± 2.87E+00
400	3.29E+00 ± 3.39E-02	1.18E+02 ± 6.23E-01	2.22E+03 ± 2.89E+00
450	3.10E+00 ± 3.25E-02	1.11E+02 ± 6.34E-01	2.10E+03 ± 2.73E+00
500	2.94E+00 ± 3.32E-02	1.05E+02 ± 6.21E-01	2.00E+03 ± 2.80E+00
600	2.73E+00 ± 3.16E-02	9.80E+01 ± 6.18E-01	1.87E+03 ± 2.99E+00
700	2.56E+00 ± 3.26E-02	9.25E+01 ± 6.56E-01	1.76E+03 ± 3.00E+00
800	2.46E+00 ± 3.25E-02	8.93E+01 ± 7.14E-01	1.70E+03 ± 3.22E+00
900	2.40E+00 ± 3.55E-02	8.69E+01 ± 7.65E-01	1.65E+03 ± 3.30E+00
1000	2.32E+00 ± 3.73E-02	8.44E+01 ± 8.01E-01	1.60E+03 ± 3.51E+00
1500	2.25E+00 ± 5.87E-02	7.96E+01 ± 8.99E-01	1.51E+03 ± 4.08E+00
2000	2.23E+00 ± 7.43E-02	7.85E+01 ± 1.22E+00	1.47E+03 ± 5.01E+00
2500	2.24E+00 ± 8.61E-02	7.89E+01 ± 1.50E+00	1.47E+03 ± 5.73E+00
3000	2.30E+00 ± 1.05E-01	8.00E+01 ± 1.68E+00	1.49E+03 ± 6.39E+00
3500	2.26E+00 ± 1.03E-01	7.87E+01 ± 1.66E+00	1.47E+03 ± 6.92E+00
4000	2.24E+00 ± 1.02E-01	7.89E+01 ± 1.89E+00	1.47E+03 ± 7.48E+00
4500	2.23E+00 ± 1.02E-01	7.83E+01 ± 1.86E+00	1.46E+03 ± 7.75E+00
5000	2.21E+00 ± 1.01E-01	7.90E+01 ± 2.31E+00	1.46E+03 ± 8.78E+00
6000	2.20E+00 ± 1.00E-01	7.87E+01 ± 2.30E+00	1.49E+03 ± 1.13E+01
7000	2.18E+00 ± 1.00E-01	8.05E+01 ± 3.36E+00	1.49E+03 ± 1.27E+01
8000	2.18E+00 ± 9.96E-02	8.03E+01 ± 3.34E+00	1.50E+03 ± 1.43E+01
9000	2.18E+00 ± 9.95E-02	8.40E+01 ± 5.06E+00	1.51E+03 ± 1.54E+01
10000	2.17E+00 ± 9.92E-02	8.37E+01 ± 5.05E+00	1.52E+03 ± 1.83E+01

TABLE B. 6
Mass stopping powers of Amber for the proton, the carbon, and the iron beams. (MeV-cm^2/g)

Energy (MeV/u)	Proton		Carbon		Iron	
1	3.56E+02	± 3.56E-02	8.30E+03	± 8.30E-01	5.28E+04	± 5.28E+00
2	1.93E+02	± 3.86E-02	5.70E+03	± 5.70E-01	4.67E+04	± 4.67E+00
3	1.40E+02	± 2.80E-02	4.45E+03	± 4.45E-01	4.27E+04	± 4.27E+00
4	1.10E+02	± 3.30E-02	3.65E+03	± 7.31E-01	3.91E+04	± 3.91E+00
5	9.28E+01	± 2.78E-02	3.15E+03	± 6.30E-01	3.64E+04	± 3.64E+00
6	7.98E+01	± 3.19E-02	2.77E+03	± 5.54E-01	3.39E+04	± 3.39E+00
7	7.09E+01	± 3.55E-02	2.47E+03	± 4.94E-01	3.21E+04	± 3.21E+00
8	6.43E+01	± 3.86E-02	2.23E+03	± 4.46E-01	3.04E+04	± 3.04E+00
9	5.88E+01	± 4.12E-02	2.04E+03	± 6.13E-01	2.81E+04	± 2.81E+00
10	5.42E+01	± 4.34E-02	1.87E+03	± 5.60E-01	2.72E+04	± 2.72E+00
20	3.00E+01	± 5.40E-02	1.07E+03	± 5.37E-01	1.82E+04	± 1.82E+00
30	2.16E+01	± 8.41E-02	7.78E+02	± 5.44E-01	1.37E+04	± 2.74E+00
40	1.71E+01	± 8.21E-02	6.11E+02	± 5.50E-01	1.09E+04	± 2.19E+00
50	1.42E+01	± 6.69E-02	5.17E+02	± 6.20E-01	9.28E+03	± 2.78E+00
60	1.23E+01	± 6.79E-02	4.50E+02	± 6.30E-01	8.07E+03	± 2.42E+00
70	1.08E+01	± 2.93E-02	3.93E+02	± 5.50E-01	7.22E+03	± 2.17E+00
80	9.83E+00	± 4.13E-02	3.52E+02	± 5.29E-01	6.56E+03	± 2.62E+00
90	8.98E+00	± 3.05E-02	3.20E+02	± 5.12E-01	6.01E+03	± 2.41E+00
100	8.28E+00	± 3.07E-02	2.98E+02	± 5.65E-01	5.54E+03	± 2.22E+00
120	7.25E+00	± 2.97E-02	2.60E+02	± 5.47E-01	4.82E+03	± 2.41E+00
140	6.45E+00	± 2.90E-02	2.32E+02	± 5.57E-01	4.37E+03	± 2.62E+00
160	5.92E+00	± 3.08E-02	2.12E+02	± 5.51E-01	3.95E+03	± 2.37E+00
180	5.47E+00	± 3.06E-02	1.95E+02	± 5.47E-01	3.66E+03	± 2.56E+00
200	5.06E+00	± 2.93E-02	1.82E+02	± 5.63E-01	3.41E+03	± 2.73E+00
250	4.40E+00	± 3.04E-02	1.58E+02	± 5.68E-01	2.96E+03	± 2.96E+00
300	3.97E+00	± 3.10E-02	1.43E+02	± 5.85E-01	2.69E+03	± 2.96E+00
350	3.62E+00	± 3.04E-02	1.31E+02	± 6.01E-01	2.49E+03	± 2.99E+00
400	3.42E+00	± 3.31E-02	1.22E+02	± 5.97E-01	2.32E+03	± 2.78E+00
450	3.24E+00	± 3.37E-02	1.15E+02	± 6.12E-01	2.18E+03	± 2.62E+00
500	3.06E+00	± 3.31E-02	1.10E+02	± 6.14E-01	2.07E+03	± 2.69E+00
600	2.85E+00	± 3.25E-02	1.02E+02	± 6.13E-01	1.94E+03	± 2.91E+00
700	2.65E+00	± 3.03E-02	9.58E+01	± 6.13E-01	1.83E+03	± 2.93E+00
800	2.57E+00	± 3.34E-02	9.23E+01	± 6.56E-01	1.76E+03	± 3.17E+00
900	2.48E+00	± 3.19E-02	8.99E+01	± 7.10E-01	1.71E+03	± 3.25E+00
1000	2.41E+00	± 3.59E-02	8.74E+01	± 7.69E-01	1.66E+03	± 3.31E+00
1500	2.26E+00	± 3.77E-02	8.30E+01	± 9.21E-01	1.57E+03	± 3.91E+00
2000	2.30E+00	± 6.93E-02	8.14E+01	± 1.20E+00	1.53E+03	± 4.73E+00
2500	2.30E+00	± 7.55E-02	8.07E+01	± 1.28E+00	1.52E+03	± 5.63E+00
3000	2.30E+00	± 8.67E-02	8.16E+01	± 1.59E+00	1.52E+03	± 6.22E+00
3500	2.32E+00	± 1.06E-01	8.08E+01	± 1.70E+00	1.51E+03	± 6.93E+00
4000	2.30E+00	± 1.05E-01	8.00E+01	± 1.69E+00	1.50E+03	± 7.36E+00
4500	2.29E+00	± 1.04E-01	8.05E+01	± 1.93E+00	1.49E+03	± 7.62E+00
5000	2.27E+00	± 1.04E-01	7.96E+01	± 1.90E+00	1.49E+03	± 8.52E+00
6000	2.26E+00	± 1.03E-01	8.08E+01	± 2.36E+00	1.51E+03	± 1.05E+01
7000	2.24E+00	± 1.03E-01	8.01E+01	± 2.35E+00	1.53E+03	± 1.27E+01
8000	2.24E+00	± 1.02E-01	8.24E+01	± 3.43E+00	1.53E+03	± 1.40E+01
9000	2.23E+00	± 1.02E-01	8.23E+01	± 3.42E+00	1.54E+03	± 1.46E+01
10000	2.22E+00	± 1.02E-01	8.74E+01	± 7.69E-01	1.54E+03	± 1.57E+01

TABLE B. 7
Mass stopping powers of Ceric sulfate dosimeter solution for the proton, the carbon, and the iron beams. (MeV-cm^2/g)

Energy (MeV/u)	Proton	Carbon	Iron
1	3.56E+02 ± 3.56E-02	8.23E+03 ± 8.23E-01	5.24E+04 ± 5.24E+00
2	1.92E+02 ± 3.84E-02	5.65E+03 ± 5.65E-01	4.62E+04 ± 4.62E+00
3	1.39E+02 ± 2.78E-02	4.42E+03 ± 4.42E-01	4.23E+04 ± 4.23E+00
4	1.09E+02 ± 3.27E-02	3.62E+03 ± 7.25E-01	3.88E+04 ± 3.88E+00
5	9.20E+01 ± 2.76E-02	3.12E+03 ± 6.25E-01	3.61E+04 ± 3.61E+00
6	7.91E+01 ± 3.16E-02	2.75E+03 ± 5.49E-01	3.36E+04 ± 3.36E+00
7	7.05E+01 ± 2.82E-02	2.45E+03 ± 4.90E-01	3.17E+04 ± 3.17E+00
8	6.36E+01 ± 3.18E-02	2.19E+03 ± 6.58E-01	2.99E+04 ± 2.99E+00
9	5.76E+01 ± 3.46E-02	2.00E+03 ± 5.99E-01	2.75E+04 ± 2.75E+00
10	5.29E+01 ± 3.70E-02	1.83E+03 ± 5.48E-01	2.65E+04 ± 2.65E+00
20	2.94E+01 ± 5.58E-02	1.05E+03 ± 6.31E-01	1.78E+04 ± 1.78E+00
30	2.11E+01 ± 2.95E-02	7.63E+02 ± 6.10E-01	1.35E+04 ± 2.69E+00
40	1.67E+01 ± 3.00E-02	6.01E+02 ± 6.01E-01	1.08E+04 ± 2.15E+00
50	1.39E+01 ± 3.07E-02	5.10E+02 ± 6.62E-01	9.12E+03 ± 2.74E+00
60	1.21E+01 ± 3.87E-02	4.43E+02 ± 6.64E-01	7.94E+03 ± 2.38E+00
70	1.07E+01 ± 4.50E-02	3.86E+02 ± 5.79E-01	7.10E+03 ± 2.13E+00
80	9.68E+00 ± 5.03E-02	3.46E+02 ± 5.54E-01	6.47E+03 ± 2.59E+00
90	8.90E+00 ± 5.69E-02	3.18E+02 ± 5.72E-01	5.92E+03 ± 2.37E+00
100	8.21E+00 ± 6.40E-02	2.93E+02 ± 5.87E-01	5.46E+03 ± 2.73E+00
120	7.14E+00 ± 3.28E-02	2.56E+02 ± 5.64E-01	4.78E+03 ± 2.39E+00
140	6.36E+00 ± 3.05E-02	2.29E+02 ± 5.73E-01	4.30E+03 ± 2.58E+00
160	5.84E+00 ± 3.15E-02	2.09E+02 ± 5.63E-01	3.89E+03 ± 2.72E+00
180	5.38E+00 ± 3.12E-02	1.92E+02 ± 5.77E-01	3.61E+03 ± 2.53E+00
200	4.99E+00 ± 3.04E-02	1.79E+02 ± 5.72E-01	3.37E+03 ± 2.69E+00
250	4.34E+00 ± 3.17E-02	1.56E+02 ± 5.91E-01	2.92E+03 ± 3.21E+00
300	3.92E+00 ± 3.22E-02	1.41E+02 ± 6.20E-01	2.69E+03 ± 2.96E+00
350	3.58E+00 ± 3.19E-02	1.29E+02 ± 6.19E-01	2.45E+03 ± 2.95E+00
400	3.38E+00 ± 3.48E-02	1.20E+02 ± 6.26E-01	2.28E+03 ± 2.74E+00
450	3.18E+00 ± 3.34E-02	1.14E+02 ± 6.39E-01	2.15E+03 ± 2.80E+00
500	3.05E+00 ± 4.39E-02	1.08E+02 ± 6.27E-01	2.05E+03 ± 2.86E+00
600	2.84E+00 ± 4.40E-02	1.01E+02 ± 6.35E-01	1.92E+03 ± 2.88E+00
700	2.63E+00 ± 3.21E-02	9.46E+01 ± 6.43E-01	1.81E+03 ± 3.07E+00
800	2.53E+00 ± 3.34E-02	9.12E+01 ± 6.84E-01	1.74E+03 ± 3.13E+00
900	2.47E+00 ± 3.65E-02	8.90E+01 ± 7.47E-01	1.69E+03 ± 3.38E+00
1000	2.38E+00 ± 3.84E-02	8.64E+01 ± 7.95E-01	1.64E+03 ± 3.44E+00
1500	2.27E+00 ± 4.94E-02	8.18E+01 ± 9.25E-01	1.55E+03 ± 4.03E+00
2000	2.33E+00 ± 8.29E-02	8.07E+01 ± 1.25E+00	1.51E+03 ± 4.99E+00
2500	2.27E+00 ± 7.59E-02	8.01E+01 ± 1.36E+00	1.51E+03 ± 5.72E+00
3000	2.30E+00 ± 8.70E-02	8.16E+01 ± 1.59E+00	1.52E+03 ± 6.40E+00
3500	2.33E+00 ± 1.06E-01	8.10E+01 ± 1.71E+00	1.51E+03 ± 7.11E+00
4000	2.32E+00 ± 1.05E-01	8.12E+01 ± 1.95E+00	1.51E+03 ± 7.54E+00
4500	2.35E+00 ± 1.17E-01	8.07E+01 ± 1.94E+00	1.50E+03 ± 7.82E+00
5000	2.34E+00 ± 1.19E-01	8.12E+01 ± 2.38E+00	1.50E+03 ± 8.87E+00
6000	2.29E+00 ± 1.05E-01	8.10E+01 ± 2.37E+00	1.52E+03 ± 1.11E+01
7000	2.41E+00 ± 1.86E-01	8.28E+01 ± 3.45E+00	1.53E+03 ± 1.27E+01
8000	2.26E+00 ± 1.03E-01	8.27E+01 ± 3.44E+00	1.54E+03 ± 1.43E+01
9000	2.25E+00 ± 1.03E-01	8.64E+01 ± 5.20E+00	1.54E+03 ± 1.47E+01
10000	2.24E+00 ± 1.03E-01	8.61E+01 ± 5.20E+00	1.55E+03 ± 1.73E+01

TABLE B. 8
Mass stopping powers of ED1S (fhw) for the proton, the carbon, and the iron beams. (MeV-cm^2/g)

Energy (MeV/u)	Proton	Carbon	Iron
1	3.45E+02 ± 3.45E-02	8.01E+03 ± 8.01E-01	5.11E+04 ± 5.11E+00
2	1.87E+02 ± 3.74E-02	5.50E+03 ± 5.50E-01	4.50E+04 ± 4.50E+00
3	1.34E+02 ± 2.68E-02	4.31E+03 ± 4.31E-01	4.12E+04 ± 4.12E+00
4	1.06E+02 ± 3.19E-02	3.53E+03 ± 7.07E-01	3.79E+04 ± 3.79E+00
5	8.97E+01 ± 2.69E-02	3.05E+03 ± 6.09E-01	3.52E+04 ± 3.52E+00
6	7.78E+01 ± 3.11E-02	2.68E+03 ± 5.35E-01	3.28E+04 ± 3.28E+00
7	6.88E+01 ± 3.44E-02	2.39E+03 ± 4.78E-01	3.10E+04 ± 3.10E+00
8	6.23E+01 ± 3.12E-02	2.15E+03 ± 6.45E-01	2.93E+04 ± 2.93E+00
9	5.67E+01 ± 3.40E-02	1.96E+03 ± 5.89E-01	2.71E+04 ± 2.71E+00
10	5.08E+01 ± 3.05E-02	1.80E+03 ± 5.39E-01	2.61E+04 ± 2.61E+00
20	2.89E+01 ± 5.78E-02	1.03E+03 ± 6.19E-01	1.75E+04 ± 1.75E+00
30	2.08E+01 ± 8.32E-02	7.50E+02 ± 6.00E-01	1.32E+04 ± 2.65E+00
40	1.64E+01 ± 2.95E-02	5.92E+02 ± 5.92E-01	1.06E+04 ± 2.11E+00
50	1.37E+01 ± 3.02E-02	5.01E+02 ± 6.52E-01	8.96E+03 ± 2.69E+00
60	1.19E+01 ± 3.92E-02	4.35E+02 ± 6.53E-01	7.80E+03 ± 2.34E+00
70	1.05E+01 ± 4.53E-02	3.79E+02 ± 5.69E-01	7.06E+03 ± 2.83E+00
80	9.53E+00 ± 5.15E-02	3.40E+02 ± 5.44E-01	6.35E+03 ± 2.54E+00
90	8.74E+00 ± 5.77E-02	3.12E+02 ± 5.62E-01	5.81E+03 ± 3.49E+00
100	8.07E+00 ± 6.45E-02	2.88E+02 ± 5.76E-01	5.36E+03 ± 2.68E+00
120	7.01E+00 ± 3.29E-02	2.52E+02 ± 5.53E-01	4.70E+03 ± 2.82E+00
140	6.25E+00 ± 3.06E-02	2.25E+02 ± 5.85E-01	4.22E+03 ± 2.53E+00
160	5.73E+00 ± 3.15E-02	2.05E+02 ± 5.74E-01	3.82E+03 ± 3.82E+00
180	5.28E+00 ± 3.06E-02	1.89E+02 ± 5.68E-01	3.55E+03 ± 2.48E+00
200	4.90E+00 ± 3.04E-02	1.76E+02 ± 5.80E-01	3.31E+03 ± 2.65E+00
250	4.26E+00 ± 3.11E-02	1.53E+02 ± 5.97E-01	2.87E+03 ± 3.15E+00
300	3.85E+00 ± 3.15E-02	1.38E+02 ± 6.09E-01	2.64E+03 ± 2.91E+00
350	3.53E+00 ± 3.28E-02	1.26E+02 ± 6.07E-01	2.41E+03 ± 2.89E+00
400	3.31E+00 ± 3.41E-02	1.18E+02 ± 6.27E-01	2.24E+03 ± 2.91E+00
450	3.12E+00 ± 3.28E-02	1.12E+02 ± 6.27E-01	2.11E+03 ± 2.75E+00
500	2.96E+00 ± 3.25E-02	1.06E+02 ± 6.26E-01	2.01E+03 ± 2.81E+00
600	2.78E+00 ± 4.20E-02	9.88E+01 ± 6.22E-01	1.88E+03 ± 3.01E+00
700	2.59E+00 ± 3.32E-02	9.31E+01 ± 6.51E-01	1.77E+03 ± 3.02E+00
800	2.48E+00 ± 3.28E-02	8.98E+01 ± 7.10E-01	1.71E+03 ± 3.25E+00
900	2.42E+00 ± 3.58E-02	8.75E+01 ± 7.61E-01	1.66E+03 ± 3.32E+00
1000	2.34E+00 ± 3.76E-02	8.50E+01 ± 8.08E-01	1.61E+03 ± 3.38E+00
1500	2.22E+00 ± 4.85E-02	8.02E+01 ± 9.06E-01	1.52E+03 ± 4.11E+00
2000	2.29E+00 ± 8.17E-02	7.91E+01 ± 1.23E+00	1.49E+03 ± 5.05E+00
2500	2.23E+00 ± 7.47E-02	7.90E+01 ± 1.42E+00	1.48E+03 ± 5.76E+00
3000	2.26E+00 ± 8.50E-02	8.00E+01 ± 1.56E+00	1.49E+03 ± 6.43E+00
3500	2.28E+00 ± 1.04E-01	7.94E+01 ± 1.67E+00	1.48E+03 ± 6.97E+00
4000	2.27E+00 ± 1.03E-01	7.95E+01 ± 1.91E+00	1.48E+03 ± 7.39E+00
4500	2.30E+00 ± 1.15E-01	7.90E+01 ± 1.90E+00	1.47E+03 ± 7.81E+00
5000	2.29E+00 ± 1.18E-01	7.96E+01 ± 2.33E+00	1.47E+03 ± 8.85E+00
6000	2.24E+00 ± 1.02E-01	7.94E+01 ± 2.32E+00	1.50E+03 ± 1.11E+01
7000	2.37E+00 ± 1.87E-01	8.11E+01 ± 3.38E+00	1.50E+03 ± 1.28E+01
8000	2.22E+00 ± 1.01E-01	8.10E+01 ± 3.37E+00	1.51E+03 ± 1.44E+01
9000	2.20E+00 ± 1.01E-01	8.47E+01 ± 5.10E+00	1.52E+03 ± 1.55E+01
10000	2.20E+00 ± 1.01E-01	8.43E+01 ± 5.09E+00	1.53E+03 ± 1.84E+01

TABLE B. 9
Mass stopping powers of ED4C (fhw) for the proton, the carbon, and the iron beams. (MeV-cm^2/g)

Energy (MeV/u)	Proton	Carbon	Iron
1	3.51E+02 ± 3.51E-02	8.16E+03 ± 8.16E-01	5.20E+04 ± 5.20E+00
2	1.90E+02 ± 3.81E-02	5.60E+03 ± 5.60E-01	4.58E+04 ± 4.58E+00
3	1.38E+02 ± 2.76E-02	4.38E+03 ± 4.38E-01	4.20E+04 ± 4.20E+00
4	1.08E+02 ± 3.25E-02	3.60E+03 ± 7.19E-01	3.85E+04 ± 3.85E+00
5	9.13E+01 ± 2.74E-02	3.10E+03 ± 6.20E-01	3.59E+04 ± 3.59E+00
6	7.86E+01 ± 3.14E-02	2.73E+03 ± 5.45E-01	3.34E+04 ± 3.34E+00
7	7.00E+01 ± 2.80E-02	2.43E+03 ± 4.86E-01	3.15E+04 ± 3.15E+00
8	6.33E+01 ± 3.17E-02	2.18E+03 ± 6.55E-01	2.98E+04 ± 2.98E+00
9	5.75E+01 ± 3.45E-02	1.99E+03 ± 5.98E-01	2.75E+04 ± 2.75E+00
10	5.15E+01 ± 3.09E-02	1.82E+03 ± 5.47E-01	2.65E+04 ± 2.65E+00
20	2.93E+01 ± 5.86E-02	1.05E+03 ± 6.28E-01	1.78E+04 ± 1.78E+00
30	2.11E+01 ± 8.23E-02	7.61E+02 ± 6.09E-01	1.34E+04 ± 2.68E+00
40	1.66E+01 ± 3.00E-02	6.00E+02 ± 6.00E-01	1.07E+04 ± 2.15E+00
50	1.39E+01 ± 3.06E-02	5.09E+02 ± 6.61E-01	9.10E+03 ± 2.73E+00
60	1.21E+01 ± 3.98E-02	4.42E+02 ± 6.62E-01	7.91E+03 ± 2.37E+00
70	1.07E+01 ± 4.49E-02	3.85E+02 ± 5.77E-01	7.17E+03 ± 2.87E+00
80	9.67E+00 ± 5.22E-02	3.45E+02 ± 5.52E-01	6.45E+03 ± 2.58E+00
90	8.87E+00 ± 5.85E-02	3.17E+02 ± 5.70E-01	5.90E+03 ± 2.36E+00
100	8.18E+00 ± 6.47E-02	2.92E+02 ± 5.85E-01	5.44E+03 ± 2.72E+00
120	7.11E+00 ± 3.27E-02	2.55E+02 ± 5.62E-01	4.77E+03 ± 2.86E+00
140	6.34E+00 ± 3.04E-02	2.28E+02 ± 5.71E-01	4.28E+03 ± 2.57E+00
160	5.82E+00 ± 3.20E-02	2.08E+02 ± 5.82E-01	3.88E+03 ± 2.71E+00
180	5.36E+00 ± 3.11E-02	1.92E+02 ± 5.76E-01	3.60E+03 ± 2.52E+00
200	4.97E+00 ± 3.08E-02	1.78E+02 ± 5.89E-01	3.36E+03 ± 2.69E+00
250	4.32E+00 ± 3.16E-02	1.55E+02 ± 6.05E-01	2.91E+03 ± 3.20E+00
300	3.90E+00 ± 3.20E-02	1.40E+02 ± 6.18E-01	2.68E+03 ± 2.95E+00
350	3.58E+00 ± 3.33E-02	1.28E+02 ± 6.16E-01	2.44E+03 ± 2.93E+00
400	3.36E+00 ± 3.46E-02	1.20E+02 ± 6.24E-01	2.27E+03 ± 2.96E+00
450	3.17E+00 ± 3.33E-02	1.14E+02 ± 6.36E-01	2.14E+03 ± 2.79E+00
500	3.00E+00 ± 3.30E-02	1.08E+02 ± 6.35E-01	2.04E+03 ± 2.85E+00
600	2.83E+00 ± 4.32E-02	1.00E+02 ± 6.32E-01	1.91E+03 ± 3.06E+00
700	2.63E+00 ± 3.36E-02	9.45E+01 ± 6.61E-01	1.80E+03 ± 3.06E+00
800	2.52E+00 ± 3.32E-02	9.12E+01 ± 7.20E-01	1.73E+03 ± 3.29E+00
900	2.45E+00 ± 3.63E-02	8.88E+01 ± 7.72E-01	1.68E+03 ± 3.37E+00
1000	2.37E+00 ± 3.82E-02	8.61E+01 ± 8.10E-01	1.63E+03 ± 3.43E+00
1500	2.26E+00 ± 4.92E-02	8.14E+01 ± 9.20E-01	1.54E+03 ± 4.17E+00
2000	2.32E+00 ± 8.27E-02	8.03E+01 ± 1.24E+00	1.51E+03 ± 4.97E+00
2500	2.26E+00 ± 7.55E-02	8.02E+01 ± 1.44E+00	1.50E+03 ± 5.70E+00
3000	2.29E+00 ± 8.63E-02	8.12E+01 ± 1.58E+00	1.52E+03 ± 6.52E+00
3500	2.31E+00 ± 1.05E-01	8.05E+01 ± 1.70E+00	1.50E+03 ± 7.07E+00
4000	2.30E+00 ± 1.05E-01	8.07E+01 ± 1.94E+00	1.50E+03 ± 7.50E+00
4500	2.34E+00 ± 1.17E-01	8.02E+01 ± 1.92E+00	1.50E+03 ± 7.93E+00
5000	2.33E+00 ± 1.19E-01	8.07E+01 ± 2.37E+00	1.50E+03 ± 8.98E+00
6000	2.27E+00 ± 1.04E-01	8.05E+01 ± 2.35E+00	1.52E+03 ± 1.12E+01
7000	2.40E+00 ± 1.89E-01	8.24E+01 ± 3.43E+00	1.52E+03 ± 1.29E+01
8000	2.25E+00 ± 1.03E-01	8.22E+01 ± 3.42E+00	1.54E+03 ± 1.46E+01
9000	2.23E+00 ± 1.02E-01	8.59E+01 ± 5.17E+00	1.54E+03 ± 1.52E+01
10000	2.23E+00 ± 1.02E-01	8.55E+01 ± 5.17E+00	1.55E+03 ± 1.78E+01

TABLE B. 10
Mass stopping powers of Ethyl cellulose for the proton, the carbon, and the iron beams. (MeV-cm^2/g)

Energy (MeV/u)	Proton	Carbon	Iron
1	3.44E+02 ± 3.44E-02	7.97E+03 ± 7.97E-01	5.06E+04 ± 5.06E+00
2	1.86E+02 ± 3.71E-02	5.47E+03 ± 5.47E-01	4.48E+04 ± 4.48E+00
3	1.35E+02 ± 2.69E-02	4.27E+03 ± 4.27E-01	4.10E+04 ± 4.10E+00
4	1.05E+02 ± 3.16E-02	3.51E+03 ± 7.01E-01	3.76E+04 ± 3.76E+00
5	8.90E+01 ± 2.67E-02	3.02E+03 ± 6.04E-01	3.49E+04 ± 3.49E+00
6	7.66E+01 ± 3.06E-02	2.66E+03 ± 5.31E-01	3.25E+04 ± 3.25E+00
7	6.80E+01 ± 3.40E-02	2.37E+03 ± 4.74E-01	3.08E+04 ± 3.08E+00
8	6.18E+01 ± 3.71E-02	2.14E+03 ± 6.43E-01	2.92E+04 ± 2.92E+00
9	5.66E+01 ± 3.96E-02	1.96E+03 ± 5.89E-01	2.70E+04 ± 2.70E+00
10	5.22E+01 ± 4.17E-02	1.80E+03 ± 5.39E-01	2.61E+04 ± 2.61E+00
20	2.89E+01 ± 5.20E-02	1.04E+03 ± 6.21E-01	1.75E+04 ± 1.75E+00
30	2.08E+01 ± 8.11E-02	7.50E+02 ± 6.00E-01	1.32E+04 ± 2.64E+00
40	1.65E+01 ± 7.93E-02	5.90E+02 ± 5.31E-01	1.06E+04 ± 2.11E+00
50	1.38E+01 ± 6.47E-02	4.99E+02 ± 5.99E-01	8.96E+03 ± 2.69E+00
60	1.19E+01 ± 6.68E-02	4.35E+02 ± 6.09E-01	7.79E+03 ± 2.34E+00
70	1.05E+01 ± 2.83E-02	3.80E+02 ± 5.70E-01	6.98E+03 ± 2.09E+00
80	9.51E+00 ± 4.09E-02	3.41E+02 ± 5.11E-01	6.33E+03 ± 2.53E+00
90	8.67E+00 ± 2.95E-02	3.09E+02 ± 4.95E-01	5.81E+03 ± 2.32E+00
100	8.05E+00 ± 5.88E-02	2.88E+02 ± 5.47E-01	5.35E+03 ± 2.68E+00
120	7.02E+00 ± 3.30E-02	2.52E+02 ± 5.54E-01	4.66E+03 ± 2.33E+00
140	6.25E+00 ± 2.87E-02	2.25E+02 ± 5.39E-01	4.22E+03 ± 2.53E+00
160	5.72E+00 ± 2.98E-02	2.05E+02 ± 5.32E-01	3.82E+03 ± 2.29E+00
180	5.29E+00 ± 2.96E-02	1.89E+02 ± 5.48E-01	3.54E+03 ± 2.48E+00
200	4.89E+00 ± 2.84E-02	1.76E+02 ± 5.44E-01	3.30E+03 ± 2.64E+00
250	4.26E+00 ± 2.98E-02	1.52E+02 ± 5.49E-01	2.86E+03 ± 2.86E+00
300	3.85E+00 ± 3.00E-02	1.38E+02 ± 5.66E-01	2.61E+03 ± 2.87E+00
350	3.51E+00 ± 2.98E-02	1.26E+02 ± 5.82E-01	2.41E+03 ± 2.89E+00
400	3.31E+00 ± 3.24E-02	1.18E+02 ± 5.78E-01	2.24E+03 ± 2.69E+00
450	3.13E+00 ± 3.29E-02	1.12E+02 ± 5.92E-01	2.11E+03 ± 2.75E+00
500	2.97E+00 ± 3.23E-02	1.06E+02 ± 6.05E-01	2.00E+03 ± 2.61E+00
600	2.76E+00 ± 3.17E-02	9.90E+01 ± 6.04E-01	1.88E+03 ± 2.82E+00
700	2.57E+00 ± 2.96E-02	9.27E+01 ± 5.93E-01	1.77E+03 ± 2.83E+00
800	2.49E+00 ± 3.26E-02	8.95E+01 ± 6.44E-01	1.71E+03 ± 3.07E+00
900	2.41E+00 ± 3.13E-02	8.71E+01 ± 6.97E-01	1.65E+03 ± 3.14E+00
1000	2.34E+00 ± 3.48E-02	8.47E+01 ± 7.54E-01	1.61E+03 ± 3.21E+00
1500	2.19E+00 ± 3.67E-02	8.04E+01 ± 9.01E-01	1.52E+03 ± 3.80E+00
2000	2.26E+00 ± 7.37E-02	7.90E+01 ± 1.17E+00	1.48E+03 ± 4.59E+00
2500	2.21E+00 ± 7.24E-02	7.83E+01 ± 1.25E+00	1.48E+03 ± 5.46E+00
3000	2.25E+00 ± 8.48E-02	7.98E+01 ± 1.56E+00	1.49E+03 ± 6.09E+00
3500	2.27E+00 ± 1.04E-01	7.90E+01 ± 1.67E+00	1.47E+03 ± 6.78E+00
4000	2.25E+00 ± 1.03E-01	7.83E+01 ± 1.65E+00	1.47E+03 ± 7.19E+00
4500	2.24E+00 ± 1.02E-01	7.87E+01 ± 1.89E+00	1.46E+03 ± 7.46E+00
5000	2.22E+00 ± 1.02E-01	7.79E+01 ± 1.86E+00	1.46E+03 ± 8.18E+00
6000	2.21E+00 ± 1.01E-01	7.91E+01 ± 2.31E+00	1.48E+03 ± 1.02E+01
7000	2.19E+00 ± 1.00E-01	7.84E+01 ± 2.30E+00	1.49E+03 ± 1.22E+01
8000	2.19E+00 ± 1.00E-01	8.07E+01 ± 3.36E+00	1.50E+03 ± 1.37E+01
9000	2.19E+00 ± 9.99E-02	8.05E+01 ± 3.35E+00	1.50E+03 ± 1.43E+01
10000	2.18E+00 ± 9.96E-02	8.40E+01 ± 5.07E+00	1.51E+03 ± 1.54E+01

TABLE B. 11
Mass stopping powers of Ferrous sulfate dosimeter solution for the proton, the carbon, and the iron beams. (MeV-cm^2/g)

Energy (MeV/u)	Proton	Carbon	Iron
1	3.56E+02 ± 3.56E-02	8.24E+03 ± 8.24E-01	5.25E+04 ± 5.25E+00
2	1.92E+02 ± 3.84E-02	5.66E+03 ± 5.66E-01	4.63E+04 ± 4.63E+00
3	1.39E+02 ± 2.78E-02	4.42E+03 ± 4.42E-01	4.24E+04 ± 4.24E+00
4	1.09E+02 ± 3.28E-02	3.63E+03 ± 7.26E-01	3.89E+04 ± 3.89E+00
5	9.22E+01 ± 2.77E-02	3.13E+03 ± 6.26E-01	3.62E+04 ± 3.62E+00
6	7.93E+01 ± 3.17E-02	2.75E+03 ± 5.50E-01	3.37E+04 ± 3.37E+00
7	7.06E+01 ± 2.82E-02	2.45E+03 ± 4.91E-01	3.18E+04 ± 3.18E+00
8	6.37E+01 ± 3.18E-02	2.20E+03 ± 6.59E-01	3.00E+04 ± 3.00E+00
9	5.77E+01 ± 3.46E-02	2.00E+03 ± 6.00E-01	2.76E+04 ± 2.76E+00
10	5.30E+01 ± 3.71E-02	1.83E+03 ± 5.49E-01	2.66E+04 ± 2.66E+00
20	2.94E+01 ± 5.59E-02	1.05E+03 ± 6.32E-01	1.79E+04 ± 1.79E+00
30	2.11E+01 ± 2.95E-02	7.64E+02 ± 6.12E-01	1.35E+04 ± 2.70E+00
40	1.67E+01 ± 3.01E-02	6.03E+02 ± 6.03E-01	1.08E+04 ± 2.16E+00
50	1.40E+01 ± 3.07E-02	5.11E+02 ± 6.64E-01	9.14E+03 ± 2.74E+00
60	1.21E+01 ± 3.87E-02	4.44E+02 ± 6.66E-01	7.95E+03 ± 2.39E+00
70	1.07E+01 ± 4.51E-02	3.87E+02 ± 5.80E-01	7.11E+03 ± 2.13E+00
80	9.70E+00 ± 5.04E-02	3.47E+02 ± 5.55E-01	6.48E+03 ± 2.59E+00
90	8.91E+00 ± 5.79E-02	3.18E+02 ± 5.73E-01	5.93E+03 ± 2.37E+00
100	8.22E+00 ± 6.41E-02	2.94E+02 ± 5.88E-01	5.47E+03 ± 2.73E+00
120	7.15E+00 ± 3.29E-02	2.57E+02 ± 5.65E-01	4.79E+03 ± 2.39E+00
140	6.37E+00 ± 3.06E-02	2.29E+02 ± 5.74E-01	4.31E+03 ± 2.58E+00
160	5.85E+00 ± 3.22E-02	2.09E+02 ± 5.64E-01	3.90E+03 ± 2.73E+00
180	5.39E+00 ± 3.13E-02	1.93E+02 ± 5.79E-01	3.62E+03 ± 2.53E+00
200	5.00E+00 ± 3.05E-02	1.79E+02 ± 5.73E-01	3.52E+03 ± 2.82E+00
250	4.35E+00 ± 3.17E-02	1.56E+02 ± 5.92E-01	3.06E+03 ± 3.06E+00
300	3.93E+00 ± 3.22E-02	1.41E+02 ± 6.22E-01	2.78E+03 ± 3.06E+00
350	3.59E+00 ± 3.19E-02	1.29E+02 ± 6.20E-01	2.57E+03 ± 3.09E+00
400	3.38E+00 ± 3.49E-02	1.21E+02 ± 6.27E-01	2.39E+03 ± 2.87E+00
450	3.19E+00 ± 3.35E-02	1.14E+02 ± 6.40E-01	2.25E+03 ± 2.93E+00
500	3.05E+00 ± 4.39E-02	1.08E+02 ± 6.28E-01	2.14E+03 ± 3.00E+00
600	2.85E+00 ± 4.41E-02	1.01E+02 ± 6.36E-01	2.01E+03 ± 3.01E+00
700	2.63E+00 ± 3.21E-02	9.48E+01 ± 6.44E-01	1.89E+03 ± 3.22E+00
800	2.54E+00 ± 3.35E-02	9.14E+01 ± 6.95E-01	1.82E+03 ± 3.28E+00
900	2.47E+00 ± 3.66E-02	8.91E+01 ± 7.48E-01	1.77E+03 ± 3.36E+00
1000	2.39E+00 ± 3.85E-02	8.65E+01 ± 7.96E-01	1.72E+03 ± 3.60E+00
1500	2.27E+00 ± 4.95E-02	8.19E+01 ± 9.26E-01	1.62E+03 ± 4.21E+00
2000	2.34E+00 ± 8.30E-02	8.08E+01 ± 1.25E+00	1.58E+03 ± 5.06E+00
2500	2.27E+00 ± 7.60E-02	8.02E+01 ± 1.36E+00	1.58E+03 ± 5.84E+00
3000	2.30E+00 ± 8.71E-02	8.17E+01 ± 1.59E+00	1.59E+03 ± 6.53E+00
3500	2.33E+00 ± 1.06E-01	8.11E+01 ± 1.71E+00	1.58E+03 ± 7.27E+00
4000	2.32E+00 ± 1.05E-01	8.13E+01 ± 1.95E+00	1.58E+03 ± 7.89E+00
4500	2.35E+00 ± 1.17E-01	8.08E+01 ± 1.94E+00	1.57E+03 ± 8.17E+00
5000	2.34E+00 ± 1.20E-01	8.13E+01 ± 2.38E+00	1.57E+03 ± 9.11E+00
6000	2.29E+00 ± 1.05E-01	8.11E+01 ± 2.37E+00	1.59E+03 ± 1.11E+01
7000	2.41E+00 ± 1.87E-01	8.29E+01 ± 3.46E+00	1.60E+03 ± 1.33E+01
8000	2.26E+00 ± 1.03E-01	8.27E+01 ± 3.44E+00	1.61E+03 ± 1.47E+01
9000	2.25E+00 ± 1.03E-01	8.65E+01 ± 5.21E+00	1.61E+03 ± 1.53E+01
10000	2.25E+00 ± 1.03E-01	8.62E+01 ± 5.20E+00	1.62E+03 ± 1.74E+01

TABLE B. 12
Mass stopping powers of Frigerio gel for the proton, the carbon, and the iron beams. (MeV-cm^2/g)

Energy (MeV/u)	Proton	Carbon	Iron
1	3.52E+02 ± 3.52E-02	8.12E+03 ± 8.12E-01	5.16E+04 ± 5.16E+00
2	1.89E+02 ± 3.78E-02	5.57E+03 ± 5.57E-01	4.56E+04 ± 4.56E+00
3	1.37E+02 ± 2.74E-02	4.35E+03 ± 4.35E-01	4.17E+04 ± 4.17E+00
4	1.07E+02 ± 3.22E-02	3.57E+03 ± 7.13E-01	3.82E+04 ± 3.82E+00
5	9.06E+01 ± 2.72E-02	3.08E+03 ± 6.15E-01	3.56E+04 ± 3.56E+00
6	7.79E+01 ± 3.12E-02	2.70E+03 ± 5.40E-01	3.31E+04 ± 3.31E+00
7	6.92E+01 ± 2.77E-02	2.41E+03 ± 4.82E-01	3.13E+04 ± 3.13E+00
8	6.25E+01 ± 3.12E-02	2.17E+03 ± 6.50E-01	2.95E+04 ± 2.95E+00
9	5.68E+01 ± 3.41E-02	1.97E+03 ± 5.92E-01	2.72E+04 ± 2.72E+00
10	5.24E+01 ± 3.14E-02	1.81E+03 ± 5.42E-01	2.62E+04 ± 2.62E+00
20	2.91E+01 ± 5.23E-02	1.04E+03 ± 6.26E-01	1.76E+04 ± 1.76E+00
30	2.09E+01 ± 7.53E-02	7.55E+02 ± 6.04E-01	1.33E+04 ± 2.66E+00
40	1.65E+01 ± 3.64E-02	5.94E+02 ± 5.35E-01	1.06E+04 ± 2.13E+00
50	1.39E+01 ± 6.65E-02	5.03E+02 ± 6.03E-01	9.03E+03 ± 2.71E+00
60	1.20E+01 ± 3.71E-02	4.38E+02 ± 6.58E-01	7.86E+03 ± 2.36E+00
70	1.06E+01 ± 4.13E-02	3.83E+02 ± 5.74E-01	7.03E+03 ± 2.11E+00
80	9.58E+00 ± 4.69E-02	3.43E+02 ± 5.49E-01	6.38E+03 ± 2.55E+00
90	8.79E+00 ± 5.27E-02	3.12E+02 ± 4.99E-01	5.86E+03 ± 2.34E+00
100	8.12E+00 ± 5.93E-02	2.90E+02 ± 5.51E-01	5.40E+03 ± 2.70E+00
120	7.08E+00 ± 3.26E-02	2.54E+02 ± 5.58E-01	4.69E+03 ± 2.35E+00
140	6.30E+00 ± 2.90E-02	2.27E+02 ± 5.44E-01	4.26E+03 ± 2.56E+00
160	5.78E+00 ± 3.06E-02	2.07E+02 ± 5.58E-01	3.85E+03 ± 2.31E+00
180	5.33E+00 ± 2.98E-02	1.91E+02 ± 5.53E-01	3.57E+03 ± 2.50E+00
200	4.93E+00 ± 2.86E-02	1.77E+02 ± 5.49E-01	3.33E+03 ± 2.66E+00
250	4.30E+00 ± 3.01E-02	1.54E+02 ± 5.54E-01	2.89E+03 ± 2.89E+00
300	3.88E+00 ± 3.07E-02	1.39E+02 ± 5.85E-01	2.63E+03 ± 2.90E+00
350	3.54E+00 ± 3.01E-02	1.28E+02 ± 5.87E-01	2.43E+03 ± 2.92E+00
400	3.34E+00 ± 3.31E-02	1.19E+02 ± 5.95E-01	2.27E+03 ± 2.72E+00
450	3.16E+00 ± 3.32E-02	1.13E+02 ± 6.09E-01	2.13E+03 ± 2.77E+00
500	2.99E+00 ± 3.23E-02	1.07E+02 ± 6.11E-01	2.02E+03 ± 2.63E+00
600	2.82E+00 ± 4.11E-02	1.00E+02 ± 6.10E-01	1.90E+03 ± 2.85E+00
700	2.60E+00 ± 3.04E-02	9.36E+01 ± 6.08E-01	1.79E+03 ± 3.04E+00
800	2.51E+00 ± 3.29E-02	9.03E+01 ± 6.50E-01	1.72E+03 ± 3.10E+00
900	2.43E+00 ± 3.18E-02	8.79E+01 ± 7.04E-01	1.67E+03 ± 3.17E+00
1000	2.35E+00 ± 3.50E-02	8.55E+01 ± 7.61E-01	1.62E+03 ± 3.24E+00
1500	2.21E+00 ± 3.73E-02	8.13E+01 ± 9.10E-01	1.53E+03 ± 3.83E+00
2000	2.28E+00 ± 7.49E-02	7.98E+01 ± 1.19E+00	1.49E+03 ± 4.63E+00
2500	2.26E+00 ± 7.59E-02	7.91E+01 ± 1.27E+00	1.49E+03 ± 5.51E+00
3000	2.28E+00 ± 8.60E-02	8.09E+01 ± 1.58E+00	1.51E+03 ± 6.17E+00
3500	2.30E+00 ± 1.05E-01	8.02E+01 ± 1.69E+00	1.49E+03 ± 6.72E+00
4000	2.29E+00 ± 1.04E-01	7.94E+01 ± 1.68E+00	1.49E+03 ± 7.30E+00
4500	2.32E+00 ± 1.14E-01	7.98E+01 ± 1.92E+00	1.48E+03 ± 7.57E+00
5000	2.31E+00 ± 1.16E-01	7.90E+01 ± 1.89E+00	1.48E+03 ± 8.30E+00
6000	2.26E+00 ± 1.03E-01	8.02E+01 ± 2.34E+00	1.50E+03 ± 1.04E+01
7000	2.38E+00 ± 1.75E-01	7.95E+01 ± 2.33E+00	1.51E+03 ± 1.24E+01
8000	2.24E+00 ± 1.02E-01	8.18E+01 ± 3.40E+00	1.52E+03 ± 1.39E+01
9000	2.22E+00 ± 1.02E-01	8.17E+01 ± 3.40E+00	1.53E+03 ± 1.45E+01
10000	2.22E+00 ± 1.02E-01	8.52E+01 ± 5.15E+00	1.53E+03 ± 1.56E+01

TABLE B. 13
Mass stopping powers of Frigerio liquid for the proton, the carbon, and the iron beams. (MeV-cm^2/g)

Energy (MeV/u)	Proton	Carbon	Iron
1	3.53E+02 ± 3.53E-02	8.15E+03 ± 8.15E-01	5.18E+04 ± 5.18E+00
2	1.90E+02 ± 3.80E-02	5.59E+03 ± 5.59E-01	4.58E+04 ± 4.58E+00
3	1.37E+02 ± 2.74E-02	4.37E+03 ± 4.37E-01	4.19E+04 ± 4.19E+00
4	1.08E+02 ± 3.24E-02	3.58E+03 ± 7.17E-01	3.84E+04 ± 3.84E+00
5	9.11E+01 ± 2.73E-02	3.09E+03 ± 6.18E-01	3.57E+04 ± 3.57E+00
6	7.83E+01 ± 3.13E-02	2.71E+03 ± 5.43E-01	3.32E+04 ± 3.32E+00
7	6.96E+01 ± 2.78E-02	2.42E+03 ± 4.84E-01	3.14E+04 ± 3.14E+00
8	6.29E+01 ± 3.14E-02	2.17E+03 ± 6.52E-01	2.97E+04 ± 2.97E+00
9	5.71E+01 ± 3.43E-02	1.98E+03 ± 5.94E-01	2.73E+04 ± 2.73E+00
10	5.26E+01 ± 3.15E-02	1.81E+03 ± 5.44E-01	2.63E+04 ± 2.63E+00
20	2.92E+01 ± 5.54E-02	1.05E+03 ± 6.27E-01	1.77E+04 ± 1.77E+00
30	2.10E+01 ± 7.77E-02	7.58E+02 ± 6.06E-01	1.34E+04 ± 2.67E+00
40	1.66E+01 ± 3.82E-02	5.97E+02 ± 5.37E-01	1.07E+04 ± 2.14E+00
50	1.38E+01 ± 2.91E-02	5.05E+02 ± 6.06E-01	9.06E+03 ± 2.72E+00
60	1.20E+01 ± 3.84E-02	4.40E+02 ± 6.60E-01	7.88E+03 ± 2.36E+00
70	1.06E+01 ± 4.25E-02	3.84E+02 ± 5.76E-01	7.05E+03 ± 2.12E+00
80	9.61E+00 ± 4.90E-02	3.44E+02 ± 5.51E-01	6.42E+03 ± 2.57E+00
90	8.82E+00 ± 5.47E-02	3.12E+02 ± 5.00E-01	5.88E+03 ± 2.35E+00
100	8.15E+00 ± 6.11E-02	2.91E+02 ± 5.53E-01	5.42E+03 ± 2.71E+00
120	7.10E+00 ± 3.27E-02	2.55E+02 ± 5.60E-01	4.73E+03 ± 2.36E+00
140	6.31E+00 ± 2.97E-02	2.27E+02 ± 5.68E-01	4.27E+03 ± 2.56E+00
160	5.80E+00 ± 3.13E-02	2.07E+02 ± 5.60E-01	3.86E+03 ± 2.70E+00
180	5.34E+00 ± 3.05E-02	1.91E+02 ± 5.54E-01	3.58E+03 ± 2.51E+00
200	4.95E+00 ± 2.97E-02	1.78E+02 ± 5.50E-01	3.34E+03 ± 2.67E+00
250	4.32E+00 ± 3.11E-02	1.55E+02 ± 5.72E-01	2.90E+03 ± 2.90E+00
300	3.90E+00 ± 3.16E-02	1.40E+02 ± 6.01E-01	2.64E+03 ± 2.90E+00
350	3.55E+00 ± 3.01E-02	1.28E+02 ± 6.01E-01	2.44E+03 ± 2.93E+00
400	3.36E+00 ± 3.43E-02	1.20E+02 ± 6.10E-01	2.27E+03 ± 2.72E+00
450	3.17E+00 ± 3.33E-02	1.13E+02 ± 6.23E-01	2.14E+03 ± 2.78E+00
500	3.00E+00 ± 3.30E-02	1.07E+02 ± 6.23E-01	2.03E+03 ± 2.84E+00
600	2.82E+00 ± 4.21E-02	1.00E+02 ± 6.21E-01	1.90E+03 ± 2.85E+00
700	2.62E+00 ± 3.19E-02	9.38E+01 ± 6.10E-01	1.79E+03 ± 3.05E+00
800	2.52E+00 ± 3.32E-02	9.04E+01 ± 6.60E-01	1.73E+03 ± 3.11E+00
900	2.44E+00 ± 3.42E-02	8.83E+01 ± 7.33E-01	1.68E+03 ± 3.18E+00
1000	2.36E+00 ± 3.54E-02	8.59E+01 ± 7.91E-01	1.63E+03 ± 3.42E+00
1500	2.23E+00 ± 4.33E-02	8.14E+01 ± 9.20E-01	1.54E+03 ± 3.99E+00
2000	2.32E+00 ± 8.19E-02	7.99E+01 ± 1.19E+00	1.50E+03 ± 4.80E+00
2500	2.26E+00 ± 7.58E-02	7.97E+01 ± 1.35E+00	1.50E+03 ± 5.53E+00
3000	2.29E+00 ± 8.62E-02	8.11E+01 ± 1.58E+00	1.51E+03 ± 6.19E+00
3500	2.31E+00 ± 1.05E-01	8.04E+01 ± 1.70E+00	1.50E+03 ± 6.89E+00
4000	2.30E+00 ± 1.05E-01	8.06E+01 ± 1.93E+00	1.50E+03 ± 7.48E+00
4500	2.33E+00 ± 1.15E-01	8.01E+01 ± 1.92E+00	1.49E+03 ± 7.75E+00
5000	2.32E+00 ± 1.17E-01	7.92E+01 ± 1.89E+00	1.49E+03 ± 8.64E+00
6000	2.27E+00 ± 1.04E-01	8.04E+01 ± 2.35E+00	1.51E+03 ± 1.06E+01
7000	2.39E+00 ± 1.80E-01	7.97E+01 ± 2.34E+00	1.52E+03 ± 1.26E+01
8000	2.24E+00 ± 1.02E-01	8.20E+01 ± 3.41E+00	1.53E+03 ± 1.39E+01
9000	2.23E+00 ± 1.02E-01	8.19E+01 ± 3.41E+00	1.53E+03 ± 1.45E+01
10000	2.23E+00 ± 1.02E-01	8.54E+01 ± 5.16E+00	1.54E+03 ± 1.65E+01

TABLE B. 14
Mass stopping powers of Goodman liquid for the proton, the carbon, and the iron beams. (MeV-cm^2/g)

Energy (MeV/u)	Proton	Carbon	Iron
1	3.52E+02 ± 3.52E-02	8.15E+03 ± 8.15E-01	5.18E+04 ± 5.18E+00
2	1.90E+02 ± 3.80E-02	5.59E+03 ± 5.59E-01	4.58E+04 ± 4.58E+00
3	1.37E+02 ± 2.74E-02	4.37E+03 ± 4.37E-01	4.19E+04 ± 4.19E+00
4	1.08E+02 ± 3.24E-02	3.58E+03 ± 7.17E-01	3.84E+04 ± 3.84E+00
5	9.11E+01 ± 2.73E-02	3.09E+03 ± 6.18E-01	3.57E+04 ± 3.57E+00
6	7.83E+01 ± 3.13E-02	2.72E+03 ± 5.43E-01	3.33E+04 ± 3.33E+00
7	6.97E+01 ± 2.79E-02	2.42E+03 ± 4.84E-01	3.14E+04 ± 3.14E+00
8	6.29E+01 ± 3.15E-02	2.18E+03 ± 6.53E-01	2.97E+04 ± 2.97E+00
9	5.72E+01 ± 3.43E-02	1.98E+03 ± 5.95E-01	2.73E+04 ± 2.73E+00
10	5.26E+01 ± 3.16E-02	1.81E+03 ± 5.44E-01	2.64E+04 ± 2.64E+00
20	2.92E+01 ± 5.55E-02	1.05E+03 ± 6.28E-01	1.77E+04 ± 1.77E+00
30	2.10E+01 ± 7.77E-02	7.59E+02 ± 6.07E-01	1.34E+04 ± 2.67E+00
40	1.66E+01 ± 3.82E-02	5.97E+02 ± 5.38E-01	1.07E+04 ± 2.14E+00
50	1.39E+01 ± 2.91E-02	5.06E+02 ± 6.07E-01	9.07E+03 ± 2.72E+00
60	1.20E+01 ± 3.84E-02	4.40E+02 ± 6.60E-01	7.89E+03 ± 2.37E+00
70	1.06E+01 ± 4.36E-02	3.84E+02 ± 5.76E-01	7.06E+03 ± 2.12E+00
80	9.62E+00 ± 4.90E-02	3.44E+02 ± 5.51E-01	6.42E+03 ± 2.57E+00
90	8.83E+00 ± 5.56E-02	3.13E+02 ± 5.00E-01	5.88E+03 ± 2.35E+00
100	8.15E+00 ± 6.12E-02	2.91E+02 ± 5.54E-01	5.42E+03 ± 2.71E+00
120	7.10E+00 ± 3.27E-02	2.55E+02 ± 5.61E-01	4.74E+03 ± 2.37E+00
140	6.32E+00 ± 2.97E-02	2.28E+02 ± 5.69E-01	4.28E+03 ± 2.57E+00
160	5.80E+00 ± 3.13E-02	2.07E+02 ± 5.60E-01	3.87E+03 ± 2.71E+00
180	5.35E+00 ± 3.05E-02	1.91E+02 ± 5.55E-01	3.59E+03 ± 2.51E+00
200	4.96E+00 ± 2.97E-02	1.78E+02 ± 5.51E-01	3.34E+03 ± 2.67E+00
250	4.32E+00 ± 3.11E-02	1.55E+02 ± 5.88E-01	2.90E+03 ± 2.90E+00
300	3.90E+00 ± 3.20E-02	1.40E+02 ± 6.02E-01	2.64E+03 ± 2.90E+00
350	3.55E+00 ± 3.01E-02	1.28E+02 ± 6.02E-01	2.44E+03 ± 2.93E+00
400	3.36E+00 ± 3.43E-02	1.20E+02 ± 6.10E-01	2.27E+03 ± 2.73E+00
450	3.17E+00 ± 3.33E-02	1.13E+02 ± 6.24E-01	2.14E+03 ± 2.78E+00
500	3.00E+00 ± 3.30E-02	1.07E+02 ± 6.23E-01	2.03E+03 ± 2.84E+00
600	2.82E+00 ± 4.21E-02	1.00E+02 ± 6.22E-01	1.90E+03 ± 2.86E+00
700	2.62E+00 ± 3.19E-02	9.39E+01 ± 6.10E-01	1.80E+03 ± 3.05E+00
800	2.52E+00 ± 3.33E-02	9.06E+01 ± 6.70E-01	1.73E+03 ± 3.11E+00
900	2.44E+00 ± 3.42E-02	8.84E+01 ± 7.33E-01	1.68E+03 ± 3.19E+00
1000	2.37E+00 ± 3.80E-02	8.60E+01 ± 7.91E-01	1.63E+03 ± 3.42E+00
1500	2.23E+00 ± 4.33E-02	8.14E+01 ± 9.20E-01	1.54E+03 ± 4.00E+00
2000	2.32E+00 ± 8.19E-02	7.99E+01 ± 1.19E+00	1.50E+03 ± 4.80E+00
2500	2.26E+00 ± 7.58E-02	7.97E+01 ± 1.35E+00	1.50E+03 ± 5.53E+00
3000	2.29E+00 ± 8.62E-02	8.11E+01 ± 1.58E+00	1.51E+03 ± 6.20E+00
3500	2.31E+00 ± 1.05E-01	8.04E+01 ± 1.70E+00	1.50E+03 ± 6.90E+00
4000	2.30E+00 ± 1.05E-01	8.06E+01 ± 1.93E+00	1.50E+03 ± 7.48E+00
4500	2.33E+00 ± 1.15E-01	8.01E+01 ± 1.92E+00	1.49E+03 ± 7.76E+00
5000	2.32E+00 ± 1.17E-01	7.92E+01 ± 1.89E+00	1.49E+03 ± 8.64E+00
6000	2.27E+00 ± 1.04E-01	8.04E+01 ± 2.35E+00	1.51E+03 ± 1.06E+01
7000	2.39E+00 ± 1.81E-01	7.97E+01 ± 2.34E+00	1.52E+03 ± 1.26E+01
8000	2.24E+00 ± 1.03E-01	8.21E+01 ± 3.41E+00	1.53E+03 ± 1.39E+01
9000	2.23E+00 ± 1.02E-01	8.19E+01 ± 3.41E+00	1.53E+03 ± 1.45E+01
10000	2.23E+00 ± 1.02E-01	8.54E+01 ± 5.16E+00	1.54E+03 ± 1.65E+01

TABLE B. 15
Mass stopping powers of Griffith muscle for the proton, the carbon, and the iron beams. (MeV-cm^2/g)

Energy (MeV/u)	Proton	Carbon	Iron
1	3.44E+02 ± 3.44E-02	7.96E+03 ± 7.96E-01	5.06E+04 ± 5.06E+00
2	1.86E+02 ± 3.71E-02	5.47E+03 ± 5.47E-01	4.48E+04 ± 4.48E+00
3	1.34E+02 ± 2.69E-02	4.27E+03 ± 4.27E-01	4.10E+04 ± 4.10E+00
4	1.05E+02 ± 3.16E-02	3.51E+03 ± 7.01E-01	3.76E+04 ± 3.76E+00
5	8.91E+01 ± 2.67E-02	3.02E+03 ± 6.04E-01	3.49E+04 ± 3.49E+00
6	7.66E+01 ± 3.06E-02	2.66E+03 ± 5.31E-01	3.25E+04 ± 3.25E+00
7	6.81E+01 ± 3.40E-02	2.37E+03 ± 4.74E-01	3.08E+04 ± 3.08E+00
8	6.17E+01 ± 3.70E-02	2.14E+03 ± 6.42E-01	2.91E+04 ± 2.91E+00
9	5.65E+01 ± 3.95E-02	1.96E+03 ± 5.88E-01	2.70E+04 ± 2.70E+00
10	5.21E+01 ± 4.17E-02	1.79E+03 ± 5.38E-01	2.61E+04 ± 2.61E+00
20	2.88E+01 ± 5.19E-02	1.03E+03 ± 6.21E-01	1.75E+04 ± 1.75E+00
30	2.08E+01 ± 8.31E-02	7.49E+02 ± 5.99E-01	1.32E+04 ± 2.64E+00
40	1.65E+01 ± 8.08E-02	5.89E+02 ± 5.31E-01	1.06E+04 ± 2.11E+00
50	1.37E+01 ± 6.60E-02	4.99E+02 ± 5.99E-01	8.95E+03 ± 2.68E+00
60	1.19E+01 ± 6.67E-02	4.35E+02 ± 6.52E-01	7.79E+03 ± 2.34E+00
70	1.05E+01 ± 2.83E-02	3.79E+02 ± 5.69E-01	6.97E+03 ± 2.09E+00
80	9.50E+00 ± 4.08E-02	3.40E+02 ± 5.10E-01	6.33E+03 ± 2.53E+00
90	8.67E+00 ± 2.95E-02	3.09E+02 ± 4.94E-01	5.81E+03 ± 2.32E+00
100	8.00E+00 ± 2.96E-02	2.88E+02 ± 5.46E-01	5.35E+03 ± 2.67E+00
120	7.01E+00 ± 3.08E-02	2.51E+02 ± 5.53E-01	4.66E+03 ± 2.33E+00
140	6.24E+00 ± 2.87E-02	2.24E+02 ± 5.39E-01	4.22E+03 ± 2.53E+00
160	5.72E+00 ± 2.97E-02	2.05E+02 ± 5.53E-01	3.81E+03 ± 2.29E+00
180	5.28E+00 ± 2.96E-02	1.89E+02 ± 5.47E-01	3.54E+03 ± 2.48E+00
200	4.89E+00 ± 2.88E-02	1.75E+02 ± 5.44E-01	3.30E+03 ± 2.64E+00
250	4.25E+00 ± 2.98E-02	1.52E+02 ± 5.64E-01	2.86E+03 ± 2.86E+00
300	3.84E+00 ± 3.03E-02	1.38E+02 ± 5.80E-01	2.61E+03 ± 2.87E+00
350	3.50E+00 ± 2.98E-02	1.26E+02 ± 5.94E-01	2.41E+03 ± 2.89E+00
400	3.31E+00 ± 3.24E-02	1.18E+02 ± 5.89E-01	2.24E+03 ± 2.69E+00
450	3.13E+00 ± 3.29E-02	1.12E+02 ± 6.03E-01	2.11E+03 ± 2.75E+00
500	2.96E+00 ± 3.23E-02	1.06E+02 ± 6.04E-01	2.00E+03 ± 2.60E+00
600	2.76E+00 ± 3.17E-02	9.89E+01 ± 6.03E-01	1.88E+03 ± 2.82E+00
700	2.57E+00 ± 2.95E-02	9.27E+01 ± 6.02E-01	1.77E+03 ± 3.01E+00
800	2.48E+00 ± 3.25E-02	8.93E+01 ± 6.43E-01	1.70E+03 ± 3.07E+00
900	2.41E+00 ± 3.36E-02	8.70E+01 ± 6.96E-01	1.65E+03 ± 3.14E+00
1000	2.33E+00 ± 3.47E-02	8.46E+01 ± 7.53E-01	1.60E+03 ± 3.21E+00
1500	2.18E+00 ± 3.67E-02	8.04E+01 ± 9.00E-01	1.52E+03 ± 3.79E+00
2000	2.29E+00 ± 8.01E-02	7.89E+01 ± 1.17E+00	1.48E+03 ± 4.74E+00
2500	2.21E+00 ± 7.23E-02	7.82E+01 ± 1.25E+00	1.47E+03 ± 5.46E+00
3000	2.25E+00 ± 8.48E-02	7.98E+01 ± 1.56E+00	1.48E+03 ± 6.09E+00
3500	2.27E+00 ± 1.04E-01	7.90E+01 ± 1.67E+00	1.47E+03 ± 6.78E+00
4000	2.25E+00 ± 1.03E-01	7.83E+01 ± 1.65E+00	1.47E+03 ± 7.20E+00
4500	2.24E+00 ± 1.02E-01	7.87E+01 ± 1.89E+00	1.46E+03 ± 7.46E+00
5000	2.22E+00 ± 1.02E-01	7.79E+01 ± 1.86E+00	1.46E+03 ± 8.34E+00
6000	2.21E+00 ± 1.01E-01	7.90E+01 ± 2.31E+00	1.48E+03 ± 1.02E+01
7000	2.19E+00 ± 1.00E-01	7.84E+01 ± 2.30E+00	1.49E+03 ± 1.24E+01
8000	2.19E+00 ± 1.00E-01	8.06E+01 ± 3.36E+00	1.50E+03 ± 1.37E+01
9000	2.19E+00 ± 9.99E-02	8.05E+01 ± 3.35E+00	1.50E+03 ± 1.43E+01
10000	2.17E+00 ± 9.96E-02	8.40E+01 ± 5.07E+00	1.51E+03 ± 1.54E+01

TABLE B. 16
Mass stopping powers of Lincolnshire bolus for the proton, the carbon, and the iron beams. (MeV-cm^2/g)

Energy (MeV/u)	Proton	Carbon	Iron
1	3.13E+02 ± 3.13E-02	7.21E+03 ± 7.21E-01	4.61E+04 ± 4.61E+00
2	1.69E+02 ± 3.39E-02	4.97E+03 ± 4.97E-01	4.06E+04 ± 4.06E+00
3	1.22E+02 ± 2.43E-02	3.90E+03 ± 3.90E-01	3.72E+04 ± 3.72E+00
4	9.61E+01 ± 2.88E-02	3.19E+03 ± 6.38E-01	3.42E+04 ± 3.42E+00
5	8.10E+01 ± 3.24E-02	2.75E+03 ± 5.50E-01	3.18E+04 ± 3.18E+00
6	6.97E+01 ± 2.79E-02	2.42E+03 ± 4.84E-01	2.96E+04 ± 2.96E+00
7	6.22E+01 ± 3.11E-02	2.16E+03 ± 6.47E-01	2.81E+04 ± 2.81E+00
8	5.68E+01 ± 3.41E-02	1.96E+03 ± 5.89E-01	2.67E+04 ± 2.67E+00
9	5.23E+01 ± 3.14E-02	1.81E+03 ± 5.43E-01	2.49E+04 ± 2.49E+00
10	4.69E+01 ± 2.81E-02	1.66E+03 ± 4.97E-01	2.41E+04 ± 2.41E+00
20	2.68E+01 ± 5.62E-02	9.54E+02 ± 5.73E-01	1.63E+04 ± 1.63E+00
30	1.93E+01 ± 7.91E-02	6.95E+02 ± 5.56E-01	1.23E+04 ± 2.45E+00
40	1.53E+01 ± 3.81E-02	5.50E+02 ± 5.50E-01	9.81E+03 ± 1.96E+00
50	1.28E+01 ± 6.91E-02	4.66E+02 ± 6.06E-01	8.33E+03 ± 2.50E+00
60	1.10E+01 ± 3.75E-02	4.05E+02 ± 6.47E-01	7.24E+03 ± 2.17E+00
70	9.79E+00 ± 4.31E-02	3.53E+02 ± 5.29E-01	6.56E+03 ± 2.62E+00
80	8.87E+00 ± 4.97E-02	3.16E+02 ± 5.05E-01	5.87E+03 ± 2.35E+00
90	8.13E+00 ± 5.53E-02	2.90E+02 ± 5.52E-01	5.41E+03 ± 2.70E+00
100	7.52E+00 ± 6.24E-02	2.68E+02 ± 5.63E-01	4.99E+03 ± 2.50E+00
120	6.53E+00 ± 3.13E-02	2.34E+02 ± 5.39E-01	4.38E+03 ± 2.63E+00
140	5.83E+00 ± 2.91E-02	2.10E+02 ± 5.45E-01	3.93E+03 ± 2.36E+00
160	5.34E+00 ± 2.99E-02	1.91E+02 ± 5.34E-01	3.56E+03 ± 2.49E+00
180	4.92E+00 ± 2.90E-02	1.76E+02 ± 5.46E-01	3.31E+03 ± 2.65E+00
200	4.57E+00 ± 2.92E-02	1.64E+02 ± 5.57E-01	3.09E+03 ± 2.78E+00
250	3.97E+00 ± 2.98E-02	1.43E+02 ± 5.71E-01	2.67E+03 ± 2.94E+00
300	3.59E+00 ± 3.01E-02	1.29E+02 ± 5.94E-01	2.47E+03 ± 2.96E+00
350	3.30E+00 ± 3.20E-02	1.18E+02 ± 5.90E-01	2.25E+03 ± 2.70E+00
400	3.09E+00 ± 3.24E-02	1.10E+02 ± 5.97E-01	2.09E+03 ± 2.72E+00
450	2.91E+00 ± 3.12E-02	1.05E+02 ± 6.06E-01	1.97E+03 ± 2.56E+00
500	2.76E+00 ± 3.18E-02	9.90E+01 ± 5.94E-01	1.88E+03 ± 2.63E+00
600	2.56E+00 ± 3.03E-02	9.22E+01 ± 5.90E-01	1.76E+03 ± 2.81E+00
700	2.41E+00 ± 3.11E-02	8.70E+01 ± 6.35E-01	1.66E+03 ± 2.98E+00
800	2.31E+00 ± 3.10E-02	8.40E+01 ± 6.80E-01	1.60E+03 ± 3.03E+00
900	2.25E+00 ± 3.40E-02	8.18E+01 ± 7.28E-01	1.55E+03 ± 3.10E+00
1000	2.18E+00 ± 3.58E-02	7.94E+01 ± 7.70E-01	1.50E+03 ± 3.31E+00
1500	2.10E+00 ± 5.14E-02	7.50E+01 ± 8.62E-01	1.42E+03 ± 3.99E+00
2000	2.10E+00 ± 7.11E-02	7.40E+01 ± 1.16E+00	1.39E+03 ± 4.87E+00
2500	2.11E+00 ± 8.23E-02	7.44E+01 ± 1.43E+00	1.38E+03 ± 5.54E+00
3000	2.17E+00 ± 1.00E-01	7.56E+01 ± 1.61E+00	1.40E+03 ± 6.17E+00
3500	2.15E+00 ± 9.89E-02	7.48E+01 ± 1.59E+00	1.40E+03 ± 6.72E+00
4000	2.15E+00 ± 9.78E-02	7.56E+01 ± 1.81E+00	1.41E+03 ± 7.17E+00
4500	2.13E+00 ± 9.73E-02	7.50E+01 ± 1.78E+00	1.40E+03 ± 7.43E+00
5000	2.12E+00 ± 9.69E-02	7.57E+01 ± 2.22E+00	1.40E+03 ± 8.42E+00
6000	2.11E+00 ± 9.62E-02	7.54E+01 ± 2.20E+00	1.43E+03 ± 1.07E+01
7000	2.09E+00 ± 9.58E-02	7.72E+01 ± 3.21E+00	1.43E+03 ± 1.21E+01
8000	2.09E+00 ± 9.54E-02	7.70E+01 ± 3.20E+00	1.44E+03 ± 1.37E+01
9000	2.09E+00 ± 9.53E-02	8.05E+01 ± 4.85E+00	1.45E+03 ± 1.48E+01
10000	2.08E+00 ± 9.51E-02	8.02E+01 ± 4.83E+00	1.46E+03 ± 1.75E+01

TABLE B. 17
Mass stopping powers of Mylar/Melinex for the proton, the carbon, and the iron beams. (MeV-cm^2/g)

Energy (MeV/u)	Proton	Carbon	Iron
1	3.04E+02 ± 6.08E-02	6.91E+03 ± 6.91E-01	4.38E+04 ± 4.38E+00
2	1.62E+02 ± 3.25E-02	4.77E+03 ± 4.77E-01	3.91E+04 ± 3.91E+00
3	1.18E+02 ± 2.36E-02	3.72E+03 ± 3.72E-01	3.57E+04 ± 3.57E+00
4	9.19E+01 ± 2.76E-02	3.04E+03 ± 6.09E-01	3.26E+04 ± 3.26E+00
5	7.65E+01 ± 2.29E-02	2.62E+03 ± 5.25E-01	3.03E+04 ± 3.03E+00
6	6.66E+01 ± 2.67E-02	2.30E+03 ± 4.61E-01	2.82E+04 ± 2.82E+00
7	5.89E+01 ± 2.35E-02	2.06E+03 ± 4.11E-01	2.68E+04 ± 2.68E+00
8	5.39E+01 ± 3.23E-02	1.89E+03 ± 3.78E-01	2.56E+04 ± 2.56E+00
9	5.03E+01 ± 3.52E-02	1.75E+03 ± 5.26E-01	2.41E+04 ± 2.41E+00
10	4.67E+01 ± 3.74E-02	1.61E+03 ± 4.82E-01	2.34E+04 ± 2.34E+00
20	2.60E+01 ± 4.42E-02	9.34E+02 ± 4.67E-01	1.58E+04 ± 1.58E+00
30	1.87E+01 ± 6.74E-02	6.71E+02 ± 4.70E-01	1.19E+04 ± 2.38E+00
40	1.49E+01 ± 6.56E-02	5.31E+02 ± 4.78E-01	9.52E+03 ± 1.90E+00
50	1.24E+01 ± 5.34E-02	4.48E+02 ± 4.93E-01	8.08E+03 ± 2.43E+00
60	1.08E+01 ± 5.39E-02	3.92E+02 ± 5.49E-01	7.04E+03 ± 2.11E+00
70	9.48E+00 ± 2.46E-02	3.44E+02 ± 4.82E-01	6.31E+03 ± 1.89E+00
80	8.58E+00 ± 3.43E-02	3.09E+02 ± 4.63E-01	5.74E+03 ± 2.30E+00
90	7.86E+00 ± 3.69E-02	2.81E+02 ± 4.49E-01	5.27E+03 ± 2.11E+00
100	7.28E+00 ± 4.81E-02	2.60E+02 ± 4.68E-01	4.85E+03 ± 2.43E+00
120	6.35E+00 ± 2.86E-02	2.28E+02 ± 4.78E-01	4.25E+03 ± 2.13E+00
140	5.66E+00 ± 2.49E-02	2.03E+02 ± 4.67E-01	3.83E+03 ± 2.30E+00
160	5.16E+00 ± 2.48E-02	1.86E+02 ± 4.83E-01	3.47E+03 ± 2.08E+00
180	4.80E+00 ± 2.59E-02	1.71E+02 ± 4.63E-01	3.21E+03 ± 2.24E+00
200	4.45E+00 ± 2.58E-02	1.59E+02 ± 4.61E-01	2.98E+03 ± 2.09E+00
250	3.86E+00 ± 2.55E-02	1.38E+02 ± 4.84E-01	2.59E+03 ± 2.33E+00
300	3.48E+00 ± 2.54E-02	1.25E+02 ± 5.01E-01	2.38E+03 ± 2.61E+00
350	3.19E+00 ± 2.62E-02	1.15E+02 ± 5.17E-01	2.20E+03 ± 2.41E+00
400	2.98E+00 ± 2.62E-02	1.07E+02 ± 5.15E-01	2.05E+03 ± 2.45E+00
450	2.86E+00 ± 2.94E-02	1.02E+02 ± 5.18E-01	1.93E+03 ± 2.31E+00
500	2.70E+00 ± 2.86E-02	9.65E+01 ± 5.31E-01	1.82E+03 ± 2.37E+00
600	2.52E+00 ± 2.82E-02	9.01E+01 ± 5.31E-01	1.71E+03 ± 2.39E+00
700	2.35E+00 ± 2.73E-02	8.46E+01 ± 5.33E-01	1.61E+03 ± 2.57E+00
800	2.26E+00 ± 2.73E-02	8.11E+01 ± 5.35E-01	1.55E+03 ± 2.64E+00
900	2.19E+00 ± 2.90E-02	7.89E+01 ± 5.76E-01	1.51E+03 ± 2.71E+00
1000	2.12E+00 ± 2.99E-02	7.67E+01 ± 6.21E-01	1.46E+03 ± 2.77E+00
1500	2.00E+00 ± 3.40E-02	7.33E+01 ± 7.92E-01	1.38E+03 ± 3.32E+00
2000	2.01E+00 ± 5.76E-02	7.10E+01 ± 8.94E-01	1.35E+03 ± 3.90E+00
2500	2.03E+00 ± 6.72E-02	7.14E+01 ± 1.10E+00	1.35E+03 ± 4.71E+00
3000	2.07E+00 ± 7.86E-02	7.36E+01 ± 1.44E+00	1.36E+03 ± 5.31E+00
3500	2.05E+00 ± 7.77E-02	7.27E+01 ± 1.43E+00	1.36E+03 ± 5.85E+00
4000	2.09E+00 ± 9.52E-02	7.27E+01 ± 1.53E+00	1.36E+03 ± 6.38E+00
4500	2.08E+00 ± 9.47E-02	7.31E+01 ± 1.75E+00	1.36E+03 ± 6.79E+00
5000	2.06E+00 ± 9.41E-02	7.25E+01 ± 1.74E+00	1.35E+03 ± 7.02E+00
6000	2.05E+00 ± 9.35E-02	7.34E+01 ± 2.14E+00	1.36E+03 ± 8.45E+00
7000	2.03E+00 ± 9.32E-02	7.28E+01 ± 2.13E+00	1.38E+03 ± 1.05E+01
8000	2.03E+00 ± 9.28E-02	7.49E+01 ± 3.11E+00	1.39E+03 ± 1.18E+01
9000	2.03E+00 ± 9.27E-02	7.48E+01 ± 3.11E+00	1.39E+03 ± 1.30E+01
10000	2.02E+00 ± 9.25E-02	7.80E+01 ± 4.70E+00	1.39E+03 ± 1.32E+01

TABLE B. 18
Mass stopping powers of Nylon-6 for the proton, the carbon, and the iron beams. (MeV-cm^2/g)

Energy (MeV/u)	Proton		Carbon		Iron	
1	3.10E+02	± 3.10E-02	7.20E+03	± 7.20E-01	4.58E+04	± 4.58E+00
2	1.68E+02	± 3.35E-02	4.95E+03	± 4.95E-01	4.05E+04	± 4.05E+00
3	1.22E+02	± 2.43E-02	3.86E+03	± 3.86E-01	3.71E+04	± 3.71E+00
4	9.53E+01	± 2.86E-02	3.17E+03	± 6.34E-01	3.40E+04	± 3.40E+00
5	8.05E+01	± 2.41E-02	2.73E+03	± 5.47E-01	3.16E+04	± 3.16E+00
6	6.92E+01	± 2.77E-02	2.40E+03	± 4.80E-01	2.94E+04	± 2.94E+00
7	6.15E+01	± 3.07E-02	2.14E+03	± 4.28E-01	2.78E+04	± 2.78E+00
8	5.57E+01	± 3.34E-02	1.93E+03	± 3.87E-01	2.63E+04	± 2.63E+00
9	5.09E+01	± 3.57E-02	1.77E+03	± 5.31E-01	2.44E+04	± 2.44E+00
10	4.70E+01	± 3.76E-02	1.62E+03	± 4.86E-01	2.35E+04	± 2.35E+00
20	2.60E+01	± 4.68E-02	9.32E+02	± 4.66E-01	1.58E+04	± 1.58E+00
30	1.87E+01	± 7.30E-02	6.75E+02	± 4.73E-01	1.19E+04	± 2.38E+00
40	1.49E+01	± 6.99E-02	5.31E+02	± 4.78E-01	9.51E+03	± 1.90E+00
50	1.24E+01	± 5.82E-02	4.49E+02	± 5.39E-01	8.06E+03	± 2.42E+00
60	1.07E+01	± 5.90E-02	3.91E+02	± 5.48E-01	7.01E+03	± 2.10E+00
70	9.43E+00	± 2.55E-02	3.42E+02	± 4.78E-01	6.28E+03	± 1.88E+00
80	8.55E+00	± 3.59E-02	3.06E+02	± 4.60E-01	5.69E+03	± 2.28E+00
90	7.80E+00	± 2.65E-02	2.78E+02	± 4.45E-01	5.23E+03	± 2.09E+00
100	7.20E+00	± 2.66E-02	2.59E+02	± 4.91E-01	4.82E+03	± 2.41E+00
120	6.30E+00	± 2.58E-02	2.26E+02	± 4.75E-01	4.18E+03	± 2.09E+00
140	5.64E+00	± 3.16E-02	2.02E+02	± 4.85E-01	3.80E+03	± 2.28E+00
160	5.15E+00	± 2.68E-02	1.84E+02	± 4.79E-01	3.43E+03	± 2.06E+00
180	4.75E+00	± 2.61E-02	1.70E+02	± 4.75E-01	3.18E+03	± 2.23E+00
200	4.40E+00	± 2.55E-02	1.58E+02	± 4.89E-01	2.96E+03	± 2.37E+00
250	3.83E+00	± 2.64E-02	1.37E+02	± 4.94E-01	2.57E+03	± 2.57E+00
300	3.46E+00	± 2.70E-02	1.24E+02	± 5.09E-01	2.35E+03	± 2.58E+00
350	3.15E+00	± 2.58E-02	1.14E+02	± 5.23E-01	2.17E+03	± 2.60E+00
400	2.98E+00	± 2.92E-02	1.06E+02	± 5.20E-01	2.02E+03	± 2.42E+00
450	2.82E+00	± 2.93E-02	1.01E+02	± 5.33E-01	1.90E+03	± 2.28E+00
500	2.66E+00	± 2.85E-02	9.54E+01	± 5.34E-01	1.80E+03	± 2.34E+00
600	2.48E+00	± 2.83E-02	8.90E+01	± 5.43E-01	1.69E+03	± 2.53E+00
700	2.31E+00	± 2.63E-02	8.33E+01	± 5.33E-01	1.59E+03	± 2.55E+00
800	2.24E+00	± 2.91E-02	8.04E+01	± 5.79E-01	1.53E+03	± 2.60E+00
900	2.16E+00	± 2.83E-02	7.83E+01	± 6.27E-01	1.49E+03	± 2.82E+00
1000	2.10E+00	± 3.15E-02	7.60E+01	± 6.61E-01	1.44E+03	± 2.88E+00
1500	1.96E+00	± 3.28E-02	7.23E+01	± 8.02E-01	1.36E+03	± 3.41E+00
2000	2.00E+00	± 6.07E-02	7.09E+01	± 1.05E+00	1.33E+03	± 4.12E+00
2500	1.99E+00	± 6.48E-02	7.03E+01	± 1.13E+00	1.33E+03	± 4.90E+00
3000	2.01E+00	± 7.59E-02	7.14E+01	± 1.39E+00	1.33E+03	± 5.45E+00
3500	2.03E+00	± 9.26E-02	7.07E+01	± 1.49E+00	1.32E+03	± 6.06E+00
4000	2.01E+00	± 9.18E-02	7.00E+01	± 1.48E+00	1.31E+03	± 6.43E+00
4500	2.00E+00	± 9.13E-02	7.04E+01	± 1.69E+00	1.31E+03	± 6.67E+00
5000	1.98E+00	± 9.09E-02	6.97E+01	± 1.67E+00	1.31E+03	± 7.32E+00
6000	1.98E+00	± 9.02E-02	7.07E+01	± 2.07E+00	1.32E+03	± 9.01E+00
7000	1.96E+00	± 8.98E-02	7.01E+01	± 2.05E+00	1.33E+03	± 1.09E+01
8000	1.96E+00	± 8.95E-02	7.22E+01	± 3.00E+00	1.34E+03	± 1.22E+01
9000	1.96E+00	± 8.94E-02	7.21E+01	± 3.00E+00	1.35E+03	± 1.28E+01
10000	1.95E+00	± 8.91E-02	7.51E+01	± 4.54E+00	1.35E+03	± 1.38E+01

TABLE B. 19
Mass stopping powers of Nylon, Du Pont Elvamide 8062 for the proton, the carbon, and the iron beams. (MeV-cm^2/g)

Energy (MeV/u)	Proton	Carbon	Iron
1	3.54E+02 ± 3.54E-02	8.24E+03 ± 8.24E-01	5.24E+04 ± 5.24E+00
2	1.92E+02 ± 3.84E-02	5.66E+03 ± 5.66E-01	4.63E+04 ± 4.63E+00
3	1.39E+02 ± 2.78E-02	4.42E+03 ± 4.42E-01	4.24E+04 ± 4.24E+00
4	1.09E+02 ± 3.28E-02	3.63E+03 ± 7.26E-01	3.89E+04 ± 3.89E+00
5	9.22E+01 ± 2.77E-02	3.13E+03 ± 6.26E-01	3.62E+04 ± 3.62E+00
6	7.92E+01 ± 3.17E-02	2.75E+03 ± 5.50E-01	3.37E+04 ± 3.37E+00
7	7.05E+01 ± 3.52E-02	2.45E+03 ± 4.90E-01	3.19E+04 ± 3.19E+00
8	6.39E+01 ± 3.83E-02	2.21E+03 ± 6.64E-01	3.01E+04 ± 3.01E+00
9	5.83E+01 ± 4.08E-02	2.02E+03 ± 6.07E-01	2.79E+04 ± 2.79E+00
10	5.37E+01 ± 4.30E-02	1.85E+03 ± 5.55E-01	2.69E+04 ± 2.69E+00
20	2.97E+01 ± 5.35E-02	1.06E+03 ± 7.45E-01	1.80E+04 ± 1.80E+00
30	2.14E+01 ± 8.56E-02	7.71E+02 ± 6.17E-01	1.36E+04 ± 2.72E+00
40	1.70E+01 ± 8.32E-02	6.07E+02 ± 5.46E-01	1.09E+04 ± 2.17E+00
50	1.41E+01 ± 6.79E-02	5.13E+02 ± 6.16E-01	9.20E+03 ± 2.76E+00
60	1.23E+01 ± 6.98E-02	4.47E+02 ± 6.70E-01	8.01E+03 ± 2.40E+00
70	1.08E+01 ± 2.91E-02	3.91E+02 ± 1.53E+00	7.16E+03 ± 2.15E+00
80	9.76E+00 ± 4.20E-02	3.49E+02 ± 5.24E-01	6.51E+03 ± 2.61E+00
90	8.91E+00 ± 3.03E-02	3.17E+02 ± 5.08E-01	5.97E+03 ± 2.39E+00
100	8.22E+00 ± 3.04E-02	2.95E+02 ± 5.61E-01	5.50E+03 ± 2.75E+00
120	7.19E+00 ± 3.02E-02	2.58E+02 ± 5.68E-01	4.80E+03 ± 2.40E+00
140	6.40E+00 ± 2.95E-02	2.31E+02 ± 5.54E-01	4.33E+03 ± 2.60E+00
160	5.88E+00 ± 3.11E-02	2.10E+02 ± 5.68E-01	3.92E+03 ± 2.35E+00
180	5.42E+00 ± 3.04E-02	1.94E+02 ± 5.62E-01	3.63E+03 ± 2.54E+00
200	5.02E+00 ± 2.96E-02	1.80E+02 ± 5.58E-01	3.39E+03 ± 2.71E+00
250	4.38E+00 ± 3.11E-02	1.57E+02 ± 5.80E-01	2.94E+03 ± 2.94E+00
300	3.95E+00 ± 3.16E-02	1.42E+02 ± 5.96E-01	2.67E+03 ± 2.94E+00
350	3.59E+00 ± 3.02E-02	1.30E+02 ± 5.96E-01	2.47E+03 ± 2.97E+00
400	3.41E+00 ± 3.44E-02	1.21E+02 ± 6.06E-01	2.30E+03 ± 2.76E+00
450	3.21E+00 ± 3.34E-02	1.15E+02 ± 6.20E-01	2.16E+03 ± 2.81E+00
500	3.04E+00 ± 3.31E-02	1.09E+02 ± 6.21E-01	2.06E+03 ± 2.67E+00
600	2.83E+00 ± 3.22E-02	1.01E+02 ± 6.19E-01	1.93E+03 ± 2.89E+00
700	2.64E+00 ± 3.17E-02	9.50E+01 ± 6.18E-01	1.82E+03 ± 3.09E+00
800	2.59E+00 ± 5.00E-02	9.16E+01 ± 6.60E-01	1.75E+03 ± 3.15E+00
900	2.47E+00 ± 3.44E-02	8.95E+01 ± 7.34E-01	1.70E+03 ± 3.22E+00
1000	2.39E+00 ± 3.61E-02	8.69E+01 ± 7.82E-01	1.65E+03 ± 3.46E+00
1500	2.26E+00 ± 4.34E-02	8.23E+01 ± 9.14E-01	1.55E+03 ± 3.89E+00
2000	2.31E+00 ± 7.62E-02	8.08E+01 ± 1.20E+00	1.52E+03 ± 4.85E+00
2500	2.30E+00 ± 7.74E-02	8.06E+01 ± 1.36E+00	1.51E+03 ± 5.59E+00
3000	2.29E+00 ± 8.64E-02	8.13E+01 ± 1.59E+00	1.51E+03 ± 6.21E+00
3500	2.34E+00 ± 1.09E-01	8.05E+01 ± 1.70E+00	1.50E+03 ± 6.90E+00
4000	2.31E+00 ± 1.05E-01	8.07E+01 ± 1.94E+00	1.50E+03 ± 7.49E+00
4500	2.29E+00 ± 1.05E-01	8.02E+01 ± 1.92E+00	1.49E+03 ± 7.76E+00
5000	2.26E+00 ± 1.03E-01	7.93E+01 ± 1.90E+00	1.49E+03 ± 8.65E+00
6000	2.25E+00 ± 1.03E-01	8.05E+01 ± 2.35E+00	1.51E+03 ± 1.06E+01
7000	2.23E+00 ± 1.02E-01	7.98E+01 ± 2.34E+00	1.52E+03 ± 1.26E+01
8000	2.23E+00 ± 1.02E-01	8.22E+01 ± 3.42E+00	1.53E+03 ± 1.39E+01
9000	2.23E+00 ± 1.02E-01	8.20E+01 ± 3.41E+00	1.53E+03 ± 1.46E+01
10000	2.22E+00 ± 1.01E-01	8.56E+01 ± 5.17E+00	1.54E+03 ± 1.57E+01

TABLE B. 20
Mass stopping powers of Polyethylene for the proton, the carbon, and the iron beams. (MeV-cm^2/g)

Energy (MeV/u)	Proton	Carbon	Iron
1	3.80E+02 ± 3.80E-02	8.95E+03 ± 8.95E-01	5.70E+04 ± 5.70E+00
2	2.08E+02 ± 4.16E-02	6.15E+03 ± 6.15E-01	5.04E+04 ± 5.04E+00
3	1.51E+02 ± 3.01E-02	4.82E+03 ± 4.82E-01	4.62E+04 ± 4.62E+00
4	1.13E+02 ± 2.27E-02	3.96E+03 ± 7.92E-01	4.24E+04 ± 4.24E+00
5	1.00E+02 ± 3.01E-02	3.41E+03 ± 6.83E-01	3.95E+04 ± 3.95E+00
6	8.64E+01 ± 3.46E-02	3.00E+03 ± 6.00E-01	3.67E+04 ± 3.67E+00
7	7.71E+01 ± 3.85E-02	2.67E+03 ± 5.34E-01	3.47E+04 ± 3.47E+00
8	6.97E+01 ± 4.18E-02	2.41E+03 ± 7.22E-01	3.28E+04 ± 3.28E+00
9	6.35E+01 ± 4.44E-02	2.20E+03 ± 6.59E-01	3.03E+04 ± 3.03E+00
10	5.68E+01 ± 4.55E-02	2.01E+03 ± 6.02E-01	2.92E+04 ± 2.92E+00
20	3.21E+01 ± 3.21E-02	1.15E+03 ± 5.73E-01	1.95E+04 ± 1.95E+00
30	2.30E+01 ± 4.37E-02	8.31E+02 ± 6.65E-01	1.47E+04 ± 2.93E+00
40	1.82E+01 ± 7.29E-02	6.56E+02 ± 6.56E-01	1.17E+04 ± 2.34E+00
50	1.52E+01 ± 3.34E-02	5.55E+02 ± 7.21E-01	9.92E+03 ± 2.97E+00
60	1.32E+01 ± 8.18E-02	4.76E+02 ± 6.66E-01	8.62E+03 ± 2.59E+00
70	1.16E+01 ± 3.25E-02	4.19E+02 ± 6.28E-01	7.78E+03 ± 3.11E+00
80	1.05E+01 ± 4.63E-02	3.75E+02 ± 6.00E-01	6.97E+03 ± 2.79E+00
90	9.58E+00 ± 3.35E-02	3.44E+02 ± 6.20E-01	6.41E+03 ± 2.56E+00
100	8.84E+00 ± 3.36E-02	3.18E+02 ± 6.35E-01	5.92E+03 ± 2.96E+00
120	7.71E+00 ± 3.32E-02	2.77E+02 ± 6.10E-01	5.19E+03 ± 3.12E+00
140	6.90E+00 ± 3.38E-02	2.48E+02 ± 6.19E-01	4.65E+03 ± 2.79E+00
160	6.31E+00 ± 3.41E-02	2.25E+02 ± 6.09E-01	4.21E+03 ± 2.95E+00
180	5.81E+00 ± 3.31E-02	2.08E+02 ± 6.25E-01	3.91E+03 ± 2.74E+00
200	5.39E+00 ± 3.29E-02	1.94E+02 ± 6.19E-01	3.65E+03 ± 2.92E+00
250	4.68E+00 ± 3.37E-02	1.68E+02 ± 6.57E-01	3.15E+03 ± 3.47E+00
300	4.22E+00 ± 3.38E-02	1.52E+02 ± 6.70E-01	2.90E+03 ± 3.19E+00
350	3.89E+00 ± 3.61E-02	1.39E+02 ± 6.67E-01	2.64E+03 ± 3.17E+00
400	3.65E+00 ± 3.75E-02	1.30E+02 ± 6.76E-01	2.46E+03 ± 2.95E+00
450	3.43E+00 ± 3.60E-02	1.23E+02 ± 6.88E-01	2.32E+03 ± 3.02E+00
500	3.25E+00 ± 3.57E-02	1.17E+02 ± 6.76E-01	2.21E+03 ± 3.09E+00
600	3.06E+00 ± 5.02E-02	1.08E+02 ± 6.61E-01	2.07E+03 ± 3.31E+00
700	2.84E+00 ± 3.70E-02	1.02E+02 ± 7.16E-01	1.94E+03 ± 3.31E+00
800	2.72E+00 ± 3.54E-02	9.85E+01 ± 7.69E-01	1.87E+03 ± 3.37E+00
900	2.64E+00 ± 3.83E-02	9.59E+01 ± 8.25E-01	1.82E+03 ± 3.64E+00
1000	2.57E+00 ± 4.05E-02	9.30E+01 ± 8.65E-01	1.76E+03 ± 3.70E+00
1500	2.48E+00 ± 6.36E-02	8.80E+01 ± 1.00E+00	1.67E+03 ± 4.50E+00
2000	2.46E+00 ± 8.02E-02	8.64E+01 ± 1.30E+00	1.62E+03 ± 5.36E+00
2500	2.48E+00 ± 9.49E-02	8.70E+01 ± 1.70E+00	1.61E+03 ± 6.27E+00
3000	2.48E+00 ± 1.13E-01	8.64E+01 ± 1.81E+00	1.60E+03 ± 6.89E+00
3500	2.44E+00 ± 1.11E-01	8.48E+01 ± 1.79E+00	1.58E+03 ± 7.44E+00
4000	2.48E+00 ± 1.29E-01	8.50E+01 ± 2.04E+00	1.58E+03 ± 8.05E+00
4500	2.43E+00 ± 1.12E-01	8.43E+01 ± 2.01E+00	1.58E+03 ± 8.51E+00
5000	2.40E+00 ± 1.10E-01	8.50E+01 ± 2.50E+00	1.57E+03 ± 9.45E+00
6000	2.49E+00 ± 1.62E-01	8.48E+01 ± 2.48E+00	1.60E+03 ± 1.22E+01
7000	2.38E+00 ± 1.12E-01	8.67E+01 ± 3.62E+00	1.60E+03 ± 1.36E+01
8000	2.37E+00 ± 1.09E-01	8.65E+01 ± 3.61E+00	1.62E+03 ± 1.54E+01
9000	2.36E+00 ± 1.08E-01	9.05E+01 ± 5.46E+00	1.62E+03 ± 1.66E+01
10000	2.36E+00 ± 1.09E-01	9.01E+01 ± 5.44E+00	1.64E+03 ± 2.04E+01

TABLE B. 21
Mass stopping powers of PEG-200 for the proton, the carbon, and the iron beams. (MeV-cm^2/g)

Energy (MeV/u)	Proton	Carbon	Iron
1	3.46E+02 ± 3.46E-02	8.02E+03 ± 8.02E-01	5.10E+04 ± 5.10E+00
2	1.87E+02 ± 3.74E-02	5.51E+03 ± 5.51E-01	4.51E+04 ± 4.51E+00
3	1.35E+02 ± 2.71E-02	4.30E+03 ± 4.30E-01	4.13E+04 ± 4.13E+00
4	1.06E+02 ± 3.19E-02	3.53E+03 ± 7.06E-01	3.78E+04 ± 3.78E+00
5	8.97E+01 ± 2.69E-02	3.04E+03 ± 6.09E-01	3.52E+04 ± 3.52E+00
6	7.71E+01 ± 3.09E-02	2.67E+03 ± 5.35E-01	3.28E+04 ± 3.28E+00
7	6.85E+01 ± 3.43E-02	2.39E+03 ± 4.77E-01	3.10E+04 ± 3.10E+00
8	6.21E+01 ± 3.73E-02	2.15E+03 ± 6.46E-01	2.93E+04 ± 2.93E+00
9	5.68E+01 ± 3.98E-02	1.97E+03 ± 5.92E-01	2.72E+04 ± 2.72E+00
10	5.24E+01 ± 4.19E-02	1.80E+03 ± 5.41E-01	2.62E+04 ± 2.62E+00
20	2.90E+01 ± 5.22E-02	1.04E+03 ± 6.24E-01	1.76E+04 ± 1.76E+00
30	2.09E+01 ± 8.15E-02	7.53E+02 ± 6.03E-01	1.33E+04 ± 2.66E+00
40	1.66E+01 ± 7.96E-02	5.93E+02 ± 5.33E-01	1.06E+04 ± 2.12E+00
50	1.38E+01 ± 6.63E-02	5.01E+02 ± 6.02E-01	9.00E+03 ± 2.70E+00
60	1.20E+01 ± 6.71E-02	4.37E+02 ± 6.55E-01	7.83E+03 ± 2.35E+00
70	1.06E+01 ± 4.12E-02	3.81E+02 ± 5.72E-01	7.01E+03 ± 2.10E+00
80	9.55E+00 ± 4.68E-02	3.42E+02 ± 5.13E-01	6.36E+03 ± 2.54E+00
90	8.75E+00 ± 5.25E-02	3.11E+02 ± 4.97E-01	5.84E+03 ± 2.34E+00
100	8.09E+00 ± 5.91E-02	2.89E+02 ± 5.49E-01	5.38E+03 ± 2.69E+00
120	7.05E+00 ± 3.31E-02	2.53E+02 ± 5.56E-01	4.68E+03 ± 2.34E+00
140	6.27E+00 ± 2.89E-02	2.26E+02 ± 5.41E-01	4.24E+03 ± 2.55E+00
160	5.75E+00 ± 2.99E-02	2.06E+02 ± 5.35E-01	3.84E+03 ± 2.30E+00
180	5.31E+00 ± 2.97E-02	1.90E+02 ± 5.50E-01	3.56E+03 ± 2.49E+00
200	4.91E+00 ± 2.90E-02	1.76E+02 ± 5.47E-01	3.31E+03 ± 2.65E+00
250	4.28E+00 ± 3.00E-02	1.53E+02 ± 5.51E-01	2.87E+03 ± 2.87E+00
300	3.86E+00 ± 3.05E-02	1.39E+02 ± 5.82E-01	2.62E+03 ± 2.88E+00
350	3.53E+00 ± 3.00E-02	1.27E+02 ± 5.84E-01	2.42E+03 ± 2.91E+00
400	3.32E+00 ± 3.26E-02	1.18E+02 ± 5.81E-01	2.25E+03 ± 2.71E+00
450	3.15E+00 ± 3.31E-02	1.12E+02 ± 5.95E-01	2.12E+03 ± 2.76E+00
500	2.98E+00 ± 3.25E-02	1.07E+02 ± 6.08E-01	2.01E+03 ± 2.62E+00
600	2.77E+00 ± 3.19E-02	9.95E+01 ± 6.07E-01	1.89E+03 ± 2.83E+00
700	2.58E+00 ± 2.97E-02	9.32E+01 ± 6.06E-01	1.78E+03 ± 2.85E+00
800	2.50E+00 ± 3.28E-02	8.99E+01 ± 6.47E-01	1.71E+03 ± 3.08E+00
900	2.42E+00 ± 3.16E-02	8.75E+01 ± 7.00E-01	1.66E+03 ± 3.16E+00
1000	2.35E+00 ± 3.50E-02	8.51E+01 ± 7.57E-01	1.61E+03 ± 3.23E+00
1500	2.19E+00 ± 3.69E-02	8.08E+01 ± 9.05E-01	1.53E+03 ± 3.81E+00
2000	2.27E+00 ± 7.43E-02	7.93E+01 ± 1.17E+00	1.49E+03 ± 4.61E+00
2500	2.25E+00 ± 7.60E-02	7.86E+01 ± 1.26E+00	1.48E+03 ± 5.49E+00
3000	2.26E+00 ± 8.52E-02	8.02E+01 ± 1.56E+00	1.49E+03 ± 6.12E+00
3500	2.28E+00 ± 1.04E-01	7.94E+01 ± 1.68E+00	1.48E+03 ± 6.81E+00
4000	2.27E+00 ± 1.03E-01	7.87E+01 ± 1.66E+00	1.48E+03 ± 7.23E+00
4500	2.30E+00 ± 1.13E-01	7.91E+01 ± 1.90E+00	1.47E+03 ± 7.50E+00
5000	2.29E+00 ± 1.15E-01	7.83E+01 ± 1.87E+00	1.47E+03 ± 8.22E+00
6000	2.24E+00 ± 1.02E-01	7.94E+01 ± 2.32E+00	1.49E+03 ± 1.03E+01
7000	2.36E+00 ± 1.75E-01	7.87E+01 ± 2.31E+00	1.50E+03 ± 1.23E+01
8000	2.22E+00 ± 1.01E-01	8.10E+01 ± 3.37E+00	1.51E+03 ± 1.37E+01
9000	2.20E+00 ± 1.00E-01	8.09E+01 ± 3.37E+00	1.51E+03 ± 1.44E+01
10000	2.20E+00 ± 1.01E-01	8.44E+01 ± 5.10E+00	1.51E+03 ± 1.54E+01

TABLE B. 22
Mass stopping powers of Polystyrene for the proton, the carbon, and the iron beams. (MeV-cm^2/g)

Energy (MeV/u)	Proton	Carbon	Iron
1	3.31E+02 ± 3.31E-02	7.71E+03 ± 7.71E-01	4.92E+04 ± 4.92E+00
2	1.80E+02 ± 3.60E-02	5.31E+03 ± 5.31E-01	4.34E+04 ± 4.34E+00
3	1.31E+02 ± 2.61E-02	4.15E+03 ± 4.15E-01	3.98E+04 ± 3.98E+00
4	1.03E+02 ± 3.08E-02	3.41E+03 ± 6.81E-01	3.65E+04 ± 3.65E+00
5	8.65E+01 ± 2.59E-02	2.94E+03 ± 5.87E-01	3.40E+04 ± 3.40E+00
6	7.44E+01 ± 2.98E-02	2.58E+03 ± 5.16E-01	3.16E+04 ± 3.16E+00
7	6.63E+01 ± 3.32E-02	2.30E+03 ± 4.60E-01	3.00E+04 ± 3.00E+00
8	6.05E+01 ± 3.63E-02	2.10E+03 ± 6.29E-01	2.85E+04 ± 2.85E+00
9	5.57E+01 ± 4.46E-02	1.93E+03 ± 5.79E-01	2.66E+04 ± 2.66E+00
10	5.13E+01 ± 4.62E-02	1.76E+03 ± 5.29E-01	2.57E+04 ± 2.57E+00
20	2.84E+01 ± 3.12E-02	1.01E+03 ± 6.08E-01	1.72E+04 ± 1.72E+00
30	2.04E+01 ± 3.87E-02	7.36E+02 ± 5.89E-01	1.30E+04 ± 2.60E+00
40	1.62E+01 ± 7.46E-02	5.81E+02 ± 5.81E-01	1.04E+04 ± 2.08E+00
50	1.35E+01 ± 3.37E-02	4.92E+02 ± 6.39E-01	8.80E+03 ± 2.64E+00
60	1.17E+01 ± 7.03E-02	4.27E+02 ± 6.40E-01	7.65E+03 ± 2.30E+00
70	1.03E+01 ± 2.88E-02	3.72E+02 ± 5.58E-01	6.94E+03 ± 2.78E+00
80	9.35E+00 ± 4.21E-02	3.33E+02 ± 5.34E-01	6.23E+03 ± 2.49E+00
90	8.53E+00 ± 3.07E-02	3.06E+02 ± 5.51E-01	5.70E+03 ± 2.28E+00
100	7.86E+00 ± 3.07E-02	2.83E+02 ± 5.65E-01	5.26E+03 ± 2.63E+00
120	6.87E+00 ± 2.95E-02	2.47E+02 ± 5.43E-01	4.61E+03 ± 2.77E+00
140	6.12E+00 ± 2.88E-02	2.21E+02 ± 5.52E-01	4.14E+03 ± 2.48E+00
160	5.62E+00 ± 3.04E-02	2.01E+02 ± 5.63E-01	3.75E+03 ± 2.62E+00
180	5.18E+00 ± 3.01E-02	1.86E+02 ± 5.57E-01	3.48E+03 ± 2.44E+00
200	4.81E+00 ± 2.98E-02	1.72E+02 ± 5.52E-01	3.25E+03 ± 2.60E+00
250	4.18E+00 ± 3.05E-02	1.50E+02 ± 5.70E-01	2.81E+03 ± 3.09E+00
300	3.78E+00 ± 3.10E-02	1.36E+02 ± 5.97E-01	2.59E+03 ± 2.85E+00
350	3.46E+00 ± 3.18E-02	1.24E+02 ± 5.96E-01	2.36E+03 ± 2.83E+00
400	3.25E+00 ± 3.31E-02	1.16E+02 ± 6.03E-01	2.20E+03 ± 2.64E+00
450	3.06E+00 ± 3.22E-02	1.10E+02 ± 6.15E-01	2.07E+03 ± 2.69E+00
500	2.90E+00 ± 3.19E-02	1.04E+02 ± 6.03E-01	1.97E+03 ± 2.76E+00
600	2.70E+00 ± 3.10E-02	9.69E+01 ± 6.01E-01	1.85E+03 ± 2.95E+00
700	2.53E+00 ± 3.19E-02	9.12E+01 ± 6.29E-01	1.74E+03 ± 2.96E+00
800	2.43E+00 ± 3.19E-02	8.81E+01 ± 6.96E-01	1.67E+03 ± 3.01E+00
900	2.37E+00 ± 3.50E-02	8.56E+01 ± 7.28E-01	1.63E+03 ± 3.25E+00
1000	2.29E+00 ± 3.67E-02	8.31E+01 ± 7.64E-01	1.58E+03 ± 3.31E+00
1500	2.18E+00 ± 4.73E-02	7.87E+01 ± 8.81E-01	1.49E+03 ± 4.03E+00
2000	2.21E+00 ± 7.32E-02	7.75E+01 ± 1.19E+00	1.45E+03 ± 4.80E+00
2500	2.16E+00 ± 7.10E-02	7.74E+01 ± 1.39E+00	1.45E+03 ± 5.50E+00
3000	2.21E+00 ± 8.32E-02	7.83E+01 ± 1.53E+00	1.46E+03 ± 6.29E+00
3500	2.23E+00 ± 1.02E-01	7.75E+01 ± 1.64E+00	1.45E+03 ± 6.81E+00
4000	2.21E+00 ± 1.01E-01	7.77E+01 ± 1.86E+00	1.44E+03 ± 7.22E+00
4500	2.19E+00 ± 1.00E-01	7.72E+01 ± 1.85E+00	1.44E+03 ± 7.63E+00
5000	2.17E+00 ± 9.96E-02	7.77E+01 ± 2.28E+00	1.44E+03 ± 8.64E+00
6000	2.17E+00 ± 9.89E-02	7.75E+01 ± 2.26E+00	1.46E+03 ± 1.08E+01
7000	2.15E+00 ± 9.85E-02	7.93E+01 ± 3.30E+00	1.47E+03 ± 1.25E+01
8000	2.15E+00 ± 9.81E-02	7.91E+01 ± 3.29E+00	1.48E+03 ± 1.41E+01
9000	2.14E+00 ± 9.80E-02	8.27E+01 ± 4.98E+00	1.48E+03 ± 1.47E+01
10000	2.13E+00 ± 9.77E-02	8.24E+01 ± 4.98E+00	1.49E+03 ± 1.72E+01

TABLE B. 23
Mass stopping powers of Polyvinyl butyral for the proton, the carbon, and the iron beams. (MeV-cm^2/g)

Energy (MeV/u)	Proton	Carbon	Iron
1	3.46E+02 ± 3.46E-02	8.03E+03 ± 8.03E-01	5.11E+04 ± 5.11E+00
2	1.87E+02 ± 3.74E-02	5.52E+03 ± 5.52E-01	4.52E+04 ± 4.52E+00
3	1.36E+02 ± 2.71E-02	4.31E+03 ± 4.31E-01	4.13E+04 ± 4.13E+00
4	1.06E+02 ± 3.19E-02	3.54E+03 ± 7.07E-01	3.79E+04 ± 3.79E+00
5	8.98E+01 ± 2.69E-02	3.05E+03 ± 6.10E-01	3.52E+04 ± 3.52E+00
6	7.72E+01 ± 3.09E-02	2.68E+03 ± 5.36E-01	3.28E+04 ± 3.28E+00
7	6.86E+01 ± 3.43E-02	2.39E+03 ± 4.78E-01	3.11E+04 ± 3.11E+00
8	6.23E+01 ± 3.74E-02	2.16E+03 ± 6.48E-01	2.94E+04 ± 2.94E+00
9	5.71E+01 ± 3.99E-02	1.98E+03 ± 5.94E-01	2.73E+04 ± 2.73E+00
10	5.26E+01 ± 4.21E-02	1.81E+03 ± 5.44E-01	2.64E+04 ± 2.64E+00
20	2.91E+01 ± 5.24E-02	1.04E+03 ± 5.22E-01	1.77E+04 ± 1.77E+00
30	2.10E+01 ± 8.18E-02	7.56E+02 ± 6.05E-01	1.33E+04 ± 2.67E+00
40	1.66E+01 ± 7.99E-02	5.95E+02 ± 5.35E-01	1.06E+04 ± 2.13E+00
50	1.39E+01 ± 6.65E-02	5.03E+02 ± 6.04E-01	9.03E+03 ± 2.71E+00
60	1.20E+01 ± 6.73E-02	4.38E+02 ± 6.14E-01	7.85E+03 ± 2.36E+00
70	1.06E+01 ± 2.85E-02	3.83E+02 ± 5.74E-01	7.03E+03 ± 2.11E+00
80	9.58E+00 ± 4.12E-02	3.43E+02 ± 5.15E-01	6.38E+03 ± 2.55E+00
90	8.74E+00 ± 2.97E-02	3.11E+02 ± 4.98E-01	5.86E+03 ± 2.34E+00
100	8.07E+00 ± 2.98E-02	2.90E+02 ± 5.51E-01	5.39E+03 ± 2.70E+00
120	7.06E+00 ± 2.96E-02	2.54E+02 ± 5.58E-01	4.69E+03 ± 2.35E+00
140	6.29E+00 ± 2.89E-02	2.26E+02 ± 5.43E-01	4.26E+03 ± 2.55E+00
160	5.77E+00 ± 3.00E-02	2.06E+02 ± 5.36E-01	3.85E+03 ± 2.31E+00
180	5.32E+00 ± 2.98E-02	1.90E+02 ± 5.52E-01	3.57E+03 ± 2.50E+00
200	4.92E+00 ± 2.86E-02	1.77E+02 ± 5.48E-01	3.32E+03 ± 2.66E+00
250	4.29E+00 ± 3.00E-02	1.54E+02 ± 5.53E-01	2.88E+03 ± 2.88E+00
300	3.87E+00 ± 3.02E-02	1.39E+02 ± 5.84E-01	2.63E+03 ± 2.89E+00
350	3.53E+00 ± 2.97E-02	1.27E+02 ± 5.86E-01	2.43E+03 ± 2.91E+00
400	3.33E+00 ± 3.26E-02	1.19E+02 ± 5.82E-01	2.26E+03 ± 2.71E+00
450	3.16E+00 ± 3.28E-02	1.13E+02 ± 6.08E-01	2.13E+03 ± 2.77E+00
500	2.99E+00 ± 3.26E-02	1.07E+02 ± 6.09E-01	2.02E+03 ± 2.62E+00
600	2.78E+00 ± 3.17E-02	9.97E+01 ± 6.08E-01	1.89E+03 ± 2.84E+00
700	2.59E+00 ± 2.98E-02	9.34E+01 ± 6.07E-01	1.78E+03 ± 2.85E+00
800	2.50E+00 ± 3.25E-02	9.00E+01 ± 6.48E-01	1.72E+03 ± 3.09E+00
900	2.41E+00 ± 3.14E-02	8.77E+01 ± 7.01E-01	1.67E+03 ± 3.17E+00
1000	2.35E+00 ± 3.53E-02	8.53E+01 ± 7.59E-01	1.62E+03 ± 3.23E+00
1500	2.20E+00 ± 3.70E-02	8.10E+01 ± 9.07E-01	1.53E+03 ± 3.82E+00
2000	2.24E+00 ± 6.80E-02	7.95E+01 ± 1.18E+00	1.49E+03 ± 4.77E+00
2500	2.23E+00 ± 7.26E-02	7.88E+01 ± 1.26E+00	1.49E+03 ± 5.50E+00
3000	2.26E+00 ± 8.51E-02	8.01E+01 ± 1.56E+00	1.49E+03 ± 6.11E+00
3500	2.28E+00 ± 1.04E-01	7.93E+01 ± 1.67E+00	1.48E+03 ± 6.80E+00
4000	2.26E+00 ± 1.03E-01	7.86E+01 ± 1.66E+00	1.47E+03 ± 7.22E+00
4500	2.25E+00 ± 1.02E-01	7.90E+01 ± 1.90E+00	1.47E+03 ± 7.49E+00
5000	2.23E+00 ± 1.02E-01	7.82E+01 ± 1.87E+00	1.47E+03 ± 8.37E+00
6000	2.22E+00 ± 1.01E-01	7.94E+01 ± 2.32E+00	1.49E+03 ± 1.03E+01
7000	2.20E+00 ± 1.01E-01	7.87E+01 ± 2.30E+00	1.50E+03 ± 1.24E+01
8000	2.20E+00 ± 1.00E-01	8.10E+01 ± 3.37E+00	1.51E+03 ± 1.37E+01
9000	2.19E+00 ± 1.00E-01	8.08E+01 ± 3.36E+00	1.51E+03 ± 1.44E+01
10000	2.18E+00 ± 1.00E-01	8.43E+01 ± 5.09E+00	1.51E+03 ± 1.54E+01

TABLE B. 24
Mass stopping powers of Rice powder for the proton, the carbon, and the iron beams. (MeV-cm^2/g)

Energy (MeV/u)	Proton	Carbon	Iron
1	3.11E+02 ± 3.11E-02	7.24E+03 ± 7.24E-01	4.66E+04 ± 4.66E+00
2	1.70E+02 ± 3.41E-02	5.00E+03 ± 5.00E-01	4.10E+04 ± 4.10E+00
3	1.24E+02 ± 3.71E-02	3.94E+03 ± 7.88E-01	3.74E+04 ± 3.74E+00
4	9.73E+01 ± 2.92E-02	3.23E+03 ± 6.46E-01	3.46E+04 ± 3.46E+00
5	8.15E+01 ± 3.26E-02	2.79E+03 ± 5.57E-01	3.22E+04 ± 3.22E+00
6	7.09E+01 ± 3.54E-02	2.45E+03 ± 7.34E-01	3.00E+04 ± 3.00E+00
7	6.36E+01 ± 3.82E-02	2.18E+03 ± 6.55E-01	2.84E+04 ± 2.84E+00
8	5.80E+01 ± 3.48E-02	1.99E+03 ± 5.96E-01	2.70E+04 ± 2.70E+00
9	5.16E+01 ± 3.10E-02	1.83E+03 ± 5.49E-01	2.52E+04 ± 2.52E+00
10	4.72E+01 ± 3.30E-02	1.68E+03 ± 6.70E-01	2.44E+04 ± 2.44E+00
20	2.70E+01 ± 3.24E-02	9.62E+02 ± 5.77E-01	1.64E+04 ± 3.29E+00
30	1.94E+01 ± 3.30E-02	7.00E+02 ± 6.30E-01	1.24E+04 ± 2.48E+00
40	1.54E+01 ± 3.24E-02	5.60E+02 ± 6.71E-01	9.92E+03 ± 2.97E+00
50	1.29E+01 ± 3.21E-02	4.73E+02 ± 7.10E-01	8.41E+03 ± 2.52E+00
60	1.12E+01 ± 4.46E-02	4.03E+02 ± 6.04E-01	7.30E+03 ± 2.92E+00
70	9.92E+00 ± 5.16E-02	3.54E+02 ± 5.66E-01	6.63E+03 ± 2.65E+00
80	8.97E+00 ± 5.92E-02	3.21E+02 ± 6.10E-01	5.95E+03 ± 2.97E+00
90	8.22E+00 ± 6.74E-02	2.94E+02 ± 6.17E-01	5.46E+03 ± 2.73E+00
100	7.60E+00 ± 7.60E-02	2.71E+02 ± 6.23E-01	5.00E+03 ± 2.50E+00
120	6.58E+00 ± 3.36E-02	2.37E+02 ± 6.16E-01	4.43E+03 ± 2.66E+00
140	5.90E+00 ± 3.36E-02	2.11E+02 ± 6.12E-01	3.96E+03 ± 2.77E+00
160	5.36E+00 ± 3.22E-02	1.93E+02 ± 6.16E-01	3.60E+03 ± 2.88E+00
180	4.96E+00 ± 3.27E-02	1.78E+02 ± 6.05E-01	3.36E+03 ± 3.02E+00
200	4.62E+00 ± 3.33E-02	1.66E+02 ± 6.29E-01	3.14E+03 ± 3.14E+00
250	4.02E+00 ± 3.42E-02	1.44E+02 ± 6.50E-01	2.69E+03 ± 3.22E+00
300	3.63E+00 ± 3.48E-02	1.30E+02 ± 6.50E-01	2.48E+03 ± 2.97E+00
350	3.34E+00 ± 3.64E-02	1.19E+02 ± 6.55E-01	2.25E+03 ± 2.93E+00
400	3.11E+00 ± 3.51E-02	1.11E+02 ± 6.44E-01	2.10E+03 ± 2.94E+00
450	2.92E+00 ± 3.36E-02	1.05E+02 ± 6.62E-01	1.99E+03 ± 2.99E+00
500	2.77E+00 ± 3.32E-02	9.94E+01 ± 6.46E-01	1.89E+03 ± 3.03E+00
600	2.58E+00 ± 3.35E-02	9.31E+01 ± 6.79E-01	1.77E+03 ± 3.19E+00
700	2.42E+00 ± 3.29E-02	8.79E+01 ± 7.30E-01	1.67E+03 ± 3.17E+00
800	2.34E+00 ± 3.60E-02	8.50E+01 ± 7.90E-01	1.61E+03 ± 3.38E+00
900	2.27E+00 ± 3.72E-02	8.30E+01 ± 8.63E-01	1.56E+03 ± 3.60E+00
1000	2.19E+00 ± 3.90E-02	8.02E+01 ± 8.74E-01	1.51E+03 ± 3.63E+00
1500	2.17E+00 ± 6.84E-02	7.62E+01 ± 1.06E+00	1.44E+03 ± 4.45E+00
2000	2.10E+00 ± 7.14E-02	7.43E+01 ± 1.24E+00	1.40E+03 ± 5.33E+00
2500	2.11E+00 ± 8.28E-02	7.48E+01 ± 1.52E+00	1.39E+03 ± 5.99E+00
3000	2.17E+00 ± 1.01E-01	7.55E+01 ± 1.61E+00	1.41E+03 ± 6.77E+00
3500	2.15E+00 ± 9.94E-02	7.56E+01 ± 1.84E+00	1.41E+03 ± 7.32E+00
4000	2.15E+00 ± 9.84E-02	7.54E+01 ± 1.80E+00	1.41E+03 ± 7.63E+00
4500	2.14E+00 ± 9.77E-02	7.66E+01 ± 2.24E+00	1.42E+03 ± 8.83E+00
5000	2.13E+00 ± 9.74E-02	7.61E+01 ± 2.23E+00	1.43E+03 ± 1.00E+01
6000	2.12E+00 ± 9.66E-02	7.81E+01 ± 3.24E+00	1.45E+03 ± 1.20E+01
7000	2.10E+00 ± 9.63E-02	7.75E+01 ± 3.22E+00	1.45E+03 ± 1.38E+01
8000	2.10E+00 ± 9.59E-02	8.10E+01 ± 4.88E+00	1.46E+03 ± 1.49E+01
9000	2.09E+00 ± 9.57E-02	8.09E+01 ± 4.87E+00	1.48E+03 ± 1.90E+01
10000	2.09E+00 ± 9.55E-02	8.08E+01 ± 4.87E+00	1.48E+03 ± 1.97E+01

TABLE B. 25
Mass stopping powers of RM-1 for the proton, the carbon, and the iron beams.
(MeV-cm^2/g)

Energy (MeV/u)	Proton	Carbon	Iron
1	3.67E+02 ± 3.67E-02	8.57E+03 ± 8.57E-01	5.45E+04 ± 5.45E+00
2	1.99E+02 ± 3.99E-02	5.88E+03 ± 5.88E-01	4.82E+04 ± 4.82E+00
3	1.44E+02 ± 2.89E-02	4.60E+03 ± 4.60E-01	4.41E+04 ± 4.41E+00
4	1.14E+02 ± 3.41E-02	3.78E+03 ± 7.55E-01	4.05E+04 ± 4.05E+00
5	9.59E+01 ± 2.88E-02	3.26E+03 ± 6.51E-01	3.76E+04 ± 3.76E+00
6	8.25E+01 ± 3.30E-02	2.86E+03 ± 5.72E-01	3.50E+04 ± 3.50E+00
7	7.34E+01 ± 3.67E-02	2.55E+03 ± 5.10E-01	3.31E+04 ± 3.31E+00
8	6.63E+01 ± 3.98E-02	2.29E+03 ± 6.88E-01	3.13E+04 ± 3.13E+00
9	6.03E+01 ± 4.22E-02	2.09E+03 ± 6.27E-01	2.88E+04 ± 2.88E+00
10	5.55E+01 ± 4.44E-02	1.91E+03 ± 5.73E-01	2.78E+04 ± 2.78E+00
20	3.07E+01 ± 5.52E-02	1.10E+03 ± 5.49E-01	1.86E+04 ± 1.86E+00
30	2.20E+01 ± 8.15E-02	7.95E+02 ± 6.36E-01	1.40E+04 ± 2.80E+00
40	1.75E+01 ± 6.98E-02	6.26E+02 ± 5.63E-01	1.12E+04 ± 2.24E+00
50	1.46E+01 ± 7.14E-02	5.30E+02 ± 6.35E-01	9.49E+03 ± 2.85E+00
60	1.26E+01 ± 7.32E-02	4.60E+02 ± 6.91E-01	8.25E+03 ± 2.48E+00
70	1.11E+01 ± 3.00E-02	4.02E+02 ± 6.02E-01	7.38E+03 ± 2.21E+00
80	1.01E+01 ± 4.32E-02	3.60E+02 ± 5.40E-01	6.72E+03 ± 2.69E+00
90	9.19E+00 ± 3.22E-02	3.30E+02 ± 5.94E-01	6.15E+03 ± 2.46E+00
100	8.47E+00 ± 3.22E-02	3.04E+02 ± 5.78E-01	5.66E+03 ± 2.83E+00
120	7.41E+00 ± 3.11E-02	2.66E+02 ± 5.85E-01	4.95E+03 ± 2.48E+00
140	6.60E+00 ± 3.10E-02	2.38E+02 ± 5.94E-01	4.46E+03 ± 2.68E+00
160	6.05E+00 ± 3.21E-02	2.16E+02 ± 5.84E-01	4.04E+03 ± 2.42E+00
180	5.58E+00 ± 3.13E-02	2.00E+02 ± 5.79E-01	3.74E+03 ± 2.62E+00
200	5.17E+00 ± 3.10E-02	1.85E+02 ± 5.75E-01	3.49E+03 ± 2.79E+00
250	4.50E+00 ± 3.20E-02	1.61E+02 ± 5.97E-01	3.02E+03 ± 3.02E+00
300	4.07E+00 ± 3.30E-02	1.46E+02 ± 6.13E-01	2.79E+03 ± 3.07E+00
350	3.71E+00 ± 3.19E-02	1.34E+02 ± 6.28E-01	2.54E+03 ± 3.05E+00
400	3.50E+00 ± 3.54E-02	1.25E+02 ± 6.23E-01	2.37E+03 ± 2.84E+00
450	3.30E+00 ± 3.43E-02	1.18E+02 ± 6.50E-01	2.23E+03 ± 2.90E+00
500	3.13E+00 ± 3.38E-02	1.12E+02 ± 6.39E-01	2.12E+03 ± 2.75E+00
600	2.91E+00 ± 3.31E-02	1.04E+02 ± 6.48E-01	1.98E+03 ± 2.98E+00
700	2.72E+00 ± 3.23E-02	9.78E+01 ± 6.36E-01	1.87E+03 ± 3.18E+00
800	2.63E+00 ± 3.44E-02	9.43E+01 ± 6.79E-01	1.80E+03 ± 3.24E+00
900	2.54E+00 ± 3.48E-02	9.21E+01 ± 7.65E-01	1.75E+03 ± 3.32E+00
1000	2.48E+00 ± 3.94E-02	8.95E+01 ± 8.14E-01	1.69E+03 ± 3.56E+00
1500	2.32E+00 ± 4.46E-02	8.46E+01 ± 9.40E-01	1.60E+03 ± 4.16E+00
2000	2.38E+00 ± 7.79E-02	8.31E+01 ± 1.22E+00	1.56E+03 ± 4.99E+00
2500	2.35E+00 ± 7.73E-02	8.28E+01 ± 1.39E+00	1.55E+03 ± 5.75E+00
3000	2.35E+00 ± 8.85E-02	8.33E+01 ± 1.62E+00	1.55E+03 ± 6.36E+00
3500	2.37E+00 ± 1.08E-01	8.25E+01 ± 1.74E+00	1.54E+03 ± 7.07E+00
4000	2.41E+00 ± 1.23E-01	8.27E+01 ± 1.98E+00	1.53E+03 ± 7.67E+00
4500	2.36E+00 ± 1.08E-01	8.21E+01 ± 1.97E+00	1.53E+03 ± 7.95E+00
5000	2.33E+00 ± 1.07E-01	8.12E+01 ± 1.94E+00	1.53E+03 ± 9.02E+00
6000	2.41E+00 ± 1.50E-01	8.25E+01 ± 2.41E+00	1.55E+03 ± 1.12E+01
7000	2.32E+00 ± 1.09E-01	8.43E+01 ± 3.52E+00	1.56E+03 ± 1.29E+01
8000	2.31E+00 ± 1.06E-01	8.42E+01 ± 3.51E+00	1.57E+03 ± 1.46E+01
9000	2.29E+00 ± 1.05E-01	8.80E+01 ± 5.30E+00	1.57E+03 ± 1.49E+01
10000	2.29E+00 ± 1.06E-01	8.76E+01 ± 5.29E+00	1.58E+03 ± 1.69E+01

TABLE B. 26
Mass stopping powers of RM/G1 for the proton, the carbon, and the iron beams.
(MeV-cm^2/g)

Energy (MeV/u)	Proton	Carbon	Iron
1	3.52E+02 ± 3.52E-02	8.14E+03 ± 8.14E-01	5.18E+04 ± 5.18E+00
2	1.90E+02 ± 3.80E-02	5.59E+03 ± 5.59E-01	4.57E+04 ± 4.57E+00
3	1.37E+02 ± 2.74E-02	4.37E+03 ± 4.37E-01	4.19E+04 ± 4.19E+00
4	1.08E+02 ± 3.23E-02	3.58E+03 ± 7.16E-01	3.84E+04 ± 3.84E+00
5	9.10E+01 ± 2.73E-02	3.09E+03 ± 6.18E-01	3.57E+04 ± 3.57E+00
6	7.82E+01 ± 3.13E-02	2.71E+03 ± 5.43E-01	3.32E+04 ± 3.32E+00
7	6.96E+01 ± 2.78E-02	2.42E+03 ± 4.84E-01	3.14E+04 ± 3.14E+00
8	6.29E+01 ± 3.14E-02	2.17E+03 ± 6.52E-01	2.97E+04 ± 2.97E+00
9	5.71E+01 ± 3.43E-02	1.98E+03 ± 5.94E-01	2.73E+04 ± 2.73E+00
10	5.25E+01 ± 3.15E-02	1.81E+03 ± 5.44E-01	2.63E+04 ± 2.63E+00
20	2.92E+01 ± 5.54E-02	1.04E+03 ± 6.27E-01	1.77E+04 ± 1.77E+00
30	2.10E+01 ± 7.76E-02	7.58E+02 ± 6.06E-01	1.34E+04 ± 2.67E+00
40	1.66E+01 ± 3.82E-02	5.97E+02 ± 5.37E-01	1.07E+04 ± 2.14E+00
50	1.38E+01 ± 2.91E-02	5.05E+02 ± 6.06E-01	9.06E+03 ± 2.72E+00
60	1.20E+01 ± 3.84E-02	4.40E+02 ± 6.60E-01	7.88E+03 ± 2.36E+00
70	1.06E+01 ± 4.36E-02	3.84E+02 ± 5.76E-01	7.05E+03 ± 2.12E+00
80	9.61E+00 ± 4.90E-02	3.44E+02 ± 5.50E-01	6.42E+03 ± 2.57E+00
90	8.82E+00 ± 5.55E-02	3.12E+02 ± 5.00E-01	5.88E+03 ± 2.35E+00
100	8.14E+00 ± 6.11E-02	2.91E+02 ± 5.53E-01	5.41E+03 ± 2.71E+00
120	7.09E+00 ± 3.26E-02	2.55E+02 ± 5.60E-01	4.73E+03 ± 2.37E+00
140	6.31E+00 ± 2.97E-02	2.27E+02 ± 5.68E-01	4.27E+03 ± 2.56E+00
160	5.80E+00 ± 3.13E-02	2.07E+02 ± 5.59E-01	3.86E+03 ± 2.70E+00
180	5.34E+00 ± 3.05E-02	1.91E+02 ± 5.54E-01	3.58E+03 ± 2.51E+00
200	4.95E+00 ± 2.97E-02	1.77E+02 ± 5.50E-01	3.34E+03 ± 2.67E+00
250	4.31E+00 ± 3.10E-02	1.55E+02 ± 5.87E-01	2.90E+03 ± 2.90E+00
300	3.90E+00 ± 3.20E-02	1.40E+02 ± 6.01E-01	2.63E+03 ± 2.90E+00
350	3.54E+00 ± 3.01E-02	1.28E+02 ± 6.01E-01	2.44E+03 ± 2.93E+00
400	3.36E+00 ± 3.46E-02	1.19E+02 ± 6.09E-01	2.27E+03 ± 2.72E+00
450	3.17E+00 ± 3.32E-02	1.13E+02 ± 6.23E-01	2.14E+03 ± 2.78E+00
500	3.00E+00 ± 3.30E-02	1.07E+02 ± 6.23E-01	2.03E+03 ± 2.84E+00
600	2.82E+00 ± 4.23E-02	1.00E+02 ± 6.31E-01	1.90E+03 ± 2.85E+00
700	2.61E+00 ± 3.19E-02	9.37E+01 ± 6.09E-01	1.79E+03 ± 3.05E+00
800	2.52E+00 ± 3.32E-02	9.05E+01 ± 6.70E-01	1.73E+03 ± 3.11E+00
900	2.44E+00 ± 3.42E-02	8.83E+01 ± 7.33E-01	1.68E+03 ± 3.18E+00
1000	2.37E+00 ± 3.79E-02	8.59E+01 ± 7.90E-01	1.63E+03 ± 3.42E+00
1500	2.23E+00 ± 4.33E-02	8.13E+01 ± 9.19E-01	1.54E+03 ± 3.99E+00
2000	2.32E+00 ± 8.19E-02	7.99E+01 ± 1.19E+00	1.50E+03 ± 4.80E+00
2500	2.26E+00 ± 7.57E-02	7.96E+01 ± 1.35E+00	1.49E+03 ± 5.53E+00
3000	2.29E+00 ± 8.62E-02	8.11E+01 ± 1.58E+00	1.51E+03 ± 6.19E+00
3500	2.31E+00 ± 1.05E-01	8.04E+01 ± 1.70E+00	1.50E+03 ± 6.90E+00
4000	2.30E+00 ± 1.05E-01	8.06E+01 ± 1.93E+00	1.50E+03 ± 7.48E+00
4500	2.33E+00 ± 1.15E-01	8.01E+01 ± 1.92E+00	1.49E+03 ± 7.76E+00
5000	2.32E+00 ± 1.17E-01	7.92E+01 ± 1.89E+00	1.49E+03 ± 8.64E+00
6000	2.27E+00 ± 1.04E-01	8.04E+01 ± 2.35E+00	1.51E+03 ± 1.06E+01
7000	2.39E+00 ± 1.81E-01	7.97E+01 ± 2.34E+00	1.52E+03 ± 1.26E+01
8000	2.24E+00 ± 1.02E-01	8.20E+01 ± 3.41E+00	1.53E+03 ± 1.39E+01
9000	2.23E+00 ± 1.02E-01	8.19E+01 ± 3.41E+00	1.53E+03 ± 1.45E+01
10000	2.23E+00 ± 1.02E-01	8.54E+01 ± 5.16E+00	1.54E+03 ± 1.65E+01

TABLE B. 27
Mass stopping powers of RM/L3 for the proton, the carbon, and the iron beams.
(MeV-cm^2/g)

Energy (MeV/u)	Proton	Carbon	Iron
1	3.51E+02 ± 3.51E-02	8.14E+03 ± 8.14E-01	5.18E+04 ± 5.18E+00
2	1.90E+02 ± 3.80E-02	5.59E+03 ± 5.59E-01	4.57E+04 ± 4.57E+00
3	1.37E+02 ± 2.75E-02	4.37E+03 ± 4.37E-01	4.19E+04 ± 4.19E+00
4	1.08E+02 ± 3.24E-02	3.58E+03 ± 7.17E-01	3.84E+04 ± 3.84E+00
5	9.10E+01 ± 2.73E-02	3.09E+03 ± 6.18E-01	3.57E+04 ± 3.57E+00
6	7.83E+01 ± 3.13E-02	2.72E+03 ± 5.43E-01	3.32E+04 ± 3.32E+00
7	6.97E+01 ± 2.79E-02	2.42E+03 ± 4.84E-01	3.14E+04 ± 3.14E+00
8	6.30E+01 ± 3.15E-02	2.18E+03 ± 6.53E-01	2.97E+04 ± 2.97E+00
9	5.72E+01 ± 3.43E-02	1.98E+03 ± 5.95E-01	2.73E+04 ± 2.73E+00
10	5.26E+01 ± 3.68E-02	1.81E+03 ± 5.44E-01	2.64E+04 ± 2.64E+00
20	2.92E+01 ± 5.55E-02	1.04E+03 ± 6.27E-01	1.77E+04 ± 1.77E+00
30	2.10E+01 ± 7.98E-02	7.58E+02 ± 6.06E-01	1.34E+04 ± 2.67E+00
40	1.66E+01 ± 2.98E-02	5.97E+02 ± 5.97E-01	1.07E+04 ± 2.14E+00
50	1.39E+01 ± 3.05E-02	5.06E+02 ± 6.58E-01	9.06E+03 ± 2.72E+00
60	1.20E+01 ± 3.84E-02	4.40E+02 ± 6.60E-01	7.88E+03 ± 2.36E+00
70	1.06E+01 ± 4.47E-02	3.84E+02 ± 5.76E-01	7.05E+03 ± 2.12E+00
80	9.62E+00 ± 5.00E-02	3.44E+02 ± 5.50E-01	6.43E+03 ± 2.57E+00
90	8.83E+00 ± 5.65E-02	3.16E+02 ± 5.68E-01	5.88E+03 ± 2.35E+00
100	8.15E+00 ± 6.28E-02	2.91E+02 ± 5.83E-01	5.42E+03 ± 2.71E+00
120	7.09E+00 ± 3.26E-02	2.55E+02 ± 5.60E-01	4.74E+03 ± 2.37E+00
140	6.32E+00 ± 3.03E-02	2.27E+02 ± 5.69E-01	4.27E+03 ± 2.56E+00
160	5.80E+00 ± 3.19E-02	2.07E+02 ± 5.60E-01	3.86E+03 ± 2.70E+00
180	5.34E+00 ± 3.10E-02	1.91E+02 ± 5.73E-01	3.59E+03 ± 2.51E+00
200	4.96E+00 ± 3.02E-02	1.78E+02 ± 5.68E-01	3.34E+03 ± 2.68E+00
250	4.31E+00 ± 3.10E-02	1.55E+02 ± 5.87E-01	2.90E+03 ± 3.19E+00
300	3.90E+00 ± 3.20E-02	1.40E+02 ± 6.16E-01	2.67E+03 ± 2.94E+00
350	3.56E+00 ± 3.16E-02	1.28E+02 ± 6.14E-01	2.44E+03 ± 2.93E+00
400	3.36E+00 ± 3.46E-02	1.20E+02 ± 6.22E-01	2.27E+03 ± 2.72E+00
450	3.16E+00 ± 3.32E-02	1.13E+02 ± 6.35E-01	2.14E+03 ± 2.78E+00
500	3.00E+00 ± 3.29E-02	1.07E+02 ± 6.23E-01	2.03E+03 ± 2.84E+00
600	2.82E+00 ± 4.26E-02	1.00E+02 ± 6.31E-01	1.90E+03 ± 2.86E+00
700	2.61E+00 ± 3.19E-02	9.39E+01 ± 6.29E-01	1.79E+03 ± 3.05E+00
800	2.51E+00 ± 3.32E-02	9.05E+01 ± 6.79E-01	1.73E+03 ± 3.11E+00
900	2.45E+00 ± 3.63E-02	8.83E+01 ± 7.42E-01	1.68E+03 ± 3.35E+00
1000	2.37E+00 ± 3.81E-02	8.58E+01 ± 7.90E-01	1.63E+03 ± 3.42E+00
1500	2.25E+00 ± 4.91E-02	8.13E+01 ± 9.18E-01	1.54E+03 ± 4.00E+00
2000	2.32E+00 ± 8.23E-02	8.01E+01 ± 1.24E+00	1.50E+03 ± 4.95E+00
2500	2.26E+00 ± 7.56E-02	7.95E+01 ± 1.35E+00	1.49E+03 ± 5.68E+00
3000	2.28E+00 ± 8.63E-02	8.10E+01 ± 1.58E+00	1.51E+03 ± 6.35E+00
3500	2.31E+00 ± 1.05E-01	8.04E+01 ± 1.70E+00	1.50E+03 ± 7.05E+00
4000	2.30E+00 ± 1.05E-01	8.06E+01 ± 1.93E+00	1.50E+03 ± 7.48E+00
4500	2.33E+00 ± 1.16E-01	8.01E+01 ± 1.92E+00	1.49E+03 ± 7.76E+00
5000	2.32E+00 ± 1.18E-01	8.06E+01 ± 2.36E+00	1.49E+03 ± 8.80E+00
6000	2.27E+00 ± 1.04E-01	8.04E+01 ± 2.35E+00	1.51E+03 ± 1.10E+01
7000	2.39E+00 ± 1.85E-01	8.22E+01 ± 3.43E+00	1.52E+03 ± 1.26E+01
8000	2.24E+00 ± 1.03E-01	8.20E+01 ± 3.41E+00	1.53E+03 ± 1.42E+01
9000	2.23E+00 ± 1.02E-01	8.58E+01 ± 5.16E+00	1.53E+03 ± 1.45E+01
10000	2.23E+00 ± 1.02E-01	8.54E+01 ± 5.16E+00	1.54E+03 ± 1.65E+01

TABLE B. 28
Mass stopping powers of RM/SR4 for the proton, the carbon, and the iron beams.
(MeV-cm^2/g)

Energy (MeV/u)	Proton	Carbon	Iron
1	3.50E+02 ± 3.50E-02	8.18E+03 ± 8.18E-01	5.21E+04 ± 5.21E+00
2	1.91E+02 ± 3.81E-02	5.62E+03 ± 5.62E-01	4.60E+04 ± 4.60E+00
3	1.38E+02 ± 2.76E-02	4.40E+03 ± 4.40E-01	4.21E+04 ± 4.21E+00
4	1.09E+02 ± 3.26E-02	3.61E+03 ± 7.22E-01	3.87E+04 ± 3.87E+00
5	9.16E+01 ± 2.75E-02	3.11E+03 ± 6.22E-01	3.60E+04 ± 3.60E+00
6	7.88E+01 ± 3.15E-02	2.73E+03 ± 5.47E-01	3.35E+04 ± 3.35E+00
7	7.02E+01 ± 3.51E-02	2.44E+03 ± 4.88E-01	3.17E+04 ± 3.17E+00
8	6.37E+01 ± 3.82E-02	2.20E+03 ± 6.61E-01	3.00E+04 ± 3.00E+00
9	5.82E+01 ± 4.08E-02	2.02E+03 ± 6.05E-01	2.78E+04 ± 2.78E+00
10	5.36E+01 ± 4.82E-02	1.84E+03 ± 5.53E-01	2.68E+04 ± 2.68E+00
20	2.96E+01 ± 5.63E-02	1.06E+03 ± 6.36E-01	1.80E+04 ± 1.80E+00
30	2.13E+01 ± 8.96E-02	7.68E+02 ± 6.15E-01	1.36E+04 ± 2.71E+00
40	1.69E+01 ± 7.09E-02	6.05E+02 ± 6.05E-01	1.08E+04 ± 2.16E+00
50	1.41E+01 ± 7.05E-02	5.13E+02 ± 6.66E-01	9.17E+03 ± 2.75E+00
60	1.22E+01 ± 7.21E-02	4.45E+02 ± 6.68E-01	7.98E+03 ± 2.39E+00
70	1.07E+01 ± 3.01E-02	3.88E+02 ± 5.82E-01	7.14E+03 ± 2.14E+00
80	9.73E+00 ± 4.28E-02	3.48E+02 ± 5.57E-01	6.50E+03 ± 2.60E+00
90	8.89E+00 ± 3.11E-02	3.19E+02 ± 5.75E-01	5.94E+03 ± 2.38E+00
100	8.19E+00 ± 3.11E-02	2.95E+02 ± 5.89E-01	5.48E+03 ± 2.74E+00
120	7.16E+00 ± 3.08E-02	2.57E+02 ± 5.66E-01	4.80E+03 ± 2.40E+00
140	6.38E+00 ± 3.00E-02	2.30E+02 ± 5.75E-01	4.32E+03 ± 2.59E+00
160	5.85E+00 ± 3.16E-02	2.09E+02 ± 5.65E-01	3.90E+03 ± 2.73E+00
180	5.40E+00 ± 3.13E-02	1.93E+02 ± 5.61E-01	3.62E+03 ± 2.54E+00
200	5.01E+00 ± 3.05E-02	1.79E+02 ± 5.74E-01	3.38E+03 ± 2.70E+00
250	4.35E+00 ± 3.13E-02	1.56E+02 ± 5.93E-01	2.93E+03 ± 3.22E+00
300	3.93E+00 ± 3.19E-02	1.41E+02 ± 6.22E-01	2.70E+03 ± 2.97E+00
350	3.59E+00 ± 3.20E-02	1.29E+02 ± 6.21E-01	2.46E+03 ± 2.95E+00
400	3.39E+00 ± 3.45E-02	1.21E+02 ± 6.15E-01	2.29E+03 ± 2.75E+00
450	3.19E+00 ± 3.32E-02	1.14E+02 ± 6.29E-01	2.16E+03 ± 2.80E+00
500	3.02E+00 ± 3.29E-02	1.08E+02 ± 6.29E-01	2.05E+03 ± 2.87E+00
600	2.81E+00 ± 3.20E-02	1.01E+02 ± 6.26E-01	1.92E+03 ± 2.88E+00
700	2.63E+00 ± 3.15E-02	9.49E+01 ± 6.45E-01	1.81E+03 ± 3.08E+00
800	2.53E+00 ± 3.29E-02	9.14E+01 ± 6.86E-01	1.74E+03 ± 3.14E+00
900	2.47E+00 ± 3.63E-02	8.92E+01 ± 7.49E-01	1.69E+03 ± 3.21E+00
1000	2.39E+00 ± 3.83E-02	8.65E+01 ± 7.87E-01	1.64E+03 ± 3.45E+00
1500	2.27E+00 ± 4.91E-02	8.19E+01 ± 9.17E-01	1.55E+03 ± 4.03E+00
2000	2.30E+00 ± 7.59E-02	8.07E+01 ± 1.24E+00	1.51E+03 ± 4.99E+00
2500	2.25E+00 ± 7.34E-02	8.01E+01 ± 1.35E+00	1.51E+03 ± 5.72E+00
3000	2.28E+00 ± 8.61E-02	8.11E+01 ± 1.58E+00	1.51E+03 ± 6.36E+00
3500	2.30E+00 ± 1.05E-01	8.02E+01 ± 1.69E+00	1.50E+03 ± 7.04E+00
4000	2.28E+00 ± 1.04E-01	8.04E+01 ± 1.93E+00	1.49E+03 ± 7.47E+00
4500	2.27E+00 ± 1.04E-01	7.99E+01 ± 1.92E+00	1.49E+03 ± 7.74E+00
5000	2.25E+00 ± 1.03E-01	8.05E+01 ± 2.36E+00	1.49E+03 ± 8.94E+00
6000	2.24E+00 ± 1.02E-01	8.03E+01 ± 2.34E+00	1.51E+03 ± 1.10E+01
7000	2.22E+00 ± 1.02E-01	8.20E+01 ± 3.42E+00	1.52E+03 ± 1.29E+01
8000	2.22E+00 ± 1.02E-01	8.19E+01 ± 3.41E+00	1.53E+03 ± 1.42E+01
9000	2.22E+00 ± 1.01E-01	8.56E+01 ± 5.16E+00	1.53E+03 ± 1.45E+01
10000	2.21E+00 ± 1.01E-01	8.53E+01 ± 5.15E+00	1.54E+03 ± 1.71E+01

TABLE B. 29
Mass stopping powers of Rossi gel for the proton, the carbon, and the iron beams. (MeV-cm^2/g)

Energy (MeV/u)	Proton	Carbon	Iron
1	3.50E+02 ± 3.50E-02	8.08E+03 ± 8.08E-01	5.14E+04 ± 5.14E+00
2	1.88E+02 ± 3.77E-02	5.54E+03 ± 5.54E-01	4.54E+04 ± 4.54E+00
3	1.36E+02 ± 2.72E-02	4.33E+03 ± 4.33E-01	4.15E+04 ± 4.15E+00
4	1.07E+02 ± 3.21E-02	3.55E+03 ± 7.10E-01	3.81E+04 ± 3.81E+00
5	9.03E+01 ± 2.71E-02	3.06E+03 ± 6.13E-01	3.54E+04 ± 3.54E+00
6	7.76E+01 ± 3.10E-02	2.69E+03 ± 5.38E-01	3.30E+04 ± 3.30E+00
7	6.90E+01 ± 2.76E-02	2.40E+03 ± 4.80E-01	3.12E+04 ± 3.12E+00
8	6.23E+01 ± 3.12E-02	2.16E+03 ± 6.48E-01	2.94E+04 ± 2.94E+00
9	5.67E+01 ± 3.40E-02	1.97E+03 ± 5.91E-01	2.71E+04 ± 2.71E+00
10	5.23E+01 ± 3.14E-02	1.80E+03 ± 5.40E-01	2.62E+04 ± 2.62E+00
20	2.90E+01 ± 5.22E-02	1.04E+03 ± 6.24E-01	1.76E+04 ± 1.76E+00
30	2.09E+01 ± 7.72E-02	7.54E+02 ± 6.03E-01	1.33E+04 ± 2.66E+00
40	1.65E+01 ± 3.79E-02	5.93E+02 ± 5.34E-01	1.06E+04 ± 2.12E+00
50	1.38E+01 ± 6.64E-02	5.02E+02 ± 6.02E-01	9.01E+03 ± 2.70E+00
60	1.19E+01 ± 3.70E-02	4.37E+02 ± 6.56E-01	7.84E+03 ± 2.35E+00
70	1.06E+01 ± 4.23E-02	3.82E+02 ± 5.73E-01	7.01E+03 ± 2.10E+00
80	9.56E+00 ± 4.78E-02	3.42E+02 ± 5.48E-01	6.37E+03 ± 2.55E+00
90	8.77E+00 ± 5.43E-02	3.11E+02 ± 4.97E-01	5.85E+03 ± 2.34E+00
100	8.10E+00 ± 6.00E-02	2.89E+02 ± 5.50E-01	5.39E+03 ± 2.69E+00
120	7.05E+00 ± 3.25E-02	2.53E+02 ± 5.57E-01	4.69E+03 ± 2.35E+00
140	6.28E+00 ± 2.95E-02	2.26E+02 ± 5.65E-01	4.25E+03 ± 2.55E+00
160	5.76E+00 ± 3.05E-02	2.06E+02 ± 5.56E-01	3.84E+03 ± 2.69E+00
180	5.32E+00 ± 3.03E-02	1.90E+02 ± 5.51E-01	3.56E+03 ± 2.49E+00
200	4.92E+00 ± 2.90E-02	1.77E+02 ± 5.48E-01	3.32E+03 ± 2.66E+00
250	4.29E+00 ± 3.04E-02	1.54E+02 ± 5.68E-01	2.88E+03 ± 2.88E+00
300	3.88E+00 ± 3.10E-02	1.39E+02 ± 5.98E-01	2.62E+03 ± 2.89E+00
350	3.53E+00 ± 3.00E-02	1.27E+02 ± 5.98E-01	2.43E+03 ± 2.91E+00
400	3.34E+00 ± 3.37E-02	1.19E+02 ± 6.07E-01	2.26E+03 ± 2.71E+00
450	3.15E+00 ± 3.31E-02	1.13E+02 ± 6.20E-01	2.13E+03 ± 2.77E+00
500	2.99E+00 ± 3.28E-02	1.07E+02 ± 6.09E-01	2.02E+03 ± 2.62E+00
600	2.81E+00 ± 4.13E-02	9.96E+01 ± 6.08E-01	1.89E+03 ± 2.84E+00
700	2.60E+00 ± 3.17E-02	9.33E+01 ± 6.07E-01	1.78E+03 ± 3.03E+00
800	2.51E+00 ± 3.31E-02	9.00E+01 ± 6.48E-01	1.72E+03 ± 3.09E+00
900	2.43E+00 ± 3.40E-02	8.78E+01 ± 7.20E-01	1.67E+03 ± 3.17E+00
1000	2.35E+00 ± 3.52E-02	8.54E+01 ± 7.77E-01	1.62E+03 ± 3.40E+00
1500	2.20E+00 ± 3.72E-02	8.10E+01 ± 9.07E-01	1.53E+03 ± 3.82E+00
2000	2.31E+00 ± 8.12E-02	7.95E+01 ± 1.18E+00	1.49E+03 ± 4.77E+00
2500	2.25E+00 ± 7.57E-02	7.93E+01 ± 1.35E+00	1.49E+03 ± 5.50E+00
3000	2.27E+00 ± 8.57E-02	8.07E+01 ± 1.57E+00	1.50E+03 ± 6.16E+00
3500	2.30E+00 ± 1.05E-01	7.99E+01 ± 1.69E+00	1.49E+03 ± 6.86E+00
4000	2.29E+00 ± 1.04E-01	7.92E+01 ± 1.67E+00	1.49E+03 ± 7.28E+00
4500	2.32E+00 ± 1.14E-01	7.96E+01 ± 1.91E+00	1.48E+03 ± 7.55E+00
5000	2.31E+00 ± 1.16E-01	7.88E+01 ± 1.88E+00	1.48E+03 ± 8.44E+00
6000	2.26E+00 ± 1.03E-01	8.00E+01 ± 2.34E+00	1.50E+03 ± 1.03E+01
7000	2.37E+00 ± 1.77E-01	7.93E+01 ± 2.32E+00	1.51E+03 ± 1.25E+01
8000	2.23E+00 ± 1.02E-01	8.16E+01 ± 3.39E+00	1.52E+03 ± 1.38E+01
9000	2.22E+00 ± 1.01E-01	8.15E+01 ± 3.39E+00	1.52E+03 ± 1.45E+01
10000	2.21E+00 ± 1.02E-01	8.50E+01 ± 5.13E+00	1.52E+03 ± 1.56E+01

TABLE B. 30
Mass stopping powers of Rossi liquid for the proton, the carbon, and the iron beams. (MeV-cm^2/g)

Energy (MeV/u)	Proton	Carbon	Iron
1	3.50E+02 ± 3.50E-02	8.08E+03 ± 8.08E-01	5.14E+04 ± 5.14E+00
2	1.88E+02 ± 3.77E-02	5.54E+03 ± 5.54E-01	4.54E+04 ± 4.54E+00
3	1.36E+02 ± 2.73E-02	4.33E+03 ± 4.33E-01	4.15E+04 ± 4.15E+00
4	1.07E+02 ± 3.21E-02	3.55E+03 ± 7.10E-01	3.81E+04 ± 3.81E+00
5	9.03E+01 ± 2.71E-02	3.06E+03 ± 6.13E-01	3.54E+04 ± 3.54E+00
6	7.76E+01 ± 3.10E-02	2.69E+03 ± 5.38E-01	3.30E+04 ± 3.30E+00
7	6.90E+01 ± 2.76E-02	2.40E+03 ± 4.80E-01	3.12E+04 ± 3.12E+00
8	6.23E+01 ± 3.12E-02	2.16E+03 ± 6.48E-01	2.94E+04 ± 2.94E+00
9	5.67E+01 ± 3.40E-02	1.97E+03 ± 5.91E-01	2.71E+04 ± 2.71E+00
10	5.23E+01 ± 3.14E-02	1.80E+03 ± 5.40E-01	2.62E+04 ± 2.62E+00
20	2.90E+01 ± 5.22E-02	1.04E+03 ± 6.24E-01	1.76E+04 ± 1.76E+00
30	2.09E+01 ± 7.51E-02	7.54E+02 ± 6.03E-01	1.33E+04 ± 2.66E+00
40	1.65E+01 ± 3.63E-02	5.93E+02 ± 5.34E-01	1.06E+04 ± 2.12E+00
50	1.38E+01 ± 6.63E-02	5.02E+02 ± 6.02E-01	9.00E+03 ± 2.70E+00
60	1.19E+01 ± 3.70E-02	4.37E+02 ± 6.56E-01	7.84E+03 ± 2.35E+00
70	1.06E+01 ± 4.23E-02	3.82E+02 ± 5.73E-01	7.01E+03 ± 2.10E+00
80	9.56E+00 ± 4.78E-02	3.42E+02 ± 5.48E-01	6.37E+03 ± 2.55E+00
90	8.77E+00 ± 5.35E-02	3.11E+02 ± 4.97E-01	5.85E+03 ± 2.34E+00
100	8.10E+00 ± 5.99E-02	2.89E+02 ± 5.50E-01	5.39E+03 ± 2.69E+00
120	7.06E+00 ± 3.25E-02	2.53E+02 ± 5.57E-01	4.69E+03 ± 2.34E+00
140	6.28E+00 ± 2.89E-02	2.26E+02 ± 5.42E-01	4.25E+03 ± 2.55E+00
160	5.76E+00 ± 3.06E-02	2.06E+02 ± 5.56E-01	3.84E+03 ± 2.30E+00
180	5.32E+00 ± 3.03E-02	1.90E+02 ± 5.51E-01	3.56E+03 ± 2.49E+00
200	4.92E+00 ± 2.90E-02	1.77E+02 ± 5.48E-01	3.32E+03 ± 2.65E+00
250	4.28E+00 ± 3.00E-02	1.54E+02 ± 5.68E-01	2.88E+03 ± 2.88E+00
300	3.87E+00 ± 3.06E-02	1.39E+02 ± 5.84E-01	2.62E+03 ± 2.89E+00
350	3.53E+00 ± 3.00E-02	1.27E+02 ± 5.98E-01	2.43E+03 ± 2.91E+00
400	3.33E+00 ± 3.30E-02	1.19E+02 ± 5.94E-01	2.26E+03 ± 2.71E+00
450	3.15E+00 ± 3.31E-02	1.13E+02 ± 6.08E-01	2.13E+03 ± 2.77E+00
500	2.99E+00 ± 3.29E-02	1.07E+02 ± 6.09E-01	2.02E+03 ± 2.62E+00
600	2.81E+00 ± 4.10E-02	9.96E+01 ± 6.08E-01	1.89E+03 ± 2.84E+00
700	2.59E+00 ± 3.04E-02	9.34E+01 ± 6.07E-01	1.78E+03 ± 3.03E+00
800	2.51E+00 ± 3.28E-02	9.00E+01 ± 6.48E-01	1.72E+03 ± 3.09E+00
900	2.42E+00 ± 3.17E-02	8.77E+01 ± 7.01E-01	1.67E+03 ± 3.17E+00
1000	2.35E+00 ± 3.52E-02	8.53E+01 ± 7.59E-01	1.62E+03 ± 3.40E+00
1500	2.20E+00 ± 3.72E-02	8.10E+01 ± 9.07E-01	1.53E+03 ± 3.82E+00
2000	2.28E+00 ± 7.47E-02	7.95E+01 ± 1.19E+00	1.49E+03 ± 4.77E+00
2500	2.25E+00 ± 7.59E-02	7.88E+01 ± 1.27E+00	1.49E+03 ± 5.50E+00
3000	2.27E+00 ± 8.57E-02	8.07E+01 ± 1.57E+00	1.50E+03 ± 6.16E+00
3500	2.30E+00 ± 1.05E-01	7.99E+01 ± 1.69E+00	1.49E+03 ± 6.86E+00
4000	2.29E+00 ± 1.04E-01	7.92E+01 ± 1.67E+00	1.49E+03 ± 7.28E+00
4500	2.32E+00 ± 1.14E-01	7.96E+01 ± 1.91E+00	1.48E+03 ± 7.55E+00
5000	2.31E+00 ± 1.16E-01	7.88E+01 ± 1.88E+00	1.48E+03 ± 8.44E+00
6000	2.26E+00 ± 1.03E-01	8.00E+01 ± 2.34E+00	1.50E+03 ± 1.03E+01
7000	2.37E+00 ± 1.76E-01	7.93E+01 ± 2.32E+00	1.51E+03 ± 1.25E+01
8000	2.23E+00 ± 1.02E-01	8.16E+01 ± 3.39E+00	1.52E+03 ± 1.38E+01
9000	2.22E+00 ± 1.01E-01	8.15E+01 ± 3.39E+00	1.52E+03 ± 1.45E+01
10000	2.21E+00 ± 1.02E-01	8.50E+01 ± 5.13E+00	1.52E+03 ± 1.56E+01

TABLE B. 31
Mass stopping powers of RW-2 for the proton, the carbon, and the iron beams. (MeV-cm^2/g)

Energy (MeV/u)	Proton	Carbon	Iron
1	3.30E+02 ± 6.60E-02	7.50E+03 ± 7.50E-01	4.78E+04 ± 4.78E+00
2	1.75E+02 ± 3.51E-02	5.14E+03 ± 5.14E-01	4.21E+04 ± 4.21E+00
3	1.27E+02 ± 2.53E-02	4.02E+03 ± 4.02E-01	3.85E+04 ± 3.85E+00
4	9.94E+01 ± 2.98E-02	3.30E+03 ± 6.59E-01	3.53E+04 ± 3.53E+00
5	8.38E+01 ± 2.51E-02	2.84E+03 ± 5.68E-01	3.29E+04 ± 3.29E+00
6	7.20E+01 ± 2.88E-02	2.50E+03 ± 5.00E-01	3.06E+04 ± 3.06E+00
7	6.41E+01 ± 3.21E-02	2.23E+03 ± 4.46E-01	2.90E+04 ± 2.90E+00
8	5.83E+01 ± 3.50E-02	2.01E+03 ± 6.04E-01	2.74E+04 ± 2.74E+00
9	5.33E+01 ± 4.26E-02	1.85E+03 ± 5.54E-01	2.54E+04 ± 2.54E+00
10	4.91E+01 ± 4.42E-02	1.69E+03 ± 5.07E-01	2.46E+04 ± 2.46E+00
20	2.72E+01 ± 2.99E-02	9.75E+02 ± 5.85E-01	1.65E+04 ± 1.65E+00
30	1.96E+01 ± 3.72E-02	7.08E+02 ± 5.67E-01	1.25E+04 ± 2.50E+00
40	1.56E+01 ± 7.17E-02	5.58E+02 ± 5.58E-01	9.98E+03 ± 2.00E+00
50	1.30E+01 ± 3.24E-02	4.73E+02 ± 6.15E-01	8.47E+03 ± 2.54E+00
60	1.13E+01 ± 6.77E-02	4.11E+02 ± 6.17E-01	7.37E+03 ± 2.21E+00
70	9.92E+00 ± 2.78E-02	3.59E+02 ± 5.38E-01	6.60E+03 ± 1.98E+00
80	8.99E+00 ± 4.05E-02	3.22E+02 ± 5.15E-01	6.01E+03 ± 2.40E+00
90	8.22E+00 ± 2.96E-02	2.95E+02 ± 5.31E-01	5.50E+03 ± 2.75E+00
100	7.58E+00 ± 2.96E-02	2.72E+02 ± 5.45E-01	5.07E+03 ± 2.53E+00
120	6.63E+00 ± 2.85E-02	2.38E+02 ± 5.24E-01	4.44E+03 ± 2.22E+00
140	5.91E+00 ± 2.84E-02	2.13E+02 ± 5.32E-01	4.00E+03 ± 2.40E+00
160	5.43E+00 ± 2.93E-02	1.94E+02 ± 5.43E-01	3.62E+03 ± 2.53E+00
180	5.01E+00 ± 2.90E-02	1.79E+02 ± 5.37E-01	3.36E+03 ± 2.35E+00
200	4.64E+00 ± 2.88E-02	1.66E+02 ± 5.32E-01	3.13E+03 ± 2.50E+00
250	4.04E+00 ± 2.95E-02	1.45E+02 ± 5.50E-01	2.71E+03 ± 2.99E+00
300	3.65E+00 ± 3.03E-02	1.31E+02 ± 5.77E-01	2.51E+03 ± 2.76E+00
350	3.33E+00 ± 2.93E-02	1.20E+02 ± 5.76E-01	2.28E+03 ± 2.74E+00
400	3.15E+00 ± 3.24E-02	1.12E+02 ± 5.82E-01	2.13E+03 ± 2.76E+00
450	2.97E+00 ± 3.14E-02	1.06E+02 ± 5.95E-01	2.00E+03 ± 2.60E+00
500	2.81E+00 ± 3.12E-02	1.01E+02 ± 5.94E-01	1.90E+03 ± 2.66E+00
600	2.61E+00 ± 3.03E-02	9.38E+01 ± 5.91E-01	1.78E+03 ± 2.68E+00
700	2.44E+00 ± 2.98E-02	8.80E+01 ± 5.98E-01	1.68E+03 ± 2.86E+00
800	2.35E+00 ± 3.13E-02	8.48E+01 ± 6.27E-01	1.62E+03 ± 2.92E+00
900	2.29E+00 ± 3.42E-02	8.28E+01 ± 7.04E-01	1.57E+03 ± 3.14E+00
1000	2.22E+00 ± 3.60E-02	8.05E+01 ± 7.48E-01	1.53E+03 ± 3.20E+00
1500	2.09E+00 ± 4.09E-02	7.62E+01 ± 8.61E-01	1.44E+03 ± 3.75E+00
2000	2.14E+00 ± 7.17E-02	7.52E+01 ± 1.17E+00	1.41E+03 ± 4.64E+00
2500	2.10E+00 ± 6.95E-02	7.47E+01 ± 1.28E+00	1.40E+03 ± 5.33E+00
3000	2.15E+00 ± 8.15E-02	7.61E+01 ± 1.49E+00	1.42E+03 ± 5.96E+00
3500	2.18E+00 ± 9.94E-02	7.59E+01 ± 1.60E+00	1.42E+03 ± 6.51E+00
4000	2.16E+00 ± 9.86E-02	7.61E+01 ± 1.83E+00	1.41E+03 ± 7.07E+00
4500	2.15E+00 ± 9.80E-02	7.56E+01 ± 1.81E+00	1.41E+03 ± 7.33E+00
5000	2.13E+00 ± 9.76E-02	7.61E+01 ± 2.23E+00	1.41E+03 ± 8.32E+00
6000	2.12E+00 ± 9.68E-02	7.59E+01 ± 2.22E+00	1.43E+03 ± 1.03E+01
7000	2.11E+00 ± 9.64E-02	7.76E+01 ± 3.24E+00	1.43E+03 ± 1.19E+01
8000	2.10E+00 ± 9.61E-02	7.75E+01 ± 3.22E+00	1.45E+03 ± 1.34E+01
9000	2.10E+00 ± 9.59E-02	8.10E+01 ± 4.88E+00	1.45E+03 ± 1.37E+01
10000	2.09E+00 ± 9.57E-02	8.07E+01 ± 4.87E+00	1.45E+03 ± 1.55E+01

TABLE B. 32
Mass stopping powers of Temex for the proton, the carbon, and the iron beams. (MeV-cm^2/g)

Energy (MeV/u)	Proton	Carbon	Iron
1	3.46E+02 ± 3.46E-02	8.08E+03 ± 8.08E-01	5.15E+04 ± 5.15E+00
2	1.89E+02 ± 3.77E-02	5.56E+03 ± 5.56E-01	4.55E+04 ± 4.55E+00
3	1.35E+02 ± 2.71E-02	4.35E+03 ± 4.35E-01	4.16E+04 ± 4.16E+00
4	1.07E+02 ± 3.22E-02	3.57E+03 ± 7.14E-01	3.82E+04 ± 3.82E+00
5	9.06E+01 ± 2.72E-02	3.08E+03 ± 6.16E-01	3.56E+04 ± 3.56E+00
6	7.79E+01 ± 3.12E-02	2.70E+03 ± 5.41E-01	3.31E+04 ± 3.31E+00
7	6.95E+01 ± 3.48E-02	2.41E+03 ± 4.82E-01	3.14E+04 ± 3.14E+00
8	6.32E+01 ± 3.79E-02	2.18E+03 ± 6.55E-01	2.97E+04 ± 2.97E+00
9	5.78E+01 ± 4.62E-02	2.00E+03 ± 6.00E-01	2.75E+04 ± 2.75E+00
10	5.18E+01 ± 4.14E-02	1.83E+03 ± 5.48E-01	2.66E+04 ± 2.66E+00
20	2.93E+01 ± 3.23E-02	1.05E+03 ± 6.29E-01	1.78E+04 ± 1.78E+00
30	2.11E+01 ± 4.00E-02	7.61E+02 ± 6.09E-01	1.34E+04 ± 2.69E+00
40	1.68E+01 ± 7.71E-02	6.01E+02 ± 6.01E-01	1.07E+04 ± 2.15E+00
50	1.39E+01 ± 3.48E-02	5.09E+02 ± 6.61E-01	9.10E+03 ± 2.73E+00
60	1.21E+01 ± 7.39E-02	4.41E+02 ± 6.62E-01	7.91E+03 ± 2.37E+00
70	1.06E+01 ± 2.98E-02	3.85E+02 ± 5.77E-01	7.16E+03 ± 2.86E+00
80	9.66E+00 ± 4.35E-02	3.45E+02 ± 5.51E-01	6.44E+03 ± 2.57E+00
90	8.82E+00 ± 3.17E-02	3.16E+02 ± 5.70E-01	5.89E+03 ± 2.36E+00
100	8.13E+00 ± 3.17E-02	2.92E+02 ± 5.84E-01	5.43E+03 ± 2.72E+00
120	7.09E+00 ± 3.05E-02	2.55E+02 ± 5.61E-01	4.77E+03 ± 2.86E+00
140	6.33E+00 ± 3.04E-02	2.28E+02 ± 5.70E-01	4.28E+03 ± 2.57E+00
160	5.80E+00 ± 3.13E-02	2.08E+02 ± 5.60E-01	3.87E+03 ± 2.71E+00
180	5.35E+00 ± 3.10E-02	1.92E+02 ± 5.75E-01	3.60E+03 ± 2.52E+00
200	4.96E+00 ± 3.08E-02	1.78E+02 ± 5.70E-01	3.35E+03 ± 2.68E+00
250	4.31E+00 ± 3.11E-02	1.55E+02 ± 6.05E-01	2.90E+03 ± 3.19E+00
300	3.90E+00 ± 3.16E-02	1.40E+02 ± 6.17E-01	2.68E+03 ± 2.94E+00
350	3.58E+00 ± 3.29E-02	1.28E+02 ± 6.15E-01	2.44E+03 ± 2.93E+00
400	3.35E+00 ± 3.42E-02	1.20E+02 ± 6.35E-01	2.27E+03 ± 2.72E+00
450	3.16E+00 ± 3.32E-02	1.13E+02 ± 6.35E-01	2.14E+03 ± 2.78E+00
500	3.00E+00 ± 3.36E-02	1.07E+02 ± 6.22E-01	2.03E+03 ± 2.85E+00
600	2.78E+00 ± 3.20E-02	1.00E+02 ± 6.20E-01	1.91E+03 ± 3.05E+00
700	2.61E+00 ± 3.29E-02	9.42E+01 ± 6.59E-01	1.80E+03 ± 3.05E+00
800	2.51E+00 ± 3.28E-02	9.09E+01 ± 7.09E-01	1.73E+03 ± 3.11E+00
900	2.44E+00 ± 3.59E-02	8.85E+01 ± 7.61E-01	1.68E+03 ± 3.36E+00
1000	2.36E+00 ± 3.76E-02	8.60E+01 ± 8.17E-01	1.63E+03 ± 3.42E+00
1500	2.25E+00 ± 4.85E-02	8.11E+01 ± 9.09E-01	1.54E+03 ± 4.15E+00
2000	2.27E+00 ± 7.50E-02	8.00E+01 ± 1.23E+00	1.50E+03 ± 4.95E+00
2500	2.23E+00 ± 7.29E-02	7.98E+01 ± 1.43E+00	1.49E+03 ± 5.68E+00
3000	2.27E+00 ± 8.55E-02	8.04E+01 ± 1.57E+00	1.50E+03 ± 6.46E+00
3500	2.29E+00 ± 1.04E-01	7.96E+01 ± 1.68E+00	1.49E+03 ± 6.99E+00
4000	2.27E+00 ± 1.04E-01	7.98E+01 ± 1.91E+00	1.48E+03 ± 7.41E+00
4500	2.25E+00 ± 1.03E-01	7.91E+01 ± 1.88E+00	1.48E+03 ± 7.84E+00
5000	2.23E+00 ± 1.02E-01	7.98E+01 ± 2.34E+00	1.48E+03 ± 8.87E+00
6000	2.23E+00 ± 1.02E-01	7.96E+01 ± 2.33E+00	1.50E+03 ± 1.11E+01
7000	2.21E+00 ± 1.01E-01	8.14E+01 ± 3.40E+00	1.51E+03 ± 1.28E+01
8000	2.20E+00 ± 1.01E-01	8.13E+01 ± 3.38E+00	1.52E+03 ± 1.44E+01
9000	2.20E+00 ± 1.01E-01	8.50E+01 ± 5.11E+00	1.52E+03 ± 1.56E+01
10000	2.19E+00 ± 1.01E-01	8.46E+01 ± 5.11E+00	1.54E+03 ± 1.85E+01

TABLE B. 33
Mass stopping powers of TH/L2 for the proton, the carbon, and the iron beams.
(MeV-cm^2/g)

Energy (MeV/u)	Proton	Carbon	Iron
1	3.51E+02 ± 3.51E-02	8.11E+03 ± 8.11E-01	5.16E+04 ± 5.16E+00
2	1.89E+02 ± 3.78E-02	5.56E+03 ± 5.56E-01	4.56E+04 ± 4.56E+00
3	1.37E+02 ± 2.73E-02	4.35E+03 ± 4.35E-01	4.17E+04 ± 4.17E+00
4	1.07E+02 ± 3.22E-02	3.57E+03 ± 7.13E-01	3.82E+04 ± 3.82E+00
5	9.06E+01 ± 2.72E-02	3.08E+03 ± 6.15E-01	3.56E+04 ± 3.56E+00
6	7.79E+01 ± 3.12E-02	2.70E+03 ± 5.41E-01	3.31E+04 ± 3.31E+00
7	6.93E+01 ± 2.77E-02	2.41E+03 ± 4.82E-01	3.13E+04 ± 3.13E+00
8	6.26E+01 ± 3.13E-02	2.17E+03 ± 6.50E-01	2.95E+04 ± 2.95E+00
9	5.69E+01 ± 3.42E-02	1.98E+03 ± 5.93E-01	2.72E+04 ± 2.72E+00
10	5.24E+01 ± 3.14E-02	1.81E+03 ± 5.42E-01	2.63E+04 ± 2.63E+00
20	2.91E+01 ± 5.53E-02	1.04E+03 ± 6.25E-01	1.77E+04 ± 1.77E+00
30	2.09E+01 ± 7.74E-02	7.56E+02 ± 6.05E-01	1.33E+04 ± 2.66E+00
40	1.66E+01 ± 3.81E-02	5.95E+02 ± 5.35E-01	1.06E+04 ± 2.13E+00
50	1.38E+01 ± 2.90E-02	5.04E+02 ± 6.04E-01	9.03E+03 ± 2.71E+00
60	1.20E+01 ± 3.83E-02	4.39E+02 ± 6.58E-01	7.86E+03 ± 2.36E+00
70	1.06E+01 ± 4.35E-02	3.83E+02 ± 5.74E-01	7.03E+03 ± 2.11E+00
80	9.58E+00 ± 4.89E-02	3.43E+02 ± 5.49E-01	6.40E+03 ± 2.56E+00
90	8.79E+00 ± 5.45E-02	3.11E+02 ± 4.98E-01	5.86E+03 ± 2.34E+00
100	8.12E+00 ± 6.09E-02	2.90E+02 ± 5.52E-01	5.40E+03 ± 2.70E+00
120	7.08E+00 ± 3.26E-02	2.54E+02 ± 5.58E-01	4.71E+03 ± 2.36E+00
140	6.30E+00 ± 2.96E-02	2.27E+02 ± 5.67E-01	4.26E+03 ± 2.56E+00
160	5.78E+00 ± 3.12E-02	2.07E+02 ± 5.58E-01	3.85E+03 ± 2.70E+00
180	5.33E+00 ± 3.04E-02	1.90E+02 ± 5.52E-01	3.57E+03 ± 2.50E+00
200	4.93E+00 ± 2.96E-02	1.77E+02 ± 5.49E-01	3.33E+03 ± 2.66E+00
250	4.30E+00 ± 3.10E-02	1.54E+02 ± 5.70E-01	2.89E+03 ± 2.89E+00
300	3.89E+00 ± 3.15E-02	1.39E+02 ± 6.00E-01	2.63E+03 ± 2.89E+00
350	3.54E+00 ± 3.00E-02	1.28E+02 ± 5.99E-01	2.43E+03 ± 2.92E+00
400	3.35E+00 ± 3.45E-02	1.19E+02 ± 6.08E-01	2.26E+03 ± 2.72E+00
450	3.16E+00 ± 3.32E-02	1.13E+02 ± 6.21E-01	2.13E+03 ± 2.77E+00
500	2.99E+00 ± 3.29E-02	1.07E+02 ± 6.21E-01	2.02E+03 ± 2.83E+00
600	2.81E+00 ± 4.19E-02	9.99E+01 ± 6.19E-01	1.90E+03 ± 2.85E+00
700	2.61E+00 ± 3.18E-02	9.35E+01 ± 6.08E-01	1.79E+03 ± 3.04E+00
800	2.51E+00 ± 3.31E-02	9.02E+01 ± 6.58E-01	1.72E+03 ± 3.10E+00
900	2.43E+00 ± 3.41E-02	8.81E+01 ± 7.31E-01	1.67E+03 ± 3.17E+00
1000	2.35E+00 ± 3.53E-02	8.57E+01 ± 7.88E-01	1.62E+03 ± 3.41E+00
1500	2.23E+00 ± 4.32E-02	8.11E+01 ± 9.17E-01	1.53E+03 ± 3.98E+00
2000	2.31E+00 ± 8.16E-02	7.97E+01 ± 1.19E+00	1.50E+03 ± 4.79E+00
2500	2.26E+00 ± 7.58E-02	7.94E+01 ± 1.35E+00	1.49E+03 ± 5.52E+00
3000	2.28E+00 ± 8.59E-02	8.09E+01 ± 1.58E+00	1.51E+03 ± 6.17E+00
3500	2.30E+00 ± 1.05E-01	8.02E+01 ± 1.69E+00	1.49E+03 ± 6.88E+00
4000	2.29E+00 ± 1.04E-01	8.03E+01 ± 1.93E+00	1.49E+03 ± 7.46E+00
4500	2.32E+00 ± 1.15E-01	7.98E+01 ± 1.92E+00	1.49E+03 ± 7.73E+00
5000	2.31E+00 ± 1.17E-01	7.90E+01 ± 1.89E+00	1.49E+03 ± 8.62E+00
6000	2.26E+00 ± 1.03E-01	8.02E+01 ± 2.34E+00	1.51E+03 ± 1.05E+01
7000	2.38E+00 ± 1.80E-01	7.95E+01 ± 2.33E+00	1.51E+03 ± 1.26E+01
8000	2.24E+00 ± 1.02E-01	8.18E+01 ± 3.40E+00	1.52E+03 ± 1.39E+01
9000	2.22E+00 ± 1.02E-01	8.17E+01 ± 3.40E+00	1.53E+03 ± 1.45E+01
10000	2.22E+00 ± 1.02E-01	8.52E+01 ± 5.15E+00	1.53E+03 ± 1.64E+01

TABLE B. 34
Mass stopping powers of the water for the proton, the carbon, and the iron beams. (MeV-cm^2/g)

Energy (MeV/u)	Proton	Carbon	Iron
1	3.11E+02 ± 3.11E-02	7.15E+03 ± 7.15E-01	4.58E+04 ± 4.58E+00
2	1.68E+02 ± 3.37E-02	4.93E+03 ± 4.93E-01	4.02E+04 ± 4.02E+00
3	1.22E+02 ± 3.66E-02	3.87E+03 ± 3.87E-01	3.69E+04 ± 3.69E+00
4	9.14E+01 ± 2.74E-02	3.17E+03 ± 6.34E-01	3.40E+04 ± 3.40E+00
5	8.04E+01 ± 3.22E-02	2.73E+03 ± 5.47E-01	3.16E+04 ± 3.16E+00
6	6.93E+01 ± 2.77E-02	2.40E+03 ± 4.80E-01	2.94E+04 ± 2.94E+00
7	6.19E+01 ± 3.10E-02	2.14E+03 ± 6.43E-01	2.79E+04 ± 2.79E+00
8	5.65E+01 ± 3.39E-02	1.95E+03 ± 5.84E-01	2.64E+04 ± 2.64E+00
9	5.18E+01 ± 3.63E-02	1.79E+03 ± 5.37E-01	2.47E+04 ± 2.47E+00
10	4.63E+01 ± 2.78E-02	1.64E+03 ± 4.92E-01	2.39E+04 ± 2.39E+00
20	2.65E+01 ± 2.91E-02	9.44E+02 ± 5.66E-01	1.61E+04 ± 3.22E+00
30	1.91E+01 ± 3.05E-02	6.89E+02 ± 5.51E-01	1.22E+04 ± 2.44E+00
40	1.51E+01 ± 3.02E-02	5.46E+02 ± 6.01E-01	9.74E+03 ± 2.92E+00
50	1.26E+01 ± 2.91E-02	4.64E+02 ± 6.49E-01	8.26E+03 ± 2.48E+00
60	1.10E+01 ± 3.95E-02	3.97E+02 ± 5.96E-01	7.19E+03 ± 2.16E+00
70	9.74E+00 ± 4.48E-02	3.50E+02 ± 5.59E-01	6.49E+03 ± 2.60E+00
80	8.81E+00 ± 5.11E-02	3.13E+02 ± 5.32E-01	5.85E+03 ± 2.34E+00
90	8.08E+00 ± 5.81E-02	2.89E+02 ± 5.48E-01	5.37E+03 ± 2.68E+00
100	7.45E+00 ± 6.49E-02	2.66E+02 ± 5.59E-01	4.96E+03 ± 2.48E+00
120	6.49E+00 ± 3.18E-02	2.33E+02 ± 5.59E-01	4.36E+03 ± 2.62E+00
140	5.80E+00 ± 3.02E-02	2.08E+02 ± 5.62E-01	3.90E+03 ± 2.73E+00
160	5.30E+00 ± 3.07E-02	1.89E+02 ± 5.50E-01	3.54E+03 ± 2.48E+00
180	4.88E+00 ± 2.98E-02	1.75E+02 ± 5.60E-01	3.29E+03 ± 2.63E+00
200	4.54E+00 ± 3.00E-02	1.63E+02 ± 5.70E-01	3.07E+03 ± 2.77E+00
250	3.94E+00 ± 3.00E-02	1.42E+02 ± 5.82E-01	2.66E+03 ± 2.92E+00
300	3.56E+00 ± 2.99E-02	1.28E+02 ± 6.03E-01	2.45E+03 ± 2.94E+00
350	3.29E+00 ± 3.36E-02	1.17E+02 ± 5.98E-01	2.23E+03 ± 2.90E+00
400	3.08E+00 ± 3.35E-02	1.10E+02 ± 6.03E-01	2.08E+03 ± 2.70E+00
450	2.90E+00 ± 3.28E-02	1.04E+02 ± 6.12E-01	1.96E+03 ± 2.75E+00
500	2.74E+00 ± 3.18E-02	9.84E+01 ± 6.10E-01	1.87E+03 ± 2.80E+00
600	2.54E+00 ± 3.03E-02	9.17E+01 ± 6.06E-01	1.75E+03 ± 2.98E+00
700	2.40E+00 ± 3.27E-02	8.65E+01 ± 6.49E-01	1.65E+03 ± 2.97E+00
800	2.30E+00 ± 3.10E-02	8.35E+01 ± 6.93E-01	1.59E+03 ± 3.17E+00
900	2.24E+00 ± 3.46E-02	8.14E+01 ± 7.57E-01	1.54E+03 ± 3.24E+00
1000	2.17E+00 ± 3.57E-02	7.92E+01 ± 8.16E-01	1.50E+03 ± 3.44E+00
1500	2.11E+00 ± 5.63E-02	7.49E+01 ± 9.29E-01	1.42E+03 ± 3.97E+00
2000	2.13E+00 ± 7.84E-02	7.35E+01 ± 1.16E+00	1.38E+03 ± 4.84E+00
2500	2.12E+00 ± 8.38E-02	7.44E+01 ± 1.51E+00	1.38E+03 ± 5.51E+00
3000	2.16E+00 ± 1.00E-01	7.51E+01 ± 1.61E+00	1.40E+03 ± 6.29E+00
3500	2.14E+00 ± 9.90E-02	7.43E+01 ± 1.59E+00	1.39E+03 ± 6.82E+00
4000	2.15E+00 ± 9.83E-02	7.52E+01 ± 1.81E+00	1.40E+03 ± 7.14E+00
4500	2.19E+00 ± 1.11E-01	7.50E+01 ± 1.78E+00	1.41E+03 ± 7.88E+00
5000	2.19E+00 ± 1.14E-01	7.58E+01 ± 2.22E+00	1.41E+03 ± 8.73E+00
6000	2.13E+00 ± 9.75E-02	7.55E+01 ± 2.20E+00	1.43E+03 ± 1.09E+01
7000	2.26E+00 ± 1.86E-01	7.72E+01 ± 3.21E+00	1.43E+03 ± 1.25E+01
8000	2.11E+00 ± 9.64E-02	7.71E+01 ± 3.21E+00	1.44E+03 ± 1.37E+01
9000	2.09E+00 ± 9.54E-02	8.06E+01 ± 4.85E+00	1.45E+03 ± 1.48E+01
10000	2.09E+00 ± 9.61E-02	8.03E+01 ± 4.84E+00	1.47E+03 ± 1.88E+01

APPENDIX C

Depth-dose distribution within 10cm x 10cm x 20cm target for ICRU-44 tissue and the soft tissue substitutes

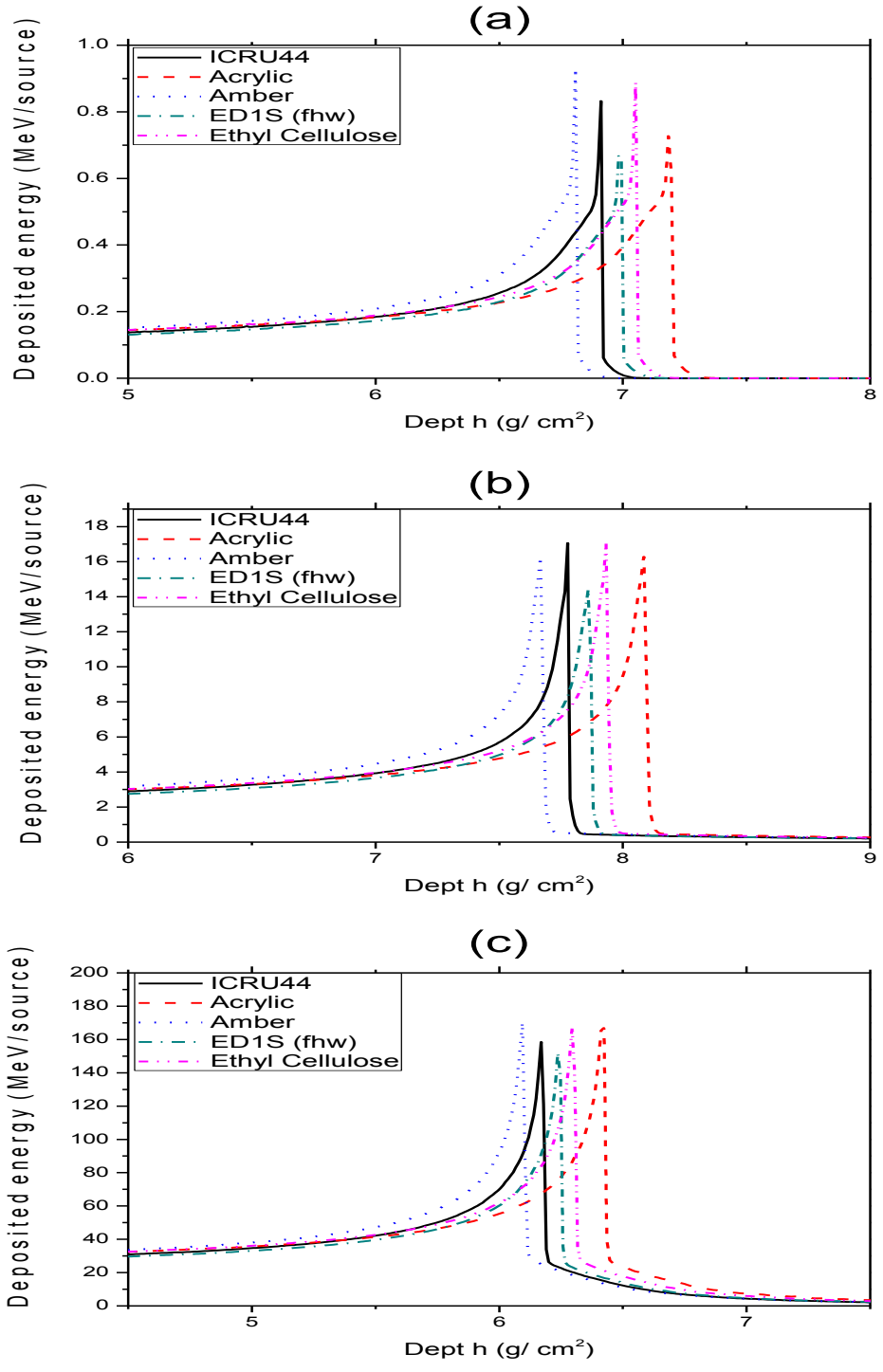

Fig. C. 1. Depth-dose distributions of the proton(a), the carbon(b), and the iron(c) beams within the media of ICRU-44 tissue, Acrylic, Amber, ED1S (fhw), and Ethyl cellulose.

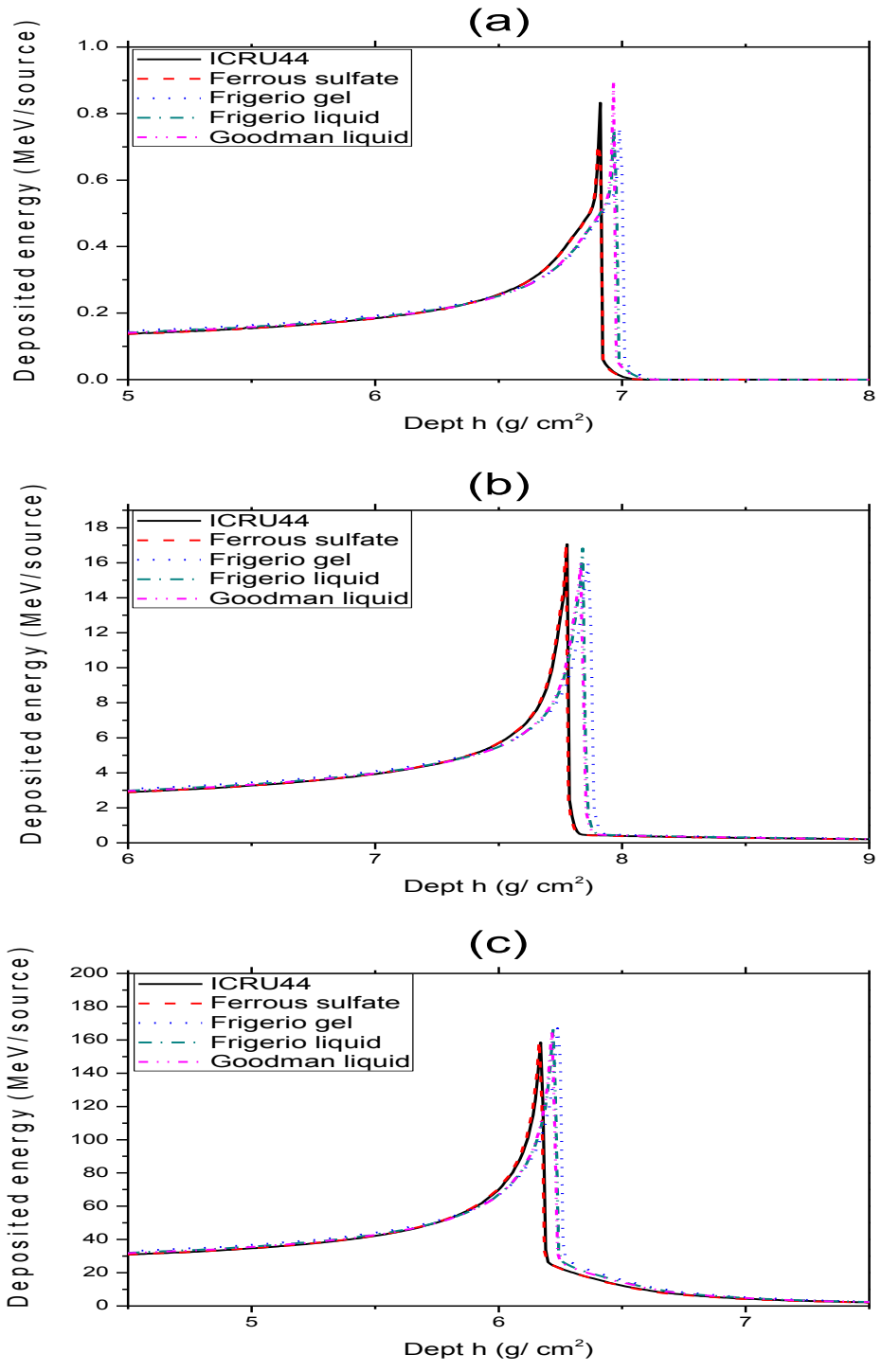

Fig. C. 2. Depth-dose distributions of the proton(a), the carbon(b), and the iron(c) beams within the media of ICRU-44 tissue, Ferrous sulfate dosimeter solution, Frigerio gel, Frigerio liquid, and Goodman liquid.

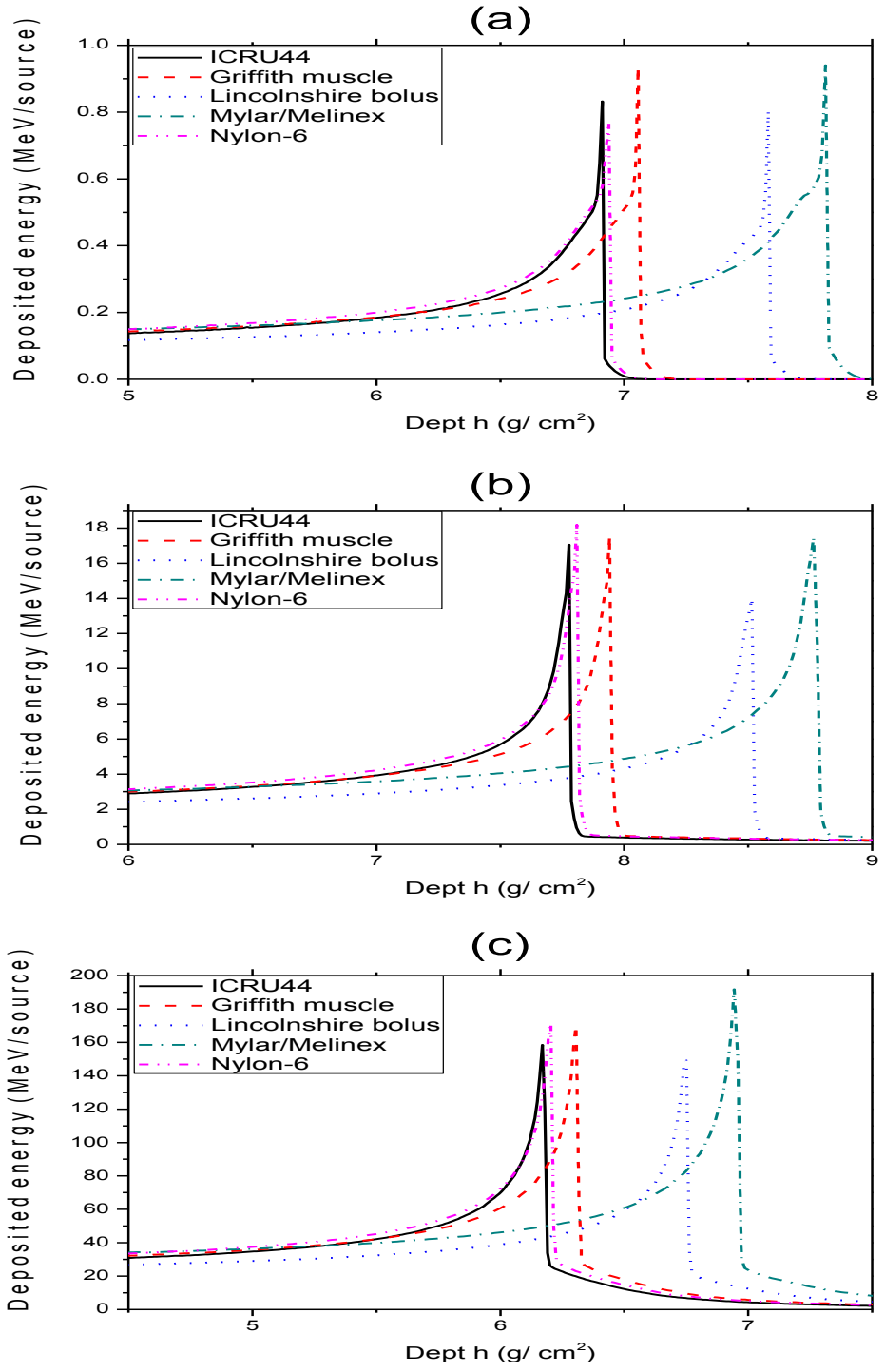

Fig. C. 3. Depth-dose distributions of the proton(a), the carbon(b), and the iron(c) beams within the media of ICRU-44 tissue, Griffith muscle, Lincolnshire bolus, Mylar/Melinex, and Nylon-6.

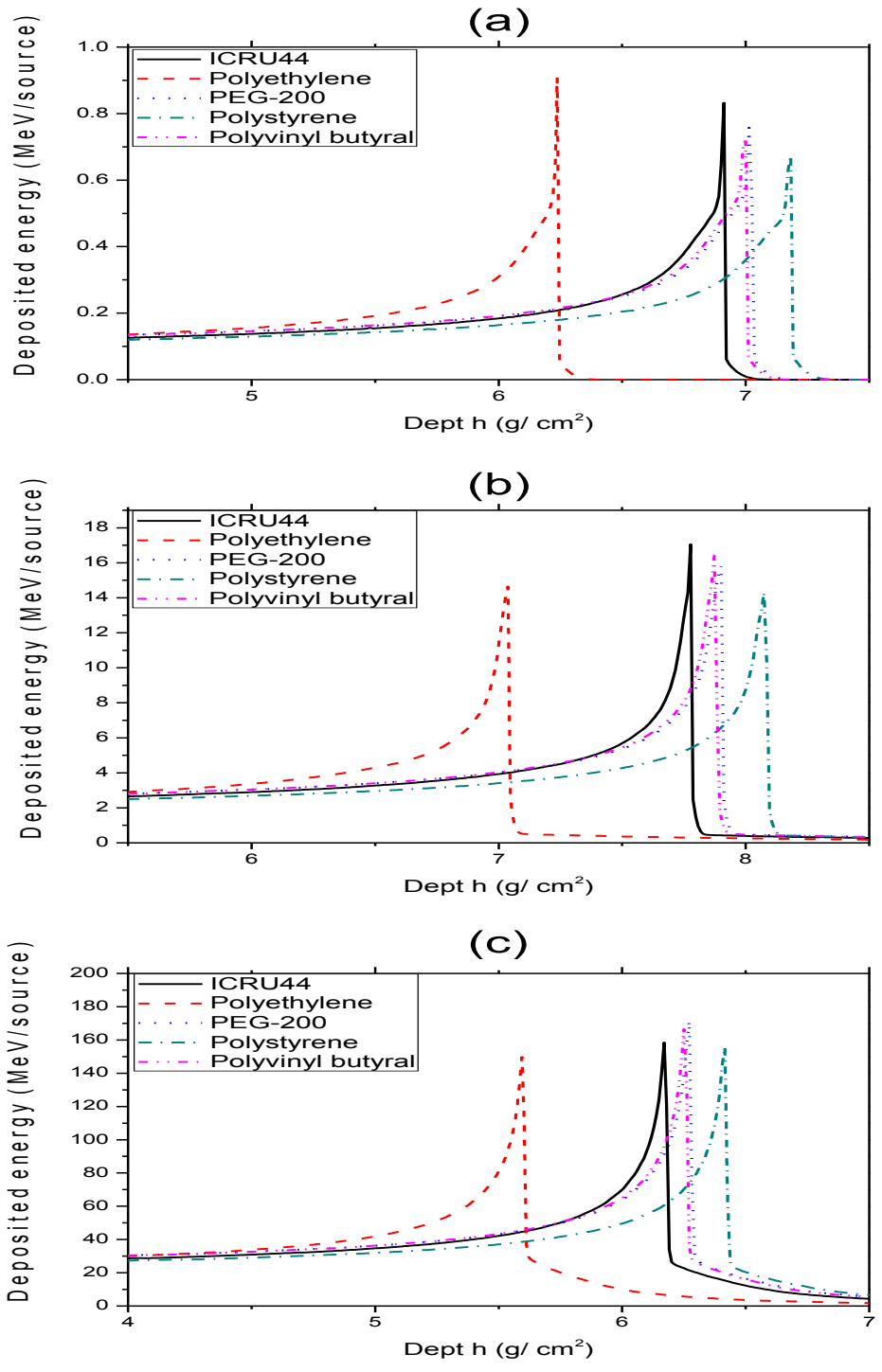

Fig. C. 4. Depth-dose distributions of the proton(a), the carbon(b), and the iron(c) beams within the media of ICRU-44 tissue, Polyethylene, PEG-200, Polystyrene, and Polyvinyl butyral.

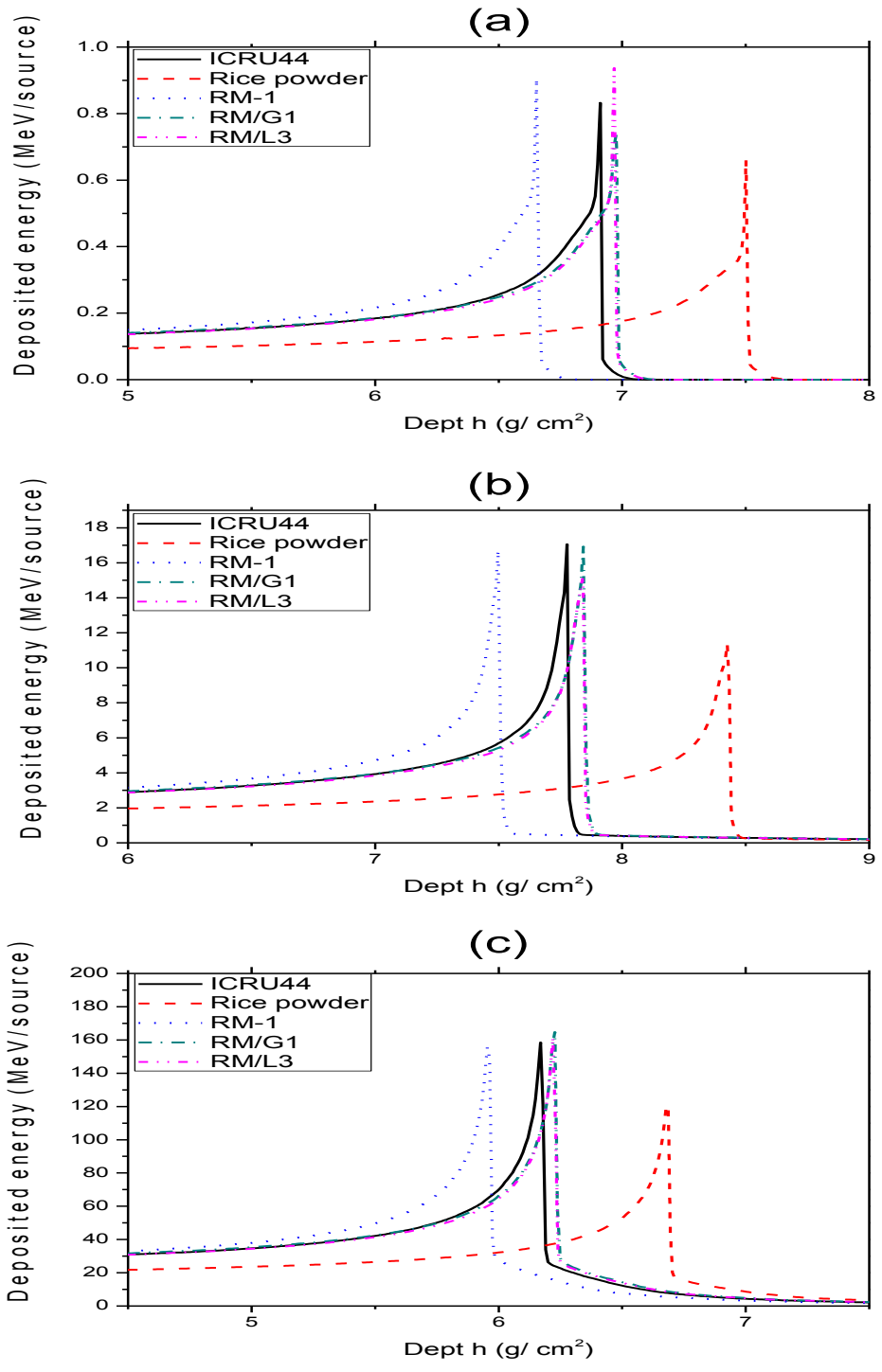

Fig. C. 5. Depth-dose distributions of the proton(a), the carbon(b), and the iron(c) beams within the media of ICRU-44 tissue, Rice powder, RM-1, RM/G1, and RM/L3.

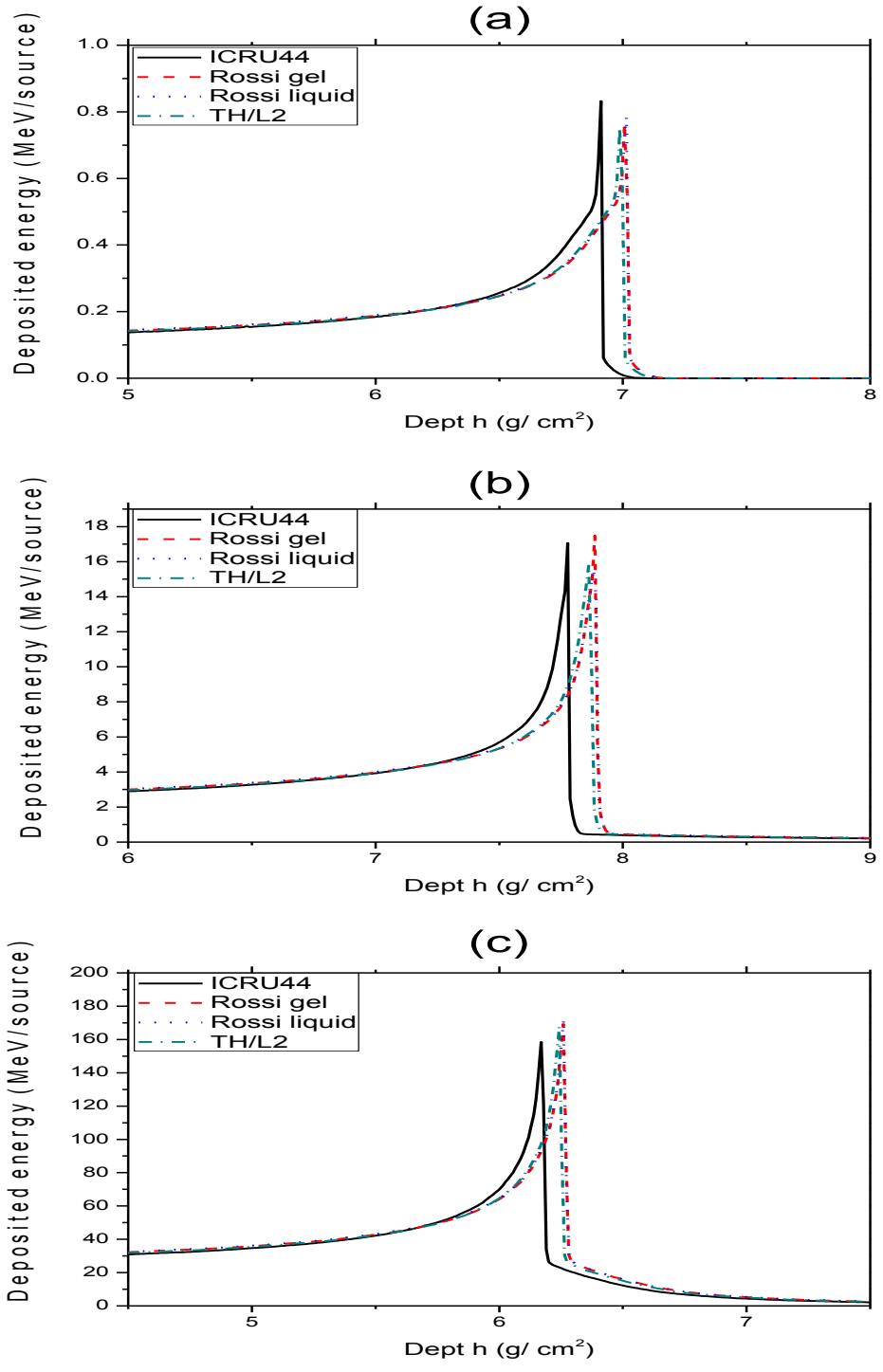

Fig. C. 6. Depth-dose distributions of the proton(a), the carbon(b), and the iron(c) beams within the media of ICRU-44 tissue, Rossi gel, Rossi liquid, and TH/L2.

APPENDIX D

Organ doses by the irradiations of each beam into the developed phantom with the suitable soft tissue substitutes by the PHITS simulations.

TABLE D. 1
Absorbed dose of each organ with an irradiation of 100 MeV proton pencil beam by simulation when they were used as the soft tissue of the phantom. Units are Gy.

	Heart tissue	Blood	Heart (all)	Left lung	Right lung	Lung (all)
ICRU-44	7.25E-12± 2.18E-15	9.14E-12± 2.74E-15	1.64E-11± 3.50E-15	2.80E-13± 3.63E-16	1.97E-15± 7.33E-17	2.82E-13± 3.71E-16
A150	8.27E-12± 2.48E-15	6.96E-12± 2.78E-15	1.52E-11± 3.73E-15	2.96E-13± 3.85E-16	1.96E-15± 7.09E-17	2.98E-13± 3.92E-16
ED4C (fhw)	7.02E-12± 2.11E-15	9.73E-12± 2.92E-15	1.68E-11± 3.60E-15	2.76E-13± 3.86E-16	1.85E-15± 6.94E-17	2.78E-13± 3.92E-16
Nylon, Elvamide	7.81E-12± 2.34E-15	7.86E-12± 3.14E-15	1.57E-11± 3.92E-15	2.90E-13± 3.77E-16	1.96E-15± 7.07E-17	2.92E-13± 3.84E-16
RM/SR4	7.28E-12± 2.18E-15	9.06E-12± 2.72E-15	1.63E-11± 3.49E-15	2.82E-13± 3.66E-16	1.98E-15± 7.19E-17	2.84E-13± 3.73E-16
Temex	7.05E-12± 2.12E-15	9.64E-12± 2.89E-15	1.67E-11± 3.58E-15	2.78E-13± 3.89E-16	2.01E-15± 7.42E-17	2.80E-13± 3.96E-16
RW-2	7.23E-12± 2.17E-15	9.09E-12± 2.73E-15	1.63E-11± 3.48E-15	2.79E-13± 3.91E-16	2.33E-15± 7.74E-17	2.82E-13± 3.99E-16
Ceric sulfate Dosimeter solution	7.23E-12± 2.17E-15	9.19E-12± 2.76E-15	1.64E-11± 3.51E-15	2.79E-13± 3.63E-16	1.84E-15± 7.10E-17	2.81E-13± 3.69E-16
Alderson muscle (B)	6.86E-12± 2.06E-15	1.03E-11± 3.08E-15	1.71E-11± 3.70E-15	2.76E-13± 3.86E-16	2.06E-15± 7.40E-17	2.78E-13± 3.93E-16
A150_corrected	7.27E-12± 2.18E-15	9.08E-12± 2.72E-15	1.64E-11± 3.49E-15	2.82E-13± 3.66E-16	1.96E-15± 7.22E-17	2.84E-13± 3.73E-16

TABLE D. 2
Absorbed dose of each organ with an irradiation of 200 MeV/u carbon pencil beam by simulation when they were used as the soft tissue of the phantom. Units are Gy.

	Heart tissue	Blood	Heart (all)	Left lung	Right lung	Lung (all)
ICRU-44	1.22E-10	3.01E-10	4.24E-10	5.66E-12± 1.59E-14	1.89E-13± 3.49E-15	5.85E-12± 1.62E-14
A150	1.29E-10± 3.87E-14	2.71E-10	4.00E-10± 3.87E-14	5.71E-12± 1.66E-14	1.84E-13± 3.40E-15	5.89E-12± 1.69E-14
ED4C (fhw)	1.20E-10	3.09E-10	4.30E-10	5.57E-12± 1.56E-14	1.90E-13± 3.47E-15	5.76E-12± 1.60E-14
Nylon, Elvamide	1.26E-10	2.83E-10	4.09E-10	5.70E-12± 1.60E-14	1.87E-13± 3.39E-15	5.88E-12± 1.63E-14
RM/SR4	1.22E-10	3.00E-10	4.22E-10	5.60E-12± 1.57E-14	1.93E-13± 3.49E-15	5.79E-12± 1.61E-14
Temex	1.20E-10	3.08E-10	4.29E-10	5.55E-12± 1.56E-14	1.90E-13± 3.42E-15	5.75E-12± 1.59E-14
RW-2	1.22E-10	3.00E-10	4.21E-10	5.59E-12± 1.57E-14	1.99E-13± 3.52E-15	5.79E-12± 1.60E-14
Ceric sulfate Dosimeter solution	1.22E-10	3.01E-10	4.23E-10	5.57E-12± 1.56E-14	1.85E-13± 3.42E-15	5.75E-12± 1.60E-14
Alderson muscle (B)	1.18E-10	3.17E-10	4.35E-10	5.51E-12± 1.54E-14	1.94E-13± 3.47E-15	5.70E-12± 1.58E-14
A150_corrected	1.22E-10	3.00E-10	4.22E-10	5.60E-12± 1.57E-14	1.90E-13± 3.46E-15	5.79E-12± 1.61E-14

TABLE D. 3
Absorbed dose of each organ with an irradiation of 400 MeV/u iron pencil beam by simulation when they were used as the soft tissue of the phantom. Units are Gy.

	Heart tissue	Blood	Heart (all)	Left lung	Right lung	Lung (all)
ICRU-44	2.12E-09± 3.82E-12	1.01E-09± 2.84E-12	3.13E-09± 4.75E-12	7.02E-11± 3.51E-13	1.34E-12± 1.24E-14	7.16E-11± 3.51E-13
A150	2.07E-09± 2.89E-12	6.73E-10± 2.22E-12	2.74E-09± 3.65E-12	7.43E-11± 3.79E-13	1.31E-12± 1.22E-14	7.56E-11± 3.79E-13
ED4C (fhw)	1.99E-09± 3.38E-12	1.20E-09± 2.16E-12	3.19E-09± 4.01E-12	6.88E-11± 3.44E-13	1.36E-12± 1.26E-14	7.01E-11± 3.44E-13
Nylon, Elvamide	2.09E-09± 3.13E-12	8.12E-10± 2.44E-12	2.90E-09± 3.97E-12	7.23E-11± 3.61E-13	1.33E-12± 1.24E-14	7.36E-11± 3.62E-13
RM/SR4	2.11E-09± 4.01E-12	1.01E-09± 2.82E-12	3.12E-09± 4.90E-12	6.99E-11± 3.50E-13	1.34E-12± 1.23E-14	7.13E-11± 3.50E-13
Temex	1.99E-09± 6.99E-12	1.19E-09± 2.14E-12	3.18E-09± 4.17E-12	6.83E-11± 3.42E-13	1.33E-12± 1.23E-14	6.96E-11± 3.42E-13
RW-2	2.11E-09± 4.00E-12	9.98E-10± 2.79E-12	3.10E-09± 4.88E-12	6.93E-11± 3.46E-13	1.36E-12± 1.24E-14	7.06E-11± 3.47E-13
Ceric sulfate Dosimeter solution	2.13E-09± 3.83E-12	1.01E-09± 2.93E-12	3.14E-09± 4.82E-12	7.00E-11± 3.50E-13	1.34E-12± 1.25E-14	7.13E-11± 3.50E-13
Alderson muscle (B)	1.82E-09± 2.74E-12	1.40E-09± 8.38E-13	3.22E-09± 2.86E-12	6.72E-11± 3.36E-13	1.35E-12± 1.25E-14	6.86E-11± 3.36E-13
A150_corrected	2.11E-09± 4.01E-12	1.01E-09± 2.83E-12	3.12E-09± 4.91E-12	6.96E-11± 3.48E-13	1.34E-12± 1.23E-14	7.10E-11± 3.48E-13

TABLE D. 4
Absorbed dose of each organ with an irradiation of 100 MeV proton broad beam by simulation when they were used as the soft tissue of the phantom. Units are Gy.

	Heart tissue	Blood	Heart (all)	Left lung	Right lung	Lung (all)
ICRU-44	2.66E-15± 1.19E-16	1.03E-15± 4.42E-17	3.69E-15± 1.27E-16	3.50E-12± 4.19E-15	2.82E-12± 3.39E-15	6.32E-12± 5.39E-15
A150	2.62E-15± 1.10E-16	1.06E-15± 4.34E-17	3.68E-15± 1.18E-16	3.58E-12± 4.30E-15	2.90E-12± 3.48E-15	6.49E-12± 5.53E-15
ED4C (fhw)	2.83E-15± 1.25E-16	9.99E-16± 4.35E-17	3.83E-15± 1.32E-16	3.45E-12± 4.14E-15	2.79E-12± 3.34E-15	6.24E-12± 5.32E-15
Nylon, Elvamide	2.66E-15± 1.13E-16	1.08E-15± 4.28E-17	3.74E-15± 1.21E-16	3.56E-12± 4.27E-15	2.89E-12± 3.46E-15	6.44E-12± 5.50E-15
RM/SR4	3.01E-15± 1.27E-16	1.07E-15± 4.29E-17	4.08E-15± 1.34E-16	3.50E-12± 4.20E-15	2.84E-12± 3.41E-15	6.34E-12± 5.41E-15
Temex	3.20E-15± 1.34E-16	1.09E-15± 4.51E-17	4.30E-15± 1.41E-16	3.45E-12± 4.14E-15	2.80E-12± 3.36E-15	6.25E-12± 5.33E-15
RW-2	3.47E-15± 1.37E-16	1.25E-15± 4.40E-17	4.73E-15± 1.43E-16	3.47E-12± 4.17E-15	2.77E-12± 3.33E-15	6.24E-12± 5.33E-15
Ceric sulfate Dosimeter solution	2.58E-15± 1.16E-16	9.62E-16± 4.42E-17	3.54E-15± 1.24E-16	3.50E-12± 4.19E-15	2.82E-12± 3.38E-15	6.31E-12± 5.39E-15
Alderson muscle (B)	3.31E-15± 1.36E-16	1.08E-15± 4.27E-17	4.39E-15± 1.43E-16	3.39E-12± 4.07E-15	2.75E-12± 3.30E-15	6.14E-12± 5.23E-15
A150_corrected	2.99E-15± 1.27E-16	1.06E-15± 4.34E-17	4.04E-15± 1.34E-16	3.50E-12± 4.19E-15	2.84E-12± 3.40E-15	6.33E-12± 5.40E-15

TABLE D. 5
Absorbed dose of each organ with an irradiation of 200 MeV/u carbon broad beam by simulation when they were used as the soft tissue of the phantom. Units are Gy.

	Heart tissue	Blood	Heart (all)	Left lung	Right lung	Lung (all)
ICRU-44	1.34E-13± 3.24E-15	7.98E-14± 2.37E-15	2.14E-13± 4.01E-15	5.79E-11± 2.14E-13	5.04E-11± 1.86E-13	1.08E-10± 2.84E-13
A150	1.33E-13± 3.20E-15	8.40E-14± 2.44E-15	2.17E-13± 4.02E-15	6.11E-11± 2.32E-13	5.31E-11± 2.02E-13	1.14E-10± 3.08E-13
ED4C (fhw)	1.35E-13± 3.29E-15	7.88E-14± 2.39E-15	2.14E-13± 4.07E-15	5.70E-11± 2.11E-13	4.97E-11± 1.84E-13	1.07E-10± 2.80E-13
Nylon, Elvamide	1.35E-13± 3.26E-15	7.85E-14± 2.39E-15	2.13E-13± 4.04E-15	5.96E-11± 2.21E-13	5.18E-11± 1.97E-13	1.11E-10± 2.96E-13
RM/SR4	1.34E-13± 3.27E-15	8.17E-14± 2.45E-15	2.16E-13± 4.08E-15	5.77E-11± 2.14E-13	5.02E-11± 1.91E-13	1.08E-10± 2.86E-13
Temex	1.37E-13± 3.26E-15	8.37E-14± 2.53E-15	2.21E-13± 4.13E-15	5.68E-11± 2.10E-13	4.95E-11± 1.83E-13	1.06E-10± 2.79E-13
RW-2	1.41E-13± 3.28E-15	8.41E-14± 2.42E-15	2.26E-13± 4.08E-15	5.74E-11± 2.12E-13	5.00E-11± 1.90E-13	1.07E-10± 2.85E-13
Ceric sulfate Dosimeter solution	1.30E-13± 3.15E-15	8.19E-14± 2.51E-15	2.12E-13± 4.03E-15	5.80E-11± 2.15E-13	5.05E-11± 1.87E-13	1.08E-10± 2.85E-13
Alderson muscle (B)	1.28E-13± 3.79E-15	8.80E-14± 2.10E-15	2.16E-13± 4.33E-15	5.60E-11± 2.07E-13	4.89E-11± 1.81E-13	1.05E-10± 2.75E-13
A150_corrected	1.33E-13± 3.23E-15	8.52E-14± 2.54E-15	2.18E-13± 4.11E-15	5.77E-11± 2.13E-13	5.02E-11± 1.91E-13	1.08E-10± 2.86E-13

TABLE D. 6
Absorbed dose of each organ with an irradiation of 400 MeV/u iron broad beam by simulation when they were used as the soft tissue of the phantom. Units are Gy.

	Heart tissue	Blood	Heart (all)	Left lung	Right lung	Lung (all)
ICRU-44	6.84E-13± 1.04E-14	5.14E-13± 9.87E-15	1.20E-12± 1.43E-14	7.62E-10± 4.27E-12	6.66E-10± 3.73E-12	1.43E-09± 5.67E-12
A150	7.02E-13± 1.06E-14	5.30E-13± 1.01E-14	1.23E-12± 1.47E-14	7.45E-10± 4.17E-12	6.52E-10± 3.65E-12	1.40E-09± 5.54E-12
ED4C (fhw)	6.80E-13± 1.05E-14	4.89E-13± 9.69E-15	1.17E-12± 1.43E-14	7.63E-10± 4.27E-12	6.66E-10± 3.73E-12	1.43E-09± 5.67E-12
Nylon, Elvamide	6.98E-13± 1.04E-14	5.20E-13± 9.99E-15	1.22E-12± 1.44E-14	7.52E-10± 4.21E-12	6.56E-10± 3.67E-12	1.41E-09± 5.59E-12
RM/SR4	6.75E-13± 1.02E-14	5.13E-13± 9.96E-15	1.19E-12± 1.43E-14	7.58E-10± 4.24E-12	6.60E-10± 3.69E-12	1.42E-09± 5.63E-12
Temex	6.90E-13± 1.03E-14	5.08E-13± 9.90E-15	1.20E-12± 1.43E-14	7.58E-10± 4.24E-12	6.61E-10± 3.70E-12	1.42E-09± 5.63E-12
RW-2	7.08E-13± 1.05E-14	5.20E-13± 9.82E-15	1.23E-12± 1.44E-14	7.55E-10± 4.23E-12	6.59E-10± 3.69E-12	1.41E-09± 5.61E-12
Ceric sulfate Dosimeter solution	6.87E-13± 1.04E-14	5.21E-13± 9.96E-15	1.21E-12± 1.44E-14	7.63E-10± 4.27E-12	6.68E-10± 3.74E-12	1.43E-09± 5.68E-12
Alderson muscle (B)	6.90E-13± 1.03E-14	5.10E-13± 9.79E-15	1.20E-12± 1.42E-14	7.60E-10± 4.26E-12	6.63E-10± 3.78E-12	1.42E-09± 5.69E-12
A150_corrected	6.84E-13± 1.03E-14	5.01E-13± 9.72E-15	1.19E-12± 1.42E-14	7.58E-10± 4.24E-12	6.60E-10± 3.70E-12	1.42E-09± 5.63E-12

VITA

Name: Dongyoul Lee

Address: Department of Nuclear Engineering
Texas A&M University
3133 TAMU
College Station, TX 77843

Email Address: dufly84@gmail.com

Education: B.S., Chemistry, Korea Military Academy, 2007
M.S., Nuclear Engineering, Texas A&M University, 2011